HOT ISOSTATIC PRESSING OF TITANIUM METAL MATRIX COMPOSITES FOR TRIBOLOGICAL APPLICATIONS

By

Malallah Mohamed Malallah Al Lawati

A thesis submitted to University of Birmingham in partial fulfilment of the requirements for the degree of

DOCTOR OF PHILOSOPHY

School of Metallurgy and Materials

College of Engineering and Physical Sciences

University of Birmingham

2022

Abstract

An investigation into developing titanium metal matrix composites (TMCs) for tribological applications while still possessing good mechanical properties has been performed using powder metallurgy (P/M) and hot isostatic pressing (HIP) process. TMCs were successfully synthesized using a wide range of process parameters such as : investigating the influence of HIP temperature and dwell time. In addition to that, the influence of reinforcement volume fraction, size, type, blending route and *in situ* reactions were studied in terms of the microstructural homogeneity, mechanical and tribological properties. The as-HIPped samples were analysed using scanning electron microscopy (SEM), optical microscopy (OM), x-ray diffraction (XRD) and Raman spectroscopy for the samples containing graphene. A wide range of reinforcements were investigated, such as silicon carbide (SiC), titanium diboride (TiB_2), boron (B), graphene nanoplatelets (GNP) and titanium carbide (TiC). In addition to that, the influence of reinforcement size from micron size (5 µm) to nano-size (20 nm) on the mechanical and tribological properties were investigated thoroughly. Furthermore, the influence of reinforcement volume fraction ranging from 5 volume percent (vol.%) to 10 vol.% on the microstructural homogeneity, mechanical and tribological properties was studied. Reinforcements such as B and GNP were used *in situ* formation work in order to synthesize phases such as TiC and TiB during the HIP process and process parameters such as the HIP temperature was investigated in terms of *in situ* phase formation and completion. Finally, functionally graded material (FGM) using SiC as a reinforcement and Ti-6Al-4V (Ti64) matrix was successfully synthesized using the HIP process and the tribological and mechanical properties were investigated.

The work will aim to solve issues of high brittleness due to the high reinforcement volume fractions, microstructural homogeneity due to powder clustering , while trying to enhance interfacial bonding and solve issues concerning TMCs blending due to the high reactivity of Ti with oxygen. Moreover, issues such as incomplete *in situ* phase formation will be investigated by HIPping at different temperatures and to reduce the size of the brittle diffusion zone due to iron (Fe) diffusion at high temperatures. The main novelty of the work will look into improving microstructural homogeneity by controlling the blending route using mechanical alloying (MA) via wet ball milling, reducing the brittle intermetallic diffusion zone by studying various HIPping temperatures and using different elemental reinforcements with high specific strengths in order to reduce agglomeration and inhomogeneity as a result of high volume fractions.

The rationale for conducting the research is that ti64 has a high specific strength to weight ratio and could provide weight savings in a wide range of engineering applications including the marine and oil and gas industry. Furthermore, Ti64 has good corrosion resistance but low tribological properties such

as coefficient of friction and sliding wear properties which is an issue at harsh environmental conditions. Therefore, reinforcing the Ti64 matrix with various chemically stable reinforcements that are stiffer than the matrix such as SiC were suggested to increase the strength and wear resistance of the composites. Furthermore, in-situ phase formation was chosen using reinforcements such as boron (B) and graphene nanoplatelets (GNP) to obtain clean in situ strengthening stiffer phases to enhance the tribological properties of the composites.

TMCs were developed for high wear resistance applications that also possess good mechanical properties using a Ti64 matrix reinforced with different additions and volume fractions of B (1 vol.%) and GNP (1-2 vol.%). The study looked into *in situ* formation of hard phases and how the HIP temperature can influence that including the consolidation behaviour. Different HIP conditions were investigated such as HIPping below the ß-transus temperature at (920℃), 1040℃ and super ß-transus temperature (1160℃). 1040℃ was selected as an optimal HIP temperature based on calculations that estimate the ß-transus temperature by taking into account the diffusion of oxygen (O) and carbon (C). The main findings of the work is that HIPping at 1160^{o}C ensured full consolidation, but resulted in grain growth, while HIPping at 920^{o}C there was lack of consolidation and no *in situ* reaction. At 1040^{o}C there was retention of TiC phase with some unreacted graphene, which improved tribological performance.

Furthermore, TMCs using SiC as a reinforcement and Ti64 as the metal matrix were developed for high wear resistant applications. The study looked into the influence of reinforcement volume fraction (5-10 vol.%) and reinforcement size (5 µm , 20 nm) on the mechanical and tribological properties. In addition to that, blending routes were investigated such as MA by ball milling and roll blending and how it affects powder homogeneity, hence the properties. The main findings of the work is that increasing the reinforcement vol.% to 5 vol.%, changes the wear mechanism from abrasive wear to mainly delamination wear, which in turn reduces the wear rate of the composite and improves the wear resistance. This could be mainly attributed to the hard *in situ* formed TiC and titanium silicide (Ti_5Si_3) phases.

Ti64 based FGMs were prepared using P/M HIP using SiC as a reinforcement. Three layers of an FGM was produced, with the bottom layer being monolithic Ti64, the second layer reinforced with 5 vol.% SiC and the third layer with 10 vol.% SiC. A super-transus HIP temperature of 1160℃ was selected for the work to ensure full consolidation, in situ reaction at the expense of grain growth. The different layers of the FGM showed good bonding and no cracking was observed along the gradient layers as seen by the micro-hardness indentations. The synthesized FGM showed promising compressive properties such as high compressive yield strength and very good ductility values even at the higher

vol.% regions. On the other hand, there was a very clear trend of a reduction in ductility and an increase in compressive yield strength as the reinforcement volume fraction was increased.

Ti64 reinforced with varying volume fractions (5 vol.%, 10 vol.%) of TiB_2 was prepared by P/M HIP. The influence of the HIP temperature (1160℃) on the microstructural evolution, mechanical and tribological properties were investigated. Furthermore, as-received MA titanium-silicon carbide (Ti-SiC) nanocomposite and titanium-titanium carbide (Ti-TiC) nanocomposite were successfully prepared by HIP at various temperature such as (950℃,1040℃) and how that influenced the mechanical and tribological behaviour. Some of the key findings of the study were that the increase of micro-hardness observed with the with the 10 vol.% TiB_2 is mainly be attributed to the load transfer mechanism and grain refinement. The large standard deviation could be attributed to the inhomogeneity, which is inherent to the blending technique used and the relatively large reinforcement size of 5 µm.

Some of the promising applications of TMCs can be used in the oil and gas industry such as pipelines as titanium is highly corrosion resistant, and the reinforcement in situ formed hard phases will provide good wear resistance properties. other areas could include engine valves and connecting rods due to the weight savings of titanium and good tribological properties provided by using graphene for example as a reinforcement that would provide lubrication.

Keywords: Powder metallurgy, Hot isostatic pressing, Titanium metal matrix composites, *In situ* phase formation

Dedication

This thesis is dedicated to my family, and without them I would not have been able to complete this work.

Acknowledgements

I would like to acknowledge the support and technical help I got from my supervisor Professor Moataz Attallah.

I would also like to acknowledge my industrial supervisor Doctor Raja Khan from the Welding Institute for all the technical help and support provided.

In addition, I would like to acknowledge the Centre of Doctoral Training in Innovative Metal Processing (IMPaCT), funded by the Engineering and Physical Sciences Research Council (EPSRC), and the National Structural Integrity Research Centre (NSIRC) for funding the PhD project at the University of Birmingham.

List of Publications

I. Irukuvarghula et al., *Development of Powder Metallurgy Based Metal Matrix Composites for Geothermal Applications,* World Geothermal Congress, 2020, Iceland. **(Co-author, Contributed to the Experimental Work)**

Papers in Preparation

I. **Chapter 4**: P/M Hot Isostatic Pressing of TMCs via In Situ Elemental Additions of B and GNP, Enhanced Mechanical and Tribological Properties
II. **Chapter 5**: Hot Isostatic Pressing of Ti-6Al-4V/SiC: Influence of HIP Temperature, Reinforcement Size and Volume fraction on Microstructural Evolution, Mechanical and Tribological Properties
III. **Chapter 6**: Characterization of Hot Isostatic Pressed Ti-6Al-4V/SiC Functionally Graded Material: Microstructure, Mechanical and Tribological Behaviour
IV. **Chapter 7**: P/M Hot Isostatic Pressing of TMCs: Influence of Reinforcement Type, HIP temperature and Reinforcement Volume Fraction on Microstructural Evolution, Mechanical and Tribological Properties

Presentations in International Conferences

I. European Powder Metallurgy Conference, 2020, Norway

Contents

List of figures

List of tables

Glossary of Terms

Term	Definition
AGA	Argon Gas Atomised
Al	Aluminium
Al_2O_3	Aluminium Oxide
APS	Average Particle Size
B	Boron
BPR	Ball-to-Powder Ratio
b	Burger vector
C	Carbon
℃	Degrees Celsius
ΔC	Thermal Mismatch between Matrix and Reinforcement
COF	Coefficient of Friction
CRTMC	Continuously Reinforced Titanium Metal Matrix Composite
CNT	Carbon Nanotubes
CTE	Coefficient of Thermal Expansion
Cu	Copper
Cubic BN	Cubic Boron Nitride
d	Grain Size
dr	Reinforcement Particle Size
DNP	Diamond Nanoparticles
DRTMC	Discontinuously Reinforced Titanium Metal Matrix Composite
EBSD	Electron Back Scatter Diffraction
EDM	Electric Discharge Machine
El%	Elongation
EDS	Energy Dispersive X-ray Spectroscopy
FG	Functionally Graded
FGL	Functionally Graded Laminate
FGM	Functionally Graded Material
f_H	Volume Fraction of Harder Phase
fr	Volume Fraction of Reinforcement
f_s	Volume Fraction of Softer Phase
g	Gram
G	Shear Modulus
GB	Grain Boundary
GND	Geometrically Necessary Dislocations
GNP	Graphene Nanoplatelets
GPa	Gigapascal
h	Hours
HF	Hydrogen Fluoride
H_h	Micro-hardness of Harder Phase
HIP	Hot Isostatic Pressing
H_{lower}	Lower Bound Composite Micro-hardness
HNO_3	Nitric Acid

H_2O	Water
H_s	Micro-hardness of Softer Phase
H_{upper}	Upper Bound Composite Micro-hardness
HV	Vickers Hardness
K	Kelvin
Kg	Kilogram
M	Taylor Factor
MA	Mechanical Alloying
mbar	Unit of Pressure
min	Minute
MMC	Metal Matrix Composite
mm	Millimetre
m^2/g	Surface Area
MPa	Mega Pascal
MPa $m^{1/2}$	Hall-Petch Constant Unit
MWCNT	Multi-Wall-Carbon-Nanotubes
N	Nitrogen
N	Newton
Ni	Nickel
nm	Nano-metre
O	Oxygen
OM	Optical Microscopy
PCA	Process Control Agent
PM	Powder Metallurgy
PSD	Particle Size Distribution
RPM	Revolutions Per Minute
SEM	Scanning Electron Microscopy
Si	Silicon
SiC	Silicon Carbide
Si_3N_4	Silicon Nitride
SPS	Spark Plasma Sintering
SWCNT	Single-Wall-Carbon-Nanotubes
Ti	Titanium
TiB	Titanium Boride
TiB_2	Titanium Diboride
TiC	Titanium Carbide
TiCN	Titanium Carbo Nitride
TMC	Titanium Metal Matrix Composite
TiN	Titanium Nitride
Ti_5Si_3	Titanium Silicide
Ti64	Ti-6Al-4V, Grade 5 Titanium
US	Ultimate Strength
V.%	Volume Percent
WC	Tungsten Carbide
Wt%	Weight Percent
XRD	X-ray Diffraction
YS	Yield Strength
µm	Micro-metre (Micron)
σ_{th}	Theoretical Stress
σ_{ym}	Yield Strength of the Matrix

$\Delta\sigma_{orowan}$	Strength Contribution from Orowan Strengthening Mechanism
$\Delta\sigma_{HP}$	Hall-Petch Grain Refinement
$\Delta\sigma_{L.T}$	Strength Contribution from Load-Transfer Mechanism
$\Delta\sigma_{CTE}$	Strength Contribution due to Coefficient of Thermal Expansion Difference
σ_o	Starting Stress for Dislocation Movement
α	Alpha Titanium Phase
ß-transus	Transformation Temperature from alpha to Beta Titanium
10^{-7} mbar*l/s	Leak Rate
±	Plus or Minus
°C/min	Rate of Cooling/Heating
λ	Wavelength
Kα	X-ray Diffraction Radiation Type

Chapter 1 Introduction

1.1 Chapter Overview

This chapter will provide a detailed insight into the significance of titanium metal matrix composites (TMCs) in various industrial applications ranging from the aerospace to the medical field. Furthermore, powder metallurgy (P/M) hot isostatic pressing concept, benefits and drawbacks will be highlighted in this chapter. In addition to that, P/M HIP will be compared to other manufacturing techniques used to synthesize TMCs and how it can solutions to fabrication issues arising from TMC manufacturing. Finally, the main objectives of the research will be mentioned and the thesis breakdown.

1.2 Brief background of TMCs and their applications

TMCs have been developed for many different industries, ranging from the aerospace industry all the way to the marine industry [1]. TMCs have been introduced in the past 30 years for aerospace applications to overcome issues such as low heat resistance , wear resistance and Young's modulus in comparison with steel and nickel-based superalloys [2]. In terms of what makes TMCs potential candidates for medical applications, is that they mainly have excellent biocompatibility while still possessing high specific strength and being light in weight [3]. There have been reports of using TMCs in high temperature compressor applications due to the TMC being able to withstand temperatures exceeding 760℃ while offering a reduction in weight approaching 50% in comparison to nickel-based superalloys [4]. It is vital to note that since TMC fabrication routes are complex and have many different issues, the National Aeronautics and Space Administration (NASA) have invested heavily in researching TMCs and make them more commercially used. NASA worked with many American companies in developing TMCs for gas turbine engines [5]. It is also worth mentioning that TMCs were replacing parts made from nickel-superalloys. For example, NASA have reported using 40% of the material in the F-22 fighter jet from TMCs. Furthermore, it is expected that newer generation fighters will compromise of even more TMCs as the development of those composites are further enhanced. It is worth mentioning that Rolls Royce Plc have developed a TMC for their advanced fan engines. The fans are comprised of titanium-carbon based TMC for the fan blades which have helped decrease the

weight of aircrafts by 680kg [6]. This would help the aircraft carry more passengers with no extra cost according to Rolls Royce. Other reports of TMCs being used are by the Royal Netherlands Air Force for their F16 fighter jets which use a TMC reinforced with SiC for their landing gear which again offers 40% decrease in weight in comparison to the previous alloys used [7]. Furthermore, there are reports of TMCs being used as an ideal material in the oil and gas industries for pipes as titanium (Ti) is highly corrosion resistant and the hard ceramic reinforcements will provide excellent wear resistance properties [8]. Finally, Toyota Motors have recently developed a TMC to be used in their new generation cars for the engine valves and connecting rods [9].

1.3 P/M HIP

P/M HIP is a manufacturing method used to either densify powders to their 100% theoretical density or as a heat treatment process for sintered parts and additively manufactured parts using a high pressure (100-200 MPa) and high temperatures in the range of (900-1250℃) for nickel superalloys and steels. The main benefit of HIP is that it applies isostatic pressure in all directions, hence resulting in optimal isotropic mechanical properties and therefore providing another method of fabricating materials other than casting and forging for example. HIP have proven to be a solid candidate as a post processing technique especially in the field of additive manufacturing and other P/M manufacturing methods such as metal injection moulding and sintering. Furthermore, HIP can be used to manufacture near net shape (NNS) components weighing up to 30 tonnes for parts to be utilized in the oil and gas and marine industries. Some HIP systems even allow for parts up to a diameter of 1 metre to be manufactured. On the other hands, HIP can be used to make small parts that are 100 grams or less and have been reported to be used to produce dental brackets. With time, HIP have proven to be cost-effective and reliable manufacturing technique that can be utilized to synthesize many different metals, ceramics and post process additively manufactured components. It should also be noted that P/M offers many benefits over other manufacturing techniques which make it a very attractive and viable option for synthesizing advanced metallurgy manufacturing [10,11].

***Table 1.1**: Industrial applications of HIP technology [10,11]*

Categories where P/M HIP is beneficial	**Advantages of P/M HIP**
Design flexibility and freedom	• Near net shape (NNS) • Ease of synthesizing composites • Fabricating large components with minimum welds required • Fabricate complex internal cavities which are very difficult to machine
Properties of HIPped samples	• Fine , homogenous microstructure due to isostatic pressure and temperature • Homogenous mechanical and tribological properties
Cost reduction	• NNS route allows for reduction in machining • Simplifying design were less parts are required for a purpose
Environmental aspect	• NNS allows for less scrap metal • No powder waste like additive manufacturing • Higher material yield in comparison with conventional metallurgy

***Table 1.2:** Applications of HIP and the typical materials used [11,12]*

Application	**Aim**	**Materials used**
Powder consolidation using canisters as encapsulations	Reach full theoretical density and reduce possibility of excessive grain growth and segregation	Advanced ceramics, MMCs, magnetic materials
Diffusion bonding	Diffusion bond dissimilar or similar materials that is a challenge with other techniques	Steel and Ni alloys , metal and ceramics bonding
Porosity removal , densification and consolidation	Reach full theoretical density	MMCs, Ni superalloys.
In situ reactive HIPping	Produce new phases from reactants at a highly negative Gibb's free energy during exothermic reaction at heating stage of HIP	MMCs, intermetallics like TiB_2, Graphene, B
Densification of casted parts	Remove porosities	Ti and its alloys, Al and its alloys
Densification of sintered parts	Reach full theoretical density	Advanced ceramics like Al_2O_3
Densification of additively manufactured parts	Porosity removal	Ti and its alloys
Heat treatment post additive manufacturing	Control grain size and microstructure and limit segregation	Ni superalloys, Ti and its alloys

Table 1.1 shows a summary of industrial areas where P/M HIP could be deemed as a solution for various issues faced by manufacturers. Furthermore, Table 1.2 Shows applications whereby P/M HIP could be employed, what the aim is of the technology and the typical materials used in each. Table 1.2 also shows the typical industries that benefit from using P/M HIP technology and the typical applications they are used to manufacture. In terms of the HIP global market, it is estimated that 25%

of the HIP used is on P/M based manufacturing. In addition to that, it is estimated that 50% of the global use of HIP is related to the densifying of sintered, casted and additively manufactured components [10]. It has also been reported that there was a rapid growth of 5000% in P/M HIP stainless steel components from 1990-2008 period. Furthermore, it was reported that in 2013 another 5000% growth in NNS components fabricated via P/M was expected for tool steel components. As summarized by Table 1.1, HIP allows for a homogenous microstructure and isotropic mechanical and tribological behaviour. For example, tool steel that is rich in carbide that is synthesized via P/M HIP has high fatigue strength and toughness due to limited segregation and the fine homogenous microstructure obtained through the technology. The main reason is attributed to the smaller carbides in steel made from P/M HIP in comparison with other manufacturing techniques such as casting or forging which in turn leads to much lower stress concentration zones, hence increasing the toughness and crack propagation rate in P/M HIPped parts. In addition to that, what makes P/M HIP an attractive manufacturing route is that parts prepared via this technology offer a comparable corrosion resistance to forged components and sometimes even better [11,12].

1.4 Aims of the project and research

The main aim of this work is to synthesize TMCs which have good tribological and mechanical properties. Most TMCs mentioned in the literature are either highly brittle with very low mechanical performance or TMCs with good mechanical properties but terrible tribological performance. This work will also aim to solve issues of high brittleness due to the high reinforcement volume fractions, microstructural homogeneity due to powder clustering , while trying to enhance interfacial bonding and solve issues concerning TMCs blending due to the high reactivity of Ti with oxygen. Moreover, issues such as incomplete *in situ* phase formation will be investigated by HIPping at different temperatures and to reduce the size of the brittle diffusion zone due to iron (Fe) diffusion at high temperatures. The main novelty of the work will look into improving microstructural homogeneity by controlling the blending route using MA via wet ball milling, reducing the brittle intermetallic diffusion zone by studying various HIPping temperatures and using different elemental reinforcements with high specific strengths in order to reduce agglomeration and inhomogeneity as a result of high volume fractions. Furthermore, the other novelty of the work will include using lower volume fractions of reinforcement to reduce the brittleness of the TMCs.

The main objectives of this research are as follows:

- Develop advanced TMCs which possess high wear resistance and good mechanical properties and evaluate the influence of the reinforcement characteristics such as (reinforcement type, volume fraction, size) and process parameters on the microstructure and properties.
- Evaluate material properties such as (Compressive strength, micro-hardness, wear resistance) and rationalise them based the microstructural characteristics of the as-HIPped TMCs.
- Create novel TMCs via in situ phase formation using P/M HIP with one or more elemental reinforcements such as boron and graphene with enhanced tribological and mechanical performance.
- Develop structure-property relations relating phase content to experimental and theoretical compressive strength values
- Synthesize TMC FGMs for high wear resistant demanding applications that are crack free

1.5 Outline of Thesis

This research looks into developing advanced TMCs that have a high wear resistance and good mechanical properties. This is presented in the following chapters: literature review (Chapter 2), experimental procedure (Chapter 3), P/M hot isostatic pressing of TMCs via in situ elemental additions of B and GNP (Chapter 4), P/M hot isostatic pressing of TMC reinforced with SiC, enhanced micro-hardness and tribological performance (Chapter 5), P/M hot isostatic pressing of Ti-6Al-4V/SiC FGM with enhanced tribological and mechanical properties (Chapter 6), Mechanical and tribological behaviour of mechanically alloyed nano TMCs synthesized via P/M hot isostatic pressing (Chapter 7), conclusions and future work (Chapter 8).

In the literature review (Chapter 2), an introduction into TMCs is provided discussing the different reinforcement categories, common powder blending routes, influence of various reinforcement characteristics such as volume fraction and size on mechanical and tribological properties. In addition to that, all the recent work done on TMCs via powder metallurgy route is summarised with the corresponding processing routes and properties. Furthermore, FGMs are discussed thoroughly in terms of their applications, production through P/M and the wide range of properties they offer depending on the design requirements.

The experimental procedure (Chapter 3) will start by highlighting an overview of the chapter and what it entails, followed by a section discussing the materials used and their processing, hot isostatic

pressing procedure, microstructural characterization and finally the mechanical and tribological testing and equipment used.

P/M hot isostatic pressing of TMCs via *in situ* elemental additions of B and GNP (Chapter 4) will start with a brief introduction and review of the current TMCs produced, followed by an experimental section discussing the material preparation route, characterization techniques used and the properties investigated both mechanical and tribological. In addition to that, the results will be presented and discussed thoroughly and the chapter will be concluded. The chapter will focus on microstructural evolution of the TMCs synthesized via *in situ* reactions, influence of HIPping temperature on phase formation, structure-property relations relating phase content to micro-hardness and tribological performance and thoroughly investigating the influence of reinforcement type such as graphene in improving wear resistance by utilising advanced characterization techniques such as Raman spectroscopy.

In the P/M hot isostatic pressing of TMC reinforced with SiC, enhanced micro-hardness and tribological performance (Chapter 5), the work looks to examine the influence of reinforcement characteristics such as the volume fraction and size on the microstructural evolution, mechanical and tribological behaviours and rationalise the properties in terms of the dominant strengthening mechanisms. The chapter includes a section summarising the most recent work done on TMCs by researchers, followed by the experimental section which describes the characterization routes and properties examined from mechanical to tribological performance. The chapter also looks into the HIP process parameters such as the influence of HIPping temperature on the microstructural evolution and formation of strengthening phases. The results are then presented, discussed and a conclusion is reached and presented.

In P/M hot isostatic pressing of Ti-6Al-4V/SiC FGM with enhanced tribological and mechanical properties (Chapter 6) , the study will investigate how to synthesize and FGM via P/M HIP and get a crack free sample with a strong bond between different layers. Compressive testing and wear testing will be conducted in order to understand whether the FGM has good bonding and to understand how the samples fail.

In chapter 7, Mechanical and tribological behaviour of mechanically alloyed nano TMCs and other reinforcements synthesized via P/M HIP will be presented and investigated.

In chapter 8, the conclusions from each chapter will be summarized and the future work will be outlined.

References

[1] S.C Tjong, Z.Y Ma., *Microstructural and mechanical characteristics of in situ metal matrix composites,* Mater. Sci. Eng. R. Rep, 2000, Vol.29(3), pp.49-113

[2] Liu, Yuanqing & Chen, L.F. & Tang, H.P. & Liu, C.T. & Liu, Boxinyue & Huang., *Design of powder metallurgy titanium alloys and composites,* Mater. Sci. Eng. A., 2006, Vol.418(1-2), pp.25-35

[3] Yuncang Li, Khurram S. Munir, Jixing Lin, Cuie Wen., *Titanium-niobium pentoxide composites for biomedical applications,* Bioactive Materials, 2016, Vol.1(2), pp.127-131

[4] O'Connell . *Production of Titanium Aluminide Products*. AFWAL-TR-83-4050,WPAFB, Ohio; 1973.

[5] Anderson . *Titanium matrix composite turbine engine component consortium(TMCTECC). The AMPTIAC Newsletter*. USA: AMPTIAC; 1998.

[6]https://www.compositestoday.com/2014/09/rolls-royce-tests-composite-fan-systems-new-engine-designs/. Accessed on 09-04-19, 16:30

[7] http://specmaterials.com/f16landingbrace.htm. Accessed on 09-06-19, 12:30

[8] K. Soorya Prakash, P.M. Gopal, D. Anburose, V. Kavimani., *Mechanical, corrosion and wear characteristics of powder metallurgy processed Ti-6Al-4V/B_4C metal matrix composites,* Ain Shams Engineering Journal, 2018, Vol.9(4), pp.1489-1496

[9] T. Saito., *Affordable High-performance Ti/TiB Metal Matrix Composites Tailored for Automobile Engine Components: Materials Design, Manufacturing Process, and Remaining Issues*, R&D Review of Toyota CRDL, 2020, Vol.51(1), pp.1-30

[10] https://www.epma.com/hot-isostatic-pressing Accessed on 03-07-19, 11:30

[11] H. Atkinson, S. Davies ., *Fundamental Aspects of Hot Isostatic Pressing: An Overview,* METALLURGICAL AND MATERIALS TRANSACTIONS A, 2000, Vol.31, pp.2981-3000

[12] Bocanegra-Bernal et al., *Review Hot Isostatic Pressing (HIP) technology and its applications to metals and ceramics,* J. Mat. Sci., 2004, Vol.39, pp.6399-6420

Chapter 2 Literature Review

2.1 TMCs overview

This section will focus on giving a detailed overview of titanium metal matrix composites (TMCs), their mechanical and tribological performance prepared and manufactured using powder metallurgy (PM) hot isostatic pressing (HIP) route. Additionally, structural-property models used to predict TMCs mechanical and tribological behaviour will be examined thoroughly. Moreover, the chapter will discuss the phase formation of phases using *in situ* techniques. Furthermore, FGM applications, preparation route using PM will be discussed. Finally, the research gap will be identified and the aims and objectives of the project will be highlighted.

2.1.1 Introduction to TMCs

TMCs are a class of materials that offer significant improvements over monolithic titanium (Ti). They have a higher specific strength, stiffness, wear resistance and heat resistance over a non-reinforced matrix alloy [1], making them ideal for petrochemical, aerospace, and maritime applications [2]. In the past decade, there has been an increased interest in researching TMCs for engine components due to the vast weight savings they offer, high specific strength and enhanced tribological performance. However, TMCs fabrication are deemed challenging and has many complications that will be discussed in greater details in later sections.

The basic principle of TMCs falls upon the matrix alloy, being reinforced with hard ceramic particles that help harden the material, however at the expense of deteriorating the ductility as the volumetric percentage (vol.%) of the reinforcement increases [3]. The mechanical properties of TMCs differ significantly from the base monolithic alloy due to in-situ reactions taking place between the reinforcement and the matrix during the consolidation process, forming new hardened phases that offer superior tribological performance over the monolithic matrix alloy.

2.1.2 Common reinforcement categories

Before dwelling into different reinforcement types and categories, it is important to define the concepts of the reinforcing phases and the matrix material. It is generally well accepted in the literature that the base material phase with the higher volume fraction is the matrix, while the reinforcement is considered the phase with the lower volume fraction that is generally mixed with the matrix material to enhance certain properties [4]. For example, if the reinforcement is a hard ceramic, it is generally added to the metallic matrix to enhance the hardness of the composite. On the other hand, a soft reinforcement could be added to a ceramic matrix to improve properties such as the ductility and impact strength of the composite.

Common TMC reinforcements can either be continuously reinforced TMCs (CRTMCs) using continuous fibres as the reinforcing phase, or discontinuously reinforced TMCs (DRTMCs) using different powder morphologies of either whiskers, particles, or even short fibres [5]. CRTMCs were widely sought after previously due to the superior tribological properties and weight reductions they offered in the aerospace industry [6]. However, the fibres were expensive to produce, hence why the focus in recent years has shifted towards DRTMCs. Nevertheless, DRTMCs still have major issues that are slowing down their implementation and expansion into different industries. The shortcomings range from particle clustering which affects the mechanical and tribological behaviour [7], reinforcement agglomeration and extreme brittleness associated with PM HIP processing route. Therefore, it is important to understand the powder blending routes, sacrificial canister material selection, HIP processing parameters to tailor a TMC with limited residual stresses, limit extremely brittle diffusion zone size and produce a homogenous microstructure to improve the properties.

Table 2.1 shows a list of common continuous-fibre and particle reinforcements used in the fabrication of TMCs. Furthermore, Table 2.2 shows a list of the most common DRTMCs, their powder characteristics, processing route and their properties. It is well noted in the literature that titanium carbide (TiC) [8] and titanium diboride (TiB_2) [9] is the most compatible reinforcement for titanium alloys due to the small coefficient of thermal expansion (CTE) mismatch between the reinforcement and matrix, hence limiting residual stress formation. Figure 2.1 shows a representation of different types of TMCs that fall under the categories of DRTMCs and CRTMCs. It is well noted in the literature that the cost of DRTMCs is way cheaper than using fibre reinforced CRTMCs. In addition to that, DRTMCs offer a more uniform isotropic distribution of properties along with a multitude of loading directions [10].

(a) Particles Reinforced

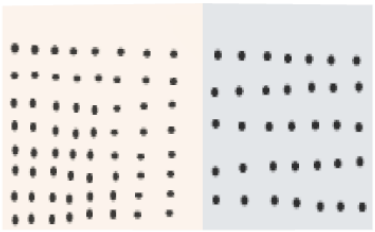

(b) Whiskers Reinforced

Figure 2.1*: Discontinuously reinforced MMC (a-b), [10]*

Table 2.1*: Common continuous and discontinuous reinforcements*

Continuous reinforcements	**Typical diameter**	**Typical reinforcements**	**Ref**	**Discontinuous reinforcements**	**Typical reinforcements**	**Typical diameter**	**Ref**
Continuous fibre	3-150 µm	SiC, B, C	[10]	Whiskers	TiB_2	1-5 µm	[11]
-	-	-		Particles	B_4C,	0.5-25 µm	[12]
-	-	-		nanoparticles	SiC , ND,GNP	< 100 nm	[13,14,15]

Table 1.2: List of common reinforcements, powder characteristics, processing route and properties from literature

Matrix	Matrix size (µm)	Reinforcement type & %	Reinforcement size	Processing route	Properties				Ref
					CTE	Hardness	Strength (MPa)	EI %	
Ti-6Al-4V	70-150	TiB_2 3 wt.%	3-5 µm	MA + HIP	7.2	347.3 HV	N/A	N/A	[11]
Ti-6Al-4V	70-150	TiB_2 5 wt.%	3-5 µm	MA + HIP	7.2	433.9 HV	N/A	N/A	[11]
Ti-6Al-4V	70-150	TiB_2 8 wt.%	3-5 µm	MA + HIP	7.2	566.3 HV	N/A	N/A	[11]
Ti-6Al-4V	100-130	TiB_2 3 wt.%	3.13 µm	MA + HIP	7.2	N/A	1063	10.1	[16]
Ti-6Al-4V	100-130	TiB_2 5 wt.%	3.13 µm	MA + HIP	7.2	N/A	1284	6.7	[16]
Ti-6Al-4V	100-130	TiB_2 8 wt.%	3.13 µm	MA + HIP	7.2	N/A	992	5.6	[16]
Ti-6Al-4V	44	SiC 5 vol. %	< 75 nm	PM	4.63	460 HV	1483	N/A	[13]
Ti-6Al-4V	44	SiC 10 vol. %	< 75 nm	PM	4.63	369 HV	1189	N/A	[13]
Ti-6Al-4V	44	SiC 15 vol. %	< 75 nm	PM	4.63	315 HV	1064	N/A	[13]
Ti-6Al-4V	<25	TiC 5 vol.%	<0.5µm	SPS	7.15	N/A	995	3	[17]
Ti-6Al-4V	<25	TiC 10 vol.%	<0.5µm	SPS	7.15	N/A	1060	3	[17]
Ti-6Al-4V	150-200	GNP 0.25 wt.%	<5 layers WT=0.5-4nm D=0.5-3 µm	SPS	N/A	N/A	940	10.0	[18]
Ti-6Al-4V	150-200	GNP 0.5 wt.%	<5 layers WT=0.5-4nm D=0.5-3 µm	SPS	N/A	N/A	938	4.3	[18]
Ti-6Al-4V	150-200	GNP 0.75 wt.%	<5 layers WT=0.5-4nm D=0.5-3 µm	SPS	N/A	N/A	892	3.6	[18]
Ti-6Al-4V	150-200	GNP 1 wt.%	<5 layers WT=0.5-4nm D=0.5-3 µm	SPS	N/A	400 HV	N/A	N/A	[18]
Ti-6Al-4V	150-200	GNP 1.5 wt.%	<5 layers WT=0.5-4nm D=0.5-3 µm	SPS	N/A	N/A	N/A	N/A	[18]
Ti	10-44	DNP 0.35 wt.%	3.0 µm	MA + SPS	N/A	333 HV	1039	39.23 compressive	[19]
Ti	10-44	DNP 0.35 wt.%	200 nm	MA + SPS	N/A	310.5 HV	938	N/A	[19]
Ti	10-44	DNP 0.35 wt.%	100 nm	MA + SPS	N/A	318 HV	957	N/A	[19]
Ti	10-44	DNP 0.35 wt.%	5 nm	MA + SPS	N/A	327.4 HV	1024	50.6 compressive	[19]
Ti	10-44	DNP 0.1 wt.%	5 nm	MA + SPS	N/A	3.7 GPa	850	55 compressive	[14]
Ti	10-44	DNP 0.25 wt.%	5 nm	MA + SPS	N/A	4.5 GPa	975	50 compressive	[14]
Ti	10-44	DNP 0.35 wt.%	5 nm	MA + SPS	N/A	5.24 GPa	981	47 compressive	[14]

Ti	10-44	DNP 0.5 wt.%	5 nm	MA + SPS	N/A	5.51 GPa	940	45 compressive	[14]
Ti	10-44	DNP 2 wt.%	5 nm	MA + SPS	N/A	N/A	N/A	N/A	[14]
Ti	20	MWCNT 0.5 wt.%	OD = 10-35nm ID = 3-10nm L = 1-10µm	MA +SPS	N/A	N/A	1056	N/A	[20]
Ti	20	MWCNT 1 wt.%	OD = 10-35nm ID = 3-10nm L = 1-10µm	MA +SPS	N/A	N/A	899	N/A	[20]

Note: Mechanical alloying (MA), spark plasma sintering (SPS), multi-walled carbon nanotubes (MWCNT), diamond nanoparticles (DNP).

Table 2.3 shows a summary of the influence of different powder characteristics such as reinforcement size and volume fraction, the dominant strengthening mechanism and the effect on the tribological and mechanical properties. The main conclusions deduced from Table 2.3 are that controlling the reinforcement characteristics can enhance the mechanical and tribological properties of a TMC due to the influence of varying strengthening mechanisms.

Table 2.2: *Influence of powder characteristics on mechanical and tribological properties*

Control parameters	Varying control variables	Dominant strengthening mechanism	Effect on mechanical and tribological properties	Ref
Reinforcement size	Sub-micron or nanoparticles	Thermal dislocation strengthening and/or orowan strengthening	Better interfacial bonding resulting in superior tribological performance	[21]
Reinforcement volume fraction	Typically, between 5-10 vol.%	Load transfer mechanism	Increase in yield strength and micro-hardness	[16]
CTE mismatch	Biggest CTE mismatch	Thermal dislocation strengthening	CTE mismatch develops a residual strain, producing geometrically necessary dislocations in the matrix around the reinforcements	[22]
Matrix size	Smallest size	Hall-petch grain boundary strengthening	Increase in yield strength	[23]

2.1.3 Phase formation using in-situ processing

There has been a rising interest in fabricating TMCs using *in situ* processing techniques over the last decade. The main reason behind the shift from ex-situ additives via ingot metallurgy to PM *in situ* processing for TMCs is primarily due to the high affinity of titanium to oxygen [24]. PM techniques ensure homogenous powder distribution and dispersion within the matrix, hence allowing an enhanced performance of the TMC [3]. *In situ* reactions can take place when the matrix reacts with the reinforcement through solid-state reaction [25]. Some common reporting of additive reinforcements used to *in situ* produce hardening phases are SiC [13], TiB_2 [11], ND [14], GNP [15]. For instance, TiB_2 can react with Ti matrix during the HIP process, resulting in TiB whiskers that are dispersed as the reinforcements phase in the matrix. If the TiB_2 powder is homogenously dispersed on

the starting Ti powder, it could result in substantial Young's modulus increase as the reported Young's modulus of TiB is (467 GPa) compared to Ti (110 GPa) [26]. It is important to note that the morphology of the *in situ* formed TiB whiskers can influence the mechanical and tribological behaviour of the TMC. It is well noted that its extremely hard to control the TiB whiskers growth as it happens in an anisotropic manner at elevated HIP temperatures during a very short dwell time. Furthermore, due to the high reactivity of titanium with boron it results in a very low aspect ratio of the formed TiB whiskers at elevated HIP temperatures [27].

Cai et al [11]. have been able to produce an *in situ* reaction between Ti64 and TiB_2 during HIP to form TiB whiskers which are homogenously dispersed along with the matrix through solid-state reaction. Sivakumar et al [13]. have successfully been able to produce the hard phase of TiC from Ti64 matrix reacting with SiC reinforcement during the PM process. Carbon has been reinforced with titanium powder by coating the titanium matrix powder with resol nanospheres which are between 10-30nm size. The *in situ* formed TiC phase from the process of pressureless sintering delivered very high compressive strength properties such as 1.5 GPa yield strength (YS) and 2.54 GPa ultimate strength (US) [28]. The study claimed that the properties achieved from the *in situ* formed TMC are better than other advanced TMCs through the use of a binary Ti-C system. It is also well noted in the literature that multi-walled carbon nanotubes (MWCNTs), are deemed to be an excellent candidate for *in situ* reactive HIP and sintering processing, synthesizing very fine titanium carbide (TiC) particles.

Other reports used MWCNT as a reinforcement with Ti matrix, resulting in an *in situ* reaction to synthesize very fine nano-sized TiC particles that are dispersed throughout the matrix around α-Ti grain boundaries (GB), hence inhibiting grain growth and the formed phase is thermally stable too. It was concluded from the report that the α-Ti phase decreased in size with the increasing vol.% of MWCNT and that the micro-hardness values increased at elevated temperatures of 573K due to the pinning effect of the *in situ* formed phase [29].

The in-situ resultant products will determine whether the TMC phase will be discrete, brittle and a cause for localised cracking or whether they are homogenous. Table 2.4 Shows a list of phases formed via *in situ* solid-state reaction during PM HIP and sintering techniques. It is quite clear that carbon-based reinforcements such as diamond, SWCNT, graphene and graphite have the highest Young's modulus > 1 TPa [30] and provide the highest hardness contribution, hence proving to be effective reinforcements and ideal in-situ reaction candidates to form clean hardening phases. Furthermore, the use of finer carbon particles will lead to finer dispersion and formation of phases, hence achieving stronger interfacial bonding, grain refinement and therefore leading to enhanced tribological and mechanical performance [31].

Table 2.3: In situ formed phases , their starting reinforcement , processing temperature and properties

Reinforcements	CTE mismatch with Ti ($X10^{-6}K^{-1}$)	In-situ formed phases	Young modulus (GPa)	Hardness (GPa)	Sintering temperature used in TMC (°C)	Ref
Few-layer Graphene	-	TiC	1000	-	920	[32]
Diamond	7.9	TiC	1220	60-100	900	[14]
Boron	-	TiB	-	-	-	[33]
SWCNT	-	TiC	1000-1260	-	-	[34]
Cubic BN	-	TiB + TiN	-	50	-	[35]
Graphite	-	TiC	-	-	1250	[36]
B_4C	3.82	TiC + TiB	445	30	1000	[37]

The phases formed during the solid-state reactive *in situ* process, depends on the diffusion rates, solubility limits of the reactants and global kinetics of the reaction [38]. For example, Sivakumar et al. have successfully fabricated a Ti-6Al-4V (Ti64) / SiC TMC via PM route. It was reported that SiC has rapidly decomposed and reacted with Ti during the *in situ* reaction, synthesizing titanium silicide (Ti_5Si_3) and titanium carbide (TiC) phases. They claimed that such a rapid *in situ* reaction was thermodynamically possible [13].

Figure 2.2 shows the Ti-Si system phase diagram, and it is quite clear that sintering that β-Ti at 1170°*C* reacts with the decomposed SiC, synthesizing the Ti_5Si_3 phase [39]. Figure 2.3 shows a backscatter micrograph of the *in situ* reaction between Ti and SiC. It can be seen that near the SiC region, both Ti_5Si_3 and TiC phases coexist in similar fractions in the form of small precipitates. However, getting closer to the Ti interface, more Ti_5Si_3 phase is greater and surrounds large TiC particles [40]. Figure 2.3 further explains the reaction path at the interface between Ti and the product interface. Furthermore, in terms of diffusion kinematics, it is well noted that carbon diffusivity is roughly 10x faster than the diffusivity of Si in β-Ti phase and that the max solubility of Si in β-Ti is approximately 3.7% [40]. In addition to that, Ti of the metal phase goes into solution in the Ti_5Si_3 phase, a counter-diffusion would take place between the decomposed SiC and Ti in the Ti_5Si_3 matrix. It is well noted by many reports that carbon solubility in this phase is relatively small, hence C would react with Ti to form small TiC precipitates. It is also worth mentioning that the coalescence of the TiC precipitates takes place due to the chemical potential gradient of C and the high diffusivity rate of carbon within the TiC precipitates [40].

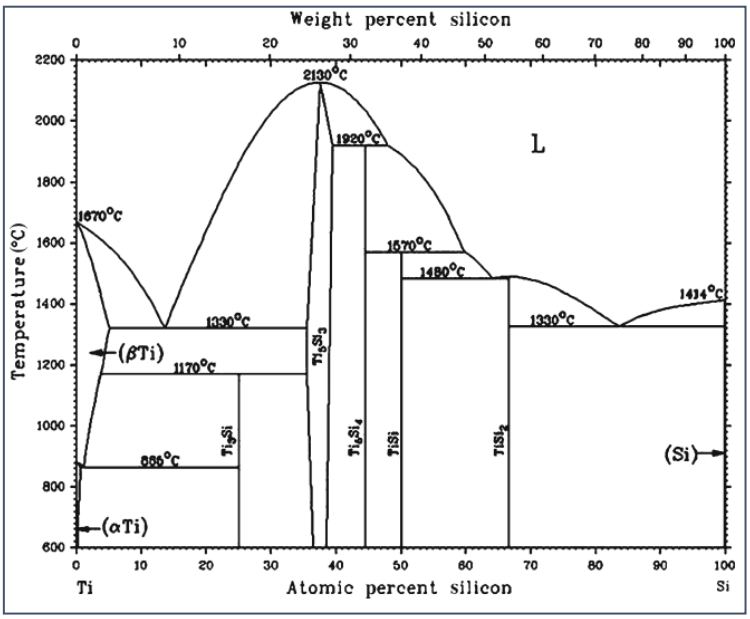

Figure 2.2*: Ti-Si phase diagram* [39]

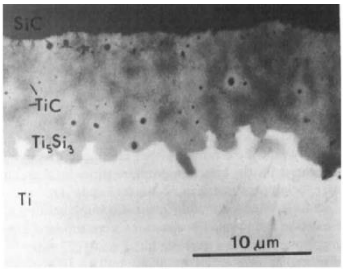

Figure 2.3*: Backscattered micrograph of Ti-SiC reaction at 1200*℃ [40]

2.1.4 MA ball milling as a blending route for MMCs

The fabrication of homogeneously mixed MMC powders is a major challenge and can detrimentally affect the mechanical and tribological performance of the composite. Conventional blending routes such as roll-blending are only affective in homogenously mixing powders if there is a large ratio difference between the matrix powder and the reinforcement powder, so that the reinforcement powder can stick to the surface of the matrix powder. Although conventional roll blending can result in homogenous powder mixing if the reinforcement to matrix powder size and volume fractions are controlled, the interfacial bonding between the matrix and reinforcement is weak, therefore negatively impacting the tribological properties of the MMC. Mechanical alloying (MA) via ball milling has been employed by many researchers successfully to mix MMCs homogenously, resulting in strong interfacial bonding [41,42,43,44].

In this section, MA as a blending route for TMCs specifically will be described and how different process variables affect the homogeneity of the composite powder. Firstly, MA is defined as a solid-state powder mixing technique that involves the repeated welding, fracturing, and re-welding of powdered particles in a high energy milling system [45]. The most widely used MA technique for blending powders is using a high energy planetary ball mill as reported by many researchers [46,47,48].

Figure 2.5 depicts a schematic of the planetary ball mill process [49]. In basic terms, a planetary ball mill works by the containers rotating around their axes generating a centrifugal force acting on the powders and grinding ball media. Since the supporting discs and containers move in opposing directions, the generated centrifugal force acts in the same and opposite direction, hence allowing the grinding ball media to fall down the inside of the container walls, which allows for the powders to be grinded via the impact generated [50].

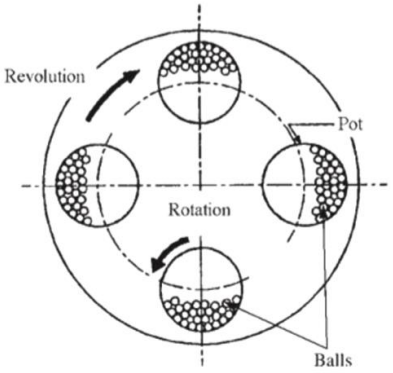

Figure 2.4*: Schematic of planetary ball mill process [49]*

In terms of MA materials, it is divided into the following categories: (a) ductile reinforcement– ductile matrix, (b) ductile matrix-brittle reinforcement, (c) brittle matrix-brittle reinforcement. In terms of ductile-ductile MA it is when a ductile reinforcement is alloyed with a ductile matrix mechanically. Ductile matrix alloyed with a brittle reinforcement is the second category that can be MA. In this category at the early stages of the milling process, the ductile metal matrix powder gets flattened by the hard ceramic balls that cause continuous collisions. Moreover, the brittle reinforcement particles become entrapped in the ductile metal matrix particles. As the milling duration continues, the metal matrix ductile powder work hardens and the spacing between the brittle reinforcement particles and

the ductile powder reduces significantly. Finally, the brittle particle is homogenously dispersed and distributed in the ductile metal matrix and becomes MA [51].

MA route has a lot of process variables that could influence the outcome of the blended powders. It is vital to note the most prominent variables and how they directly influence the outcome which is as follows:

2.1.4.1 Milling speed (RPM)

The milling speed is an important variable that affects the morphology of the matrix, reinforcement and homogeneity of the MA MMCs. It is therefore vital to understand how varying the speed from (<200-250 RPM) [52] to (>300 RPM) [53] affects the characteristics of the milled MMCs. It is well known that the higher the milling speed is, the higher the produced collision energy is, hence exerting a higher impact force. There have been countless reports in the literature that have employed lower milling speeds to MA TMCs [54,55,56]. The reason is that the aim of using lower RPM is not to deform and smash the inherent shape of the matrix, but rather to adhere the fine reinforcement powders to the surface of the matrix. Furthermore, it ensures a homogenous reinforcement network distribution, while limiting the absorption of Oxygen (O) in Ti-based matrices, hence reducing the chance of embrittling the TMC. Another important reason why controlling the milling speed is a fundamental aspect of fabricating TMCs, is to limit a temperature spike which could cause the Ti matrix to catch a spark. On the other hand, the temperature increase due to the high milling speeds could be used when diffusion is needed when alloying powders is the main objective. It could be thought that increasing the RPM would result in more energy being transmitted to the powders, however if the RPM is increased beyond a critical speed, most of the grinding media balls will be restrained on the inner walls of the containers, hence not applying much impact force on the powders and not enough collision energy will be employed as a result [57].

Zhang et al., MA titanium nanodiamond composite using ball milling at a lower RPM (250 RPM) , keeping the titanium morphology spherical and retaining a well distributed homogenous interfacial bonding between the nanodiamond and the matrix powder [58].

2.1.4.2 Milling duration

It should be well noted that duration is one of the most important factors that influences the characteristics of the milled powder. Time is a vital parameter that is used to attain an equilibrium state between cold welding and fracturing of the powders. There are multiple factors reported in the literature that affect the milling duration. This is primarily based on mainly the ball-to-powder ratio (BPR) and the temperature rise due to the intensity of the milling procedure. Furthermore, contamination due to the grinding media used could influence the time duration as contamination would increase as the powders are milled for a longer duration, hence why finding the ideal milling duration is important [59].

2.1.4.3 BPR

BPR is one of the most fundamental control variables used in the MA process. BPR is the ratio between how many grams of ball there is to powder in the milling process. For example, a BPR of 4:1 means for every 4g of grinding media, there is 1g of powder. There has been different BPR used from 1:1 up to 220:1. Most reports that aim to MA work between a BPR of 4:1 up to 10:1. The higher the BPR the shorter the milling time is the resultant contamination would be higher too [60]. The main reason for a reduction in milling time with increasing the BPR, is because of the rate of collisions increase as the weight of the balls increase, hence more energy is being transferred to the powders, therefore reducing the time it takes for MA to take place successfully. However, as a result of a higher collision rate, temperature could rise which could be a factor in choosing a lower more suitable BPR [61]. Cai et al., has successfully MA Ti-6Al-4V/TiB_2 MMC using a 4:1 BPR [11].

2.1.4.4 Process control agent

When powders are milled using high RPMs and milling parameters, they get cold-welded especially if the matrix powder is ductile such as titanium, hence they may undergo severe plastic deformation. It is also important to note that mechanical alloying between the matrix and reinforcement particles happens only when an equilibrium state is reached between cold welding and fracturing of the particles. This is why a process control agent is used in many cases to reduce the impact of cold welding hence making it easier to alloy powders. The process control agents adheres to the surface of the powders hence limiting the impact of cold welding and therefore minimizing the chances of powder agglomeration which results in a more homogenous distribution of powders. Furthermore, the agents reduce the surface energy of powders which helps in limiting the milling duration [57]. The most widely reported process control agents are stearic acid [62], hexane [63], methanol [64] and ethanol

[65]. Al-Sherbini et al., has successfully milled graphite into graphene using 2-ethylhexanol as a process control agent. The main reasoning behind using 2-ethyhexanol in his work, was due to the agent's high viscosity of 10.3 centipoise compared to ethanol which has a low viscosity of < 1 centipoise at room temperature [66]. Choosing a viscous process control agent helps reduce the effects of the number of collisions, hence the resultant deformation of the powders. Furthermore, a solvent agent such as 2-ethylhexanol has a high boiling point of around 184 °C [66] which means that milling for a long period of time using high RPMs could be a viable option if needed. There have been other process control agents (PCA) used in the literature which are summarised in Table.4 with the corresponding materials and milling parameters.

2.1.4.5 Milling atmosphere

Selecting the atmosphere where the milling takes place depends solely on the material. Two factors that influence the selection of milling atmosphere is the level of contamination that the powders could experience and the temperature rise inside the milling chamber due to constant collisions. Inert gases such as argon have been used to purge milling containers or using glovebox environments for the milling process to stop oxidation and reduce the chances of powder contamination. There have been many reports indicating that milling in air produce oxides which can cause embrittlement to powder such as titanium based alloys [67]. Moreover, there have been reports showing that milling in different atmospheres such as nitrogen could be utilized in a way to produce nitrides, therefore the milling atmosphere can be used and tailored to suit different purposes [68].

Table 2.5 Shows more reports of different TMCs with varying volume fractions and reinforcement sizes, and the corresponding milling speed used.

Table 2.4: TMCs milling parameters from the literature

Matrix	Matrix size	Reinforcement type & size	Milling speed (RPM)	Milling duration (hr)	Grinding media	BPR	Process control agent	Ultrasonication (YES/NO)	Ultrasonication duration (min)	Ref
Ti-6Al-4V	100-130 µm	TiB_2 (3-5µm)	200	4	Steel balls	4:1	-	-	-	[16]
Ti-6Al-4V	70-150 µm	TiB_2 (3.13 µm)	200	4	Steel balls	4:1	-	-		[11]
Ti-6Al-4V	20 µm	SiC (<75nm)	300	8	-	40:1	C6H6—CH			[13]
Ti	10-44 µm	DNP (3 µm)	250	5	-	10:1	Ethanol	Yes	30	[19]
Ti	10-44 µm	DNP (200 nm)	250	5	-	10:1	Ethanol	Yes	30	[19]
Ti	10-44 µm	DNP (100 nm)	250	5	-	10:1	Ethanol	Yes	30	[19]
Ti	10-44 µm	DNP (5 nm)	250	5	-	10:1	Ethanol	Yes	30	[19]
Ti	0-35 µm	GNP	350	2.5	-	5:1	Ethanol	Yes	20	[69]
Ti	13.75 µm	DNP (4-6 nm)	-	16	Zirconium oxide	10:1	Hexane	No	-	[70]
Ti	13.75 µm	DNP (4-6 nm)	-	16	Zirconium oxide	10:1	Hexane	No	-	[70]
Ti	13.75 µm	DNP (4-6 nm)	-	16	Zirconium oxide	10:1	Hexane	No	-	[70]

2.1.5 Importance of Coefficient of thermal expansion in reinforcement selection

Choosing reinforcements based on their coefficient of thermal expansion (CTE) and density compatibility with the matrix powder will limit the formation of residual stresses at brittle reaction zones during the cooling process in HIPping. This issue becomes more evident when microstructural control via rapid cooling is used, hence thermal compatibility is key. Many reports in the literature of TMCs have indicated that TiB_2, TiC and TiN are the best candidate reinforcements for a Ti-based matrix due to the CTE mismatch being relatively small [71,72].

On the other hand, there have been reports suggesting that a relatively large CTE mismatch between the reinforcement and matrix in question, could strengthen the composite using thermal dislocation strengthening mechanism. This simply works on the basis that the CTE mismatch will develop a residual strain that will in turn produce geometrically necessary dislocations (GNDs) in the matrix around the reinforcement to accommodate the CTE mismatch and critical strain misfit, hence increasing yield strength specifically in cases on using nano-reinforcements [73,74]. However, Ho et al., in his review of thermal residual stress in metal matrix composites indicated that a large CTE mismatch can induce thermal residual stresses in the MMC, which could negatively impact the mechanical behaviour of the composite such as the fatigue life, accelerated stress corrosion and cracks induced from thermal stresses [75]. Kouzeli et al., reported that the thermal mismatch between Al and Al_2O_3 resulted in a higher dislocation density, hence resulting in a higher yield strength increase from 73 MPa to 148 MPa [76]. While Dong et al., reported that when the volume fraction of the reinforcement is increased, the dislocation strengthening effect due to CTE mismatch would result in an increase in the yield strength [73]. Finally, Kumar et al., looked into the influence of reinforcement volume fraction on the composite's CTE. The study reported that the dislocation density increases as the CTE decreases, and an increase in thermal mismatch, leading to an increase in yield strength. Furthermore, the CTE of the composite was determined based on the rule of mixture more specifically using the Kerner model [77].

2.1.6 TMCs as potential candidates for tribological applications

Titanium alloys have never been sought after for tribological applications due to the low micro-hardness of the material compared to nickel superalloys. However, titanium is selected as a metal matrix as it offers a high strength to weight ratio and corrosion resistance [78,79], which makes it an

ideal metal matrix candidate for the marine industry, aerospace industry that require a long service life in harsh environments and a high wear resistance which could be achieved by reinforcing the metal matrix with hard ceramic particles [80]. Continuously reinforced titanium matrix composites (CRTMC) with fibres have not gained a huge interest for research because of the high cost and extremely anisotropic properties of the composite from the inherent fibre characteristics [81]. However, lately discontinuously reinforced titanium matrix composites (DRTMC) have gained a wide interest in tribological applications due to the weight reductions and enhanced wear resistant properties they provide [7]. It is well noted that reinforcing a ductile titanium-based matrix with hard ceramic particles/whiskers increases the composites hardness which is a desirable trait in tribological based applications. This is directly proportional to the volume fraction of the reinforcement. There have been several studies conducted on DRTMCs specifically looking into the wear resistance and tribological performance [82,83]. For instance, An et al., was able to synthesize a TiB/Ti64 composite using an *in situ* reaction by P/M manufacturing process. The study found that the *in situ* formed TiB network boundary was like a barrier and helped in reducing wear features such as abrasion in comparison with un-reinforced monolithic Ti64. In addition to that, the main conclusion derived from the study was that the dominant wear mechanism was dependant on the network size as it changed from micro-cutting to brittle debonding when the network size increased from 60 µm to 200µm [84]. On the other hand, Chaudhari et al., synthesized a Ti-4Al-2Fe/TiC/TiB FGM using SPS and concluded that the fine TiC phase and TiB whiskers reduced the wear rate significantly due to the increase in micro-hardness [85].Cai et al., studied the friction and micro-hardness behaviour of in-situ TiB/Ti-6Al-4V via hot isostatic pressing. The study concluded that both micro-hardness and wear resistance increased with the increase in the volume fraction of TiB [11]. In another study, Saba et al., fabricated a Ti/nano-diamond composite using SPS. The result showed that reducing the reinforcement size significantly enhanced the wear resistance of the composite, while increasing the micro-hardness and retaining ductility due to Orowan looping mechanism [19]. The tribological behaviour of MMCs depends on the matrix and reinforcement characteristics such as the volume fraction of hard particles embedded in the matrix, the reinforcement particle size, reinforcement morphology, and spatial distribution [86]. Furthermore, it is well noted in TMC fabrication literature that the interfacial bonding between the matrix and reinforcement can influence the tribological performance of the composites substantially, therefore it is one of the more important factors to consider in synthesizing TMCs with enhanced properties [87].Recently, there have been a wide interest in carbon-based reinforcements such as CNTs and few-layer graphene because of their ultra-high strength contributions and lubrication characteristics of graphene. Cao et al. studied the mechanical and tribological properties of graphene nanoflakes-reinforced TMCs via P/M route [88]. The study concluded that 1.2 vol% of

GNPs reduced the coefficient of friction (COF) of the composite compared to monolithic Ti alloy from 0.42 to 0.39 due to the self-lubricating properties of graphene. Furthermore, the study claimed that the wear volume loss was reduced due to the strong interfacial bonding between the nano-reinforcements and the matrix in addition to other strengthening mechanisms such as orowan , grain refinement and load transfer strengthening contribution, hence reducing volumetric wear loss [88].

Figure 2.7 shows an illustration of how hard reinforcing particles in the composite protect against abrasive wear in a ductile matrix. This is due to the hard stiffer reinforcement having better load bearing capability and protecting the inner ductile matrix from the hard abrasive particles as a result of particles being pulled out due to delamination wear.

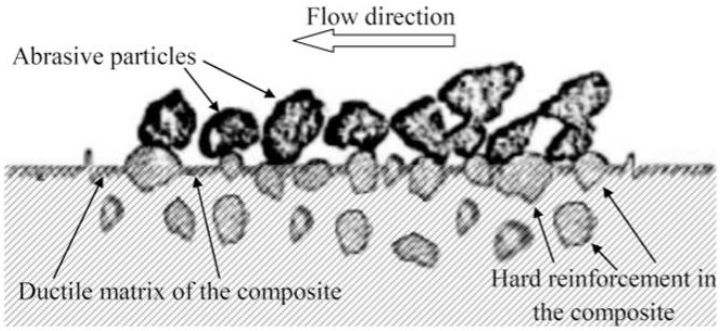

Figure 2.5*: hard reinforcement protecting against abrasive wear* [139]

2.1.6 influence of volume fraction on tribological performance of MMCs

One of the most influential control variables that affects the tribological performance of TMCs is the volume fraction. It is well noted in the literature that increasing the volume fraction of hard reinforcing particles improves the wear properties of the composite in question. This trend was observed in many TMCs, such as Ti-6Al-4V/TiB composite [11], Ti/nano-diamond composite [19], and Ti/GNPs composite [88]. It was noted in all these reports that the hard in-situ formed phases act as a barrier to abrasive wear as shown in Figure 7 . However, the reports mentioned that as sliding continues, the delaminated hard particles from the matrix, start three body abrasion on the wear surface, hence increasing the wear rate.

There have been some experiments conducted on the influence of volume fraction of the reinforcement in MMCs. The nanocomposites used are materials that are lower than 100 nm diameter or form phases that have grain boundaries in the nanoscale. It is well noted in the literature that titanium metal matrix nanocomposites (TMMNCs) exhibit superior tribological and mechanical performance over TMMCs that use micron sized reinforcements. MMCs reinforced with nanoparticles have been reported to be dispersed best using a PM route. However, fabricating TMCs using nano-reinforcements has been described to be challenging due to the intrinsic characteristics of the nanoparticles, having a higher surface area relative to their volume, hence they tend to agglomerate to reduce their surface energy [19]. Several researchers have looked into TMMNCs and reported their tribological and wear properties. Shang et al., studied the effect of network size on the wear resistance of titanium/ nanodiamond nanocomposites and deduced that the COF of composites decrease as the volume fraction of the reinforcement increases however, increasing the volume fraction more than 5 vol.% tends to increase the COF value far beyond the monolithic material [89].

In another study, Savalani et al. [90], looked into *in situ* formation of TiC using Ti and CNTs via laser cladding. The study concluded that as the volume fraction of CNT increased, the wear depth decreased due to the higher microhardness that the composite exhibits. It is also important to note that many studies have concluded that increasing the volume fraction beyond 5 vol.% reduces the effectiveness of the wear resistance. This is speculated to be due to certain inherent defects such as voids and agglomeration of the nano reinforcements. The defects would weaken the composite, hence affecting the wear properties negatively [90]. Singh et al., synthesized a silicon nitride (Si_3N_4) titanium matrix composite using sintering process. The study concluded that as the content of Si_3N_4 volume fraction increased, the wear rate decreased due to the solid solution strengthening effect on nitrogen (N) and silicon (Si) [91].

2.1.7 Influence of reinforcement size on mechanical and tribological properties of MMCs

It is a well reported that the tribological performance of MMCs heavily depends on the size of the reinforcement. The wear resistance capability and COF value can vary depending on the size of reinforcement used, hence why research has been focused on studying the influence of the reinforcement size on both mechanical and tribological performance [92]. The main factor that has been reported to ensure good tribological performance is a strong interfacial bonding between the matrix and reinforcement powder, which depends on the reinforcement particle size. It has been

reported by many studies [91-94] that reinforced materials have a tendency to show a much lower wear rate than monolithic unreinforced alloys. This is mainly due to the load bearing capabilities and hardness of the reinforcement. In addition to that, studies have reported a trend of enhanced wear resistance as the reinforcement particle size moves from the micron scale to nano-scale [19]. However, it is not clear yet whether there is a critical size that influences the tribological behaviour of the MMCs. For example, El-Kady et al., looked into the influence of SiC particle size ranging from 40µm to 70nm and the volume fraction from 5 weight percent (wt.%) to 10wt.% on the properties of the Al-SiC composite. The study concluded that in order to maximise the compressive strength of the composite, the smallest particle size and highest content of reinforcement would achieve that [93]. Bapu et al., worked on developing a nickel (Ni) titanium carbo nitride (TiCN) metal matrix nanocomposite. The study concluded that the incorporation of nanoparticles enhanced the wear resistance of the composite and the authors attributed that to the grain refinement mechanism and the micro-hardness contribution of the TiCN phase [94].

There have extensive work carried out in both micron and nano-reinforcement areas, however sub-micron reinforcement particles have not gained a lot of interest in research yet. For instance, Kumar et al [95]., was able to simultaneously improve the strength, ductility and corrosion resistance and wear resistance of Al7075-2% SiC composite by reducing the reinforcement size to nanoparticles. The authors attributed that to the strengthening effect of Hall-Petch grain refinement, Orowan strengthening due to the incorporation of nanoparticles and the enhanced interfacial bonding between the matrix and reinforcement as a result of using nanoparticles. Singh et al [96]., studied the tribological behaviour of SiC based Al MMCs under dry and lubricated conditions. The study found that as the reinforcement size reduced the tribological behaviour improved due to a higher micro-hardness. Zaiemyekeh [97] et al., investigated the influence of Al_2O_3 on the mechanical and tribological behaviour of Al-based matrix composite via P/M. The investigation concluded that the compressive strength and wear resistance of the composite improved drastically with the addition of the Al_2O_3 nanoparticles. The result was an enhanced micro-hardness, scratch resistance and strength improvement. However, the author's reported that once the volume fraction exceeded 5 vol.%, the performance reduced due to the increased brittleness.

In addition to that, Saba [19] et al., looked into the tribological performance of Ti reinforced with NDs. The study concluded that as the size of the reinforcement was reduced from 200 nm to 5 nm, the micro-hardness increased resulting in a lower wear rate. The authors attributed this to orowan strengthening which is a dominant strengthening mechanism that is highly sensitive to particle size in the nano-scale. Recently, Shang [89] et al., have successfully fabricated Ti/NDs composite via SPS technique. The authors claimed that the compressive yield strength and hardness have increased by

42.7% compared to monolithic Ti. Furthermore, the paper concluded that as the matrix network size decreased while using the same reinforcement ND size of 5nm, the ductility of the composite increased from 8% to 33% compared to monolithic Ti. In addition to that, the COF and wear loss of the nanocomposites relative to monolithic Ti decreased significantly. The reason that the authors suggested is that the using a smaller matrix size that produced a quasi-continuous network microstructure, the in-situ formation of TiC phase and dislocation strengthening due to CTE mismatch from the ND reinforcements contributed to the wear resistance properties.

2.1.8 Strengthening mechanisms in MMCs

2.1.8.1 Predicting yield strength of TMCs

There have been many different approaches taken to predict the yield strength of TMCs, taking into account the size of the matrix, size of the reinforcement, volume fractions of both the reinforcement and the matrix, CTE mismatch, load-bearing mechanisms, grain size and orowan strengthening mechanisms [98]. The contribution of each mechanism changes vastly, depending on the scale of reinforcement used, moving from micrometre to nanometre scale as reported by [99,100].

Saba et al [19]., has reported that if the volume fraction of the reinforcement and the particle size are both small, the matrix will bare most of the load, hence load-transfer mechanism can be ignored if the volume fraction is less than 5 vol%. Some articles have reported that CTE mismatch dislocation strengthening is the most effective way to increase the yield strength, due to the generation of geometrically necessary dislocations (GNDs) that arise from the critical strain misfit from thermal mismatch. Furthermore, Saba et al., reported that if the reinforcement size is below 100 nm, dislocation strengthening due to thermal mismatch could be neglected, due to the fact that the critical misfit strain from thermal mismatch cannot be achieved, hence Orowan strengthening mechanism dominates in the nanoscale below 100 nm. Zhang et al [58]., has also found that there is a critical size for the reinforcement which is 5.44x the burger vector, in which the orowan mechanism breaks down.

$$\sigma_{th} = \sigma_{ym} + \Delta\sigma_{orowan} + \Delta\sigma_{HP} + \Delta\sigma_{L.T} + \Delta\sigma_{CTE} \qquad (2.1)$$

Equation (1) [101] is the theoretical estimated yield strength of MMCs that have been modified based on the shear lag model and used in the work of Zhang et al [102] who looked into the contribution of the Orowan-strengthening mechanism in particulate reinforced metal matrix nanocomposites. Where

σ_{ym} is the matrix yield strength, σ_{orowan} is the strength contribution due to orowan mechanism, σ_{HP} is the well-known Hall-Petch grain size relationship, σ_{LT} is the load transfer contribution, and finally σ_{CTE} is the dislocation strengthening mechanism.

2.1.8.2 Grain refinement

The Hall-Petch equation describes the contribution of grain refinement on the overall strength of the material:

$$\Delta\sigma_{H-P} = \sigma_o + kd^{-\frac{1}{2}} \qquad (2.2)$$

σ_o is the starting stress for dislocation movement (845 MPa) for Ti, while k is the Hall-Petch constant used for the Ti-matrix is 0.3 MPa $m^{1/2}$ [19], and d is the average grain size of the matrix. As mentioned earlier, reducing the reinforcement size to the nanoscale has a significant contribution to the overall strength of the TMC. Grain size is highly receptive to the matrix size, reinforcement particle size, HIP temperature, dwell time and cooling rate, hence it is why these parameters need to be considered to achieve an optimal grain refinement contribution to the composite's strength [67]. The grain refinement mechanism influence on the strength of a composite is based on a reduction in grain size area, which results in more grain boundary interfaces hence inhibiting dislocation movement and effectively increasing the strength of a composite [103].

2.1.8.3 Thermal mismatch strengthening

The contribution due to thermal mismatch strengthening could be expressed by the following equation [104]:

$$\Delta\sigma_{CTE} = \alpha Gb\sqrt{\left(\frac{12\Delta T}{b(\frac{\Delta c.fr}{dr}}\right)} \qquad (2.3)$$

Where k is a material constant (1.25) for Ti [105], G=45 GPa (shear modulus of Ti) [106], b=0.29nm (Burger vector for Ti) [107], ΔT (the difference between the HIP temperature and property testing

temperature), ΔC (*thermal mismatch between matrix and reinforcement*), fr (volume fraction of reinforcement) and dr (*reinforcement particle size*). It is well known that the difference in CTE mismatch between the matrix and reinforcement results in the generation of Geometrically necessary dislocations (GNDs) during the cooling process, hence increasing the strength of the TMC. It can be seen in from equation 2.3 that reducing dr from the micron scale to the nanoscale can significantly increase the strength, while the contribution is not sensitive to increasing the fr. It is also to note that some reports have mentioned that as the size of the reinforcement is change from the micron to nanoscale, the strengthening effect due to thermal mismatch strengthening decreases significantly [19].

2.1.8.4 Orowan strengthening

Reinforcing metal matrices with nanoparticles strengthens the metal matrix by forming loops around the scattered nanoparticles, hence impeding dislocations movement, increasing the strength of the TMC. The contribution due to orowan looping could be evaluated using the following equation [108]:

$$\Delta\sigma_{orowan} = \frac{0.81\,MGb}{2\pi(1-\theta)^{\frac{1}{2}}} \frac{ln\frac{d_r}{b}}{\left(\frac{1}{2}d_r\sqrt{\frac{3\pi}{2f_r}-d_r}\right)} \qquad (2.4)$$

Where M=2.6 (Taylor factor for Ti) [109], G= 44GPa (shear modulus for Ti) , b=0.29nm (burger vector), dr (*particle size of reinforcement*) , fr (*volume fraction of reinforcement*), Θ=0.37 (poisson ratio of Ti) [106]. It can be deduced from equation 2.4 that the orowan contribution in micron-sized reinforcements is insignificant and can be negligible. This is because the inter-particle spacing is huge. On the other hand, it is clear from the same equation that the orowan strengthening mechanism plays a significant part in strengthening the matrix when nano-reinforcements is used, due to the ability of the nano-reinforcements to impede dislocation movement.

2.1.8.5 Load transfer

The load transfer mechanism is highly sensitive to the volume fraction of the reinforcement. It operates on the basis that the load is transferred from the matrix to the stiffer reinforcements. It is important to note that having a strong between the matrix and reinforcement will enhance the ability of this mechanism to enhance load bearing capability. The contribution due to load transfer could be expressed in the following equation [110]:

$$\Delta\sigma_{L.T} = 0.5 f_r \sigma_{ym} \qquad (2.5)$$

Where σ_{ym} =845 MPa (yield strength of Ti matrix) and f_r (volume fraction of reinforcement).

2.1.8.6 Predicting hardness of TMCs using ROM

In terms of predicting the hardness of TMCs based on the phase fractions, Hashin and Shtrikman have come up with the upper bound (Voist model) based on the equal strain assumption and lower bound (Reus model) that is based on equal stress assumption [111]. Effectively, the Reus model can be used for effective hardness of a composite which corresponds to a soft matrix surrounded by a stiffer reinforcement phase. f_h and H_h are the volume fraction and hardness of the harder phase, while f_s and H_s are the volume fraction and hardness of the softer phase. Kim [111] studied the validity of the ROM in predicting the hardness of particle reinforced composites. The study concluded that the stress states for high volume fraction of hard reinforcement is nearly iso-strain (Voist model) and that the stress state for low volume fraction reinforcement is nearly iso-stress (Reus model) as validated by finite element results.

$$H_{upper} = f_h H_h + f_s H_s \qquad (2.6)$$

$$H_{lower} = \left(\frac{f_h}{H_h} + \frac{f_s}{H_s}\right)^{-1} \qquad (2.7)$$

2.1.8.7 Theoretical deviation of structural property modelling from experimental data

There are many factors that could lead to a deviation in the prediction of a material's strength using structural property models. Being able to predict the strength of an MMC using equation (2.1) and taking into account all the strengthening contributions could help tailor different MMCs for different applications. Saba et al [19]., successfully modelled the strength of titanium reinforced with different particle sizes of nano diamonds. The results have been compiled in Figure 2.9 It is clear from the figure that the predictions of yield strength are very close to the experimental data. This shows that if correct initial assumptions are taken depending on the particle size, a very accurate prediction could be made. According to the study, the deviation between the experimental and theoretical yield strength as the reinforcement particle size is reduced is mainly attributed to the internal stresses due to the CTE mismatch are drastically reduced between the metal matrix and nano-reinforcement.

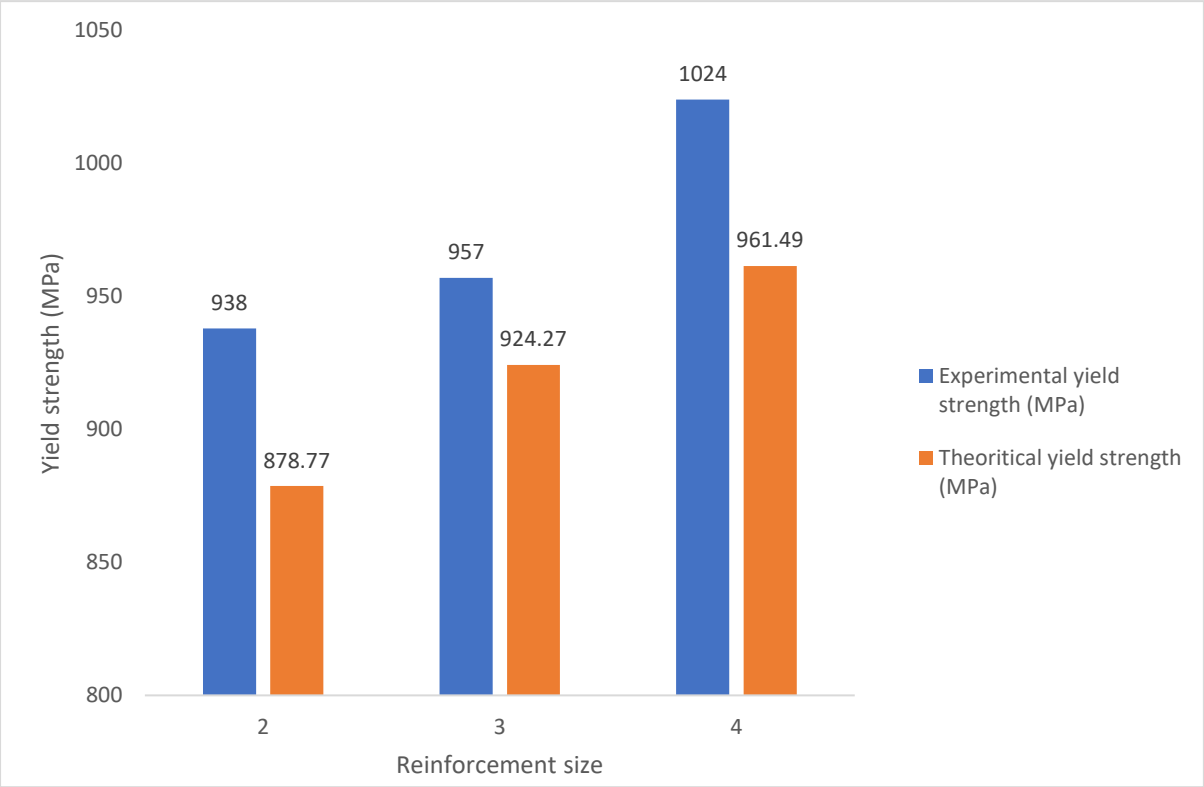

Figure 2.6: *Experimental and theoretical yield strength for Ti nanodiamonds using structure property relations [19]*

2.2 FGMs overview

Functionally graded materials (FGMs) will be discussed thoroughly in terms of their concept, classification, preparation, applications, recent and future developments, mechanical and tribological properties as prepared via PM route.

2.2.1 Introduction to FGMs

In recent years there have been a rising demand in materials that can satisfy a wide range of properties such as high wear resistance, resistance to thermo-mechanical mismatch, corrosion and impact resistance [112]. This is where the concept of FGMs was born in order to satisfy many different irreconcilable properties. The basic definition of FGMs are a class of inhomogeneous materials that consist of two or more different materials [113]. An FGM can either be classified as a chemical composition FGM, porosity FGM or a microstructure FGM [114]. The different classifications of FGMs will be discussed thoroughly in later sections. In the most basic terms, FGMs are tailored to have a variation of properties with dimension of the component. For example, an FGM could be made to have a very high wear resistant surface and a softer core material. Some of the mechanical components whereby FGMs have been used are shafts, gears and bearings, with a surface that is resistant to abrasion and a core that is crack resistant [115]. Some of the major advantages that FGMs offer over conventional MMCs are such as [114]:

(1) Improving the bond strength between di-simmilar and incompatible materials
(2) Grading reinforcement volume fraction can reduce thermal and residual stresses and thermal shocks
(3) Can be used to remove stresses at the interface
(4) Grading can reduce cracking in the material

2.2.2 Classification of FGMs

There are three types of FGM classifications, one being a chemical composition FGM, porosity FGM , a microstructure FGM as seen in figure 10 [114]. In terms of a chemical composition FGM, it is whereby the chemical composition is varied along a gradient layer gradually. It could be either a multi-phased or a single phase material. Generally, an accepted classification of a single-phased FGM is whereby the FGM is synthesized from a single phase origin. The FGM in this case is created by progressively

varying the chemical elements in the single phase, hence resulting in an FGM. In terms of a multi-phased FGM, it is when the phases and chemical composition are graded along gradient layers, causing the formation of different phases which help achieve the desired properties. For a multi-phased FGM, the FGM properties can be controlled by either varying the volume fraction of the reinforcement or matrix material, reinforcement or matrix size and the processing conditions such as the HIPping or sintering temperature, cooling rate and any heat treatments that the FGM undergoes. The most conventional technique used in synthesizing a chemical composition FGM is by powder metallurgy [116]. This is whereby the various powder compositions are stacked on top of each other and then sintered. FGMs are also quite important in the biomedical field. This is in the form of porosity gradient FGMs. Porosity gradient FGMs can have a change of porosity content along different gradient layers, while the size of the porosity and shape can be tailored accordingly to the desired specs. They are typically used in the biomedical field in applications such as implants and the tissues they surround [117]. Porosity gradient FGMs can be achieved by either varying the powder particle size in different regions or by changing process control parameters such as the sintering parameters like sintering temperature in order to get different porosity content along the gradient [118]. The last classification of FGMs are microstructure gradient FGMs whereby the FGM is tailored to have different microstructures at different layers of the FGM to change in a gradual manner [119]. One of the most conventional methods to achieve a microstructure gradient FGM is through heat treatment. This is done for example by rapidly cooling the upper surface by quenching and letting the rest of the layers cool slowly at different rates, resulting in a graded microstructure [114]. Some of the applications that demand varying graded microstructure FGMs are typically ones that require a wear resistant surface and a softer matrix material at the bottom. Some application examples are bearings, gears and shafts [120]. Figure 2.10 shows a schematic of the different classifications of FGMs.

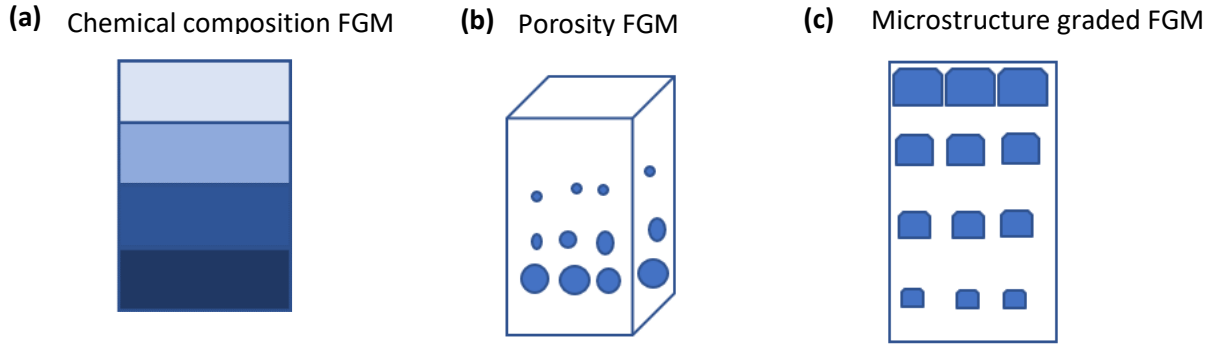

Figure 2.7*: Schematic classification of FGMs (a) Chemical composition FGM, (b) Porosity FGM, (c) Microstructure graded FGM [114]*

2.2.3 FGM applications

This section will discuss some of the applications and fields that FGMs can be considered for as a valid solution. There have been extensive research in synthesizing Aluminium (Al) based FGMs for Defense based applications. For example, Al based FGMs have been used to fabricate armours due to the lightweight properties of Al. Other applications of FGMs include the automotive industry, whereby Al based FGMs have been used in braking rotor disc which is graded to have a tough inner section and a wear resistant shell [121].Table 2.6 shows a summary of the literature review of current FGMs, their current processing routes and applications.

***Table 2.5**: Literature review of current FGMs, processing route and applications*

Matrix	Reinforcement	Manufacturing Process	Application	Reference
Al	SiC	Centrifugal casting method	Brake rotor disc	[122]
Al	SiC	-	FGM graded gear	[123]
AlSi	CNT		FGM piston ring	[124]
Ti	Si	P/M	Orthopaedic implants	[125]
Ti	Silk fibroin	Electron beam melting	Bone repair	[126]

2.2.4 FGMs by PM

PM is the most conventional method of synthesizing FGMs due to the many benefits it offers over other techniques. Some of the main advantages of using PM as a manufacturing technique to synthesize FGMs is that it opens the possibility of producing FGMs with complex geometries and helps in reducing the shrinkage due to CTE mismatch between different gradient layers. The PM technique to make FGMs work by blending powders with different compositions, volume fractions or particle sizes, stacking them on top of each other and ending with the sintering process [127].

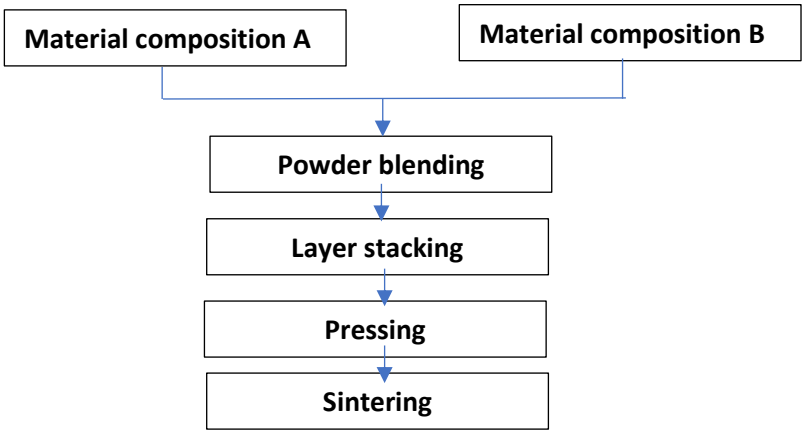

Figure 2.8*: Flowchart displaying FGM manufacturing by PM technique [127]*

Figure 2.11 shows a schematic flowchart showing a typical way of synthesizing an FGM via PM manufacturing technique. The most vital parameters that can influence the FGM microstructural development, properties and bond strength are the process control parameters such as dwell time, pressure and temperature which are the main drivers of diffusion. Salama et al [115]., successfully synthesized an Al-CNT FGM via PM. The FGM was graded with un-reinforced Al bottom layer and then 2 layers with 1 vol.% CNT and 2 vol.% CNT. It was shown in the study that the upper layer reinforced with 2 vol.% CNT achieved the highest micro-hardness and strength values. Kirmizi et al [128]., looked into fabricating an Al-SiC FGM via PM with 5 graded layers with varying vol.% of SiC and studied the FGMs ballistic and mechanical performance of the FGM.

2.2.5 Mechanical and tribological properties of FGMs

This section will discuss the mechanical and tribological performance of FGMs. So far, most of the studies conducted on FGMs are mainly concerning Al and nickel (Ni) based FGMs, with very little research done on Ti and its alloys FGMs [129,130]. For example, Ma et al [131]., successfully synthesized a Ti-6Al-4V (Ti64) FGM reinforced with TiC using direct energy deposition. The FGM was layered from 0 vol.% TiC up to 50 vol.% TiC. The study concluded that when the vol.% of TiC was at 40 vol.% and beyond, cracks propagated heavily on the thin-walled pipe part. On the other hand, Weng et al [132]., successfully fabricated a Ti64 FGM reinforced with TiC and Ti_5Si_3 particles which resulted in an enhanced wear resistance performance and micro-hardness increase. Zhang et al [133]., worked on fabricating an FGM based on a Ti64 matrix reinforced with TiC particles. It was discovered that as the vol.% of TiC increased along different layers, the ductility and tensile strength decreased a little.

Other investigations conducted by Joo et al [134]., looked into synthesizing an FGM consisting of an aluminium (Al) matrix reinforced with layers of carbon nanotubes (CNTs) and concluded that at high vol.% of CNTs, the ductility of the FGM dropped sharply. There have been work also done by Udupa et al [135]., whereby they successfully synthesized a functionally graded laminate (FGL) with the matrix being Al reinforced with CNTs ranging from 0.5 wt.% , 0.1 wt.% and then a pure Al layer. It was concluded by the study that the use of thin layers of CNTs helped reduce the coefficient of thermal mismatch (CTE) between the different gradient layers, hence reduce thermal shock and damage to the part. On the other hand, Kwon et al [136]., studied the effect of CNT vol.% on hardness of Al matrix FGM reinforced with different layers of CNT. The study found that the layer reinforced with 15 vol.% CNT, resulted in the hardness reaching seven times that of pure Al. Ekici et al [137]., studied the indentation behaviour of an FGM system based on Al-SiC MMC with random particle distribution. It was concluded by the study that randomly dispersing the SiC reinforcement caused non-uniform residual stress and strain levels. Sindhu et al [138]., investigated the in-situ formation of Al/TiB_2 FGM and the influence of reinforcement gradation on the mechanical, tribological behaviour and thermal properties of the FGM composite. The study concluded that the reinforcement gradation resulted an increase in micro-hardness as the vol.% of reinforcement was increased resulting in an enhanced wear resistance. Furthermore, it was found that when the vol.% of reinforcement was increased in the outer surface, it resulted in lowering the CTE value.

2.3 Research gap

In terms of assessing the gap in the literature, there seems to be a lot of work done on TMCs but there are generally investigating high volume fraction of reinforcements which is known to give brittle behaviour. Furthermore, there seems to be an inconsistency in studies investigating the influence of reinforcement volume fraction, reinforcement particle size, reinforcement type and blending method on the microstructural homogeneity, mechanical and tribological behaviour of resulting TMC. Moreover, there are a lack of studies investigating the control process parameters such as the influence of HIPping temperature on the completion of *in situ* reactions and consolidation behaviour of the TMCs and how that affects the mechanical and tribological performance. In addition to that, there is a lack of studies looking into the structure-property relations of the TMCs and how different phases affect the mechanical and tribological behaviour. In terms of *in situ* formation of TMCs from elemental powders via P/M HIP there is very limited work done on the subject. Most of the work is concentrated on aluminium and its alloys. The studies do not look into the influence of HIPping temperature and its parameters on the *in situ* formation of hard phases and the affect that has on the

properties. Finally, in terms of FGMs there is again very limited work done on Ti-based FGMs and most of the work is done on Al-based FGMs due to the issues concerning Ti ex-situ processing techniques and its reactivity.

2.3.1 Summary of literature review: key findings and areas of investigation

A thorough literature review have been conducted looking into TMCs and their classification, reinforcement categories, influence of matrix and reinforcement parameters on the mechanical and tribological properties, while also thoroughly discussing the dominant strengthening mechanisms in each parameter change. Furthermore, phase formation via *in situ* formation was looked into in great detail while also discussing the different blending routes used in the literature to synthesize homogenous TMCs. Finally, FGMs were classified, discussed in terms of their applications while summarising the mechanical and tribological properties of FGMs from the available literature. The following points summarise what was found from the literature.

- According to the literature, the homogeneity of the TMC microstructure is heavily influenced by the reinforcement powder size and blending route used. Mechanically alloying via low-energy ball milling and using reinforcement size of sub-micron or nanoparticles ensures an enhanced homogeneity.
- The tribological and mechanical properties are heavily influenced by the reinforcement volume fraction and the dominant strengthening mechanism is the load transfer mechanism from the less stiff matrix to the stiffer phases. Most researchers use a reinforcement volume fraction from 5 vol.% up to 10 vol.% anymore and the TMC is very brittle.
- Most studies have looked at the *in situ* formation of phases from additive reinforcements such as SiC, TiB_2, however there are very limited studies looking at *in situ* formation of phases from elemental additives such as B , graphite and GNP.
- None of the studies looked into using two or more elemental additives to get two or more strengthening phases with enhanced tribological behaviour.
- None of the studies looked into the influence of HIP temperature on the completion of the *in situ* reaction and consolidation behaviour of the TMCs.
- Lack of studies looking at fabricating Ti based FGMs as most studies look into Al based FGMs for high wear resistance applications.
- Lack of studies looking into structure-property models relating the microstructure and the properties to theoretical models

2.3.2 Potential for further study

In summary, after conducting a thorough literature review on the current work on TMCs via powder metallurgy, it can be concluded that very limited work and studies have been conducted on rationalising the microstructure, mechanical and tribological properties to theoretical models and trying to predict the properties based on the reinforcement volume fraction, size , matrix size and processing parameters. Furthermore, most current studies focus on using vol.% of reinforcement which leads to crack propagation and that leads to deteriorating mechanical and tribological performance. Even though in recent years there have been a gradual increase in the number of publications regarding TMCs fabricated either via powder metallurgy or additive manufacturing, there seems to still be a lack of a comprehensive studies looking at the following:

- Relating the reinforcement characteristics , process parameters to the microstructure and properties.
- Studying how the process parameters influence *in situ* phase formation and consolidation behaviour.
- Achieve a crack free fully consolidated FGM via P/M HIP and develop a way to stack the powder layers without getting them mixed.

References

[1] G. Lütjering , J. Williams,. *Titanium engineering materials and progresses*, vol. 379, 2nd ed. Berlin: Springle; 2007

[2] C. Leyens, M. Peters., *Titanium and Titanium Alloys: Fundamentals and Applications*. Weinheim: [Chichester: Weinheim: Wiley-VCH; Chichester: John Wiley distributor c2003; 2003

[3] K. Kondoh, *Titanium metal matrix composites by powder metallurgy (PM) routes,* Titanium Powder Metallurgy, Technology and Applications, 2015, pp.277-297

[4] K. Chawla. (2012) Metal Matrix Composites. In: Composite Materials. Springer, New York, NY

[5] Chandran, K. S. Ravi & Panda, Krutibas & Sahay, Satyam., *TiBw-reinforced Ti composites: processing, properties, application prospects, and research needs.* JOM, 2004;vol.56(5), pp.42–48

[6] S. Bahl, *Fiber reinforced metal matrix composites- a review.* Materials Today: Proceedings, 2021 vol.39, pp.317-323

[7] L. Huang, L. Geng ., *Introduction. Discontinuously Reinforced Titanium Matrix Composites: Microstructure Design and Property Optimization*. Singapore:Springer Singapore; 2017. pp. 1–15.

[8] S.Li, B. Sun, H. Imai, K. Kondoh ., *Powder metallurgy Ti-TiC metal matrix composites prepared by in situ reactive processing of Ti-VGCFs system*. Carbon, 2013; vol.61, pp.216–228.

[9] H. Attar, K. Prashanth, L. Zhang, ., *Effect of powder particle shape on the properties of in situ Ti–TiB composite materials produced by selective laser melting*. J Mater Sci Technol, 2015, vol.31(10), pp.1001–1005.

[10] M. Hayat, H. Singh, Z. He, P. Cao ., *Titanium metal matrix composites: An overview.* Composites Part A, 2019, vol.121, pp.418-438

[11]C. Cai, B. Songa, C. Qiub, L. Lia , P. Xuea , Q. Weia , J. Zhoua , H. Nanc , H. Chend , Y. Shi ., *Hot isostatic pressing of in-situ TiB/Ti-6Al-4V composites with novel reinforcement architecture, enhanced hardness and elevated tribological properties.* Journal of Alloys and Compounds, 2017, vol.710, pp.364-374

[12] S. Li, K. Kondoh, H. Imai, B. Chen, L. Jia, J. Umeda, Y. Fu., Strengthening behavior of *in situ*-synthesized (TiC-TiB)/Ti composites by powder metallurgy and hot extrusion, Materials and Design, 2016, vol.95, pp.127-132

[13] Sivakumar, Ganesan & Ananthi, V. & Ramanathan., *Production and mechanical properties of nano SiC particle reinforced Ti–6Al–4V matrix composite*. Trans Nonferrous Metals Soc China, 2017, vol.27(1),pp.82–90

[14] Zhang, Faming & Liu, Suli & Zhao, Peipei & Liu, Tengfei & Sun, Jing., *Titanium/nanodiamond nanocomposites: Effect of nanodiamond on microstructure and mechanical properties of titanium.* Materials and Design, 2017, vol.131, pp.144-155

[15] Qi, Yan & Chen, Biao & Li., *Super-high-strength graphene/titanium composites fabricated by selective laser melting.* Carbon, 2021, vol.174, pp.451-462

[16] C. Cai, S. He, L. Li, Q. Teng, B. Song, C. Yan, Q. Wei, Y. Shi,., *In-situ TiB/Ti-6Al-4V composites with a tailored architecture produced by hot isostatic pressing: Microstructure evolution, enhanced tensile properties and strengthening mechanisms.* Composites part B: Engineering, 2019, vol.164, pp.546-558

[17] M.A Lagos, I. Agote, G. Atxaga, O. Adarraga, L. Pambaguian., *Fabrication and characterisation of Titanium Matrix Composites obtained using a combination of Self propagating High temperature Synthesis and Spark Plasma Sintering.* Mater Sci Eng, A, 2016, vol.655, pp.44-49

[18] M. Nasr, S. Anwar, A. Al-Samhan, H. Abdo, A. Dabwan., *On the machining analysis of graphene nanoplatelets reinforced Ti6Al4V matrix nanocomposites.* Journal of Manufacturing Processes, 2021, vol.61, pp.574-589

[19] F. Saba, F. Zhang, S. Liu, T. Liu,., *Reinforcement size dependence of mechanical properties and strengthening mechanisms in diamond reinforced titanium metal matrix composites.* Composites Part B: Engineering, 2019, vol.167, pp.7-19

[20] F. Wang, Z. Zhang, Y. Sun, Y. Liu, Z. Hu, H. Wang., *Rapid and low temperature spark plasma sintering synthesis of novel carbon nanotube reinforced titanium matrix composites*. Carbon, 2015, vol.95, pp.396–407.

[21] O. Falodun, B. Obadele, S. Oke, ., *Titanium-based matrix composites reinforced with particulate, microstructure, and mechanical properties using spark plasma sintering technique: a review.* The International Journal of Advanced Manufacturing Technology, 2019, vol.102, pp.1689-1701

[22] A. Sanaty ., *Comparison between current models for the strength of particulate-reinforced metal matrix nanocomposites with emphasis on consideration of Hall-Petch effect.* Mater Sci Eng A, 2012, vol.531, pp.112-118

[23] P. Luo, D.T. McDonald, W. Xu, S. Palanisamy, M.S. Dargusch, K. Xia., *A modified Hall-Petch relationship in ultrafine-grained titanium recycled from chips by equal channel angular pressing.* Scr Mater, 2012, vol.66(10), pp.785-788

[24] D. Ni, L. Geng, Z. Zheng ., *Fabrication and tensile properties of in situ TiBw and TiCp hybrid-reinforced titanium matrix composites based on Tin4Chy.* Mat. Sci. Eng. A, 2008, vol.478, pp.291-296

[25] D. Ni, L. Geng, Z. Zheng., *Effect of B_4C on microstructure of in situ titanium matrix composites prepared by reactive processing of Ti- B_4C system.* Script. Mater., 2006, vol.55, pp.429-432

[26] S. Gorsse, Y. Petitcorps, S. Matar, F. Rebillat., *Investigation of the Young's modulus of TiB needles in situ produced in titanium matrix composite.* Mat. Sci. Eng. A, 2003, vol.340, pp.80-87

[27] S. Lieberman, A. Gokhale, S. Tamirisakandala, R. Bhat., *Three-dimensional microstructural characterization of discontinuously reinforced Ti64-TiB composites produced via blended elemental powder metallurgy*. Mater. Charact., 2009, vol.60, pp.957-963

[28] S. Luo, Q. Li, J. Tian, C. Wang, M. Yan, G. Schaffer, M. Qian ., *Self-assembled, aligned TiC nanoplatelet-reinforced titanium composites with outstanding compressive properties*. Script. Mater., 2013, vol.69, pp.29-32

[29] K. Kondoh, T. Threrujirapapong, J. Umeda, B. Fugetsu., *High-temperature properties of extruded titanium composites fabricated from carbon nanotubes coated titanium powder by spark plasma sintering and hot extrusion.* Compos. Sci. Technol., 2012, vol.72, pp.1291-1297

[30] E. Solvas, D. García, A. Rodríguez., *Towards physical properties tailoring of carbon nanotubes-reinforced ceramic matrix composites*, J. Eur. Ceram. Soc., 2012, vol.32, pp.3001–3020

[31] Y. Mai, F. Chen, M. Zhou, Q. Xiao, G. Cai, X. Jie ., *Anchored graphene nanosheet films towards high performance solid lubricants,* Materials and Design, 2018, vol.160, pp.861-869

[32] Q. Yan, B. Chen, B. Zhang, T. Zhang, J. Wan, J. Shen, H. Kou ., *Inhibiting the interfacial reaction between few-layered graphene and titanium via SiC nanoparticle decoration* , Journal of Alloys and Compounds, 2022, vol.893

[33] D. Hastings, N. Rodriguez, H. McCann, M. Schoenitz, E. Dreizin., *Titanium-boron reactive composite powders with variable morphology prepared by arrested reactive milling,* Fuel. B, 2022, vol.310

[34] K. Wilson, E. Barrera, Y. Bayazitoglu., *Processing of Titanium Single-Walled Carbon Nanotube Metal-Matrix Composites by the Induction Melting method,* Journal of Composite Materials, 2010, vol.44, pp.1037-1048

[35] B. Zhao, W. Ding, J. Xu, H. Su., *Comparative study on cutting behaviour of vitrified cubic boron nitride wheel and electroplated cubic boron nitride wheel in high-speed grinding of (TiC_p + TiB_w)/Ti-6Al-4V composites,* Journal of Engineering Manufacture, 2016, vol.230(3), pp.428-438

[36] S. Teoh, R. Thampuran, W. Seah ., *Coefficient of friction under dry and lubricated conditions of a fracture and wear resistant P/M titanium-graphite composite for biomedical applications,* Wear, 1998, vol.214(2), pp.237-244

[37] K. Yoganandam, V. Mohanavel, J. Vairamuthu, V. Kannadhasan ., *Mechanical properties of titanium matrix composites fabricated via powder metallurgy method,* materialstoday Proceedings, 2020, vol.33(7), pp.3243-3247

[38] S. Gorsse, Y. Petitcorps., *A new approach in the understanding of the SiC/Ti reaction zone composition and morphology,* Composites Part A, 1998, vol.29A, pp.1221–1227

[39] S. Sabooni, F. Karimzadeh, M. Abbasi., *Thermodynamic aspects of nanostructured Ti5Si3 formation during mechanical alloying and its characterization,* Bull. Mater. Sci., 2012, Vol. 35(3), pp.439–447

[40] M. Backhaus-Ricoult, *Solid State Reactions Between Silicon Carbide and Various Transition Metals*, Ber. Bunsenges. Phys. Chem., 1989, vol.93, pp.1277-1281

[41] C. Suryanarayana., *Mechanical alloying and milling,* Prog. Mater. Sci., 2001, vol.46(1), pp.1-184

[42] L. Lu, M. Lai, C. Ng., *Enhanced mechanical properties of an Al based metal matrix composite prepared using mechanical alloying,* Mat. Sci. Eng. A, 1998, vol.252(2), pp.203-211

[43] J. Fogagnolo, F. Velasco, M. Robert, J. Torralba., *Effect of mechanical alloying on the morphology, microstructure and properties of aluminium matrix composite powders,* Mat. Sci. Eng. A, 2003, vol.342(1-2), pp.131-143

[44] E. Ruiz-Navas, J. Fogagnolo, F. Velasco, J. Ruiz-Prieto, L. Froyen., *One step production of aluminium matrix composite by mechanical alloying,* Composites Part A: Applied Science and Manufacturing, 2006, vol.37(11), pp.2114-2120

[45] C. Suryanarayana, E. Ivanov, V. Boldyrev., *The science and technology of mechanical alloying,* Mat. Sci. Eng. A, 2001, vol.304-306, pp.151-158

[46] A. Tiwari, V. Gopinathan, P. Ramakrishnan., *PROCESSING OF MODIFIED AI (7010)-SIC PARTICULATE COMPOSITES BY MECHANICAL ALLOYING AND HOT-PRESSING,* Materials and Manufacturing Processes, 1991, vol.6(4), pp.621-633

[47] K. Hanada, K. Khor, M. Tan, Y. Murakoshi, H. Negishi, T. Sano., *Aluminium-lithium/SiC_P composites produced by mechanically milled powders,* Journal of Materials Processing Technology, 1997, vol.67(1-3), pp.8-12

[48] J. Fogagnolo, M. Robert, F. Velasco, J. Torralba., *Aluminium Matrix Composites Reinforced with Si_3N_4, AlN and ZrB_2, Produced by Conventional Powder Metallurgy and Mechanical Alloying,* Kona Powder and Particle Journal, 2004, vol.22, pp.143-150

[49] S. Chauruka, A. Hassanpour, R. Brydson, K. Roberts, M. Ghadiri, H. Stitt., *Effect of mill type on the size reduction and phase transformation of gamma alumina,* Chemical Engineering Science, 2015, vol.134, pp.774-783

[50] O. Neikov, N. Yefimov, S. Naboychenko., *Handbook of Non-Ferrous Metal Powders (Second Edition),* Chapter 3- Mechanical Alloying, Technologies and Applications, 2019, pp.91-124

[51] J. Benjamin, T. Volin., *The mechanism of mechanical alloying,* Metall. Trans. A., 1974, vol.5, pp.1929-1934

[52] B. Zeeshan, O. Mamat, M. Mustapha., *Low energy solution ball milling of graphene nanoplatelets (GNPs) reinforced aluminium nanocomposites and its mechanical properties,* IOP Conference Series: Materials Science and Engineering. 380. 012009

[53] H. Liao, J. Chen, L. Peng, J. Han, H. Yi, F. Zheng, Y. Wu, W. Ding., *Fabrication and characterization of magnesium matrix composite processed by combination of friction stir processing and high-energy ball milling,* Mat. Sci. Eng. A, 2017, vol.683, pp.207-214

[54] B. Kaveendran, G. Wang, L. Huang, L. Geng, H. Peng., *In situ (Al_3Zr + Al_2O_{3np})2024Al metal matrix composite with novel reinforcement distributions fabricated by reaction hot pressing,* Journal of Alloys and Compounds, 2013, vol. 581, pp.16-22

[55] A. Srivastava., *A Review on Fabrication and Characterization of Aluminium Metal Matrix Composite (AMMC),* International Journal of Advance Research and Innovation, 2014, Vol. 2(2), pp.516-521

[56] H. Ye, X. Liu, H. Hong., *Fabrication of metal matrix composites by metal injection molding-A review,* Journal of Materials Processing Technology, 2008, Vol.200(1-3), pp.12-24

[57] C. Suryanarayana., *Mechanical alloying and milling,* Progress in Materials Science, 2001, Vol.46, pp.1-184

[58] F. Zhang, S. Liu, P. Zhao, T. Liu, J. Sun., *Titanium/nanodiamond nanocomposites: Effect of nanodiamond on microstructure and mechanical properties of titanium,* Materials and Design, 2017, vol.131, pp.144-155

[59] C. Koch, J. Whittenberger., *Mechanical milling/alloying of intermetallics,* Intermetallics, 1996, Vol.4(5), pp.339-355

[60] P. Kuziora, M. Wyszyńska, M. Polanski, J. Bystrzycki., *Why the ball to powder ratio (BPR) is insufficient for describing the mechanical ball milling process,* International Journal of Hydrogen Energy, 2014, Vol.39(18), pp.9883-9887

[61] Z. Zhao, X. Shao, K. Wang., *Effect of Ball-to-Powder Ratio on Morphology, Structure, and Flowability of Ball-Milled Gray Cast Iron powder,* J. Therm. Spray. Tech., 2021, Vol.30, pp.1679-1691

[62] Y. Saberi, S. Zebarjad, G. Akbari., *On role of stearic acid on morphology of Al-SiC_p composite powders produced by mechanical alloying method,* Powder Metallurgy, 2009, Vol.52(1), pp.61-64

[63] A. Restrepo, J. Rios, F. Arango., *Characterization of titanium powders processed in n-hexane by high-energy ball milling,* The International Journal of Advanced Manufacturing Technology, 2020, Vol.110, pp.1681-1690

[64] Y. Chen, X. Zhang, E. Liu., *Fabrication of in-situ grown graphene reinforced Cu matrix composites,* Sci. Rep., 2016,Vol.6(19363)

[65] K. Rashidi, M. Goudarzi, A. Masoudi., *Powder processing, characterization and mechanical properties of Al/GNP composites,* Materials Chemistry and Physics, 2020, Vol.256, 123719

[66] A. Al-Sherbini, M. Bakr, M. Saad., *Exfoliation of graphene sheets via high energy wet milling of graphite in 2-ethylhexanol and kerosene,* Journal of Advanced Research, 2017, Vol.8(3), pp.209-215

[67] Z. Cai, J. Chen, P. Du, T. Xiang, J. Chen, G. Xie., *Mechanical behavior and microstructure control of the low-cost titanium-oxygen alloy prepared by ball milling and spark plasma sintering,* Journal of Alloys and Compounds, 2021, Vol.887, 161349

[68] Y. Chen, T. Halstead, J.S. Williams., *Influence of milling temperature and atmosphere on the synthesis of iron nitrides by ball milling,* Materials Science and Engineering A, 1996, Vol.206(1), pp.24-29

[69] X. Mu, H. Zhang, H. Cai, Q. Fan, Z. Zhang, Y. Wu, Z. Fu, D. Yu., *Microstructure evolution and superior tensile properties of low content graphene nanoplatelets reinforced pure Ti matrix composites,* Materials Science and Engineering A, 2017, Vol.687, pp.164-174

[70] I. Melendez, E. Neubauer, P. Angerer, H. Danninger, J. Torralba ., *Influence of nano-reinforcements on the mechanical properties and microstructure of titanium matrix composites,* Composites Science and Technology, 2011, Vol.71(8), pp.1154-1162

[71] L. Geng, D. Ni, J. Zhang, Z. Zheng ., *Hybrid effect of TiBw and TiCp on tensile properties of in situ titanium matrix composites,* J. Alloy. Compd., 2008, Vol.463(1), pp.488-492

[72] K. Morsi, V. Patel., *Processing and properties of titanium-titanium boride (TiBw) matrix composites- a review,* J. Mater. Sci., 2007, Vol.42(6), pp.2037-2047

[73] S. Dong, J. Zhou, D. Hui, Y. Wang, S. Zhang., *Size dependent strengthening mechanisms in carbon nanotube reinforced metal matrix composites,* Composite Part A: Applied Science and Manufacturing, 2015, Vol.68, pp.356-364

[74] R. Vogt, Z. Zhang, Y. Li, M. Bonds, N.D. Browning, E.J. Lavernia, J.M. Schoenung., *The absence of thermal expansion mismatch strengthening in nanostructured metal–matrix composites,* Scripta Materialia, 2009, Vol.61(11), pp.1052-1055

[75] S. Ho, E. Lavernia., *Thermal residual stresses in metal matrix composites: A review,* Applied Composite Materials, 1995, Vol.2, pp.1-30

[76] M. Kouzeli, A. Mortensen., *Size dependant strengthening in particle reinforced aluminium,* Acta. Mater., 2002, Vol.50, pp.39-51

[77] G B, Veeresh & Pramod, Ramakrishna & Reddy., *Investigation of the Tribological Characteristics of Aluminum 6061-Reinforced Titanium Carbide Metal Matrix Composites,* Nanomaterials, 2021, Vol.11(11), 3039

[78] I. Yadroitsev, P. Krakhmalev, I. Yadroitsava., *Selective laser melting of Ti6Al4V alloy for biomedical applications: temperature monitoring and microstructural evolution,* J. Alloy. Compd., 2014, Vol.584, pp.404-409

[79] J. Williams, E. Starke., *Progress in structural materials for aerospace systems,* Acta. Mater., 2003, Vol.19, pp.5755-5799

[80] Dipankar Banerjee, J. William., *Perspectives on titanium science and technology,* Acta. Mater., 2013, Vol.3,pp.844-879

[81] P. Smith, F. Froes., *Developments in titanium metal matrix composites,* JOM, 1984, Vol.36(3), pp.19-26

[82] H. Singh, M. Hayat, H. Zhang, P. Cao ., *The decomposition of Si3N4 in titanium and its effect on wear properties,* Wear, 2019.

[83] J. Kim, K. Lee, D. Cho, Y. Lee ., *Fretting wear characteristics of titanium matrix composites reinforced by titanium boride and titanium carbide particulates,* Wear, 2013, Vol.301(1), pp.562-568

[84] Qi An, L.J. Huang, Yang Bao, Rui Zhang, Shan Jiang, Lin Geng, Miaomiao Xiao., *Dry sliding wear characteristics of in-situ TiBw/Ti6Al4V composites with different network parameters,* Tribol. Int., 2018, Vol.121, pp.252-259

[85] R. Chaudhari, R. Bauri*., A novel functionally gradient Ti/TiB/TiC hybrid composite with wear resistant surface layer*, J. Alloy. Compd., 2018, Vol.744, pp.438–444

[86] T. Ram Prabhu, V.K. Varma, Srikanth Vedantam., *Effect of SiC volume fraction and size on dry sliding wear of Fe/SiC/graphite hybrid composites for high sliding speed applications,* Wear, 2014, Vol.309(1-2), pp.1-10

[87] Uvaraja, V & Nanjappan, Natarajan., *Optimization of friction and wear behaviour in hybrid metal matrix composites using Taguchi technique,* J. Miner. Mater. Charact. Eng., 2012, Vol.11(8)

[88] Z. Cao, X. Wang, J. Li, Y. Wu, H. Zhang, J. Guo, S. Wang., *Reinforcement with graphene nanoflakes in titanium matrix composites,* J. Alloy. Compd., 2017, Vol.696, pp.498-502

[89] C. Shang, T. Liu, F. Zhang, F. Chen., *Effect of network size on mechanical properties and wear resistance of titanium/nanodiamonds nanocomposites with network architecture,* Composites Communications, 2020, Vol.19, pp.74-81

[90] M. Savalani, C. Ng, Q. Li, H. Man., In situ formation of titanium carbide using titanium and carbon-nanotube powders by laser cladding, Applied Surface Science., 2012, Vol.258(7), pp.3173-3177

[91] H. Singh, M. Hayat, H. Zhang, P. Cao ., *The decomposition of Si_3N_4 in titanium and its effect on wear properties,* Wear, 2019, Vol.420-421, pp.87-95

[92] J. Jiang, Y. Wang ., *Microstructure and mechanical properties of the semisolid slurries and rheoformed component of nano-sized SiC/7075 aluminum matrix composite prepared by ultrasonic-assisted semisolid stirring,* Mater. Sci. Eng., 2015, Vol.639, pp. 350-358

[93] O. El-Kady, A. Fathy., *Effect of SiC particle size on the physical and mechanical properties of extruded Al matrix nanocomposites,*Mater. Des.,2014, Vol.54, pp. 348-353

[94] G. Ramesh Bapu, S. Jayakrishnan., *Development and characterization of electro deposited Nickel–Titanium Carbo Nitride (TiCN) metal matrix nanocomposite deposits,* Surface and Coatings Technology, 2012, Vol.206, pp.2330-2336

[95] A. Kumar, K. Pal, S. Mula., *Simultaneous improvement of mechanical strength, ductility and corrosion resistance of stir cast Al7075-2% SiC micro- and nanocomposites by friction stir processing,* Journal of Manufacturing Processes, 2017, Vol.30, pp.1-13

[96] K. Singh, S. Singh, A. Shrivastava., *Study of Tribological Behavior of Silicon Carbide Based Aluminum Metal Matrix Composites under Dry and Lubricated Environment,* Advances in Materials Science and Engineering, 2016, p.11

[97] Zaiemyekeh, Z. Liaghat, Gholamhossein & Khan, Muhammad Kashif., *Effect of Al2O3 nanoparticles on the mechanical behaviour of aluminium-based metal matrix composite synthesized via powder metallurgy,* Proc IMechE Part L: J Materials: Design and Applications, 2021, Vol.235(10), pp.2340-2355

[98] K. Deng, J. Shi, C. Wang, X. Wang, Y. Wu., *Microstructure and strengthening mechanism of bimodal size particle reinforced magnesium matrix composite,* Compos. A. Appl. Sci. Manuf., 2012, Vol.43(8), pp. 1280-1284

[99] N. Babu, K. Kallip, M. Leparoux, K. AlOgab., *Influence of microstructure and strengthening mechanism of AlMg5–Al_2O_3 nanocomposites prepared via spark plasma sintering,* Materials & Design, Vol.85, 2016, pp.534-544

[100] S. Choi, H. Awaji., *Nanocomposites-a new material design concept,* Science and Technology of Advanced Materials, 2005, Vol.6, pp.2-10

[101] M. Korayem, R. Mahmudi, W. Poole., *Enhanced properties of Mg-based nano-composites reinforced with Al2O3nano-particles, ,* Mater. Sci. Eng. A., 2009, Vol.519, pp.198-203

[102] Z. Zhang, D. Chen., *Contribution of Orowan strengthening effect in particulate-reinforced metal matrix nanocomposites, ,* Mater. Sci. Eng. A., 2008, Vol.483-484, pp.148-152

[103] W. Li, Y. Yang, M. Li, J. Liu., *Enhanced mechanical property with refined microstructure of a novel γ-TiAl/TiB_2 metal matrix composite (MMC) processed via hot isostatic press,* Materials & Design, 2018, Vol.141, pp.57-66

[104] C. Goh, J. Wei, L. Lee, M. Gupta., *Properties and deformation behaviour of Mg–Y2O3nanocomposites,* Acta Materialia, 2007, Vol.55, pp.5115-5121

[105] W. Kim, Y. Yu., *The effect of the addition of multiwalled carbon nanotubes on the uniform distribution of TiC nanoparticles in aluminum nanocomposites*, Scripta Mater, 2014, Vol.72, pp.25–28

[106] F.X. Li, P.D. Hao, J.H. Yi, Z. Chen, K.G. Prashanth, T. Maity, J. Eckert., *Microstructure and strength of nano-/ultrafine-grained carbon nanotube-reinforced titanium composites processed by high-pressure torsion*, Mater. Sci. Eng. A, 2018, Vol.722, pp.122-128

[107] H. Frost., *Deformation mechanism maps: the plasticity and creep of metals and ceramics*, Pergamon press; 1982

[108] Q. Yuan, X. Zeng, Y. Liu, L. Luo, J. Wu., *Microstructure and mechanical properties of AZ91 alloy reinforced by carbon nanotubes coated with MgO*, Carbon, 2016, Vol.96, pp.843–855.

[109] M.J. Starink, S.C. Wang., *A model for the yield strength of overaged Al–Zn–Mg–Cu alloys*, Acta Mater, 2003, Vol.51, pp.5131–5150

[110] A. Sanaty-Zadeh., *Comparison between current models for the strength of particulate-reinforced metal matrix nanocomposites with emphasis on consideration of Hall–Petch effect*, Mater. Sci. Eng. A, 2012, Vol.531, pp.112–118

[111] H. Kim., *on the rule of mixtures for the hardness of particle reinforced composites*, Mater. Sci. Eng. A, 2000, Vol. 289, pp. 30-33

[112] A.G. Arsha, E. Jayakumar, T.P.D. Rajan, V. Antony, B.C. Pai., *Design and fabrication of functionally graded in-situ aluminium composites for automotive pistons*, Mater. Des., 2015, Vol.88, pp.1201–1209

[113] R. Jojith, Manu Sam, N. Radhika., *Recent advances in tribological behavior of functionally graded composites: A review,* Engineering Science and Technology, an International Journal, 2021

[114] R. Mahamood, E. Akinlabi., *Types of functionally graded materials and their areas of application. In Functionally graded materials*, Springer, Cham, 2017, pp. 9-21

[115] Ehab I. Salama, Sherry S. Morad, Amal M.K. Esawi., *Fabrication and mechanical properties of aluminum-carbon nanotube functionally-graded cylinders,* Materialia, 2019, Vol.7, 100351

[116] Z. Wang, C. Li, H. Wang., *Wear and Corrosion Behavior of Functionally Graded Nano-SiC/2014Al Composites Produced by Powder Metallurgy,* J. of Materi. Eng. and Perform., 2017, Vol.26, pp.729-735

[117] M. Thieme, K. Wieters, F. Bergner., *Titanium powder sintering for preparation of a porous functionally graded material destined for orthopaedic implants*, J. Mater. Sci. Med., 2001, Vol.12(3), pp.225-231

[118] I. Matuła, G. Dercz , M. Sowa A. Barylski, P. Duda P., *Fabrication and Characterization of New Functional Graded Material Based on Ti, Ta, and Zr by Powder Metallurgy Method,* Materials, 2021, Vol.14, 660

[119] Y. Geng, W. Xie, Y. Tu ., *Ti–6Al–4V microstructural functionally graded material by additive manufacturing: Experiment and computational modelling,* , Mater. Sci. Eng. A, 2021, Vol.823, 141782

[120] L. Lu, M. Chekroun, O. Abraham, V. Maupin., *Mechanical properties estimation of functionally graded materials using surface waves recorded with a laser interferometer*, NDT and E Int., 2011, Vol.44(2), pp.169–177

[121] S.N. Naveen Kumar, R.M. Devarajaiah, T. Ram Prabhu ., *Review on aluminium based functionally graded composites,* materialstoday: Proceedings, 2021, Vol.39, pp.1743-1749

[122] K. Vinoth Babu, S. Marichamy, P. Ganesan, D. Madan, M. Uthayakumar, T.P.D. Rajan., *Processing of functionally graded aluminium composite brake disc and machining parameters optimization,* Materials Today: Proceedings, 2019, in printing.

[123] M. Surya, G. Prasanthi., *Effect of Silicon Carbide Weight Percentage and Number of Layers on Microstructural and Mechanical Properties of Al7075/SiC Functionally Graded Material,* Silicon, 2021,

[124] A. Pasha, B. Rajaprakash., *Functionally graded materials (FGM) fabrication and its potential challenges & applications,* Materials Today: Proceedings, 2021, in press.

[125] Thieme M, Wieters KP, Bergner F, Scharnweber D, Worch H., *Titanium Powder Sintering for Preparation of a Porous FGM Destined as a Skeletal Replacement Implant,* Materials Science Forum, 1999, Vol.308, pp.374-382

[126] Y. Guo, J. Guan, H. Peng, X. Shu, L. Chen, H. Guo ., *Tightly adhered silk fibroin coatings on Ti6Al4V biometals for improved wettability and compatible mechanical properties,* Materials & Design, 2019, Vol.175, 107825

[127] A. Kawasaki, R. Watanabe., *Concept and P/M Fabrication of Functionally Gradient Materials*, Ceramics International, 1997, Vol.23, pp.73-83

[128] G. Kırmızı, H. Arık, H. Çinici ., *Experimental study on mechanical and ballistic behaviours of silicon carbide reinforced functionally graded aluminum foam composites,* Composites part B: Engineering, 2019, Vol.164, pp.345-357

[129] J.K.M Kwok, S.C Lim., *High-speed tribological properties of some Al/SiCp composites: I. Frictional and wear-rate characteristics,* Composites Science and Technology, 1999, Vol.59(1), pp.55-63

[130] Karnati, S. Zhang, Y. Liou, F. Newkirk, J.W., *On the Feasibility of Tailoring Copper–Nickel Functionally Graded Materials Fabricated through Laser Metal Deposition,* Metals, 2019, Vol.9(3),p.287

[131] G. Ma, C. Yu, B. Tang, Y. Li, F. Niu., *High-mass-proportion TiCp/Ti6Al4V titanium matrix composites prepared by directed energy deposition,* Additive manufacturing, 2020, Vol.35, 101323

[132] F. Weng, H. Yu, J. Liu, C. Chen, J. Dai, Z. Zhao., *Microstructure and wear property of the Ti5Si3/TiC reinforced Co-based coatings fabricated by laser cladding on Ti-6A1-4V,* Opt. Laser Technol., 2017, Vol.92, pp.156–162

[133] Y. Zhang, Z. Wei, L. Shi, M. Xi., *Characterization of laser powder deposited Ti-TiC composites and functional gradient materials,* J. Mater. Process. Technol., 2008, Vol.206, pp.438–444.

[134] S. Joo, S. Yoon, C. Lee., *Microstructure and tensile behavior of Al and Al-matrix carbon nanotube composites processed by high pressure torsion of the powders,* J. Mater. Sci., 2010, Vol.45, pp. 4652-4658

[135] S. Udupa., *Fabrication of functionally graded carbon nanotube-reinforced aluminium matrix laminate by mechanical powder metallurgy technique—part 1,* J. Mater. Sci. Eng., 2015, Vol.4,p.169

[136] H. Kwon, M. Leparoux, A. Kawasaki ., *Functionally graded dual-nanoparticulate-reinforced aluminium matrix bulk materials fabricated by spark plasma sintering,* J. Mater. Sci. Technol.,2014,Vol.30, pp.736-742

[137] Recep Ekici, M. Kemal Apalak, M. Yildirim., *Indentation behavior of functionally graded Al–SiC metal matrix composites with random particle dispersion,* Composites Part B: Engineering, 2011, Vol.42(6), pp.1497-1507

[138] N. Sindhu, R. Kumar Goyal, Thankachan T. Pullan., *Study on Al/TiB2 functionally graded metal matrix composites,* Composites Part B: Engineering, 2011, Vol.42(6), pp.1497-1507

[139] Rohatgi, Pradeep & Tabandeh-Khorshid, Meysam & Omrani, Emad & Lovell, Michael & Menezes, Pradeep., *Tribology of metal matrix composites,* In Tribology for scientists and engineers, Springer, New York, pp.233-268

Chapter 3 Experimental Procedure

3.1 Experimental chapter overview

This chapter will thoroughly discuss the experimental techniques used to fabricate and characterize the various TMCs and FGMs used in this research and papers written. Details such as powder characterization techniques, powder blending routes used, canister fabrication, canister filling, outgassing, crimping, HIPping process parameters used, post processing such as EDM cutting and sample preparation using grinding and polishing will be discussed comprehensively. Furthermore, the chapter will include information on the microscopic techniques and various phase characterization techniques including XRD and Raman spectroscopy. Information regarding mechanical and tribological testing will also be mentioned in detail and the machine used to map the wear tracks. An overview of the HIP system at the University of Birmingham (UoB) will also be provided.

3.2 Materials and their processing

3.2.1 GA Ti-6Al-4V powder

The argon GA Ti64 powder used in this research was supplied by (LPW Technology, UK) and was produced by the gas atomising process. The as-received powder had a size range of (15-45µm) and an average particle size of 33µm as provided by the data sheet from the manufacturer. The powder morphology was mostly spherical with a few satellites and irregular particles due to the inherent atomisation process used.

3.2.2 SiC powders

Alpha SiC used in this research (99.5% purity with an average particle size of 4.14µm) was procured from (Reade Advanced Materials, USA). On the other hand, SiC nanoparticles (98% purity with an average particle size of 20nm) was supplied by (PlasmaChem GmbH, Germany). Powder particle size distribution (PSD) for the micron-sized SiC were acquired following the ASTM B822-10 standard.

3.2.3 Boron powder

Boron (B) (purity: >95%) amorphous powder used in this research with an average particle size of < 1µm was procured from (Sigmaaldrich, Germany). The powder morphology was assessed by a scanning electron microscope (SEM) and an energy dispersive X-Ray (EDX) to confirm the morphology and chemical composition.

3.2.4 Graphene nanoplatelets powder

Graphene nanoplatelets (GNPs) used in this research was purchased form (Sigmaaldrich, Germany). The powder had a thickness range between (5-20nm), a high surface area of 750m^2/g and a length that is less than < 2µm. The data was provided powder specification sheet by the manufacturer. The powder was also checked by an SEM in order to look at the morphology.

3.2.5 Ti-TiC, Ti-SiC, Ti-WC powders

Mechanically alloyed Ti-TiC, Ti-SiC, Ti-WC powders were procured from (MBN Nanomaterialia, Italy). Grade 2 titanium (Ti) powder with an average particle size (APS) of (45µm-150µm) was used as the matrix. Tungsten carbide (WC) with a weight of (22.5 wt.%), titanium carbide (TiC) with a weight of (25 wt.%) and silicon carbide (SiC) with a weight of (42 wt.%) were used as the reinforcements and mechanically alloyed (MA) with the Ti matrix. SEM was used to look at the powder morphologies and cross sections to check for internal defects such as porosities and cracks.

3.2.6 Powder blending

In this research , two powder blending routes were used and evaluated in terms of the powder homogeneity. The first method was using a powder mixing machine and the second method was using ball milling via mechanical alloying (MA) the powders. Ti64 matrix was reinforced with various reinforcement as listed in table 3.1 and table 3.2. In terms of the nano-reinforcements, they were suspended in ethanol with Ti64, de-agglomerated using ultrasonication for 30 minutes. The de-agglomerated powders in the ethanol solution were then added to stainless steel jars ready for MA via low-energy ball milling (HMK-1901, University of Birmingham). The process control agent used was

ethanol and the ball-to-powder ratio (BPR) used was 4:1 and a rotational speed of 200 RPM was used in order to limit the deformation of the powder morphology and overheating of Ti powder. The grinding media used were aluminium oxide (Al_2O_3) that have a micro-hardness value exceeding 1600HV and the balls diameter are 8mm. After the powders were MA, there were left to dry on a hot plate overnight inside a glovebox. The other blending method was roll blending which was used for the micron-sized reinforcement powders. The parameters used are shown in table 3.2.

Table 3.6: *Roll blending parameters used for micron sized reinforcements*

Matrix	Reinforcement	Milling speed	Milling duration
Ti64	SiC (4µm)	80	4

Table 3.7: *MA ball milling parameters used for nano-sized reinforcements*

Matrix	Reinforcement	Ultrasonication duration (min)	Process control agent	Ball to powder ratio (BPR)	Milling speed (RPM)	Milling duration (h)
Ti64	SiC (20nm)	30	ethanol	4:1	200	4
Ti64	GNPs	30	Ethanol	4:1	200	4
Ti64	B	30	Ethanol	4:1	200	4
Ti64	B + GNPs	30	Ethanol	4:1	200	4

3.2.7 Hot Isostatic Pressing procedure

The powders were consolidated using PM HIP using the (EPSI HIP, University of Birmingham). The HIP works by consolidating the powders using process parameters such as temperature, pressure and dwell time. In order to get the powders to consolidate and reach theoretical density, the powder encapsulation material used needs to deform under high temperature and pressure, hence why mild steel is generally used. Prior to welding the mild steel cans, the cans were cleaned by submerging them in acetone and ultrasonicating them for 15 mins to get rid of any contamination. Mild steel cans were fabricated and welded at the University of Birmingham. The diameter used was 20.8mm, length of 80mm and a wall thickness of 2.03mm. canisters were checked for leaks prior to powder filling using (Smart test, Pfeiffer vacuum) helium leak detector that can detect leaks with a leak rate that are smaller than $5x10^{-12}$ mbar l/s as shown by figure 3.1. Powder filling of the canisters was done inside the (Glovebox, Saffron) as seen in figure 3.2 followed by using a vibratory station to tap the powders and help achieve a better tap density shown in figure 3.3.

Figure 3.1*: Helium leak detector photograph*

Figure 9: *Glovebox used to fill powders photograph*

Figure 3.3*: Vibratory station to tap powder filled canisters*

The canisters were then outgassed overnight until they reached a vacuum level of 10^{-5} mbar or lower using an-inhouse outgassing rig at the University of Birmingham as shown in figure 3.4. Once the cans reached the desired vacuum level, they were crimped and welded at the top to ensure that they are sealed and vacuum tight. The cans were then placed in the HIP furnace (EPSI HIP, University of

Birmingham) as shown in figure 3.5. Different HIPping parameters were used for different powder blends ; however, a constant heating rate of 10℃/min and a cooling rate of 5℃/min were used and a dwell time of 3h. The pressure and temperature of the HIP furnace were slowly increased until the point that the desired temperature and pressure are reached.

Figure 3.4*: Outgassing rig setup photograph*

Figure 3.5*: EPSI HIP located at the University of Birmingham*

The EPSI HIP shown in Figure 3.5 can reach a maximum HIP temperature of 1450℃ and a maximum pressure of 200 MPa. The EPSI HIP system contains two heating elements, one at the top of the furnace and one located at the bottom of the furnace. The system also contains a heating shield, a jet water cooling system that can cool at a rate of 80℃/min and an argon gas compressor. Furthermore, the system contains thermocouples at the top and bottom of the furnace that is connected to a computer in order to monitor any temperature fluctuations in the system. Finally, it is important to mention that the temperature fluctuation within the furnace are within ± 3 ℃.

3.3 Microstructural characterization

3.3.1 Sample preparation

The first thing step was to analyse the As-received powders and take micrographs of the morphology using a scanning electron microscope (SEM). The As-received powders were mounted on a conductive Bakelite sticker and mounted into the (Hitachi TM3000 SEM) for characterization. Furthermore, the As-received mechanically alloyed (MA) powders were mounted on Bakelite using a mounting press and then grinded for 30s a SiC grit 1200 with water ready to be examined under an SEM. In order to characterize the microstructure of the as-HIPped samples, they were first cut using the electric discharge machine (EDM) , followed by hot mounting them into Bakelite for the grinding and polishing procedure. The grinding and polishing procedure was carried out using the (Struers Tegramin) at the University of Birmingham.

The metallographic sample preparation steps in terms of grinding and polishing are highlighted and summarised in table 3.3. After the grinding and polishing procedure was conducted, the samples were etched in order for the microstructural features to be spotted for SEM analysis and optical microscopy. The etchant used was Kroll's reagent consisting of 10 vol.% nitric acid and 2 vol.% hydrogen fluoride and the remaining balance of water. The samples were etched for roughly 10 seconds.

***Table 3.8**: Grinding and polishing procedure used for TMCs*

Disc/ abrasion media used	RPM	Force (N)	Time (min)
MD Piano Grit 220 with water	300	15	2
MD Piano Grit 1200 with water	300	15	5
MD largo diamond suspension	150	10	3
Chem 0.05 um OP-S Colloidal Silica (SiO_2) +10% Hydrogen Peroxide (H_2O_2)	150	10	20

3.3.2 Characterization techniques

A back scattered electron (BSE) scanning electron microscope (SEM) was used to take micrographs of etched samples using a Hitachi TM3000, while the energy dispersive X-ray (EDX) was used in conjunction with the SEM to identify the chemical composition of the samples. Furthermore, Image J

software was used to quantify the volume fraction of the different phases of polished samples to be used in structure-property modelling using thresholding methods on grey scale images. Image analysis using Image J was also used to measure the grain size of 200 grains along each sample. X-ray diffraction (XRD) analysis was performed using (AXRD, Proto) which is the machine name at the University of Birmingham on As-polished samples in order to identify the different phases. The parameters used on the XRD were a copper (Cu) Kα radiation, a wavelength of (λ = 1.5406°A), a step size of 0.02º and 1s time/step. Finally, to characterize as-received graphene nanoplatelets (GNPs), Raman spectroscopy was used using the (Invia Raman Microscope, Renishaw) at the University of Warwick facility. The parameters used during testing were a wavelength excitation of 532nm, acquisition time of 30 s with a focus of x50 and 4 scans per sample. The same parameters were used on the as-HIPped samples that included GNPs as reinforcements. The Raman spectra scans were conducted on samples before and after wear testing.

3.3.3 Mechanical and tribological testing

In terms of Micro-hardness testing, they were carried out using a diamond micro-indenter at the University of Birmingham (Buehler Wilson VH1202, Buehler) as shown in Figure 3.6. Large indentations were done using a load of 1 Kg, dwell time of 10 s and 10 indentations were carried out on different regions of the samples to get a good average of the composites micro-hardness using the recommended spacing in accordance with ASTM E384-17 standard. The micro-hardness indentations were carried out on flat as-polished samples. Furthermore, small indents were carried on some samples along a matrix area of 0.2 mm by 0.2 mm and matrix size of 9x7 using the smallest load of 10 g to hit all the different phases in the composites. Wear tests were carried out at the University of Birmingham using a (Phoenix TE79) sliding in-house reciprocating machine as shown in figure 3.7. The machine has the capability to record COF readings. The counter-body ball used was aluminium oxide (Al_2O_3) with a diameter of 10 mm and a hardness value of 1600 HV. The ball was rotated each time a different sample was used. The tests were carried out at room temperature using a constant load of 20N, sliding distance of 5 mm and sliding speed of 10mm/s, 750 cycles and a sliding time of 30 minutes per test. The wear depth was analysed and mapped using an (Infinitefocus microscope, Alicona). Cylinders with a diameter of 5mm and a height of 10mm were extracted from the HIPped canisters using electric discharge machine (EDM) for coefficient of thermal expansion analysis. The measurements for linear coefficient of thermal expansion was carried out using a dilatometer (Netzsch TMA 402 F1) at a temperature reaching 1000 ℃ using a 5 ℃/min heating rate. The furnace was set to

go from 30℃ to 200℃ at a rate of 5℃/min under a positive flow of nitrogen, held at 200℃ for 1h and returned to 30℃ at a rate of 5℃/min. The samples used for compression testing were cylindrical samples with a diameter of 6 mm and height of 10 mm and were cut with the aid of an EDM.The machine used for compression testing was a universal testing machine (ESH Testing 200) located at the University of Birmingham. The testing was performed at a constant crosshead speed of 2mm/min using a maximum load cell of 100 KN

Figure 3.6*: Buehler Micro-hardness tester photograph*

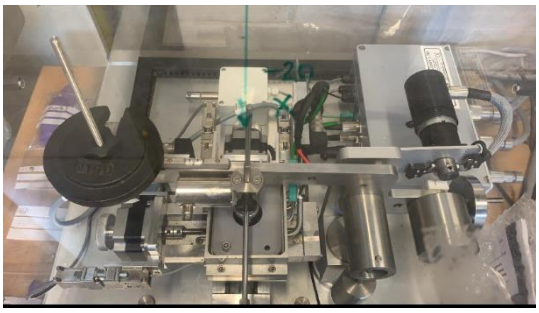

Figure* 3.7: Reciprocating wear test machine photograph*

Chapter 4: P/M Hot Isostatic Pressing of TMCs via *In Situ* Elemental Additions of B and GNP, Enhanced Mechanical and Tribological Properties

Abstract

(1) Ti64 titanium metal matrices reinforced with graphene nanoplatelets (GNP) of varying volume fractions (1-2 vol.%) have been prepared and developed using the powder metallurgy (PM) hot isostatic pressing (HIP) technique. Furthermore, novel advanced TMCs were developed by reinforcing the Ti64 matrix with 1 vol.% boron (B) and 1 vol.% GNP. The powders were MA by means of wet ball milling and vacuum dried in the glovebox prior to HIP. Experiments were conducted to examine and understand the influence of HIP temperature on the *in situ* reaction and consolidation behaviour of the TMCs. HIP temperatures of sub β-transus (920°C), 1040 °C and super β-transus (1160 °C) were investigated. 1040 °C was selected as a temperature below the β-transus temperature based on calculations taking into account the diffusion of carbon (C) and oxygen (O) on raising the β-transus temperature. In addition, the influence of reinforcement vol.% on the micro-hardness and wear resistance were investigated. Micro-hardness maps were also plotted using a load of 10g in order to examine the phase micro-hardness contribution to the TMC and further understand the phase homogeneity, and ultimately the tribological performance of the materials. The as-received GNP powder was analysed using Raman spectroscopy (InVia Raman Microscope) to confirm the presence of graphene. The microstructure and tribological performance of the as-HIPped TMCs were characterised using EDX, SEM, XRD, dry-sliding reciprocating with coefficient of friction (COF) tests, micro-hardness and coefficient of thermal expansion (CTE) measurements, and Raman spectroscopy to further understand the graphene lubrication behaviour on the worn surfaces. One of the main findings of this work was that an increase in the vol.% of GNP reduced the COF due to an increase in micro-hardness and a higher GNP content at the surface of the composite, which lubricated the surface. Furthermore, raising the vol.% of GNP increased the micro-hardness due to a higher retention of TiC hard phase. HIPping at 1160°C ensured full

consolidation, but resulted in grain growth, while HIPping at 920^{o}C there was lack of consolidation and no *in situ* reaction.

4.1 Introduction

Titanium (Ti) and its alloys are known to provide excellent mechanical properties, including and providing high strength and weight reductions [1]. However, they have not been used extensively in a variety of applications due to their poor tribological performance [2]. Metal matrix composites (MMCs) are composed of at least two constituent parts, one being the metal and the other usually a ceramic, which can offer a solution to the shortcomings of Ti and its alloys [3]. Reinforcing the matrix with ceramic, either as continuous fibres or discontinuous particulates, can enhance strength and wear resistance immensely, while the matrix offers both ductility and toughness, thus opening up the possibility of tailoring composites for many different applications [4].

Research into the wide range of application possibilities of titanium matrix composites (TMCs) has advanced over recent years. A number of TMCs, either continuously reinforced with fibres or discontinuously reinforced with particulates or whiskers, have been developed, such as titanium diboride ($TiB_{2)}$ [5], silicon carbide (SiC) [6], titanium carbide (TiC) [7], diamond nanoparticles (DNP) [8] and graphene [9]. Conventional techniques used to develop MMCs by way of ex situ additions of the reinforcement phases are prepared prior to synthesising the composite but suffer from various shortcomings that limit their development. This is mainly due to Ti being extremely reactive at high temperatures as well as the poor interfacial bonding between the matrix and reinforcement [10]. On the other hand, *in situ* synthesization techniques for the preparation of TMCs have gained interest in recent years. An *in situ* method allows for a chemical reaction to take place between the metal matrix and ceramic reinforcement, resulting in phases that are high in strength, thermodynamically stable and exhibit superior interfacial bonding, improving the mechanical and tribological behaviour of the composite in comparison with ex situ routes [11]. Lately, graphene has been deemed an attractive reinforcement choice for MMCs due to its exceptional mechanical properties [12]. It has an elastic modulus value of 1 TPa and is much stronger than diamond, and with its high specific area of 2600m^2/g would contribute to stronger interfacial bonding between the matrix and reinforcement, improving the load-transfer capabilities and reducing the rate of delamination during severe wear applications [13]. Further studies have shown graphene is an effective reinforcement in reducing the coefficient of friction (COF) and wear rate due to its ultra-high strength and lubrication sliding-like properties, attributed to the shear potential, that form a protective layer on the contact surfaces [14]. Some research has been carried out on use of graphene nanoplatelets (GNP) as a potential reinforcement for metal matrices, including magnesium (Mg), aluminium (Al) and nickel alloys [15-17]. Algul et al.[18] studied the influence of graphene volume fraction on the wear properties of nickel graphene composite. They concluded that an increase of graphene content caused a decrease in COF and wear

rate, due to the elevated hardness and lubricating properties of graphene. It is also worth mentioning that TiB_2 has recently been at the forefront of TMC research due to the excellent properties that it exhibits, such as a hardness (25-35 GPa), high elastic modulus (425-480 GPa) and a coefficient of thermal expansion (CTE) value of $8.1x10^{-6}K^{-1}$ and is compatible with Ti and its alloys [19]. Research on the CTE behaviour of the various TMCs is vital, as the inherent CTE mismatch between the matrix and reinforcement can result in the generation of thermal residual stresses that are detrimental to the mechanical properties of TMCs when used in high temperature applications and could result in cracks or spallation. Being able to predict the CTE can help in the design of TMCs for specific applications. Turner's model [28] for particulate composites assumes only hydrostatic stresses are acting on the composite as expressed in equation 4.1.

$$\alpha_c = \frac{\alpha_m V_m K_m + \alpha_p V_p K_p}{V_m K_m + V_p K_p} \quad (4.1)$$

where V is volume fraction, K is bulk modulus, m and p subscripts are matrix and reinforcement respectfully. Another model, which takes into account the shear and hydrostatic stresses, is the Kerner model [28], represented by equation 4.2.

$$\beta_c = \beta_m v_m + \beta_p v_p - \left(\beta_m - \beta_p\right) \times \frac{\frac{1}{K_m} - \frac{1}{k_p}}{\frac{v_m}{k_p} + \frac{v_m}{k_m} + \frac{3G_m}{4}} \quad (4.2)$$

where G is the shear modulus and the other subscripts are like the Kerner model mentioned above.

To date there has been little work carried out on the use of the HIP technique to synthesise Ti64/GNP, Ti64/B and Ti64/GNP +B composites Therefore, this study will focus on synthesising TiC and TiB_2 reinforced Ti64 using elemental *in situ* reactive hot isostatic pressing (RHIP) with GNP and B additions. The influence of HIP temperature and reinforcement powder characteristics, such as volume fraction of GNP and B, on microstructural evolution and phase formation, and mechanical and tribological performance will be investigated. As to the authors knowledge, not a lot of work has been done on HIP technique to consolidate Ti64 reinforced with elemental additions to synthesize Ti64/GNP, Ti64/B and Ti64/GNP +B composites.

4.2 Experimental

4.2.1 Material preparation

Argon gas atomised (AGA) Ti-6Al-4V (Ti64) powder (Figure 4.1a), with an average particle size (APS) of 15-45µm, was used as the metal matrix and purchased from (LPW Technology, UK). Graphene nanoplatelets (GNP) with a length of < 2µm, thickness of 5-20nm, average number of layers of 5 to 7 layers and a high surface area of 750m^2/g were purchased from (Sigma-Aldrich, Germany). B powder (purity: >95%) with an APS of < 1µm was also purchased from (Sigma-Aldrich, Germany). Four different powders blends were prepared: Ti64+ 1 vol.% B, Ti64 + 1 vol.% GNP, Ti64 + 2 vol.% GNP, Ti64 + 1 vol.% B + 1 vol.% GNP. Firstly, the GNP underwent deagglomeration using ultrasonication for a time period of 30 min in ethanol with a concentration of approximately 0.1mg/ml. Ti64 was added to the GNP suspension and ultrasonicated for an additional 30 min. The blended powders were allowed to rest and drained to remove excess solution. The blended powders were then MA using low-energy ball milling (HMK-1901) using ethanol as a process control agent, for a duration of 4h, with ball to powder ratio (BPR) of 4:1 and a speed of 200 revolutions per minute (RPM) to limit the deformation and overheating of Ti powders. The grinding media used was aluminium oxide (Al_2O_3) balls with a diameter of 8mm.

.

4.2.2 Powder HIP

The MA composites were then consolidated by use of HIP. Mild steel canisters with an outer diameter of 20.8mm, length of 80mm and wall thickness of 2.03mm were welded prior to being filled with the composite powders and vibrated. The canisters were then outgassed at 100℃ until they reached a vacuum level of 10^{-5} bar, before being crimped. The canisters were HIPped using (EPSI, HIP) at three different temperatures, 920℃ (sub β-transus), 1040℃ and 1160℃ (super β -transus), at a constant pressure of 140MPa and for 3h.

4.2.3 Microstructural characterisation

The as-HIPped samples were wire cut using an electrical discharge machine (EDM), ground, and polished for XRD. The samples were then etched using Kroll reagent (2% HF, 92% H2O and 6% HNO3) for approximately 10 seconds before microstructural analysis using a SEM followed by an EDX. In-situ

phase identification was performed on the samples by X-ray diffractometer (XRD;AXRD, Proto) using Cu Kα radiation (λ = 1.5406˚A), and spectrums were collected by a fixed parameter of 0.02º step size and 1s time/step. Raman spectroscopy (Renishaw InVia Raman Microscope), a powerful non-destructive method used for characterising carbonaceous materials in terms of quality and structure, was used to confirm the presence of GNP in the HIPped composites with a 532nm wavelength, an acquisition time of 30 s and a x50 focus of. Four scans were conducted on each sample pre- and post-slide wear testing, to develop a comprehensive understanding of the GNP contribution to the improvement of composites wear resistance. The average grain size was determined, using image analysis software (ImageJ), by sampling and individually measuring 200 grains. The phase fractions of the α and β Ti, and *in situ* formed hard phases were also measured with ImageJ software on back-scattered electron (BSE) microscope images and using thresholding methods on grey scale images of the different phases in the micrographs.

4.2.4 Tribological and mechanical properties

The wear properties of the TMCs were studied using a sliding reciprocating machine with coefficient of friction (COF) recording capabilities. Wear tests were carried out at room temperature and the counter-body material used was Al_2O_3 balls with a diameter of 10 mm and a Vickers hardness value exceeding 1600HV. The Al_2O_3 balls were slide over polished flat specimens in a reciprocating motion using a load of 20N, sliding speed of 10mm/s, sliding distance of 5mm for a duration of 30 min. The worn surfaces were examined using SEM and EDX to understand the prominent wear mechanisms on the specimens. Furthermore, the wear depth was measured using an infinitefocus microscope, (Alicona). Micro-hardness of the TMCs was determined in order to understand the phase strengthening contribution of the composite's and their deformation patterns, using a micro-hardness tester (Wilson VH1202, Buehler). Using the smallest load of 10g, in order to indent individual phases, 100 small indents were made on a matrix of 0.2mm x 0.2mm. Furthermore, 10 large linear indentations were made with a 1kgf load, with recommended spacing according to ASTM E384-17, in order to obtain an average of the composite micro-hardness value.

4.2.5 Coefficient of thermal expansion

Cylinders with a diameter of 5mm and a height of 10mm were extracted from the HIPped canisters using EDM. The measurements for linear coefficient of thermal expansion were carried out using a dilatometer (Netzsch TMA 402 F1) at a temperature reaching 1000℃ with a 5℃/min heating rate. The furnace was set to rise from 30℃ to 200℃ at a rate of 5℃/min under a positive flow of nitrogen, held at 200℃ for 1h before being brought back to 30℃, again at a rate of 5℃/min.

4.3 Results and discussion

4.3.1 Powder characterisation

Figure 4.1a presents SEM micrographs of Ti64 (15-45µm) with an APS of 33µm. The powder is mostly spherical, but shows some satellites attached to it, particle breakage and irregular morphology, which are common features of the AGA method used to manufacture the powders. Figure 4.1b shows MA Ti64+1vol.%GNP using low-energy milling, with GNP seen to homogenously decorating the metal matrix, due to the MA method used, however there are a few GNP agglomerates associated with the high surface energy of the nanoplatelets. Figure 4.1c shows Ti64+2vol.%GNP with less agglomerations present and the reinforcement GNP are sticking and decorating the titanium matrix homogenously, exhibiting a strong interfacial bond. Figure 4.1d shows a micrograph of Ti64+ 1vol.% B with the reinforcement powder again decorating homogenously spread over the metal matrix. Figure 4.1e shows the micrograph of Ti64+1 vol% GNP + 1 vol.% B. Both the GNP and B are homogenously spread and decorating the Ti matrix. It is also important to note that the Ti64 powder morphology remains highly spherical due to the low-energy milling parameters and the 4:1 BPR used.

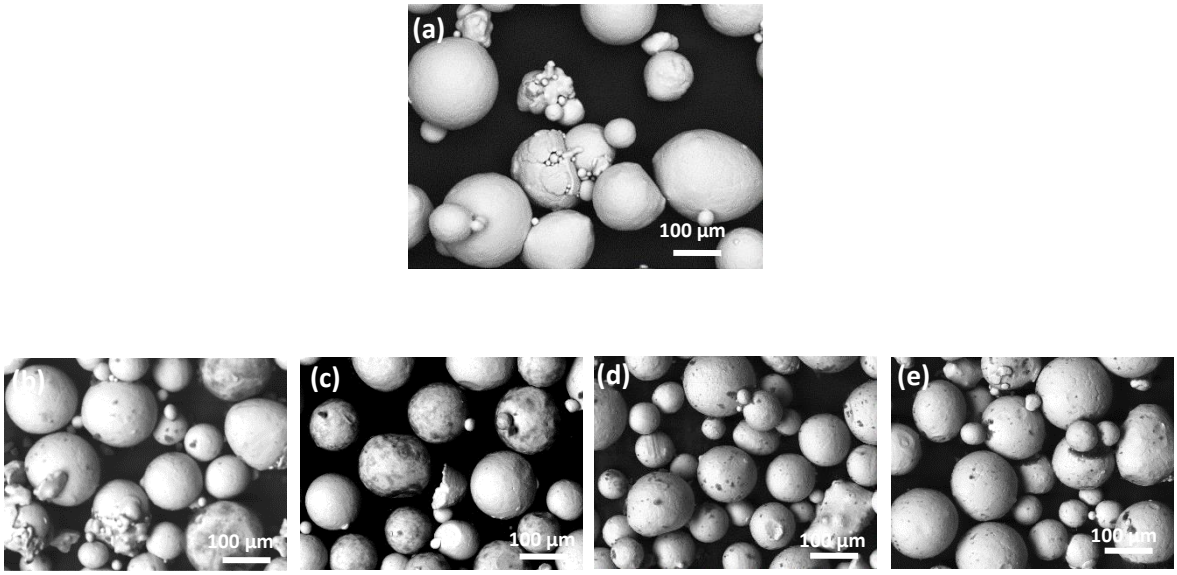

Figure 4.1*: SEM micrographs of as-received Ti64 powder (a) and MA powder (b-e).*
(a) Ti64, (b) Ti64 + 1 vol.% GNP, (c) Ti64 + 2 vol.% GNP, (d) Ti64 + 1 vol.% B, (e) Ti64 + 1 vol.% B+1 vol.% GNP

4.3.2 Microstructural evolution of in situ TMCs

4.3.2.1 Graphene characterisation

Figure 4.2 displays the Raman spectra of the as-received graphene powder. The D band present, known as the disorder or defect band, which is known to be extremely weak in graphite but has a strong intensity in graphene, confirmed the as-received powder was graphene. Furthermore, the number of defects is proportional to the intensity suggesting that the as-received graphene powder had a lot of defects. However, the 2D band visible, the second order of the D band, and is a strong visible band in graphene. Further confirmation is provided by the presence of the G band, that distinctively appears at 1587cm^{-1} as an in-plane vibrational mode of SP2 carbon [14].

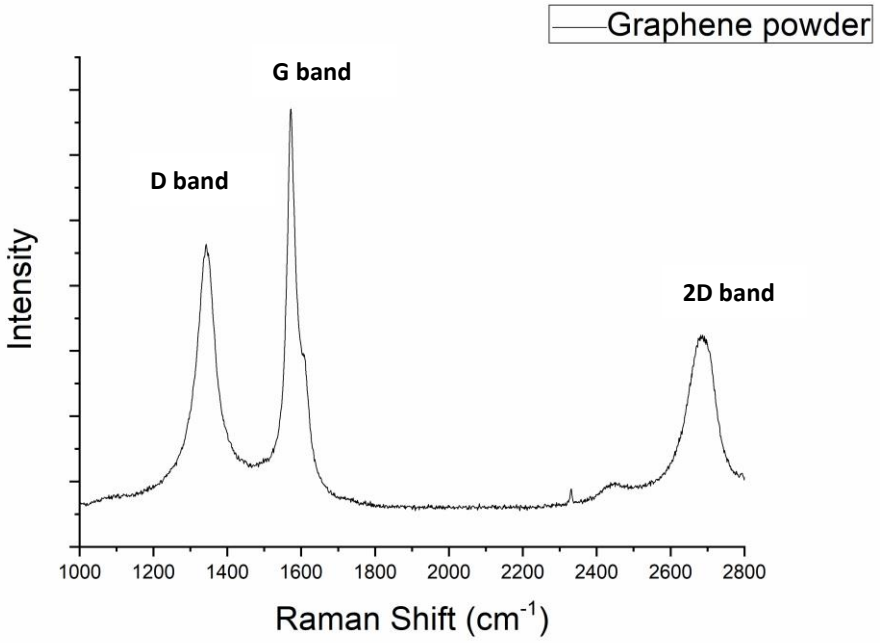

Figure 4.2*: Raman spectra of graphene powder*

4.3.2.2 X-ray diffraction (XRD) characterization

Figure 4.3 shows scans from the XRD analysis of the as-HIPped Ti64-GNP composites, which consists of α Ti, β Ti and TiC peaks and confirmed that an *in situ* reaction took place between the Ti matrix and graphene reinforcement resulting in the formation of a TiC phase at the HIP temperature of 1040°C. Furthermore, it is also clear that increasing the vol.% of GNP from 1-2 vol.% resulted in retaining a higher fraction of TiC phase.

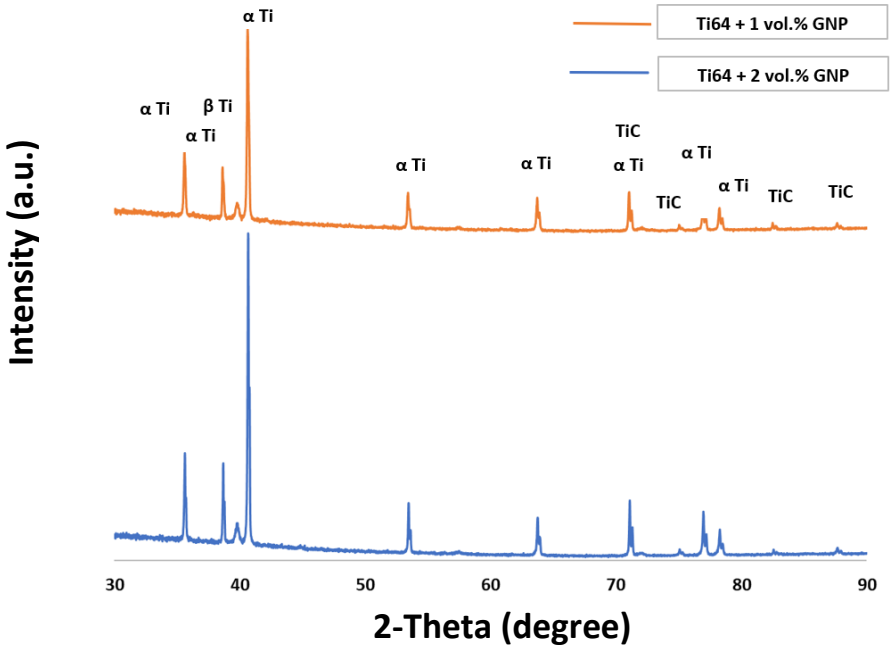

Figure 4.3*: XRD scans of Ti64 + 1 vol.% GNP and Ti64 + 2 vol.% GNP processed at 1040 ℃*

Figure 4.4 shows the scans for Ti64 + 1vol.% B and Ti64 + 1vol.% B + 1vol.% GNP composites, with both diffraction patterns displaying a dominant α-Ti intensity peak. From reviewing the scans, it can be seen that for Ti64 + 1vol.%B + 1vol.% GNP there is overlapping of some TiC peak with certain α-Ti peaks, due to carbon being an α stabiliser and diffusing into the titanium lattice structure. Furthermore, there is no indication of the any residual B, indicating that it was involved in a complete *in situ* reaction with the Ti matrix, resulting in TiB whiskers.

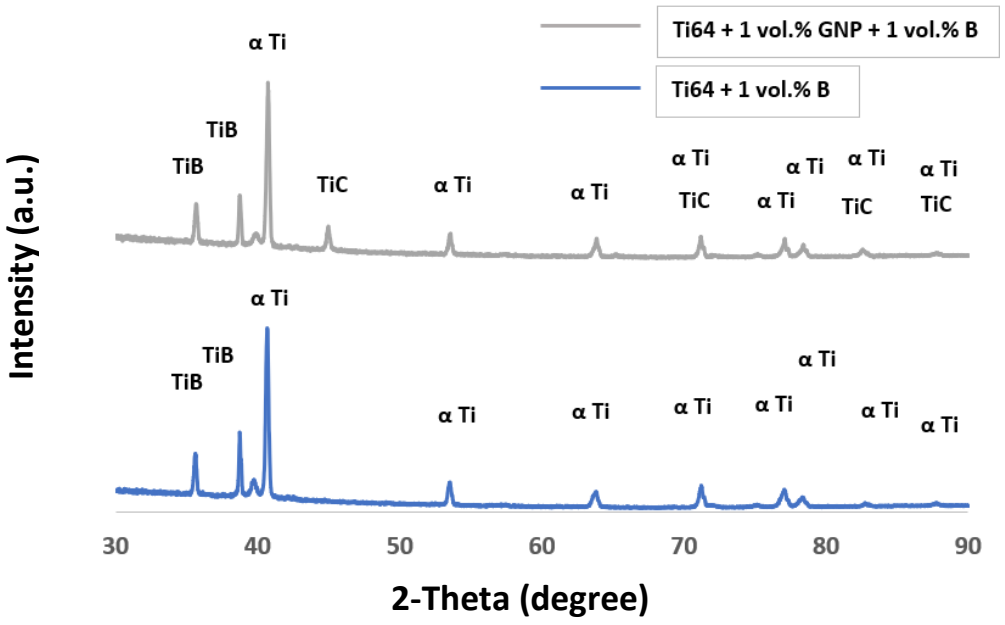

Figure 4.4: *XRD scans of Ti64+ 1 vol.% B and Ti64+ 1 vol.% B + 1 vol.% GNP processed at 1040 ℃*

4.3.2.3 influence of HIP temperature on phase formation

The micrographs in figure 4.5 reveal the influence of HIP temperature on the consolidation behaviour of the Ti64+ 1 vol.% GNP. Three HIP temperature conditions were selected sub-ß transus (920℃), (1040℃) and super-ß transus (1160℃). It is quite evident from large micron-sized porosities visible in figure 4.5a that the Ti64 + 1 vol% GNP HIPped at sub-ß transus temperature used in Ti64 lacks consolidation as shown by the. Furthermore, it is evident that an *in situ* reaction was taking place though it was incomplete in nature. Most of the graphene present was in sub-micron and nano-size ranges, which could be beneficial for enhanced mechanical properties. HIP at 920℃ kept the microstructural nature of Ti64 as the grain size is quite refined and small which is always beneficial for mechanical behaviour. Figure 4.5b shows the microstructural evolution of Ti64 + 1 vol.% GNP HIPped at 1040℃. Ti64 has a ß-transus temperature of 980℃ [20]. Oxygen is a well-known alpha stabiliser that raises the transformation temperature of Ti and is an interstitial that raises the strength but can be detrimental to the ductility and toughness. Based on assuming the O and C contents, the ß-transus temperature was estimated to be 1070℃, hence the reason for 1040℃ being selected as an optimal HIP temperature for this composite. At 1040℃ shown in figure 4.5b there is limited grain growth and the ß phase fraction has not increased significantly. Furthermore, an in-situ reaction took place between α-Ti and GNP to produce a fine hard TiC phase. In addition, figure 4.5c shows that a complete reaction took place between α-Ti and GNP to produce coarse TiC particles, due to HIP being conducted at higher than β-transus temperature.

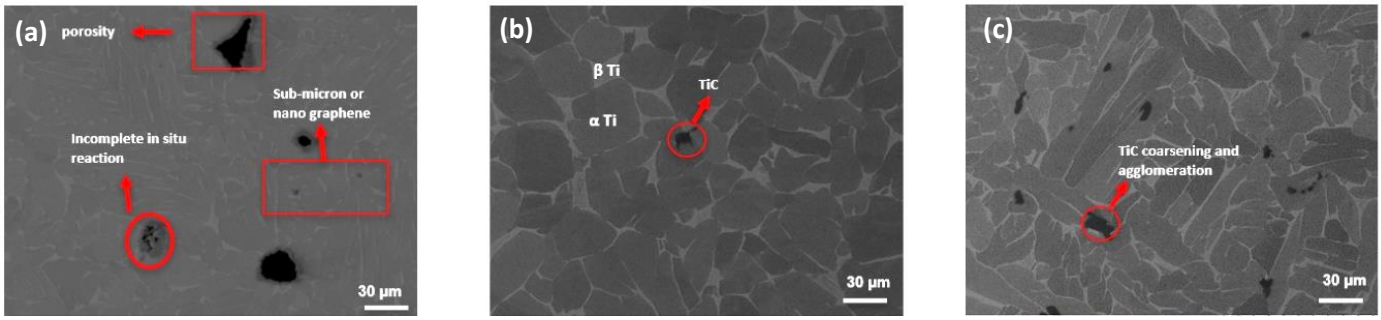

Figure 4.5*: Influence of HIP temperature on microstructural evolution of Ti64+ 1 vol.% GNP (a) 920 ℃, (b) 1040 ℃, (c) 1160 ℃*

4.3.2.4 Ti64 MMCs HIPped at 1040℃

Figure 4.6 shows the consolidation and microstructural evolution of as-HIPped composites processed at 1040℃. Figure 4.6a-b show the influence of different GNP volume fractions, 1 vol.% and 2 vol.%, on the microstructural evolution of the composites. Carbon is an α stabiliser and during the exothermic reaction the heat released was sufficient to convert Ti and C into the TiC. TiC phase is feasible as per the reaction shown below due to releasing a highly negative Gibbs free energy (ΔG) , as expressed in equation 5.1 [21].

$$Ti + C \longrightarrow TiC \ (\Delta G^{o} \text{ at } 1000\ K) = -150\ kJmol^{-1} \qquad (5.1)$$

Figure 4.6c shows the SEM micrograph of the TiB needles formed from the *in situ* reaction that took place between Ti-6Al-4V and B. Numerous studies have investigated the ΔG formation of TiB and concluded that it is highly negative, suggesting that an *in situ* reaction between Ti and B can proceed and form TiB if a high vol.% of B is present [22]. However, others have reported that the diffusion of B from TiB_2 to the Ti matrix can further facilitate the formation of TiB [23]. Furthermore, Figure 4.6c shows the hard and fine TiB phase decorating the prior particle boundaries (PPBs), while some neighbouring TiB coalesced at regions of agglomeration due to inhomogeneities in the blending method. Figure 4.5d shows the microstructure of Ti64 + 1 vol.% B + 1 vol.% GNP composite. In conclusion, an *in situ* reaction took place between the matrix and reinforcements resulted in two hard phases TiB and TiC, as expressed in equations 4 and 5.

$$Ti + 2B \longrightarrow TiB_2 \quad (\Delta G^{o} \text{ at } 1000\ K) = -308\ kJmol^{-1} \qquad (4)$$

$$TiB_2 + Ti \longrightarrow 2TiB \qquad (5)$$

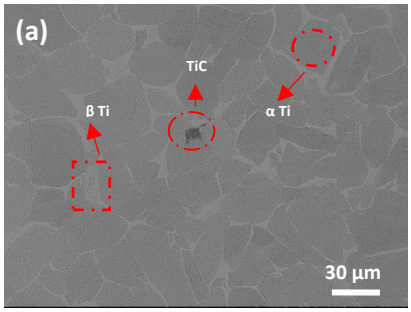

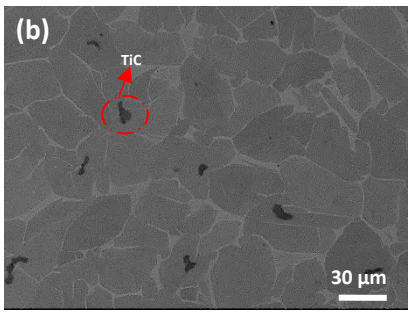

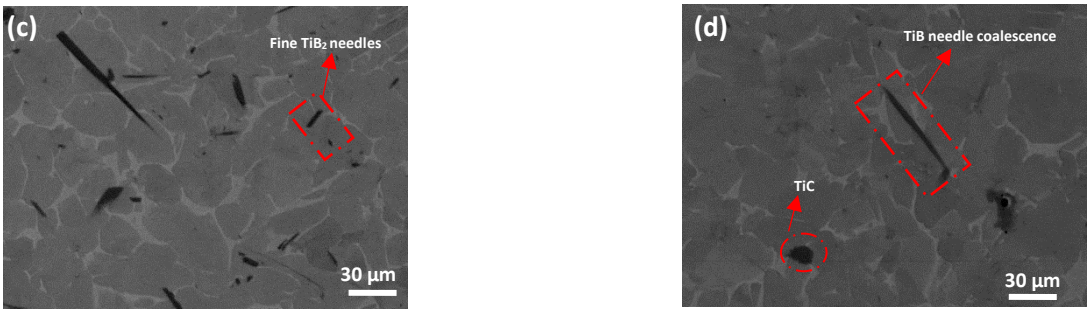

Figure 4.6*: SEM micrographs of as-HIP composites at 1040°C: (a) Ti64+1 vol.% GNP, (b) Ti64+2 vol.% GNP, (c) Ti64+1 vol.% B, (d) Ti64+ 1vol.% B + 1vol.% GNP*

Figure 4.7 shows the effect of HIP temperature on the grain growth of Ti64-GNP composites at 1vol.% GNP. There is a clear trend that as the HIP temperature was raised from the sub β-transus temperature (920°C) to super β-transus temperature of (1160°C) the level of grain growth in the α Ti platelets increased from 3.3µm to 8.1µm.

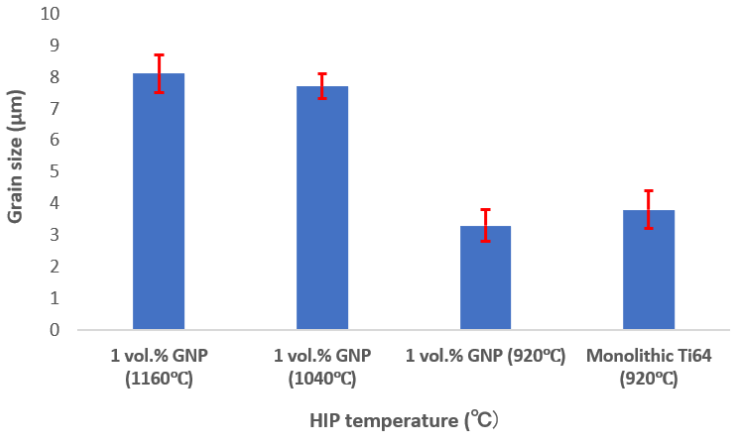

Figure 4.7*: Influence of HIP temperature on Ti64+ 1 vol.% GNP grain size*

Furthermore, figure 4.8 shows the influence of GNP vol.% in refining the microstructure. It is quite clear that as the vol.% of GNP increased from 1-2 vol.%, more *in situ* reaction took place between the reinforcement and matrix resulting in a higher volume of hard fine TiC precipitates, which impede grain growth, causing a grain size reduction from roughly 8µm to 6.2µm.

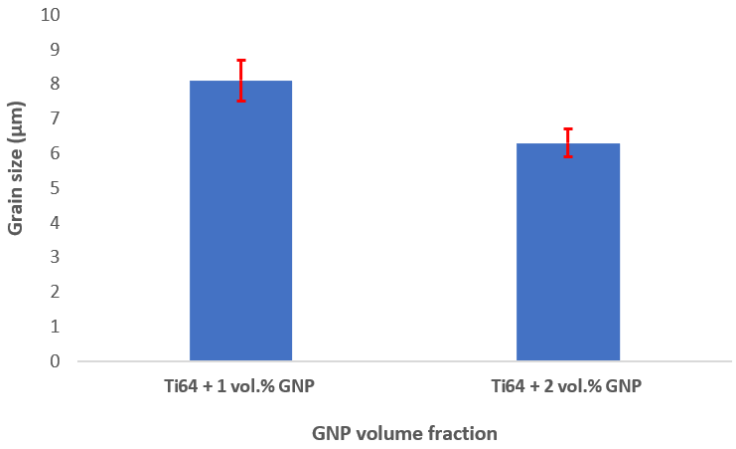

Figure 4.8: *Influence of GNP volume fraction on grain size processed at 1040°C*

Figure 4.9 shows the TMCs prepared by HIP at 1040°C, whereby there is a clear trend of grain size reduction with an increase in the vol.% of the reinforcement. The chart shows that Ti64+1vol.%GNP+1vol.%B further reduced the grain size from 6.3µm to 5.1µm in spite of the reinforcement volume fraction remaining constant at 2 vol.%. This could be attributed to the *in situ* formed TiC phase acting as obstacles for TiB growth, further refining the microstructural development. Bermingham et al. [24] suggested that B has a high growth restriction factor and helps reduce the α grain size.

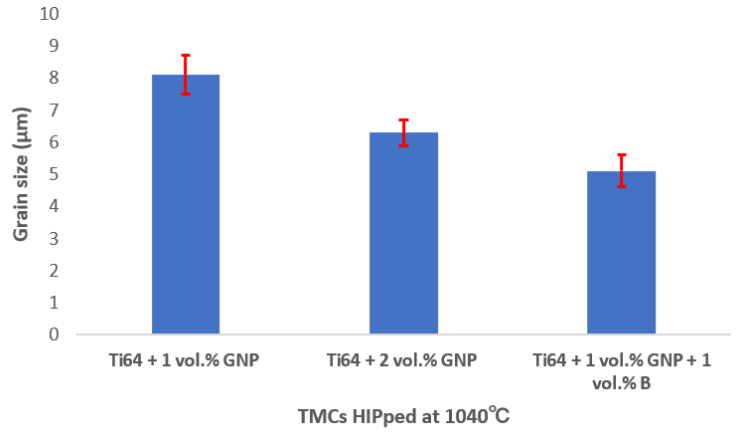

Figure 4.9: *Grain size of TMCs HIPped at 1040°C*

Figure 4.10 shows image analysis of the *in situ* HIPped TMCs at 1040°C. This was used to quantify the different phase fractions formed during HIP from the elemental powders used. α-Ti, β-Ti, TiC and TiB were all quantified in order to be used in structure-property relations and help predict TMC properties. The red colour thresholding highlights the phase as indicated by the label on each individual image. For example, in Figure 4.1b, it corresponds to TiB phase and so on. In figures 4.10a-10d image analysis of Ti64+1vol.%B TMC is shown. The yielded phase fraction of TiB (figure 4.10b) was 1.24%, for α-Ti it was 86.99% (figure 4.10c) and for β-Ti was 11.77% (figure 4.10d). Figures 4.10e-h shows the image analysis of Ti64+1vol.% GNP TMC. The yield TiC phase is 1.02%, α-Ti is 87.95% and β-Ti is 11.03%. Figures 4.10i-l shows the analysis of Ti64+ 2vol.% GNP TMC. The phases formed yielded 2.08% TiC, 84.67% α-Ti and 13.25% β-Ti. The reason the α-Ti phase of the Ti64+2 vol.% GNP is less than the TMC with 1 vol.% GNP is due to C being an α stabilizing element that reacts with the α-Ti matrix, resulting in more TiC phase and due to the higher starting vol.% of GNP used.

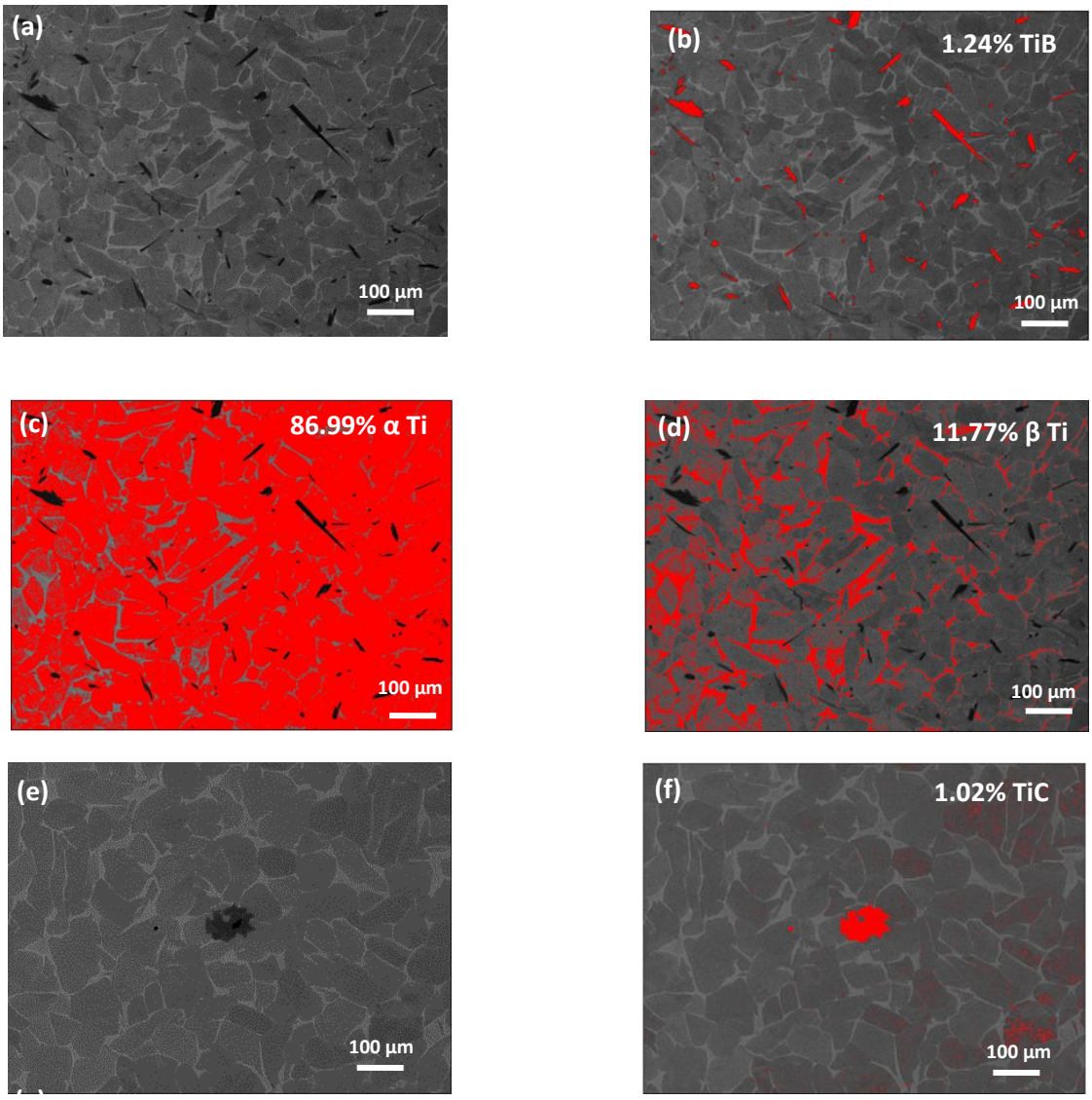

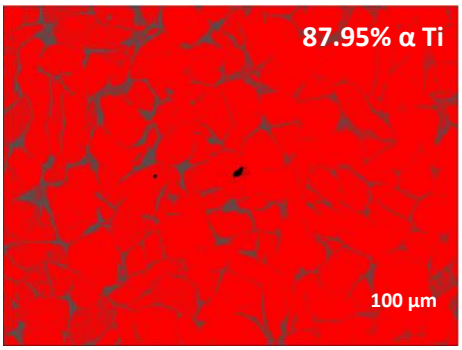
87.95% α Ti
100 µm

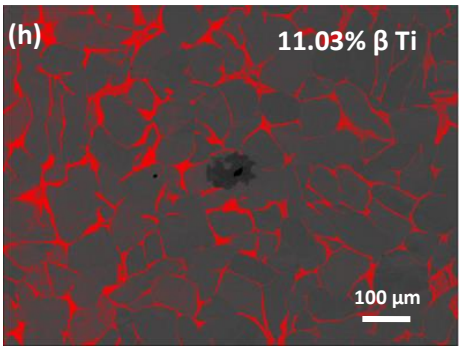
(h)
11.03% β Ti
100 µm

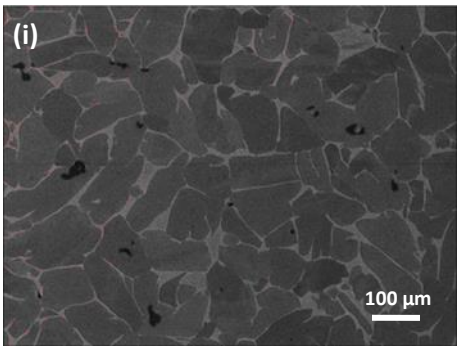
(i)
100 µm

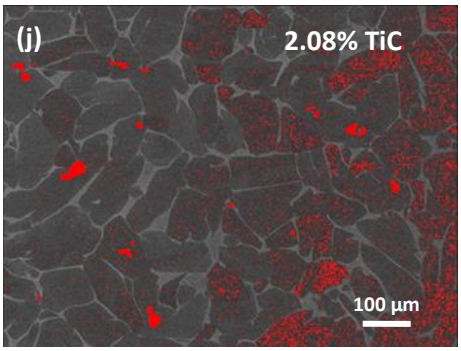
(j)
2.08% TiC
100 µm

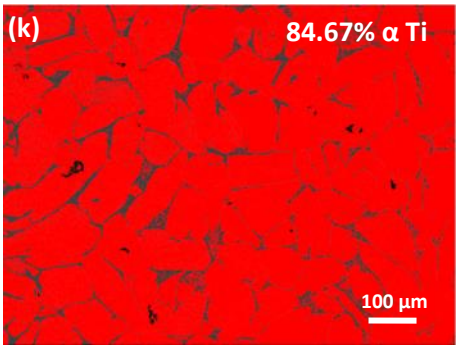
(k)
84.67% α Ti
100 µm

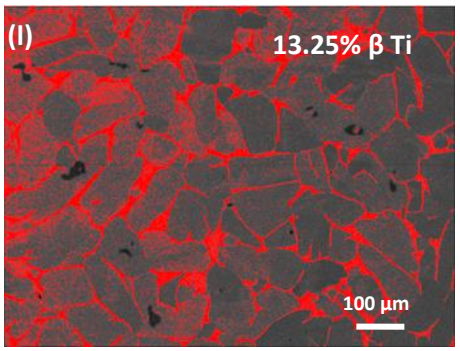
(l)
13.25% β Ti
100 µm

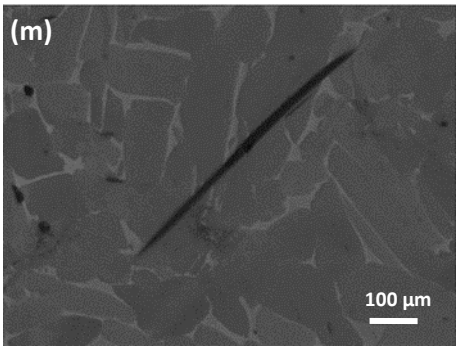
(m)
100 µm

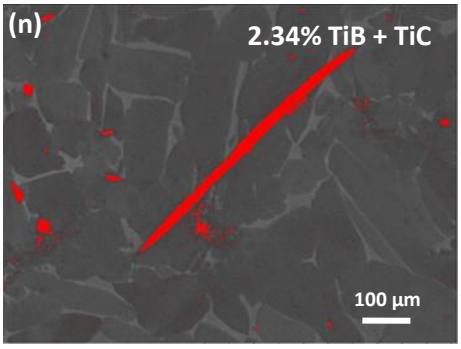
(n)
2.34% TiB + TiC
100 µm

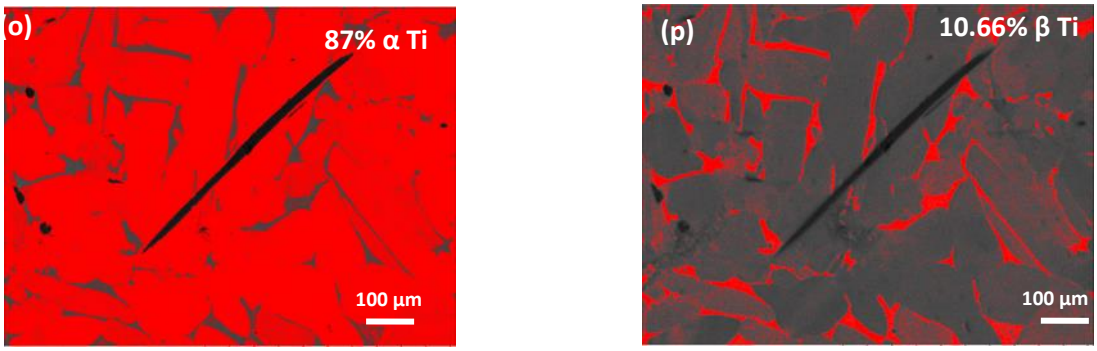

Figure 4.10: *Image Analysis of as-HIP TMCs at 1040°C: (a-d) Ti64 + 1 vol.% B, (e-h) Ti64 + 1 vol.% GNP, (i-l) Ti64 + 2 vol.% GNP, (m-p) Ti64 + 1 vol.% B + 1 vol.% GNP*

Table 4.1 *Phase fractions of as-HIPped TMCs from Image Analysis*

TMC	α Ti (%)	β Ti (%)	TiC (%)	TiB (%)
Ti64 + 1 vol.% GNP	**87.95**	**11.03**	**1.02**	-
Ti64 + 2 vol.% GNP	**84.67**	**13.25**	**2.08**	-
Ti64 + 1 vol.% B	**86.39**	**11.77**	-	**1.84**
Ti64 + 1 vol.% B + 1 vol.% GNP	**87.00**	**10.66**	**2.34 total TiB and TiC phases**	

Table 4.1 shows the phase fractions collected from image analysis using ImageJ, which will aid in the structure-property relations calculated.

4.3.3 Mechanical properties

4.3.3.1 Micro-hardness

Figure 4.11a shows the micro-hardness as a function of GNP vol.% processed at 1040°C. As the volume fraction of the reinforcement increased from 1 vol.% to 2 vol.%, there is a clear trend of increasing micro-hardness from 350 HV to 380HV., which could be attributed to the hardening effect induced by the increase in TiC phase content. Furthermore, load-transfer mechanism plays an important role in

transferring the load from a soft metallic matrix to a harder phase. It is important to note that the load-transfer mechanism is heavily sensitive to a change in reinforcement volume fraction. Figure 4.11b shows micro-hardness of Ti64+1vol.% GNP prepared at different HIP temperatures ranging from sub β-transus to super β-transus. HIP at 920°C (sub β-transus) resulted in a micro-hardness gain of 1.5%,very close to that of wrought Ti64, suggesting that the *in situ* reaction was incomplete and did not result in the harder TiC phase. However, Ti64+1vol.% GNP HIP at 1040°C resulted in a 5.5% micro-hardness gain, due to more diffusion taking place and a highly negative Gibbs-free energy resulting in TiC phase formation, which is agreement with the SEM micrographs seen in figure 4.6a. Finally, the TMC HIP at the super-transus condition of 1160°C resulted in the highest micro-hardness increase of approximately 7.8% due to more TiC phase formation taking place and a complete in-situ reaction.

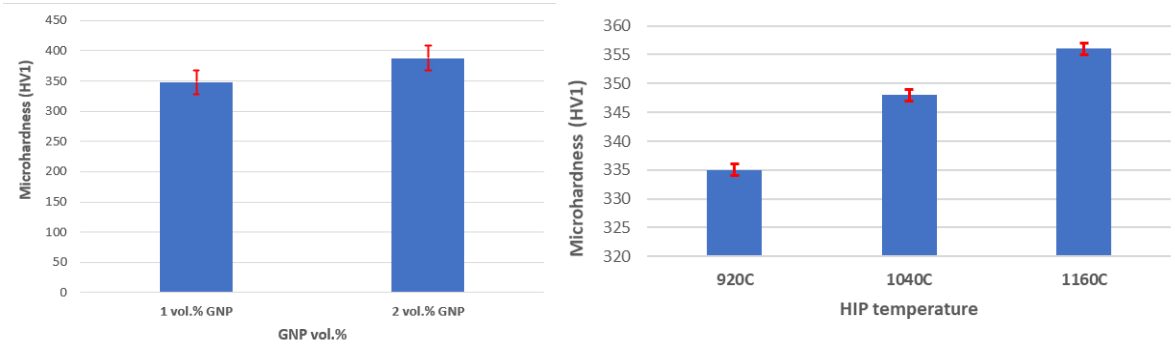

Figure 4.11: *(a) Micro-hardness as a function of GNP vol.%, (b) Microhardness as function of HIP temperature for Ti64+ 1vol.% GNP*

4.3.3.2 Micro-hardness structure relations

Figure 4.12 shows the micro-hardness structure relations of the different TMCs. Experimental micro-hardness data were compared to theoretical micro-hardness values. In order to theoretically predict the micro-hardness of the TMCs based on the phase fractions obtained from image analysis in Figure 4.10 and table 4.1, the rule of mixture (ROM) based on the Reus model was used [28], which takes into account the effective hardness of a composite that corresponds to a soft matrix surrounded by a stiffer reinforcement phase , as expressed in equation 6.1 [25], where f_h and H_h are the volume fraction and hardness of the harder phase, respectively, and f_s and H_s are the volume fraction and hardness of the softer phase, respectively. However, it does not take into account chemical in situ reactions.

$$H_{low} = (\frac{f_h}{H_h} + \frac{f_s}{H_s})^{-1} \qquad (6.1)$$

In figure 4.12, the Ti64+1 vol.% GNP experimental value is slightly lower than the theoretical value calculated using the ROM, could be due to the homogeneity of the TMC, as seen in figure 4.6a, resulting from the powder mixing method, whereby the graphene was not homogenously attached to the matrix powder, as seen in figure 4.1d. By increasing the volume fraction to 2 vol.%, the experimental and theoretical values are in closer agreement, as the microstructure was more homogenous and the soft Ti64 matrix surrounded by the harder TiC phase, validating the use of the Reus model [25]. Furthermore, the Ti64 + 1 vol.% B TMC theoretical value is slightly higher than the experimental value, which again can be rationalised in terms of revisiting the microstructure in figure 4.6c. The microstructure is homogenous; however, some regions are richer in TiB phase while others are lean In addition to that, some regions agglomeration of B took place, which could explain why some areas of the microstructure neighbouring TiB needles were coalescing and strengthening some regions more than others. Finally, the Ti64 + 1vol.% B + 1 vol.% GNP theoretical and experimental micro-hardness values are very close, which shows that the model used works better at higher volume fractions, due to potentially more of the harder phase is surrounding the softer matrix.

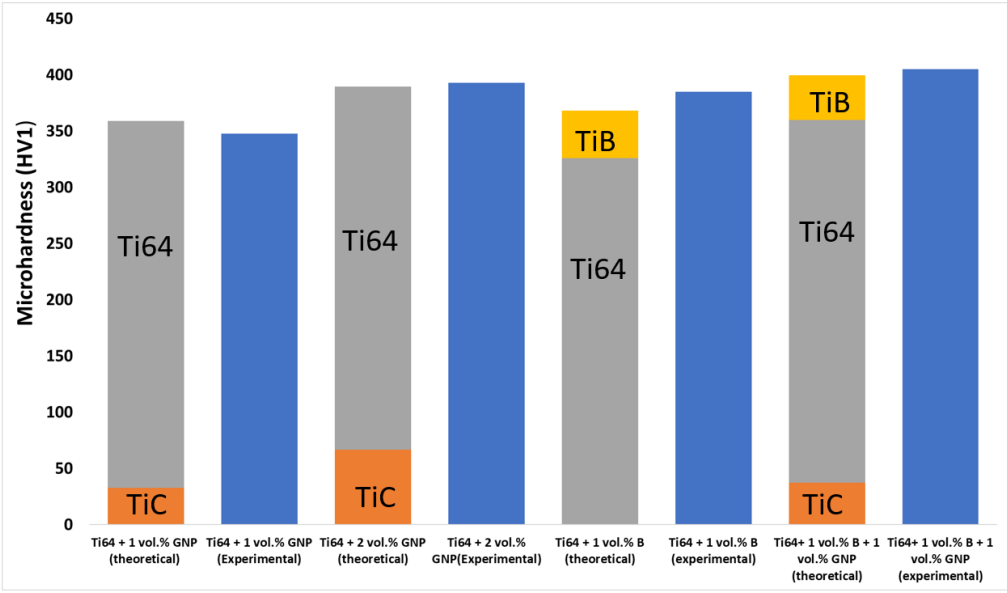

Figure 4.12: *Micro-hardness structure-property relations for different TMCs theoretical and experimental values*

4.3.3.3 Micro-hardness maps for TMCs

Vickers micro-hardness maps for different TMCs are presented in figure 4.13, conducted on a matrix of 7 x 9 with a load of 10g in order to hit the different *in situ* phases below. Figure 4.13a shows the indentations of the Ti64+1vol.% B and its corresponding micro-hardness map. It is quite clear that the heterogeneous spread of micro-hardness of the dependent on the reinforcement distribution along the matrix. It can be seen that the areas that contribute the highest micro-hardness are the regions of the matrix that are surrounded by the harder TiB phase, resulting in smaller indentations. Figure 4.1b shows the indentations of the Ti64+1vol.%B+1vol.% GNP and its corresponding micro-hardness map. It is visible from the map that the upper half of the indentations are more homogenous in terms of micro-hardness compared to the lower half, which can be rationalised and attributed to the phase distribution. The indentations that hit the hard phase, or are in close proximity to it, exhibit the highest micro-hardness readings due to the TiB and TiC phase and their high density in relation to Ti64. Figure 4.1c shows the indentation matrix and the corresponding map for the Ti64+1vol.% GNP TMC. It can be seen that the micro-hardness distribution is heterogeneous as some regions are lean in TiC phase, while other regions are rich. Finally, figure 4.13d displays the Ti64+2 vol.% GNP TMC, showing a wide range of micro-hardness readings depending on which phases the indentations hit. It can be seen from the micrograph that the regions of coalescence of neighbouring TiC particles resulted in the highest micro-hardness as indicated by the yellow and red map colour codes.

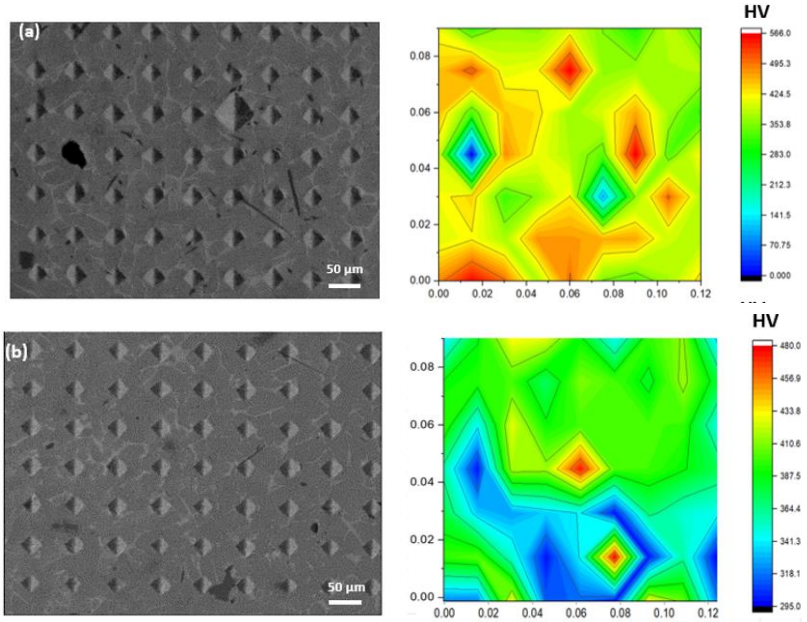

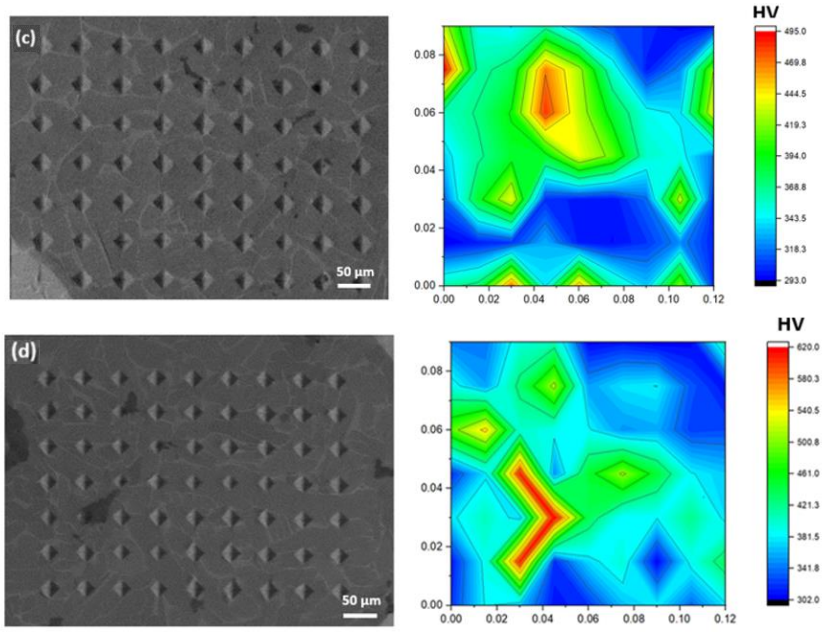

Figure 4.13: *Micro-hardness distribution profiles of in situ TMCs synthesized via HIP: (a) Ti64 + 1 vol.% B, (b) Ti64 + 1 vol.% B + 1 vol.% GNP, (c) Ti64 + 1 vol.% GNP, (d) Ti64 + 2 vol.% GNP*

4.3.3.4 CTE measurements

The CTE results of the TMCs processed at 1040 °C were conducted at a temperature up to 180°C. The plots in figure 4.14 as change of length over original length as a percentage as a function of temperature.

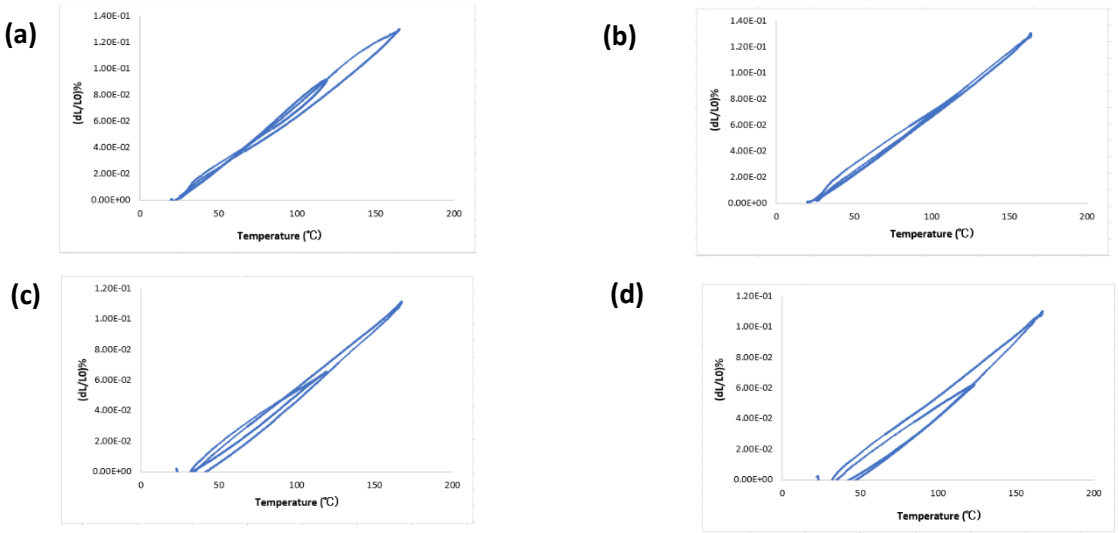

(e)

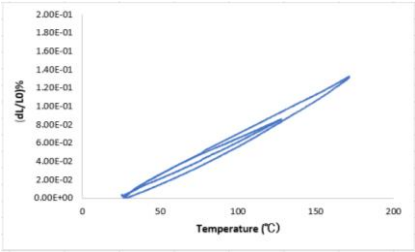

Figure 4.14: *CTE measurements for TMCs processed at 1040°C: (a) Ti64, (b) Ti64 + 1 vol.% B, (c) Ti64 + 1 vol.% GNP, (d) Ti64 + 2 vol.% GNP, (e) Ti64 + 1 vol.% B + 1 vol.% GNP*

Table 4.2 *CTE measurements of TMCs*

TMC	CTE value
Ti64	$9.1 \times 10^{-6} °C^{-1} \pm 0.2$
Ti64 + 1 vol.% B	$9.06 \times 10^{-6} °C^{-1} \pm 0.1$
Ti64 + 1 vol.% GNP	$7.93 \times 10^{-6} °C^{-1} \pm 0.2$
Ti64 + 2 vol.% GNP	$7.72 \times 10^{-6} °C^{-1} \pm 0.1$
Ti64 + 1 vol.% GNP + 1 vol.% B	$8.53 \times 10^{-6} °C^{-1} \pm 0.1$

The CTE of monolithic Ti64 was measured as 9.1 x 10^{-6}°C^{-1} which is within the range of acceptable CTE for the alloy (8.7-9.1 x 10^{-6}°C^{-1}) [26]. Adding 1 vol.% B reduced the COF to 9.06 x 10^{-6}°C^{-1} due to the *in situ* formation of the TiB phase, which has a CTE value of 8.6 x 10^{-6}°C^{-1}, similar to the theoretical value of 8.8 x 10^{-6}°C^{-1} calculated using the Kerner ROM equation . On the other hand, reinforcing Ti64 matrix with GNP seems to have a more positive effect in lowering the CTE values. The *in situ* formed TiC phase is known to have a CTE value of 6.52 x1 0^{-6}-7.12 x 10^{-6}°C^{-1} at the temperature ranges of (25-500°C), hence why the measured CTE for the TMC with 1 vol.% GNP was 7.93 x 10^{-6}°C^{-1} (the theoretical value calculated using the Kerner model is 7.81 x 10^{-6}°C^{-1}). Increasing the vol.% of GNP to 2 vol.% reduced the CTE value further to 7.72 x 10^{-6}°C^{-1} due to the higher retained vol.% of the TiC phase. Finally, the Ti64 reinforced with 1 vol.% GNP and 1 vol.% B has a measured CTE of 8.53 x 10^{-6}°C^{-1} (theoretical value of 8.3 x 10^{-6}°C^{-1}) due to the TiB and TiC phase being present. It can be concluded that *in situ* formed TiC from GNP are ideal for reducing the CTE of TMCs in accordance with the modified ROM Kerner model. It should be noted that all the CTE readings were taken at a constant temperature range of 35-110°C as values will slightly change with varying temperature ranges. Table 4.2 shows a summary of the CTE measurements of the TMCs discussed above.

4.3.4 Tribological properties

4.3.4.1 Worn surfaces

Figure 4.15 shows the morphologies of the worn surfaces of all the TMCs. Generally speaking, they all displayed rough surfaces with deep ploughed grooves and parallel furrows, caused by the hard Al_2O_3 counter-body and the detached debris resulting in three-body-abrasive wear during reciprocating motion of the ball. This suggests that plastic deformation due to the abrasive nature of the wear mechanism is dominant during friction. It should be noted that increasing the vol.% of the reinforcement phase, should cause the number of furrows and wear debris to decrease. However, increasing the vol.% of GNP from 1-2 vol.% (figures 4.15a-b,)resulted in more wear debris being present, but there are no deep ploughed grooves visible. This implies that the increase in micro-hardness in the Ti64 + 2 vol.% GNP TMC helps resist abrasive wear more than the TMC with 1 vol.% GNP. In figure 4.16c, Ti64 + 1 vol.% B TMC worn surface is shown, with deep ploughed grooves, micro-cracks and wear debris clearly visible, but to lesser extent than with the Ti64 + 1 vol.% GNP TMC. Since both vol.% are the same, the reason for the improved wear resistance could be attributed to a stronger interfacial bonding between the *in situ* formed TiB and Ti matrix, as well as the higher micro-hardness displayed by the Ti64 + 1 vol.% B TMC, making it more resistant to abrasion. Lastly, figure 4.15d shows the worn surface track of Ti64 + 1 vol.% B + 1 vol.% GNP TMC. It exhibits far less wear debris and abrasive wear features compared to any other TMC shown in figure 4.15. This is due to the two *in situ* formed nano sized phases TiB and TiC, resulting in superior wear performance reduced abrasive wear mechanisms, such as micro-cutting and sub-surface crack initiation, due to the nano formed phases inhibiting grain growth and ultimately having better interfacial bonding, while having a more efficient load transfer to two harder phases.

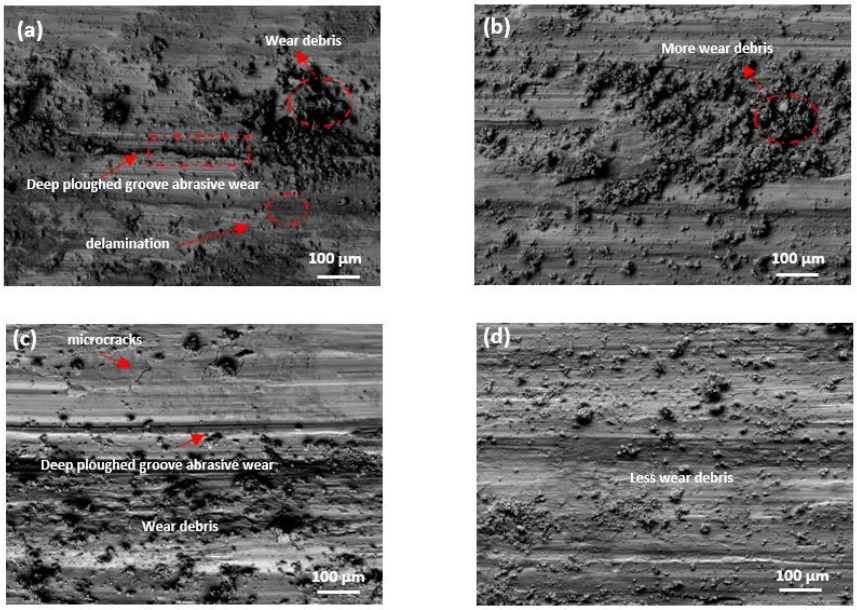

Figure 4.15: micrographs of worn surfaces *(a) Ti64 + 1 vol.% GNP, (b) Ti64 + 2 vol.% GNP, (c) Ti64 + 1 vol.% B, (d) Ti64 + 1 vol.% B + 1 vol.% GNP*

4.3.4.2 COF

Figure 4.16 shows the COF readings of the different as-HIPped TMCs. Generally speaking, the COF values kept rising as the wear test initiated until it reached a maximum value and then stabilised. This is attributed to something known as the break in period and the surface roughness of the TMCs at the preliminary sliding stage [27]. It is also well known that COF= τ_s/H_b, whereby τ_s is surface shear strength (variable) and H_b bulk hardness (constant). The surface shear strength is dependent on the contact area of the counter-body, which in this study was Al_2O_3 balls, and the TMC its reciprocating on. According to the literature the shear strength of the surface increases with an increase in contact area, [28]. It can be seen in figure 4.16 that increasing the vol.% of GNP from 1-2 vol.% after the break-in period, causes the value of COF to stabilise with less fluctuation than the sample containing 1 vol.% GNP. It can therefore be concluded that the delaminated regions of GNP on the surface help reduce the COF value due to the lubrication and sliding-like properties of graphene, improving the tribological performance. It can also be seen in figure 4.16 that the TMC containing 1 vol.% B had the highest and most unstable COF value, which could be attributed to the low vol.% of B used, and the micro-hardness contribution of TiB phase did not provide much strengthening compared to monolithic Ti64.

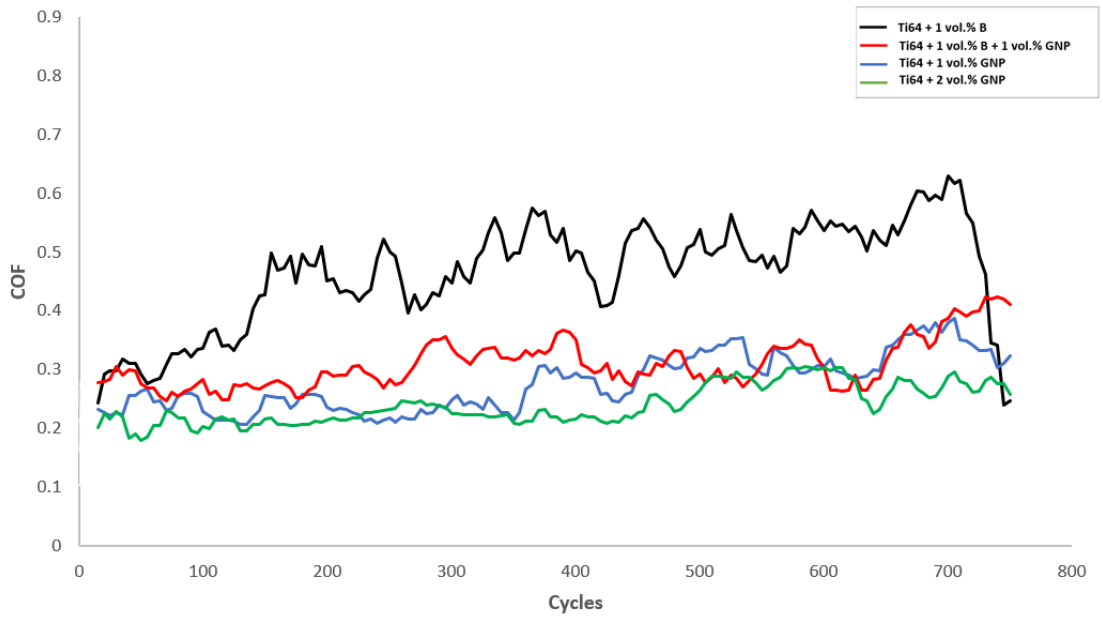

Figure 4.16: *COF readings of different TMCs*

4.3.4.3 Wear maps

Figure 4.17 shows wear maps obtained for the TMCs after wear testing using Alicona. It can be clearly seen that increasing the vol.% of GNP from 1 vol.% to 2 vol.% reduced the wear depth, which is in agreement wear track morphologies and micro-hardness data presented in figure 4.1. Ti64 + 1 vol.% B had the lowest micro-hardness reading and the most abrasive wear features as seen from Figure 16c, which is in agreement with the Alicona map shown in figure 4.17c. It can be seen from the Alicona map that most of the regions of the wear surface are heavily worn corresponding to more depth, indicated by the colour codes. Lastly, figure 4.17d shows Ti64 + 1 vol.% B + 1 vol.% GNP, where it is visible there is less wear depth, hence wear rate in comparison to figure 4.17c. On the other hand, in correspondence with the COF data, the wear of the Ti64 + 1 vol.% B + 1 vol.% GNP was higher than Ti64 + 2 vol.% GNP even though the micro-hardness of Ti64 + 1 vol.% B + 1 vol.% GNP was higher. It is therefore concluded that the TiB phase formed from B (1µm) does not provide much strengthening effect compared to TiC nor strong enough interfacial bonding, resulting in delamination and abrasive wear mechanisms taking place.

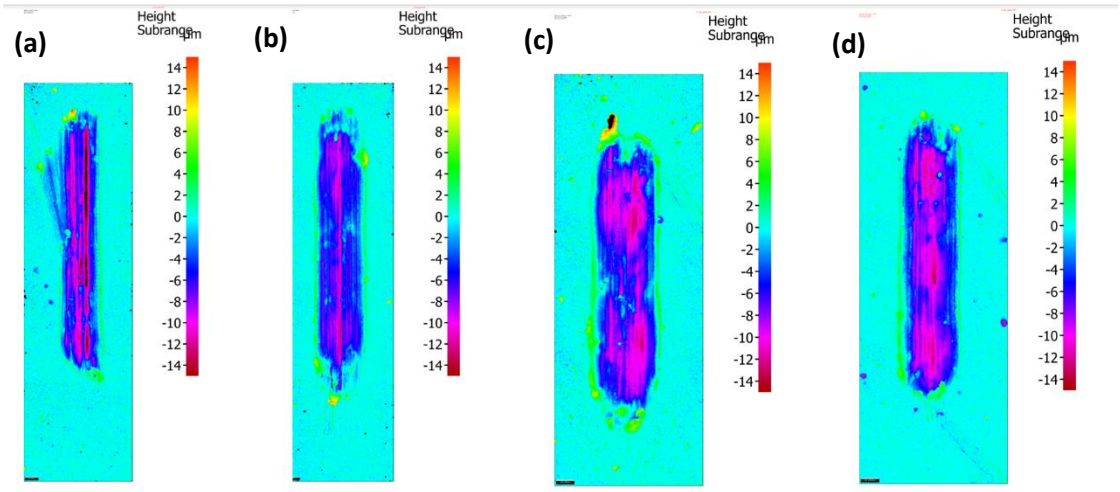

Figure 4.17: *Alicona maps of worn surfaces: (a) Ti64 + 1 vol.% GNP, (b) Ti64 + 2 vol.% GNP, (c) Ti64 + 1 vol.% B, (d) Ti64 + 1 vol.% B + 1 vol.% GNP*

Figure 4.18 shows the wear rate of the composites. The volume loss was analysed using the Alicona optical profilometer. The data of the wear rate is in agreement with the worn surfaces shown in figure 17 above and the COF data plotted in figure 4.16. The wear rate data is also in alignment with the micro-hardness data as shown in figure 4.12. The main reason for a decrease in wear rate could be attributed to an increase in the reinforcement vol.% and *in situ* formed TiC phase, and the lubricating effect of the un-reacted GNP.

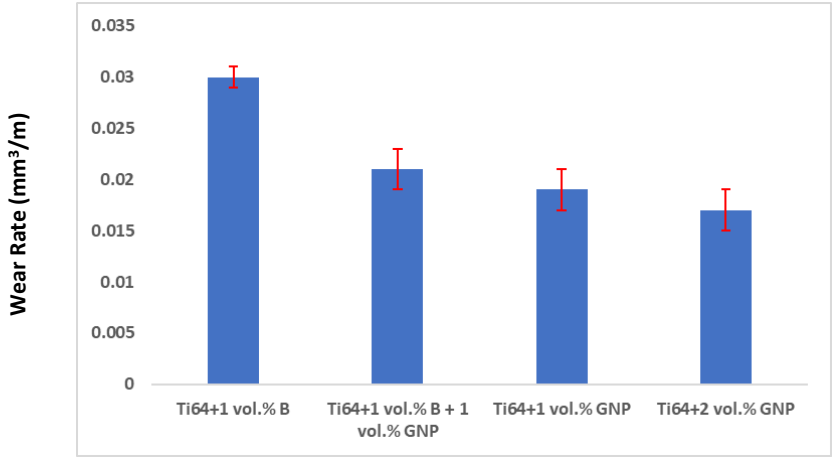

Figure 4.18: *Wear rate of as-HIPped composites*

4.3.4.4 Raman spectra of worn surfaces

The worn surfaces of the TMCs containing GNP were analysed before and after the wear tests in order to understand how graphene influences the wear resistance. figure 4.19a shows the Raman spectra of Ti64 + 1 vol.% GNP before and after wear, while figure 4.19b shows the Raman spectra of Ti64 + 2 vol.% GNP before and after wear testing. It can be seen in figure 4.19a that the (2D and G) peaks of graphene are much lower compared to pre-wear test analysis, suggesting that the structure of GNP was destroyed during the wear test. It is known that GNP exhibit extremely high flexural strength and it is assumed that they will bend and tilt towards the surface of the composite under the contact of a load and help lubricate the surface, hence the lower COF values seen in Figure 16. In addition, the before wear image (figure 19b) exhibits higher (2D and G) peaks in comparison to figure 4.19a, suggesting that there was a higher retention of GNP due to the higher vol.% used, with not all the GNP reacting *in situ* to produce TiC precipitates. Again, it can be seen that the (2D and G) peaks after wear test is far lower suggesting that the graphene on the surface was acting as a lubricant.

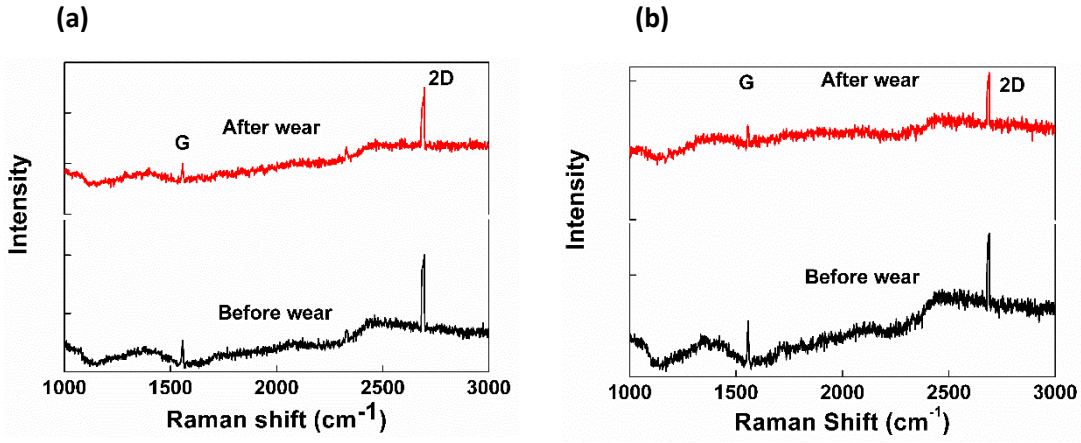

Figure 4.19: *Raman spectra of worn surfaces: (a) Ti64 + 1 vol.% GNP, (b) Ti64 + 2 vol.% GNP*

4.4 Conclusions

The aim of this study was to develop TMCs by way of *in situ* reactions using reinforcements such as B and GNP with differing vol.% and analyse them for their potential use in high wear resistance applications, as well as tackle the main challenges of fabrication, such as the homogeneity of the blended powders and dispersion the reinforcement in the matrix. The formation of hard phases by way of *in situ* reactions during HIP and their influence on the tribological performance of the TMCs investigated. Furthermore, an attempt to understand how different HIP conditions above and below the β-transus temperatures that affected the completion of the *in situ* reactions, consolidation behaviour and microstructure. Finally, structure-property modelling was conducted to see whether it was possible to predict the behaviour of the advanced TMCs using the ROM and test the validity of the equations. The conclusions are as follows:

(2) Raising the vol.% of GNP increased the micro-hardness due to load transfer mechanism and higher retention of TiC phase.

(3) HIPping at 1160^{o}C ensured full consolidation, but resulted in grain growth, while HIPping at 920^{o}C there was lack of consolidation and no *in situ* reaction. At 1040^{o}C there was retention of TiC phase with some unreacted graphene, which improved tribological performance.

(4) Raising the vol.% of GNP reduces the COF due to an increase in micro-hardness and a higher GNP content at the surface of the composite lubricating the surface

(5) The theoretical micro-hardness values were generally in agreement with the experimental micro-hardness values, hence validating the equations

(6) Ti64 +1 vol.% B + 1 vol.% GNP TMC had the highest measured micro-hardness and least abrasive wear features, as shown by the worn surface micrographs. However, TMCs reinforced with graphene had better wear resistance due to the lubricating properties of GNP.

(7) Ti64 with 2 vol.% GNP has the lowest CTE measurement in comparison with Ti64 with 1 vol.% B + 1 vol.% GNP and other reinforcements, due to the higher retention of *in situ* formed TiC phase.

(8) The experimental and theoretical values of CTE were generally in agreement, validating the modified ROM Kerner model.

Acknowledgements

The authors acknowledge the Centre of Doctoral Training in Innovative Metal Processing (IMPaCT), funded by the Engineering and Physical Sciences Research Council (EPSRC), and the National Structural Integrity Research Centre (NSIRC), for funding this PhD at the University of Birmingham.

References

[1] L. Cai, Y. Zhang, L. Shi, H. Yang, M. Xi., (2006) 'Research on development of *in situ* titanium matrix composites and *in situ* reaction thermodynamics of the reaction systems', Jou*rnal of University of Science and Technology Beijing*, 13, pp. 551.

[2] C. Cai, B. Song, C. Qiu, L. Li, P. Xue, Q. Wei, J. Zhou, H. Nan, H. Chen, Y. Shi., *Hot isostatic pressing of in-situ TiB/Ti-6Al-4V composites with novel reinforcement architecture, enhanced hardness and elevated tribological properties*. Journal of Alloys and Compounds, vol.710, 2017, pp. 364-374

[3] K. Kondoh, T. Threrujirapapong, H. Imai, J. Umeda, B. Fugetsu., *Characteristics of powder metallurgy pure titanium matrix composite reinforced with multi-wall carbon nanotubes*, Compos.Sci. Technol. vol.69, 2009, pp.1077-1081

[4] S. Li, B. Sun, H. Imai, T. Mimoto, K. Kondoh., *Powder metallurgy titanium metal matrix composites reinforced with carbon nanotubes and graphite*, Compos. Part A. vol.48, 2013, pp.57-66

[5] S. Gorsse, D.B Miracle., *Mechanical properties of Ti-6Al-4V/TiB composites with randomly oriented and aligned TiB reinforcements,* Acta Ma*terialia.* Vol.59(9)*,* 2003, pp.2427-2442

[6] C. Poletti, M. Balog, T. Schubert, V. Liedtke, C. Edtmaier., *Production of titanium matrix composites reinforced with SiC particles,* Compos.Sci.Technol. vol.68, 2008, pp.2171-2177

[7] D. Liu, S.Q. Zhang, A. Li, H.M. Wang., *Microstructure and tensile properties of laser melting deposited TiC/TA15 titanium matrix composites,* J. Alloys Compd. vol.485, 2009, pp.156-162

[8] F. Zhang, S. Liu, P. Zhao, T. Liu, J. Sun., *Titanium/nanodiamond nanocomposites: Effect of nanodiamond on microstructure and mechanical properties of titanium,* Mater. Des. vol.131, 2017, pp.144-155

[9] Cao, Z., Li, Jl., Zhang, Hp., *Mechanical and tribological properties of graphene nanoplatelets-reinforced titanium composites fabricated by powder metallurgy*, J. Iron Steel Res. Int. 2020

[10] K.Kondoh, *Titanium metal matrix composites by powder metallurgy (PM) routes,* Science, technology and Applications, 2015, pp.277-297

[11] P.B Joshi, G.R Marathe, N.S.S Murti, V.K Kaushik, P. Ramakrishnan, *Reactive synthesis of titanium matrix composite powders,* Muter.LRtt., vol.56, 2002, p.322

[12] Ö. Güler, N. Bağcı., *A short review on mechanical properties of graphene reinforced metal matrix composites,* J MATER RES TECHNOL, vol.9(3),2020, pp.6808-6833

[13] C. Soldano, A. Mahmood, E. Dujardin., *Production, properties and potential of graphene,* Carbon, vol.48, 2010, pp.2127-2150

[14] Y. Song, Y. Chen, W.W. Liu, W.L. Li, Y.G. Wang, D. Zhao, X.B. Liu., *Microscopic mechanical properties of titanium composites containing multi-layer graphene nanofillers,* Mater. Des*., vol.109 , 2016, pp.256-263*

[15] X. Du, W. Du, Z. Wang, K. Liu, S. Li., *Ultra-high strengthening efficiency of graphene nanoplatelets reinforced magnesium matrix composites,* Mater Sci Eng A, vol.711, pp.633-642

[16] J. Wang, Z. Li, G. Fan, H. Pan, Z. Chen, D. Zhang., *Reinforcement with graphene nanosheets in aluminum matrix composites,* Scr Mater, vol.66, 2012,pp.594-597

[17] K. Fu, X. Zhang, C. Shi, E. Liu, F. He., *An approach for fabricating Ni@graphene reinforced nickel matrix composites with enhanced mechanical properties,* Mater Sci Eng A, vol.715(7), 2018, pp.108-116

[18] H. Algul, M. Tokur, S. Ozcan, M. Uysal, T. Cetinkaya, H. Akbulut, A. Alp., *The effect of graphene content and sliding speed on the wear mechanism of nickel-graphene nanocomposites,* Appl Surf Sci, vol.359, 2015, pp.340-348

[19] M. Hayat, H. Singh, Z. He, P. Cao., *Titanium metal matrix composites: An overview,* Compos.A, vol.121, 2019, pp.418-438

[20] Rogoff, E. & Antony, M. & Markle., *Calculating Ti-6Al-4V b Transus Through a Chemistry Based Equation Derived from Combined Element Binary Phase Diagrams*, Journal of Materials Engineering and Performance, Volume 27(10) October 2018—5227

[21] N.S. Karthiselva, S. R. Bakshi., *Carbon nanotube and in-situ titanium carbide reinforced titanium diboride matrix composites synthesized by reactive spark plasma sintering* , Mater Sci Eng A, vol.663, 2016, pp.38-48

[22] S. Schmidt, S. Beyer, H. Knabe, H. Immich, R. Meistring, A. Gessler., *Advanced ceramic matrix composite materials for current and future propulsion technology applications,* Acta Astronaut, vol.55, 2004, pp.409-420

[23] P. Verma, S. Warghane, U. Nichul, P. Kumar., *Effect of boron addition on microstructure, hardness and wear performance of Ti-6Al-4V alloy manufactured by laser powder bed fusion additive manufacturing,* Materials Characterization, vol.172, 2021

[24] M.J. Bermingham, S.D. McDonald, K. Nogita, D.H. St. John, M.S. Dargusch., *Effect of boron on microstructure in cast titanium alloys*, Scripta Materialia, vol.59,2008, pp.538-541

[25] H. Kim, *on the rule of mixtures for the hardness of particle reinforced composites*. Mater Sci Eng A. vol. 289, 2000, pp. 30-33

[26] A.M. Russell, B.A. Cook., *Coefficient of thermal expansion anisotropy and texture effects in ultra-thin titanium sheet,* Acta Materialia, Vol.37, 1997, pp.1461-1477

[27] M. Suh, Y. Chae, S. Kim ., *Friction and wear behaviour of structural ceramics sliding against zirconia*, Wear, vol. 264 (9), 2008 ,pp.800-806.

[28] J. L.Basse, *Basic theory of solid friction*, ASM Int. 1992, pp.27-36. Materials Park, OH.

[29] R. Vaidya, K.K Chawla., *Thermal Expansion of Metal-Matrix Composites,* Comp Sci tech, vol.50, 1994, pp.13-22

Chapter 5: Hot Isostatic Pressing of Ti-6Al-4V/SiC: Influence of HIP Temperature, Reinforcement Size and Volume Fraction on Microstructural Evolution, Mechanical and Tribological Properties

Abstract

Ti-6Al-4V-based matrix composites (TMCs) reinforced with silicon carbide (SiC) particles have been developed by powder metallurgy (P/M) and hot isostatic pressing (HIP) route. SiC with varying particle sizes (5 µm and 20nm), volume fractions (5-10 vol.%), blending routes (MA ball milling, roll blending) have been investigated in this research. Experiments were also conducted to assess the influence of HIP parameters, such as temperature below β-transus temperature and super β-transus temperature (950°C and 1160°C) and dwell time (3h,6h), on the consolidation behaviour of the TMCs. Moreover, structural property modelling work has been carried out to understand the contribution of different strengthening mechanisms, such as load transfer and CTE, on enhancing the wear resistance of the TMCs. The microstructure and tribological properties of the as-fabricated TMCs were characterized using SEM, EDX, XRD, micro-hardness, and dry-sliding reciprocating tests. With the volume fraction increasing from 0 vol.%. to 5 vol.%, the wear regime changes from abrasive wear to delamination wear, thereby reducing the wear rate of the composite. However, increasing the volume fraction to 10 vol.% shows an increase in wear rate due to 3 body abrasive wears taking place. Reducing the reinforcement size from 5µm to 20nm tended to reduce the wear rate due to an increase in the hardness of the material, an improvement in the interfacial bonding between the matrix and reinforcement, and the ability of the nano reinforcement to bridge between subsurface cracks.

5.1 Introduction

Titanium (Ti) and its alloys are extensively known to be light in weight while exhibiting excellent mechanical performance, such as high specific strength, creep resistance, and specific stiffness [1]. Ti alloys are widely used in the aerospace and automobile industry [2] due to the superior mechanical performance they provide; however, the aerospace and automobile industries are constantly developing and requiring materials that can operate in severe environmental conditions for a long service period. This is where the concept of titanium metal matrix composites (TMCs) comes into play, as they offer superior wear resistance [3], tribological performance, and weight reductions [4] in many advanced applications. For instance, TMCs have been reported in high-temperature compressor applications to offer 50% weight cuts [5] and to work at high operating temperatures, reaching 760°C [6]. TMCs are generally classified as either continuously reinforced or discontinuously reinforced, depending on whether continuous fibres or particles are used as the reinforcement [7]. Discontinuously reinforced TMCs are known to have a higher specific strength, wear resistance, and thermal stability than monolithic titanium alloys [8]. PM *in situ* routes, such as HIP, are widely employed to synthesise TMC parts over ex situ additive routes due to the chemical reactivity of titanium [9]. It is vital to note that to fabricate TMCs that offer enhanced performance capabilities, homogenous powder processing is a key dominant factor in the process [10]. Generally, reinforcements are chosen on the basis of having a similar coefficient of thermal expansion (CTE) value to the matrix material [11], to restrain residual stress formation during the cooling process. There have been many reported discretely reinforced TMCs reinforcements in the literature, ranging from SiC [12], TiC [13], TiB_2 [14], Si_3N_4 [15], B_4C [16], and CNTs [17]. Cai et al. [2-3] have used TiB_2 as a reinforcement for Ti-6Al-4V matrix, due to the CTE compatibility of TiB_2 (7.2×10^{-6}) and Ti-6Al-4V (8.2×10^{-6}), and therefore the materials were thermodynamically stable. The literature also suggests that in-situ synthesised formation of TiC and TiB_2 is the best reinforcement for Ti matrix due to the close CTE values and the elevated hardness contributions that they provide, and due to the chemical compatibility with titanium [9]. Cai et al. [2-3] have been able to produce an *in situ* reaction between Ti-6Al-4V and TiB_2 during HIP to form TiB whiskers that are homogenously dispersed along with the matrix through solid-solution reaction. While Saba et al. [18] have tackled the poor ductility of TMCs by reinforcing Ti with diamond nanoparticles and successfully retained some ductility. This works based on Orowan's strengthening mechanism, whereby nanoparticles strengthen the matrix by having dislocations loop around the particles, since the inter-particle spacing is small, thereby increasing the dislocation density inside the grain interior, which in turn will help in simultaneously raising the ductility and yield strength of the material. It is vital to note that to fabricate TMCs that offer enhanced

performance capabilities, homogenous powder processing is the key initiating factor in the process. Sivakumar et al. [12] have successfully produced the hard phase of TiC from Ti-6Al-4V matrix reacting with SiC reinforcement during the P/M process. Their findings showed that at 5 vol.% the reinforced composite was the optimal reinforcement content and increasing vol.% to 10% and beyond did not result in considerable gains in hardness or strength due to particle agglomeration. Furthermore, Sivakumar et al. reported a compressive strength of 1483 MPa for the nano-reinforced Ti-6Al-4V composite, showing almost a 17% strength gain with the addition of 5 vol.% SiC content. Poletti et al. [19] successfully demonstrated that milling at 150 rpm for 5h was enough to adhere fine SiC particles to Ti without deforming the spherical morphology of Ti particles. Many reports indicate that the MA route via ball milling offers superior homogeneity in mixed powders in comparison with roll blending routes. However, the agglomeration of fine nano-reinforcements causes a deterioration in the wear and tribological performance of the TMCs, hence research lately is being focused on developing a powder blending route to solve this inherent issue. Wu et al. [20] successfully blended graphene nano-platelets (GNPs) reinforced AlSi10Mg composite via an MA ball milling technique, using a process control agent to de-agglomerate the nano-reinforcements. Li et al. [21] used a lubricant oil to distribute carbon-nanotubes (CNTs) uniformly on Ti powder using an MA milling route. Saba et al. [18] first mixed Ti powders with different sized diamond nanoparticles through bath sonication using ethanol solution to de-agglomerate the particles, followed by ball milling for 5h. The trend in the literature clearly shows that the fabrication of nano reinforced TMCs requires a control agent to homogenously distribute the nanoparticles on the matrix surface which in turn will improve the tribological properties and mechanical properties of the TMC due to a stronger bond between the reinforcement and matrix.

There have been many different approaches taken to predict the strength of TMCs, taking into account the size of the matrix, size of the reinforcement particle, volume fractions of both the reinforcement and the matrix, CTE mismatch, load-bearing mechanisms, grain size, and Orowan strengthening mechanisms. The contribution of each mechanism changes vastly, depending on the scale of reinforcement used, moving from micrometre to nanometre scale. Saba et al.[18] report that if the volume fraction of the reinforcement and the particle size are both small, the matrix will take most of the load, so load-transfer mechanism can be ignored, if the volume fraction is less than 5 vol.%. Some articles reports that CTE mismatch strengthening is the most effective way to increase the yield strength [2-3], due to the generation of geometrically necessary dislocations that arise from the critical strain misfit from the thermal mismatch. However, other reports indicates that if the reinforcement size is below 100nm, dislocation strengthening due to thermal mismatch could be neglected, since the critical misfit strain from thermal mismatch cannot be achieved, hence the Orowan strengthening mechanism dominates in the nanoscale below 100nm and above 1nm range. Zhang et al. [22] also find

that there is a critical size for the reinforcement, roughly 5.44x the magnitude of the burger vector, in which the Orowan mechanism breaks down and yield strength decreases.

Since titanium alloys have poor tribological performance, this work focuses on improving the hardness, compressive strength, and the wear resistance properties, and reducing the high unstable coefficient of friction (COF) of Ti alloys. Very little work, as yet, has been done investigating the tribological properties of Ti-6Al-4V reinforced with SiC particles. This research studies phase formation, microstructure evolution, and dry sliding wear properties with COF data and rationalising them in terms of micro-hardness data, in addition to theoretical compression strength values calculated from structure-property models. This work aims to establish a relationship between reinforcement volume fraction, size, micro-hardness, compression strength structure-property models, and tribological performance of Ti-6Al-4V composite reinforced with SiC using multiple powder processing routes.

5.2 Experimental

5.2.1 Material preparation

Argon gas atomised (AGA) Ti-6Al-4V powder (figure 5.1a) (average particle size of 15-45µm) was used as the metal matrix (LPW Technology, UK). SiC (average particle size of 5µm) was purchased from Reade Advanced Materials USA (figure 5.1b). SiC powder (average particle size of 20nm) was supplied by PlasmaChem GmbH Germany. Ti-6Al-4V was roll blended (RB) with SiC 5 µm with different volume percentages (0%, 5%, and 10%) for 6h. Ti-6Al-4V/SiC (average particle size 20nm) with a volume percentage of (5%) was MA by ball milling. The Ti-6Al-4V/SiC (20nm) were both mixed in ethanol for bath sonication (30 mins) to de-agglomerate the nanoparticles and then MA using ball milling for 6h (HMK-1901, the ball to powder ratio (BPR); 4:1, 200 RPM) to limit the deformation and overheating of Ti particles.

5.2.2 Powder HIPping

The Blended powders were consolidated via HIP. Mild steel canisters with an outer diameter of 50.8mm, length of 170mm, and a wall thickness of 2.03mm were produced and used to contain the roll blended powders before being outgassed and crimped. MA powders were contained in mild steel canisters with an outer diameter of 50.8mm, length of 65mm, and a wall thickness of 2.03mm. The

samples were hot outgassed at 100℃ until they reached a vacuum level of 10^{-5} bar before being HIPped at both 950℃ and 1160℃, 140 MPa for 3h using a (EPSI, HIP) furnace.

5.2.3 Microstructural characterization

The as-HIPped samples were wire EDM cut, ground, and polished for XRD. The samples were then etched using Kroll reagent (2% HF, 92% H_2O and 6% HNO_3) for around 10 seconds before microstructural analysis using an SEM with an EDX. XRD was used to identify the different in-situ phases present in the samples. Phase identification was performed by XRD (AXRD, Proto) with Cu Kα radiation (λ = 1.5406°A), and XRD spectrums were collected by a fixed parameter of 0.02º step size and 1s time/step. The grain size was measured using ImageJ by sampling 200 grains, measuring them individually, and then getting an average size.

5.2.4 Tribological behaviour and mechanical properties

The wear properties of the Ti-6Al-4V/SiC matrix composites were examined using a reciprocating machine with a coefficient of friction measuring capabilities. The wear tests were carried out at room temperature. The counter-body material used was Al_2O_3 with a ball diameter of 10mm and Vickers hardness value of 1600HV. Al_2O_3 balls were used to slide over as-polished flat specimens in a reciprocating motion under a dry surface. A load of 20N, a sliding speed of 10mm/s, a sliding distance of 5mm, and a time duration of 30 min have been used. The worn surfaces have been examined using an SEM with an EDX to understand the dominant wear mechanisms exhibited on the specimens. Finally, as-polished specimens were mounted on micro-hardness tester (Wilson VH1202, Buehler) for Vickers hardness measurement. The test for each sample was performed with 100g load and 10 times linearly indented with recommended spacing according to ASTM E384-17.

5.3 Results & discussion

5.3.1 Powder characterization

Figure 5.1a shows the powder morphology of AGA Ti-6Al-4V and particle size distribution. The powder has an average particle size of 33µm. It is also clear that satellites, irregular particles, agglomeration, and particle breakage are common features in the AGA powder route used. Figure 5.1b shows the

morphology of micron-sized SiC particles. The particles were faceted and irregular and the average particle size was less than 5 µm. Figure 5.1c shows the morphology of as-received SiC nanoparticles. It is quite clear from the micrograph that the nanoparticles are agglomerated due to the surface energy of the nanoparticles. The average particle size as reported by the supplier was 20 nm. Figure 5.1d shows the morphology of SiC nanoparticles after de-agglomeration using ultrasonication method as shown in Figure 5.2.

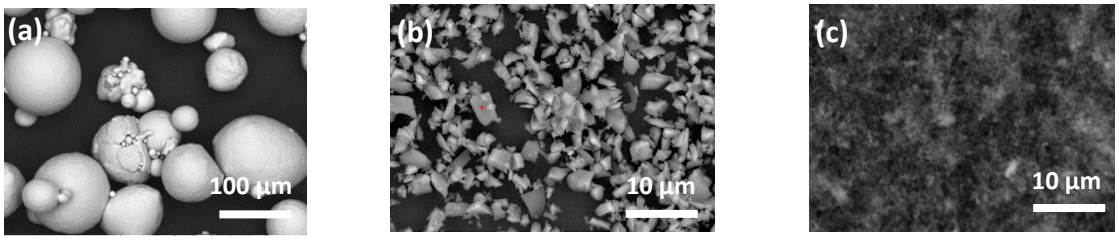

Figure 5.1: *(a) SEM micrograph of As-received GA Ti64 powder; (b) As-received SiC (5µm) powder; (c) As-received SiC (20nm) powder*

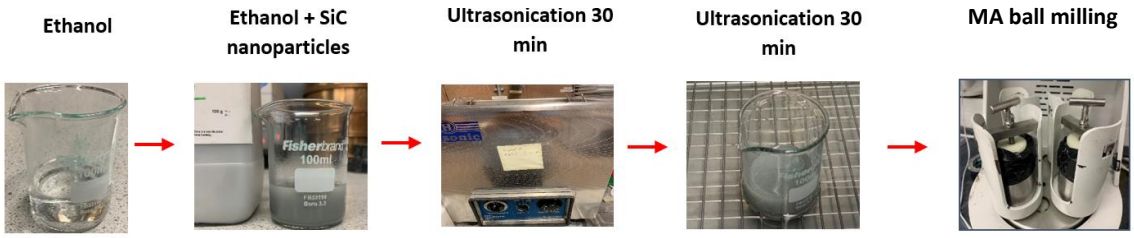

Figure 5.2: *Preparation procedure of Ti64/SiC nanocomposite*

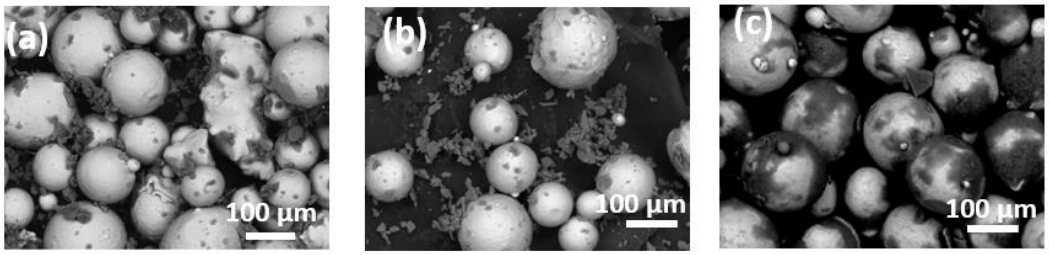

Figure 5.3: *SEM micrographs showing RB Ti64 + SiC (a) 5 vol.%, (b) 10 vol.%, (c) MA Ti64 + 5% SiC 20nm*

5.3.2 Nanocomposite fabrication

SiC nanoparticles were mixed with Ti64 using a volume fraction of 5 vol.%. The fabrication process is illustrated in figure 5.2. The first step was dispersing the SiC nanoparticles in ethanol solution. The solution was then ultrasonicated for a duration of 30 mins to help de-agglomerate the nanoparticles. Ti64 powders were then dispersed in the same solution and ultrasonicated for another 30 mins. Furthermore, the mixture was then MA using ball milling for 6h as described in section 5.1. After MA the powders, the powders were filtered using filter paper and then left to dry prior to HIP stage.

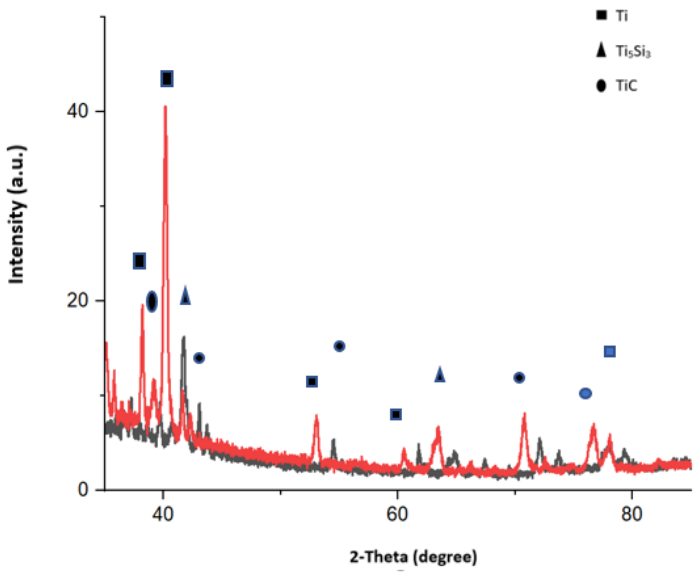

Figure 5.4*: XRD analysis for as-HIPped Ti64+5 vol.% SiC black plot 5 µm, red plot 20nm*

Figure 5.3a shows Ti-6Al-4V reinforced with 5 vol%. SiC (5 µm) decorating the matrix. However, the majority of the SiC particles (dark grey contrast) are clustered and not sticking to the matrix. As the size of the reinforcement (5 µm) is large relative to the matrix (15-45 µm), hence why the reinforcement is not sticking to the titanium surface. Figure 5.3b shows Ti-6Al-4V + 10 vol.% SiC (5 µm), more clustering of SiC can be seen due to the higher vol.% of reinforcement used, in addition to the same inherent problem of reinforcement not sticking to the matrix is again observed, which could also be attributed to the mixing route used and the reinforcement to matrix size ratio selected. Finally, figure 5.3c shows Ti-6Al-4V with 5 vol.% SiC (20 nm) decorating the surface of the matrix homogeneously. This could be attributed to the strong interfacial bonding between the nanoparticles

with high surface energy and the MA using ball milling route used in this study. Even after MA Ti-6Al-4V with the nano-reinforcement, the Ti-6Al-4V morphology remains highly spherical due to the small BPR of 4:1 and ball milling parameters used.

5.3.3 The microstructure of as-HIPped specimens

5.3.3.1 Microstructural evolution of TMCs

Figure 5.4 shows the XRD analysis for the as-HIPped Ti-6Al-4V + 5 vol.% SiC (20nm) to confirm the phases present in the TMCs. The analysis clearly shows that SiC has completely disintegrated and reacted with the titanium matrix, in-situ forming Ti_5Si_3 (titanium silicide) and TiC (titanium carbide) during the HIPping process at elevated temperatures (1160°C). SEM micrographs have been taken in figure 5.5 to understand how the addition of SiC reinforcements influence the microstructural development concerning volume fraction and size. It is quite clear that the microstructure of synthesized TMCs has been dominated by Ti_5Si_3 phase formation along the β grain boundaries (figure 5.5f). Grain growth has taken place in the SiC free-sample (figure 5.5a-b), in contrast to the SiC containing samples, suggesting that the in-situ formed phases are impeding grain growth. Furthermore, the (α+β) SiC free sample (figure 5.5a-b) has a lamellar microstructure with a higher volume fraction of the β phase due to the super-transus HIPping temperature used in this work. It can also be noted that the in-situ phases are decorating the Prior-Particle-Boundaries (PPBs), forming a homogenous network of strengthening phases that coalesce as the volume fraction of the reinforcement is increased as seen in figure 5.5c-f. Furthermore, the Ti_5Si_3 and TiC phases are growing into the PPBs, coalescing, and forming bridges between neighbouring titanium particles. It can also be noted from table 5.1 that reducing either the reinforcement particle size or increasing the reinforcement volume fraction impedes grain growth.

5.3.3.2 Titanium silicide phase formation

In figure 5.5f and 5.5h, some small precipitates have formed. It is suspected that TiC precipitates formation because of the reaction between β-Ti and SiC. Figure 5.5c and 5.5d show that the darker shades are rich in Ti, while the lighter shades are rich in Si. It is therefore suspected that the darker region is TiC rich due to its higher density, while the lighter region is Ti_5Si_3 rich, which agrees with the

XRD scans presented. Furthermore, carbon diffusivity is roughly 10x faster than the diffusivity of Si in the β-Ti phase, and the max solubility of Si in β-Ti is approximately 3.7% [23]. Additionally, Ti of the metal phase goes into solution in the Ti_5Si_3 phase, a counter-diffusion would take place between the decomposed SiC and Ti in the Ti_5Si_3 matrix. Carbon solubility in this phase is relatively small, hence C would react with Ti to form small TiC precipitates [23]. It is also worth mentioning that the coalescence of the TiC precipitates takes place due to the chemical potential gradient of C and the high diffusivity rate of carbon within the TiC precipitates. The coalescence of the TiC phase between neighbouring precipitates can be seen in figure 5.5f. Figure 5.5g-h shows the Ti64+ 5vol.% SiC 20nm. The in situ formed TiC and Ti_5Si_3 phases are more refined due to the smaller reinforcement size used, however grain growth of the nanoparticles is evident due to the high HIP temperature used and the dwell time used to ensure consolidation.

5.3.3.3 Influence of HIP parameters on microstructural evolution

Figure 5.7 shows the effect of HIPping temperature on the consolidation and microstructural evolution of 10 vol%. SiC TMCs. Figures 5.7a-7b has been HIPped at sub-transus temperature of 950°*C* with a dwell time of 6h, while figure 5.7c-7d have been HIPped at super-transus temperature of 1160℃ with a dwell time of 3h. It is clear that the as-HIPped sample HIPped at sub-transus temperature (figure 5.7a-6b), shows a lack of consolidation due to the temperature being too low to reduce the yield strength of SiC and to enhance the diffusivity in the material to cause pore closure. However, it is also apparent from a microstructural evolution standpoint, that an in-situ reaction between the matrix and reinforcement did take place. Furthermore, it is also vital to note that the size of the diffusion zone is on the scale of a few microns. Figure 5.7c-7d shows a microstructure that is fully consolidated, with a complete in-situ reaction taking place. However, the diffusion zone is eloquently large, due to the increased solubility of Fe in Ti with increasing temperature beyond the β-transus temperature.

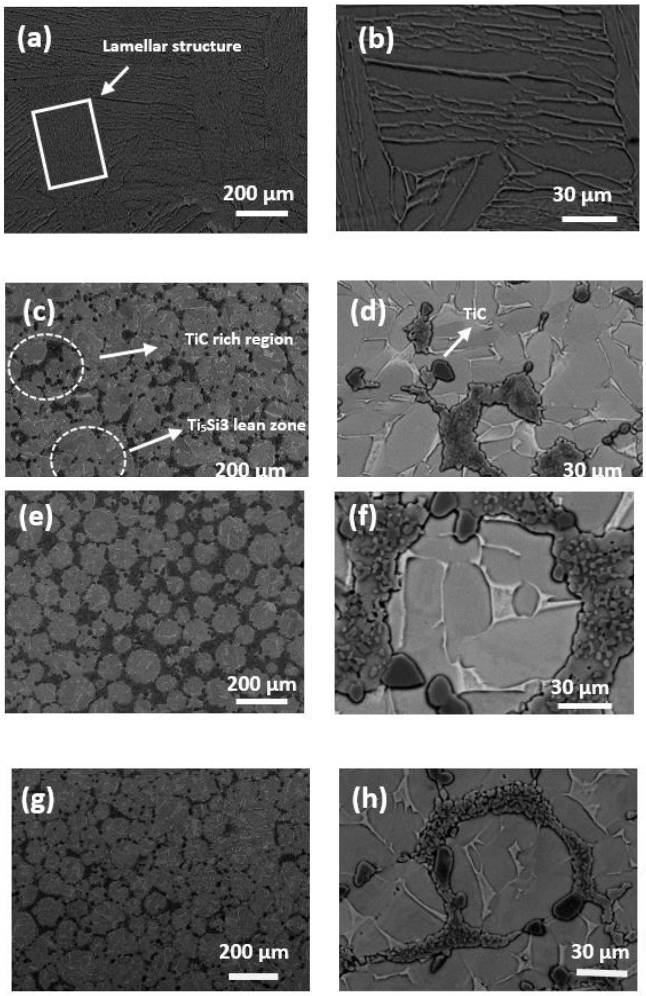

Figure 5.5: *SEM micrographs of as-HIPped samples (1160℃) reinforced with SiC (a-b) 0 vol.%, (c-d) 5 vol.%, (e-f) 10 vol.%, (g-h) 5 vol.% 20nm*

***Table 5.9**: Average grain size of TMCs measured using ImageJ*

Material	Average grain size (µm)
Ti-6Al-4V + 5 vol% SiC (5 µm)	8.2±0.8
Ti-6Al-4V + 10 vol% SiC (5 µm)	7.1±0.6
Ti-6Al-4V + 5 vol% SiC (20 nm)	5.8±0.6

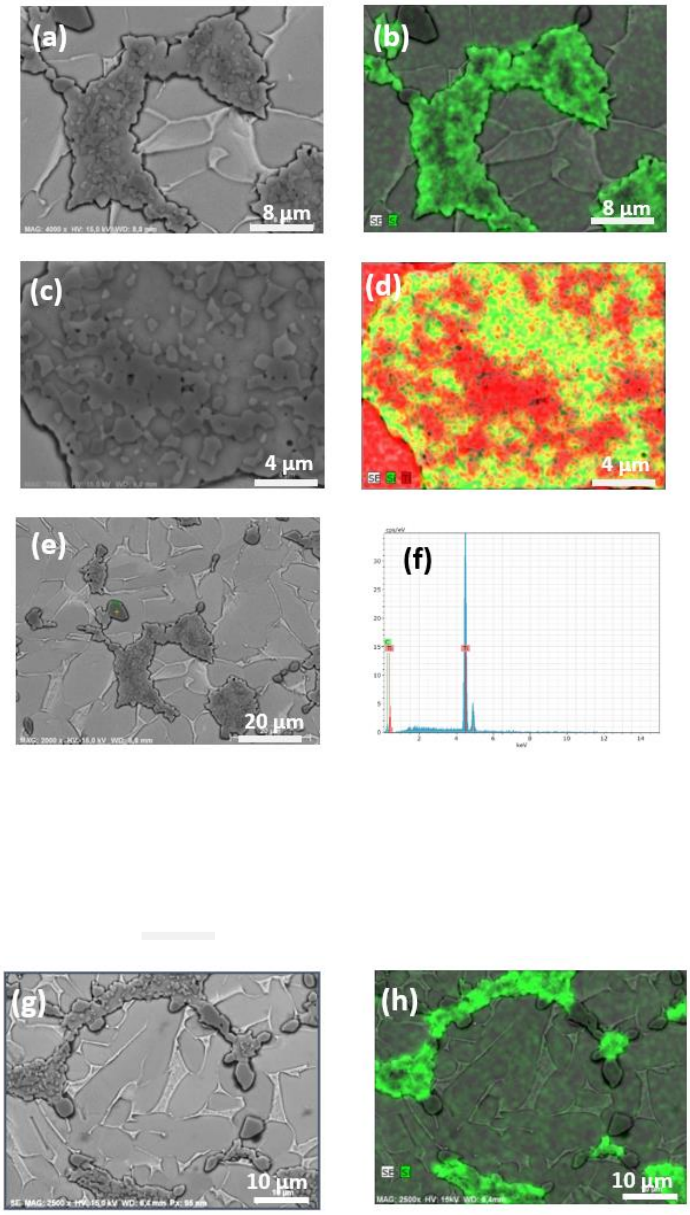

Figure 5.6*: EDX scans showing the formation of titanium silicide and titanium carbide (a-f) 5 vol.% SiC 5µm, (g-h) 5 vol.% SiC 20nm*

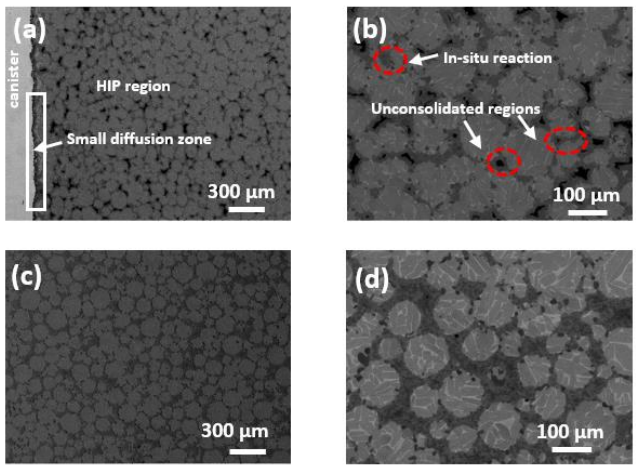

Figure 5.7: *SEM micrographs of as-HIPped samples with 10 vol.% SiC processed at 950*℃ (a-b), processed at 1160℃ (c-d)

5.3.4 Mechanical properties

5.3.4.1 Micro-hardness

Figure 5.8 shows the variation in micro-hardness values of as-HIPped Ti-6Al-4V/SiC TMCs with varying reinforcement size and volume fractions. Figure 5.8a shows an increase in micro-hardness by reducing the reinforcement particle size even though they all fall within the margin of error. The micro-hardness has roughly increased by 28% with adding 5 vol.% SiC. Furthermore, reducing the reinforcement size from 5µm to 20nm shows roughly a 3% strength gain. The micro-hardness gains could be ascribed generally to the hardening induced effect of the TiC phase. Additionally, the surge in micro-hardness values with reducing the reinforcement size could be specifically attributed to grain refinement due to nano-reinforcements inhibiting grain growth. This phenomenon could also be credited to the Orowan strengthening mechanism, whereby the nano-reinforcement inhibits dislocation motion. Figure 5.8b shows that increasing the volume fraction from 5 to 10 vol.% increases the micro-hardness by roughly 11%. This contribution to the strength could be attributed to the load-transfer from the soft metallic matrix to the stiffer harder phases. The load transfer mechanism is known to be heavily influenced by the volume fraction of the reinforcement. It also relies on other compositional parameters, such as a strong interfacial bonding between the reinforcement and matrix, which could be enhanced by decreasing the reinforcement size. The TMC reinforced with 10 vol.% SiC had a lot of clustering and weak interfacial bonding, hence the micro-hardness not significantly increasing with the doubling of the vol.% from 5-10%. Therefore, the load transfer effect could not be maximised.

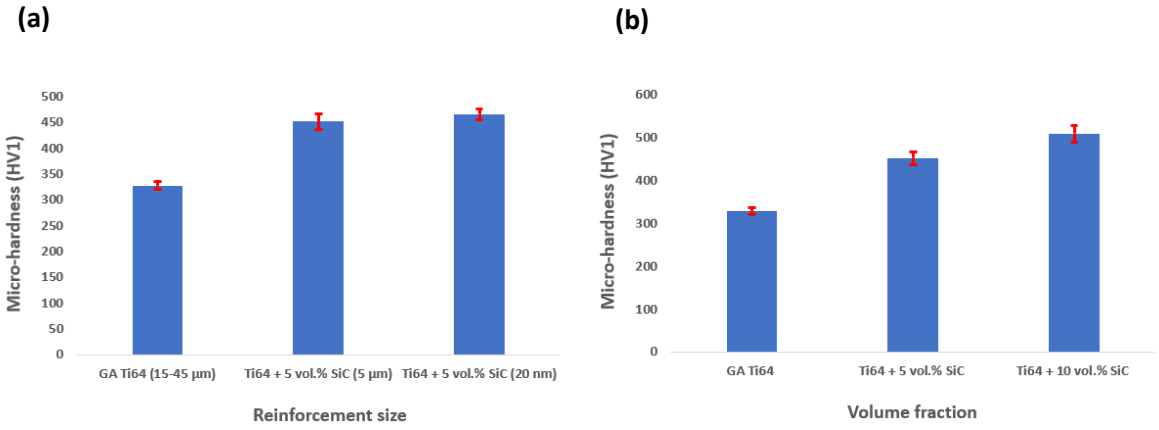

Figure 5.8: *(a)The influence of reinforcement size on micro-hardness, (b) Influence of reinforcement volume fraction on micro-hardness*

5.3.5 Tribological properties

5.3.5.1 Wear rate

Figure 5.9 shows the worn surface morphologies of the Ti-6Al-4V/SiC TMCs and their respective depth maps. The worn surfaces generally exhibit rough surfaces with deep ploughed grooves. Furthermore, the deep ploughed groove as seen in figure 5.9a, which shows the un-reinforced Ti-6Al-4V sample, is caused by the hard Al_2O_3 counter-body, which is a sign of severe plastic deformation and abrasive wear. As the reinforcement volume fraction has been increased to 5 vol.%, the wear track depth decreases from 13µm to 8.6µm. Moreover, the main wear feature present in the 5 vol.% SiC sample is delamination, and the amount of wear debris tends to increase with the addition of more SiC. The trend of increasing delamination and wear debris seen with increasing the volume fraction of the reinforcement deteriorates the wear resistance through abrasive wear mechanism and delamination. It also clearly indicates a debonding between the reinforcement and matrix interface, which is due to the weak interfacial bonding in the micron-reinforced samples. The amount of delamination and signs of ploughed grooves notably in the nano-reinforced sample are far less than the micron-reinforced sample. This indicates that the wear track depth, and consequently the wear rate, will be lower. The reason is that the nano-reinforced sample has a higher micro-hardness and stronger interfacial bonding, so its exhibit superior wear resistance. This is supported by looking at both the wear track depth reduction from 8.6µm to about 6.2µm, and the wear rate values, as seen in figure 5.10, whereby the nano-reinforced material has the lowest wear rate values. It is therefore conclusive to say that reducing the particle size to the nano-scale ascribes superior resistance to abrasive wear mechanisms, such as micro-cutting and sub-surface crack initiation, due to the nano-particles inhibiting grain growth and having stronger interfacial bonding.

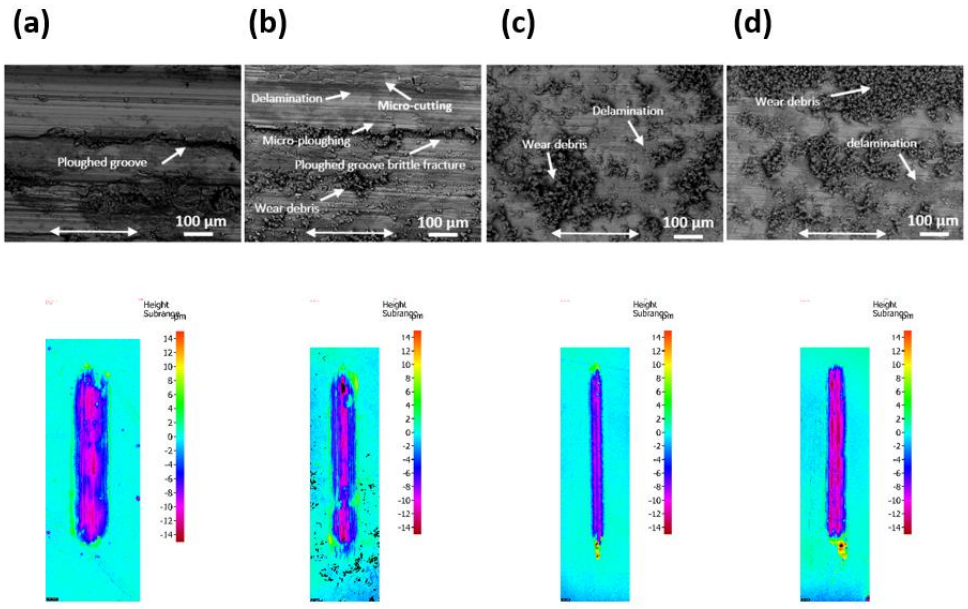

Figure 5.9: *SEM micrographs of worn surfaces and depth maps with varying reinforcement volume fraction and reinforcement particle size; (a) GA Ti64 , (b) Ti64 + 5 vol.% SiC (5µm), (c) Ti64 + 5 vol.% SiC (20nm), (d) Ti64 + 10 vol.% SiC*

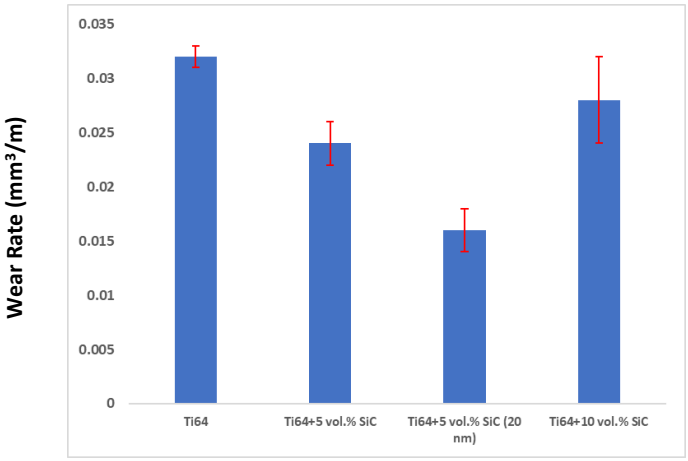

Figure 5.10: *Wear rate as a function of reinforcement size and volume fraction*

5.3.5.2 Coefficient of friction

Figure 5.11 shows the COF data as a function of varying reinforcement volume fraction and reinforcement size of as-HIPped TMCs. There is a clear trend in terms of the COF value decreasing from 0.45 to 0.38 with the addition of 5 vol.% SiC, which indicates a clear enhancement of the tribological performance. The increase in reinforcement content up to 5 vol.% increases the resistance of the material to thermal softening and abrasive wear mechanisms. This could be attributed to the fact that TiC particles are extremely hard, so they can strengthen the matrix and protect it from abrasive wear. With further additions of SiC, the COF value increases even beyond the un-reinforced

Ti-6Al-4V with a value transcribing to 0.48, which could be attributed to 3-body abrasive wear taking part between the wear debris and hard counter-body. These findings agree with Baradeswaran et al. [24] who reported a similar trend with AA7075-Al_2O_3 composites. As the reinforcement size is decreased from 5 µm to 20nm, the data clearly shows a drop in COF values from monolithic Ti-6Al-4V and the micron-reinforced 5 vol.% TMC. The COF value of the nano-reinforced TMC was roughly 0.36, compared with the 0.38 recorded value for the micron-reinforced sample. This could be due to the increase in hardness, stronger interfacial bonding, and grain refinement contribution from the nano-reinforcements.

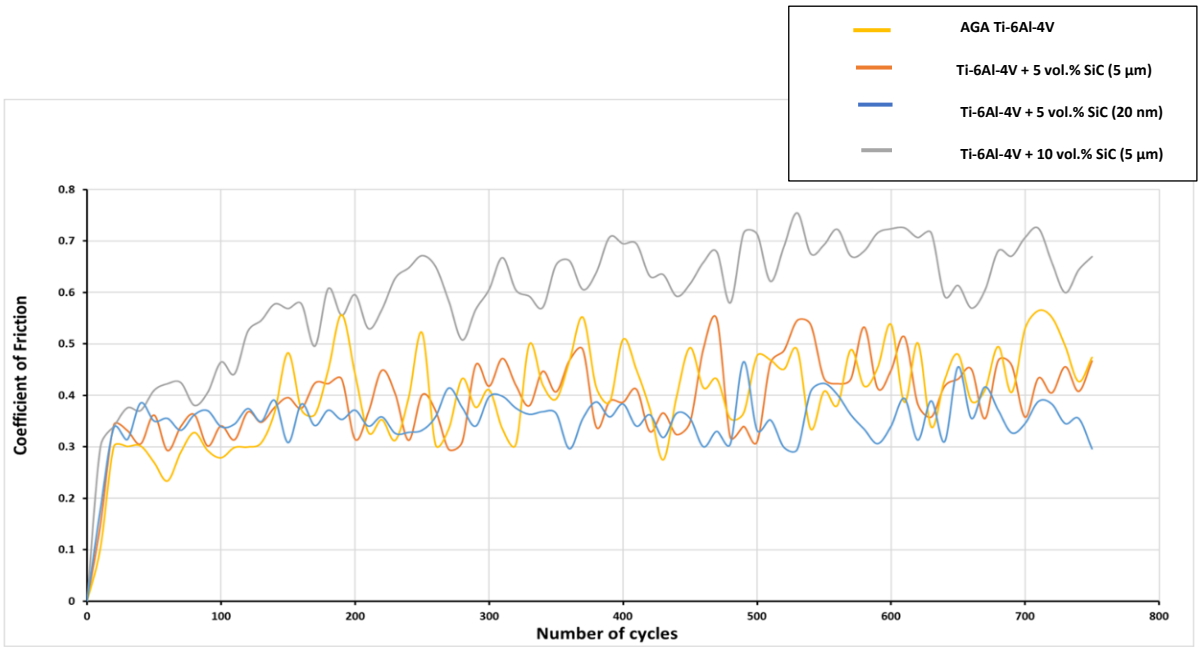

Figure 5.11: *COF data of TMCs*

5.3.6 Strengthening mechanisms in Ti-SiC TMCs

To predict the structure-property relations of TMCs, understanding the different strengthening contributions from secondary phases to the overall strength of the composite is vital. Many papers studying the effect of discontinuously reinforced TMCs have concluded how the secondary phases influence the compressive strength of the composite with accordance to different strengthening mechanisms. The strength contributing mechanisms change depending on whether nano-reinforcement or micron-sized reinforcements are used. However, generally, the overall strength could be predicted by summing the contribution of load transfer, dislocation strengthening via CTE mismatch, grain refinement strengthening, and Orowan dispersion strengthening mechanisms as shown in equation 7.1 below [25].

$$\sigma_{th} = \sigma_{ym} + \sigma_{H-P} + \sigma_{L.T} + \sigma_{CTE} + \sigma_{orowan} \qquad (7.1)$$

5.3.6.1 Grain refinement

The Hall-Petch equation describes the contribution of grain refinement on the overall strength of the material:

$$\Delta\sigma_{H-P} = \sigma_o + kd^{-\frac{1}{2}} \qquad (7.2)$$

σ_o is the starting stress for dislocation movement (845 MPa), while k is the Hall-Petch constant used for the Ti-matrix is 0.3 MPa $m^{1/2}$ [26], and d is the average grain size of the matrix. The average grain sizes used to calculate the grain refinement contribution have been drawn from Table 5.1. Reducing the matrix grain size to the nanoscale has a significant contribution to the overall strength of the TMCs, which can be seen in figure 5.12 where the grain refinement contribution due to reinforcement size reduction from 5 µm to 20nm was 19 MPa.

5.3.6.2 Thermal mismatch strengthening

The contribution due to thermal mismatch strengthening can be expressed by the following equation [25]:

$$\Delta\sigma_{CTE} = \alpha Gb\sqrt{\left(\frac{12\Delta T}{b(\frac{\Delta c.fr}{dr}}\right)} \qquad (7.3)$$

where k is a material constant (1.25) for Ti [27], G=44 GPa (shear modulus of Ti) [28], b=0.29nm (Burger vector for Ti) [29], ΔT (the difference between the HIP temperature and property testing temperature), ΔC (thermal mismatch between matrix and reinforcement), fr (volume fraction of reinforcement), and dr (reinforcement particle size). It is well known that the difference in CTE mismatch between the matrix and reinforcement results in the generation of geometrically necessary dislocations (GNDs) during the cooling process, hence the increasing strength of the TMC. It can be

seen in figure 5.12 that reducing the reinforcement particle size from 5 µm to 20 nm significantly increased the strength, while the contribution is not sensitive to increasing the volume fraction, as outlined in equation 7.3.

5.3.6.3 Orowan strengthening

Reinforcing metal matrices with nanoparticles, such as SiC nanoparticles, strengthens the metal matrix by forming loops around the scattered nanoparticles, impeding dislocations movement and increasing the strength of the TMC. The contribution due to Orowan looping could be evaluated using the following equation [25]:

$$\Delta\sigma_{orowan} = \frac{0.81\,MGb}{2\pi(1-\theta)^{\frac{1}{2}}} \frac{ln\frac{d_r}{b}}{\left(\frac{1}{2}d_r\sqrt{\frac{3\pi}{2f_r}-d_r}\right)} \qquad (7.4)$$

where M=2.6 (Taylor factor for Ti) [30], G= 44GPa (shear modulus for Ti) , b=0.29nm (burger vector), dr (particle size of reinforcement) , fr (volume fraction of reinforcement), and Θ=0.31 (poisson ratio of Ti) [31]. It can be seen in figure 5.12 that the Orowan contribution in micron-sized reinforcements is insignificant and can be negligible. This is because the inter-particle spacing is huge. On the other hand, it is clear from figure 5.12 that the Orowan strengthening mechanism plays a significant part in strengthening the matrix when nano-reinforcements are used, due to the ability of the nano-reinforcements to impede dislocation movement.

5.3.6.4 Load transfer

The load transfer mechanism is highly sensitive to the volume fraction of the reinforcement. It operates on the basis that the load is transferred from the matrix to the stiffer reinforcements. It is important to note that having a strong between the matrix and reinforcement will enhance the ability of this mechanism to strengthen the material. The contribution due to load transfer could be expressed in the following equation [32]:

$$\Delta\sigma_{L.T} = 0.5 f_r \sigma_{ym} \qquad (7.5)$$

where σ_{ym} =845 MPa (yield strength of Ti matrix) and f_r (volume fraction of reinforcement). Results presented in figure 5.11 prove that the load transfer capability only changes in relation to the volume fraction of the reinforcement used, while other reinforcement powder characteristics, such as reinforcement size and morphology, are irrelevant.

5.3.6.5 The deviation between experimental and theoretical data

A few notable reasons explain why there is a deviation between theoretical and experimental structure-property relations. Firstly, the equation assumes the yield strength of monolithic Ti. However, as seen in figure 5h, there is a clear diffusion of silicon into the Ti matrix, which is known to have a very profound strengthening contribution to titanium [33]. Secondly, interstitials, such as O, are known to strengthen Ti, and that could suggest that the yield strength drawn from literature is not accurate. Finally, there is weak interfacial bonding between the matrix and the reinforcement in micron-reinforced composites, so the load transfer may have not been effective. Another issue that could cause deviation between experimental and theoretical data are that the constants used are approximate values derived from different experimental parameters, hence should be used for estimate values and not absolute values.

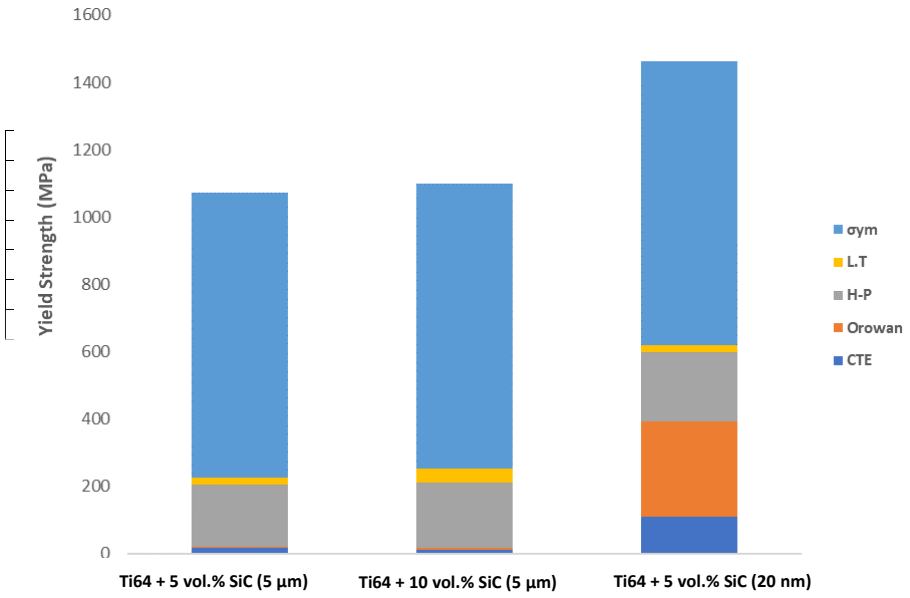

Figure 5.12: *Structure property model relating the reinforcement size and fraction to the strength of TMCS*

5.4 Conclusions

This study has investigated the microstructural evolution and the mechanical and tribological properties of Ti-6Al-4V/SiC composites concerning varying the volume fraction and reinforcement particle size synthesized via P/M HIP route while rationalizing them with structural-property models. The effect of reinforcement characteristics on the strengthening contributions has been studied thoroughly and relationships between the theoretical and experimental values have been validated. The conclusions are as follows:

1) HIPping Ti-6Al-4V/SiC composite at 950℃ has many regions of unconsolidated SiC. Incomplete in-situ reactions occur. In contrast, HIPping at 1160℃ ensures full synthetization of in-situ Ti_5Si_3 and TiC phase formation.
2) Reducing the reinforcement particle size from 5µm to 20nm has a positive influence on the tribological properties, due to stronger interfacial bonding and dominant strengthening mechanisms contributions from Orowan looping and grain refinement.
3) Increasing the volume fraction of the reinforcement shows a positive increase in micro-hardness due to load transfer effect; however, it has a deteriorating effect on the tribological performance due to delamination and abrasive wear.
4) The deviation between experimental and theoretical structure integrity models could possibly be due to Si diffusion in the Ti matrix.

Acknowledgements

The authors acknowledge the Centre of Doctoral Training in Innovative Metal Processing (IMPaCT), funded by the Engineering and Physical Sciences Research Council (EPSRC), and the National Structural Integrity Research Centre (NSIRC) for funding the PhD project at the University of Birmingham.

References

[1] M. Hayat, H. Singh, Z. He, P. Cao., *Titanium metal matrix composites: An overview*. Composites part A, vol.121, 2019, pp. 418-419

[2] C. Cai, S. He, L. Li, Q. Teng, B. Song, C. Yan, Q. Wei., *In-situ TiB/Ti-6Al-4V composites with a tailored architecture produced by hot isostatic pressing: Microstructure evolution, enhanced tensile properties and strengthening mechanisms*. Composites part B, vol.164, 2019, pp. 546-558

[3] C. Cai, B. Song, C. Qiu, L. Li, P. Xue, Q. Wei., *Hot isostatic pressing of in-situ TiB/Ti-6Al-4V composites with novel reinforcement architecture, enhanced hardness and elevated tribological properties.* Journal of Alloys and Compounds, vol.710, 2017, pp. 364-374

[4] D. Banerjee, J.C. Williams., *Perspectives on titanium science and technology*, Acta Materialia, vol.61(3), 2013, pp.844-879

[5] R. Singerman et al., *Superalloys 1996,* Warrendale, 1996, p.579

[6] O'Connell, *Production of Titanium Aluminide Products,* AFWAL-TR-83-4050, WPAFB, Ohio, 1973

[7] V.K. Lindroos, M.J. Talvitie ., *Recent advances in metal matrix composites,* J. Mater. Process. Technol., vol.53, 1995, pp.273-284

[8] M. Hayat, H. Singh, Z. He, P. Cao., *Titanium metal matrix composites: An overview*. Composites part A, vol.121, 2019, pp. 418-419

[9] L. Huang, L. Geng., *Discontinuously Reinforced Titanium Matrix Composites.* National Defense Industry Press, 2017, p.26

[10] K. Kondoh, *Titanium metal matrix composites by powder metallurgy* (PM) *routes.* Titanium Powder Metallurgy, 2015, pp.277-297

[11] F. Zhang, J. Wang, T. Liu, C. Shang., *Enhanced mechanical properties of few-layer graphene reinforced titanium alloy matrix nanocomposites with a network microstructure*. Materials and Design, vol.186, 2020

[12] G. SIVAKUMAR, V. ANANTHI, S. RAMANATHAN., *Production and mechanical properties of nano SiC particle reinforced Ti-6Al-4V matrix composite.* Trans Nonferrous Metals Soc China, vol.27(1), 2017, pp. 82-90

[13] M.A Lagos, I. Agote, G. Atxaga, O. Adarraga, L. Pambaguian., *Fabrication and characterisation of Titanium Matrix Composites obtained using a combination of Self propagating High temperature Synthesis and Spark Plasma Sintering.* Mater Sci Eng, A, vol. 655, 2016, pp. 44-49

[14] Z. Yan, F. Chen, Y. Cai, Y. Zheng., *Microstructure and mechanical properties of in-situ synthesized TiB whiskers reinforced titanium matrix composites by high-velocity compaction.* Powder Technol, vol.267, 2014, pp. 309-314

[15] T. Dougherty, Y. Xu, A. Hanizan., *Mechanical Properties and Microstructure of PM Ti-Si3N4 Discontinuous Fibre Composite.* Springer international publishing, Cham, 2016, pp.721-728

[16] J. Wang, X. Guo, J. Qin, D. Zhang, W. Lu., *Microstructure and mechanical properties of investment casted titanium matrix composites with B4C additions.* Mater Sci Eng,A,2015, vol.628, pp.366-373

[17] X. Sun, Y. Han, S. Cao, P. Qiu, W. Lu., *Rapid in-situ reaction synthesis of novel TiC and carbon nanotubes reinforced titanium matrix composites.* Mater Sci Tech, vol.33, 2017,pp.1165-1171

[18] F. Saba, F. Zhang, S. Liu, T. Liu., *Reinforcement size dependence on mechanical properties and strengthening mechanisms in diamond reinforced titanium metal matrix composites*. Composites Part B, vol. 167, 2019, PP. 7-19

[19] C. Poletti, M. Balog, T. Schubert, V. Liedtke, C. Edtmaier., *Production of titanium matrix composites reinforced with SiC particles*. Compos Sci Technol, vol.68, pp. 2171–217

[20] L. Wu, Z. Zhao, P. Bai, W. Zhao, Y. Li ., *Wear resistance of graphene nano-platelets (GNPs) reinforced AlSi10Mg matrix composite prepared by SLM.* Applied Surface Science. Vol.503, 2020

[21] S. Li, B. Sun, H. Imai, T. Mimoto, K. Kondoh., *Powder metallurgy titanium metal matrix composites reinforced with carbon nanotubes and graphite.* Comp Part A Applied Science and Manufacturing, Vol.48(1), 2013, pp.57-66

[22] Z. Zhang, D.L. Chen., *Contribution of Orowan strengthening effect in particulate-reinforced metal matrix nanocomposites*. Mater Sci Eng A. vol. 483-484, 2008, pp. 148-152

[23] M. Backhaus-Ricoult, *Solid State Reactions Between Silicon Carbide and Various Transition Metals.* Laboratoire de Physique des Matkriaux. Vol.93(11), 1989, pp.1277-1281

[24] A. Baradeswaran, A. Elaya Perumal., *Study on mechanical and wear properties of Al7075/Al_2O_3/graphite hybrid composites.* Composites Part B: Engineering, Vol.56, 2014, pp.464-471

[25] M. Habibnejad-Korayem, R. Mahmudi, W.J. Poole., *Enhanced properties of Mg-based nano-composites reinforced with Al2O3nano-particles, ,* Mater. Sci. Eng. A., 2009, Vol.519, pp.198-203

[26] F. Saba, F. Zhang, S. Liu, T. Liu., *Reinforcement size dependence of mechanical properties and strengthening mechanisms in diamond reinforced titanium metal matrix composites.* Composites Part B: Engineering, 2019, vol.167, pp.7-19

[27] C.S. Goh, J. Wei, L.C. Lee, M. Gupta., *Properties and deformation behaviour of Mg–Y2O3 nanocomposites,* Acta Materialia, 2007, Vol.55, pp.5115-5121

[28] W.J. Kim, Y.J. Yu., *The effect of the addition of multiwalled carbon nanotubes on the uniform distribution of TiC nanoparticles in aluminum nanocomposites*, Scripta Mater, 2014, Vol.72, pp.25–28

[29] F.X. Li, P.D. Hao, J.H. Yi, Z. Chen, K.G. Prashanth, T. Maity, J. Eckert., *Microstructure and strength of nano-/ultrafine-grained carbon nanotube-reinforced titanium composites processed by high-pressure torsion*, Mater. Sci. Eng. A, 2018, Vol.722, pp.122-128

[30] H. Frost., *Deformation mechanism maps: the plasticity and creep of metals and ceramics*, Pergamon press; 1982

[31] M.J. Starink, S.C. Wang ., *A model for the yield strength of overaged Al–Zn–Mg–Cu alloys*, Acta Mater, 2003, Vol.51, pp.5131–5150

[32] Sanaty-Zadeh, *Comparison between current models for the strength of particulate-reinforced metal matrix nanocomposites with emphasis on consideration of Hall–Petch effect*, Mater. Sci. Eng. A, 2012, Vol.531, pp.112–118

[33] T. Deng, S. Li, Y. Liang, L. Sun, Y. Zhang, ., *Effects of Scandium and Silicon addition on the microstructure and mechanical properties of Ti-6Al-4V alloy,* Journal of Materials Research and Technology, 2020, Vol.9(3), pp.5676-5688

[34] C. Bortolan, L. Campanelli., *Effect of oxygen content on the mechanical properties and plastic deformation mechanisms in the TWIP/TRIP Ti-12Mo alloy,* Mat. Sci. Eng. A., 2021, Vol.817, 141346

Chapter 6: Characterization of Hot Isostatic Pressed Ti-6Al-4V/SiC Functionally Graded Material: Microstructure, Mechanical and Tribological Behaviour

Abstract

Ti-6Al-4V (Ti64)-based functionally graded titanium (Ti) composites reinforced with silicon carbide (SiC) particles were successfully synthesised using the powder metallurgy (PM) hot isostatic pressing (HIP) technique. The microstructure and micro-hardness values varied along different gradient layers as the volume fraction of SiC increased (0-5-10 vol%.). The different layers of the FGM showed good bonding and no cracking was observed along the gradient layers. The Ti64 and SiC powders were blended using roll blending and the average reinforcement particle size (APS) used was 5 µm. The following study investigated the influence of HIP parameters, such as temperature (1160°C) on the consolidation behaviour of the Ti-6Al-4V/SiC FGM and the microstructural evolution along different gradient layers. The microstructure and tribological behaviour of the as-fabricated Ti-6Al-4V/SiC FGM was characterised by means of optical microscopy (OM), x-ray diffraction (XRD), scanning electron microscopy (SEM), micro-hardness testing, the dry-sliding reciprocating test with coefficient of friction (COF) and compression testing. Furthermore, structural-property models were established with the aid of ImageJ to quantify the different phase fractions along the FGM gradient layers, enabling prediction of the strength of the material, which were then compared to compression test values. It is important to note that the study successfully synthesised a Ti64/SiC FGM using the PM HIP technique that had strong interface bonding between the different FGM layers as confirmed by the crack-free micro-hardness readings recorded at each interface zone. Moreover, the FGM showed promising compressive properties even at the highest reinforcement volume fraction regions, including good compressive yield strength values and ductility, there was also a clear trend of improving compressive yield strength and reduction in ductility values as the reinforcement volume fraction was increased. For example, even at the interface region between Ti64 + 5vol.% SiC to Ti64 + 10 vol.% SiC, it had a satisfactory ductility of 9%.

6.1 Introduction

Titanium metal matrix composites (TMCs) offer substantial weight reductions and a higher specific strength compared to steel alloys [1]. Data has been published suggesting that TMCs can operate in high temperature applications, providing a 50% weight reduction while still providing a similar strength, for instance in jet-propulsion systems in the aerospace industry [2]. Incorporating continuous fibres, discontinuous particulates or whisker reinforcements helps to enhance the specific strength, tribological behaviour and thermal stability of the material operating at high temperatures [3]. However, TMCs reinforced with a high reinforcement fraction of tend to suffer with low fracture toughness [4] as the fraction of brittle phases increase and are more prone to thermal stress changes induced by the coefficient of thermal mismatch (CTE) between the metal matrix and ceramic reinforcement. This is where functionally graded metal matrix composites (FGMMC) become the principal choice for demanding applications that require an interior bulk material with greater toughness and an outer shell that is highly wear resistant [5].FGM is a type of composite characterised by a gradient of varying particle type, size and volume fraction that offer different microstructural and compositions with tailored properties along the gradient [6]. Some demanding engineering applications require a high hardness at high operating temperatures and high toughness at lower temperatures [7], and as a result of the grading in FGMMCs, this incompatible set of properties is a possibility. FGMMCs also solve a major problem faced by metal matrix composites (MMCs), which is the metal-ceramic debonding caused by the CTE mismatch that tends to affect the dry-sliding properties of the material [8]. Additionally, FGMMCs have optimisable properties in certain directions along a gradient line such as strength and ductility, hence they can be tailored for very specific applications [9]. Extensive research has been conducted on aluminium (Al) based FMMCs, investigating the different properties ranging from tensile strength [10], wear [11] and hardness [12]. Carvalho et al.[13] synthesised an FGMMC carbon nanotube (CNT) reinforced Al alloy with varying volume fractions of CNT. The results showed that 2 vol.% CNT had the highest tensile strength contribution along the FGMMC. Salama et al. [14] successfully produced a FGMMC CNT reinforced Al alloy using the high energy ball milling (HEBM) PM method. The innermost layer was constructed of pure Al to allow for maximum ductility, while the other layers were reinforced with 1% and 2% CNT to increase the wear resistance. Li et al. [6] successfully synthesised a TiC/Ti-6Al-4V FGM with vary volume fractions (vol.%) of the reinforcing TiC phase from 0-50 vol.% using laser melt deposition. It was reported that when the vol.% of TiC reached 40-50 vol.% severe cracking was observed indicating that the material was very brittle . Panda et al.,[15] fabricated a Ti-TiB FGM by use of sintering varying the TiB vol.% from 0-80 vol.%, with each layer incrementally increasing in 20 vol.% TiB content. The

study deduced that the micro-hardness was increased from 420 HV at the base Ti layer up to 1600 HV at the TiB rich layer.

To date there has been little work carried to investigate the possibility of manufacturing a Ti based FGMMCs by use of the powder metallurgy (PM) hot isostatic pressing (HIP) technique. Therefore, this study was conducted in order to understand the relationship constituting the influence of reinforcement volume fraction on the microstructural development, mechanical and tribological performance of the FGMMC along different gradient layers using HIP as it opens the possibility of manufacturing large FGM components that are microstructurally homogeneous and is a simpler method of synthesizing an FGM.

6.2 Experimental

6.2.1 Material preparation

AGA Ti64 powder, shown in figure 6.3a, has an average particle size (APS) of 15-45µm and was purchased from (LPW Technology, UK). SiC powder with an APS of 5 µm was supplied by (Reade Advanced Materials, USA). Powders were mechanically alloyed (MA) using low-energy ball milling (HMK-1901) for a duration of 6h, with a ball to powder ratio (BPR) of 4:1 and at a constant 250 revolutions per minute (RPM). To create the FGM, three different powders were prepared: monolithic Ti64 (0 vol.% SiC), Ti64 + 5 vol.% SiC and Ti64 + 10 vol.% SiC. The powders reinforced with SiC were MA in the same run. The schematic presented in figure 6.2 shows the FGM preparation route and how different layers were stacked inside the mild steel canister.

6.2.2 Powder HIP

A mild steel canister was fabricated and used to encapsulate the powder layers. The outer diameter was 28mm, with a length of 85 mm and wall thickness of 2.03mm. The powder HIP process of the FGM is depicted in figure 6.1 whereby the powders were MA using ball milling, encapsulated in the canisters with each layer of the FGM being 28mm in height, and the canister was kept static to avoid mixing of different layers. The base layer was Ti64, the second layer was Ti64 + 5 vol.% SiC and final top layer was Ti64 + 10 vol.% SiC, as displayed in figure 6.2. The canister was then outgassed overnight until it

reached a vacuum level of at least 10^{-5} bar and then sealed by hot crimping. The canister then underwent HIP at a temperature of 1160°C, for a period of 3h at a pressure of 140 MPa.

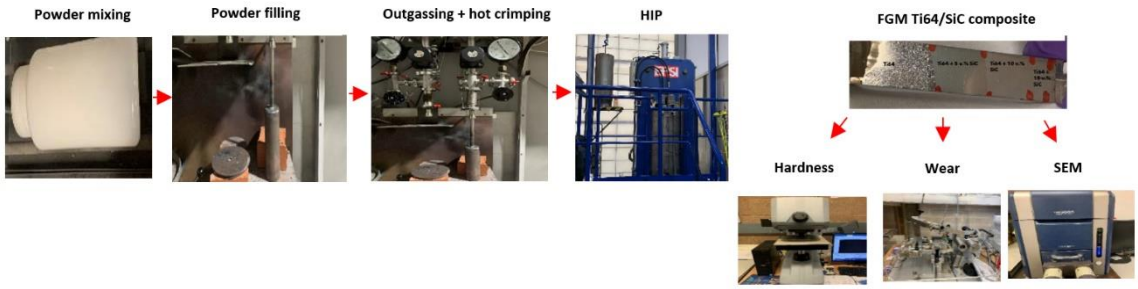

Figure 6.1: *FGM Ti64/SiC composite fabrication process*

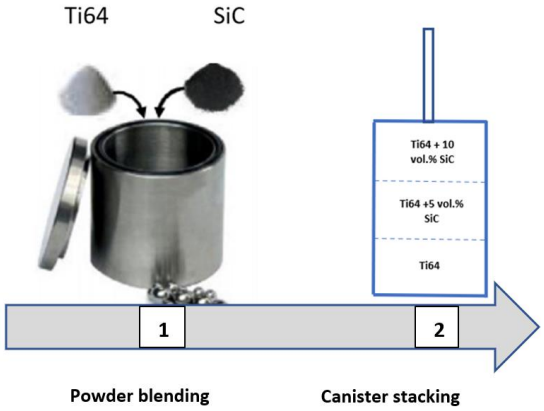

Figure 6.2: *FGM preparation method*

6.2.3 Microstructural characterisation

The as-HIPped FGM was wire cut using an electrical discharge machine (EDM), ground and polished for microstructural characterisation. Scanning electron microscopy (SEM) was first used to analyse the microstructure followed by an energy dispersive spectroscopy detector (EDX), in order to rationalise the FGM phase contents along different gradient layers, in relation to their mechanical and tribological

properties. Optical microscopy (OM) was also utilised to study the different gradient layers of the FGM.

6.2.4 Mechanical and tribological properties

Compression testing was conducted on FGM samples with a diameter of 8mm and a height of 10mm. Five samples were extracted using an EDM Ti64 (FGM 1), Ti64 + 5 vol.%, Ti64 + 10 vol.% interface (FGM 2), Ti64 + 10 vol.% SiC (FGM 3), Ti64 + 5 vol.% SiC (FGM 4), Ti64 + 5 vol.% SiC (FGM 5). The machine used to conduct the compression testing at room temperature was a universal testing machine (ESH Testing 200). The testing was conducted at a constant crosshead rate of 2mm/min using a load cell of 100 kN, the maximum load of the machine. For the micro-hardness measurements, a load of 1kgf was placed on the as-polished samples using a micro-hardness tester (Wilson VH1202, Beuhler) to obtain an average of 10 readings of the different FGM layers. The recommended spacing used was as specified in the ASTM E384-17 standard. Furthermore, four micro-hardness indents using a load of 100g were applied on two of the FGM sample FGM 5 and FGM 2 along the gradient layer and the micro-hardness values rationalised using EDX line scans and mapping of related phase content to the micro-hardness. In terms of the tribological properties of the FGM, a reciprocating wear testing machine with COF measuring capabilities was utilised at room temperature. The counter-body used was an aluminium oxide (Al_2O_3) ball with a diameter of 10mm and a reported hardness of 1600 HV. The test was conducted on a dry surface over the as-polished samples in a reciprocating motion. In terms of the test parameters used, a load of 20N, a sliding speed of 10mm/s and a sliding distance of 5mm were used for a duration of 30 minutes. Finally, the worn surfaces were extensively examined using an SEM and EDX to analyse the wear mechanisms that were at play on the FGM surfaces.

6.3 Results and discussion

6.3.1 Powder characterisation

Figure 6.3a shows an SEM micrograph of as-received AGA Ti64 powder, and the morphology is observed to be mostly spherical with lots of satellites and a few irregular particles due to the inherent production process of gas atomisation. The Ti64 powder size range was 15-45µm as reported by the supplier. Figure 6.3b shows Ti64 reinforced with 5 vol.% SiC, and it can be seen that even after MA the powders, there was a substantial volume of powder clustering and ineffective interfacial bonding

between the SiC reinforcement and Ti64 matrix due to the large size of the reinforcement relative to the matrix. Figure 6.3c the micrograph of Ti64 reinforced with 10 vol.% SiC shows that as the volume fraction of the reinforcement was increased, more clustering and agglomeration of the reinforcement took place, due to the higher volume fraction and relative size to the matrix used.

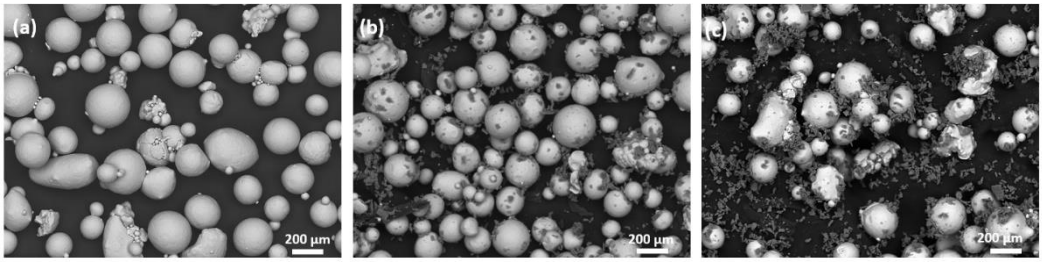

Figure 6.3*: SEM micrographs: (a) AGA Ti64 15-45µm, (b) Ti64+5 vol.% SiC, (c) Ti64+10 vol.% SiC*

6.3.2 Microstructural evolution of Ti64/SiC FGM

Figure 6.4 shows OM images of Ti64/SiC FGM at different layers. The red line in the figure has been drawn in order to separate the interface between one layer of an FGM with the other layer and provide an easier illustration of the figure. Figure 6.4a shows a layer of Ti64 + 5 vol.% SiC on the left and a layer of Ti64 on the right. It can be seen from figure 6.4b that the interface is only a few microns in size while it is also clear that moving from the reinforced side on the left with 5 vol.% SiC to the unreinforced side on the right, the grains change from more equiaxed grains to lamellar grains when observing the reinforced 5 vol.% SiC on the left to the unreinforced layer on the right. This could be attributed to the grain refinement of the reinforcement and how the *in situ* formed hard phases are inhibited grain growth. Figure 6.4c shows Ti64 + 5 vol.% SiC on the left and a layer of Ti64 + 10 vol.% SiC on the right. Again, it can be seen that the layer with 10 vol.% SiC has more equiaxed grains and grain refinement.

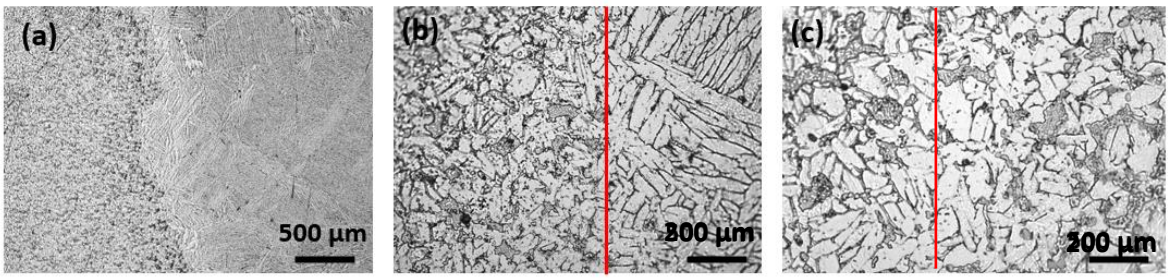

Figure 6.4: *OM of Ti64/SiC FGM: (a) Ti64+ 5vol.% SiC left to Ti64 on right, (b)Ti64+5vol.% left to Ti64 layer on right, (c) Ti64+ 5vol.% SiC on left and Ti64 + 10 vol.% SiC on the right*

Figure 6.5 shows SEM micrographs of the Ti64/SiC FGM at different layers and scales. Figure 6.5a shows an FGM layer changing from a lamellar Ti64 microstructure on the left to a more refined microstructure reinforced with 5 vol.% SiC on the right. The grading helps achieve a wide range of properties from fatigue crack growth resistance due to the coarse lamellar α plates achieved by using the HIP method above the ß-transus temperature, to better wear resistance with reinforcing Ti64 with SiC particles. Figure 6.5b shows the microstructure of Ti64 + 5 vol.% SiC, which clearly demonstrates that the SiC had *in situ* reacted with Ti and resulted in the formation of titanium silicides (Ti_5Si_3) along the ß-grain boundaries and titanium carbide (TiC) that homogenously decorated the prior particle boundaries (PPBs),the presence of Ti_5Si_3 and TiC both had been confirmed by XRD in a previous study. Figure 6.5d shows a micrograph of Ti64 + 5 vol.% SiC on the left and Ti64 + 10 vol.% SiC on the right. In figure 6.5e it can be seen that there was a higher formation of Ti_5Si_3 and TiC due to the higher volume fraction of SiC used, leading to a coalescence between neighbouring Ti particles. Figure 6.5f shows a micrograph of Ti64 + 10 vol.% SiC at a higher magnification and reveals micro-cracks at the brittle zones of the Ti_5Si_3 and TiC.

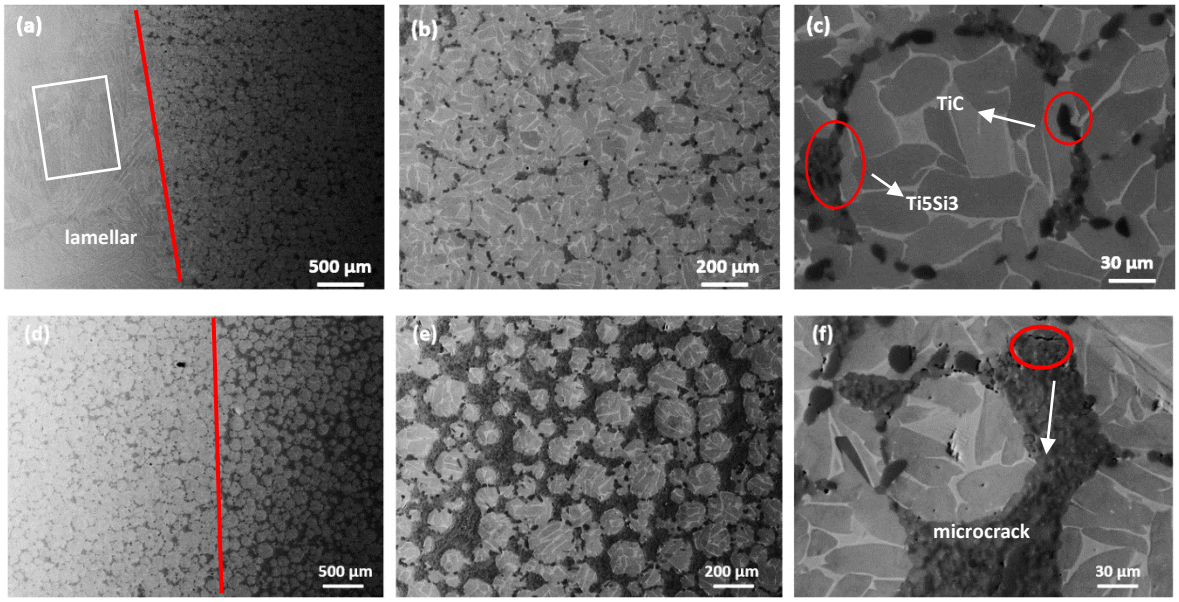

Figure 6.5: *SEM micrographs of Ti64/SiC FGM*

Figure 6.6 shows an EDS line scan along different gradient layers. In figure 6.6a a scan of Ti64 layer to Ti64 + 5 vol.% SiC moving from left to right shows. varying silicon (Si), Ti, Al, vanadium (V) and carbon

(C) content along the gradient layers. In figure 6.6b the line scan confirms that there is no Si diffused into Ti64 on the left, however, a high peak of Si is detected when the scan reaches the Ti64 + 5 vol.% SiC area. Furthermore, moving from left to right there is a higher ß-Ti content, which could be attributed to Si diffusing and being a ß phase stabilising element. The scan presented in figure 6.6c shows the Ti64 + 5 vol.% SiC layer on the left and Ti64 + 10 vol.% SiC on the right. The scan in figure 6.6d confirms a higher peak of Si moving from left to the right, indicating that more Si reacted with Ti resulting in a higher retention of *in situ* formed Ti_5Si_3 phase. Furthermore, show the change from one gradient layer to the next both line scans confirmed the synthesis of a Ti64/SiC FGM via PM HIP.

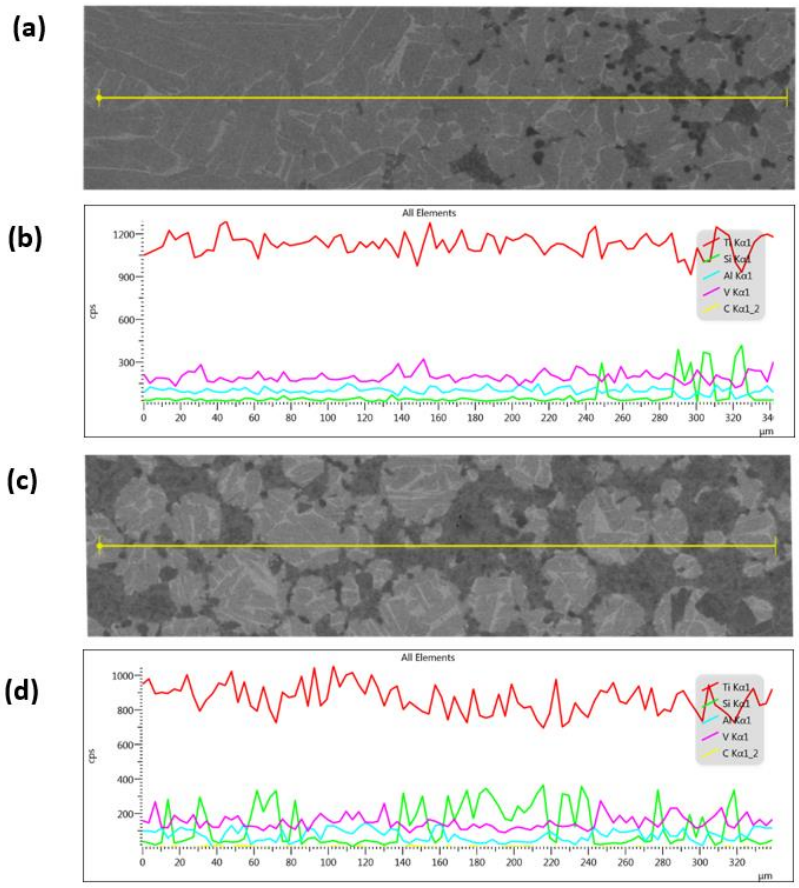

Figure 6.6*: EDX line scans: (a) Ti64 (left) to Ti64 + 5 vol.% SiC (right), (b) EDX line scan of image (a), (c) Ti64+5vol.%SiC (left) Ti64 + 10 vol.% SiC (right), (d) EDX line scan of image (c)*

6.3.3 Mechanical properties

6.3.3.1 Micro-hardness

Figure 6.7 shows the variation of micro-hardness at different layers of the FGM from the unreinforced Ti64, Ti64 + 5 vol.% SiC and Ti64 + 10 vol.% SiC. There is a clear trend of improved micro-hardness as the volume fraction is increased, which is assumed be attributed to the strengthening mechanism of load transfer from the softer matrix to the stiffer reinforcement. It is vital to note that the load transfer mechanism is sensitive to volume fraction due to the load being transferred from the less stiff matrix to the stiffer and harder reinforcement, as seen from equation 6.1 below, whereby f_r is the volume fraction and σ_{ym} is the yield strength of the matrix [3].

$$\Delta\sigma_{L.T} = 0.5 f_r \sigma_{ym} \quad [6.1]$$

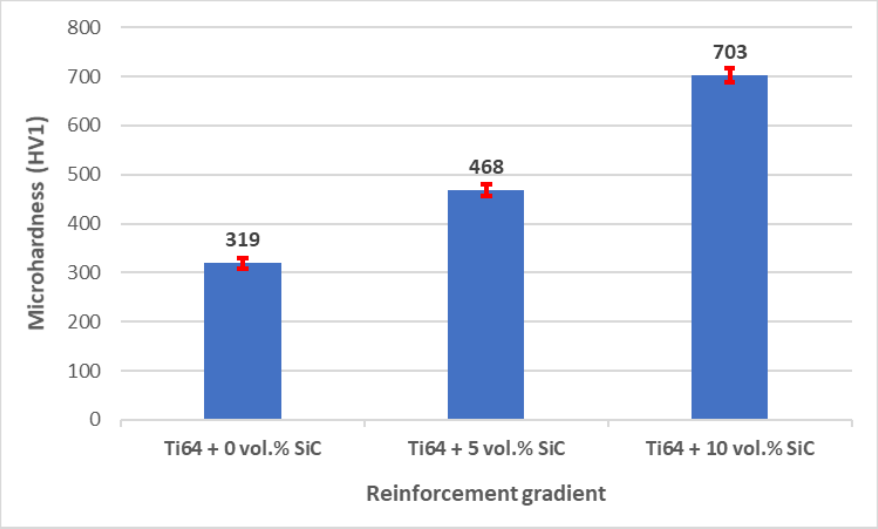

Figure 6.7: *Micro-hardness readings at different gradient layers*

Figure 6.8 shows OM images of micro-hardness indents using a load of 100g along different layers of the FGM. Figure 6.8a shows a line of micro-hardness indentations from the Ti64 layer to the Ti64+5vol.% SiC layer and figure 6.8b shows an indent around the interface area between both the monolithic Ti64 region and the reinforced region. It is quite clear from these two images that there is a variation of micro-hardness. In figure 6.8c indentations can be seen along a layer of Ti64+5vol.% SiC at the bottom and Ti64+10vol.% SiC at the top, with the variation in size due to differing micro-hardness due to the reinforcement volume fraction. Looking at figure 6.8b and 6.8d close to the

interface, micro-cracks can be observed at the indentation, suggesting that the phase was quite brittle. Figure 6.9 presents the graphical representation of the measured micro-hardness values corresponding to the indentations seen in figure 6.8. It is quite clear that the micro-hardness was highest at the top where the Ti64 matrix was reinforced with two strengthening phases: TiC and Ti_5Si_3. In figure 6.9b there is a clear trend of increasing micro-hardness values as the reinforcement volume fraction is raised from 5 vol.% to 10 vol.%, due to the load transfer mechanism discussed earlier. The numbers on the figures corresponds to different locations on the figure, for example number 1 is the indent corresponding to the bottom indent on figure 6.8a and so on.

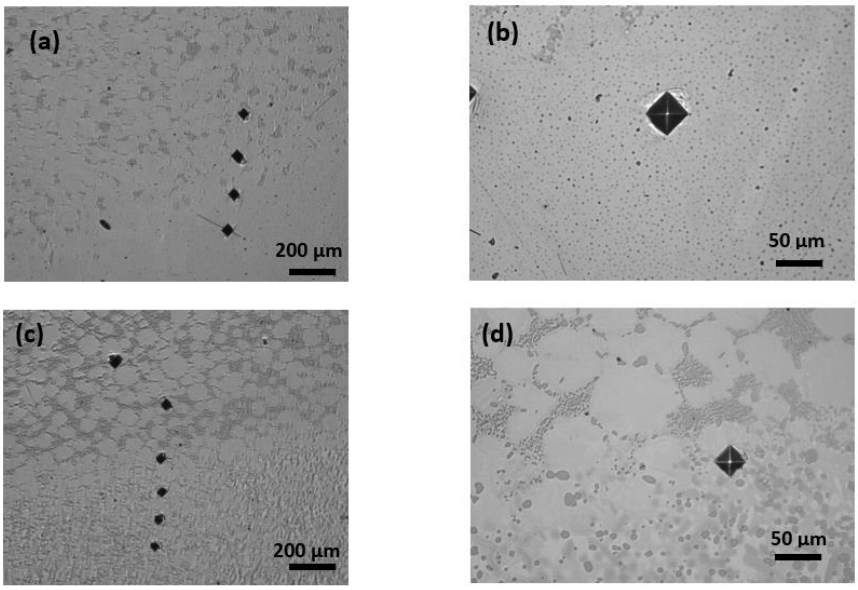

Figure 6.8*: OM micrographs of micro-hardness indents: (a) Ti64 (bottom) Ti64+ 5 vol.% SiC (top), (b) interface between Ti64 and Ti64+5vol.%SiC (c) Ti64+5vol.%SiC (bottom) Ti64+10vol.%SiC top (d) interface between 5 and 10 vol.% SiC*

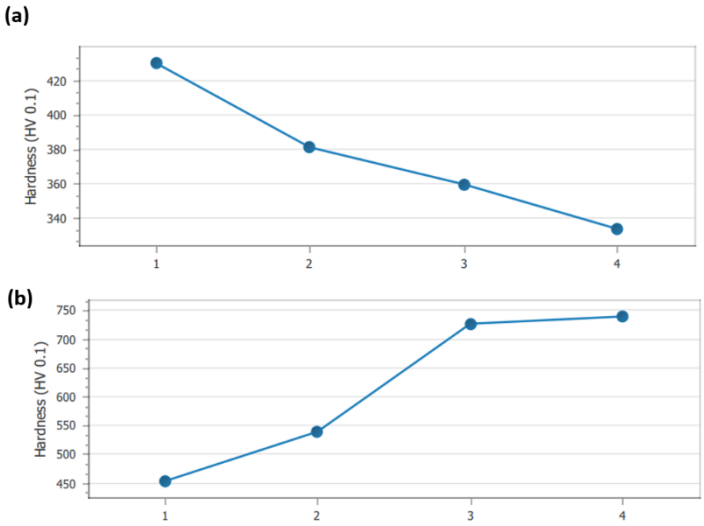

Figure 6.9: *(a) Micro-hardness indents from Ti64+5vol.% SiC to Ti64, (b) micro-hardness indents from Ti64+5vol.% SiC to Ti64+10vol.% SiC layer*

Figure 6.10 shows the EDX mapping of the Ti64 region through to the Ti64+5vol.% SiC region. It can be observed that a very small amount of Si diffused into Ti due to Si being a ß-stabilising element, which could explain the small increase of micro-hardness in the Ti64 region. However, there is a higher count of Si on the right side of the FGM that is reinforced with 5 vol.% SiC, confirming that an *in situ* reaction occurred with the Si and Ti forming Ti_5Si_3.

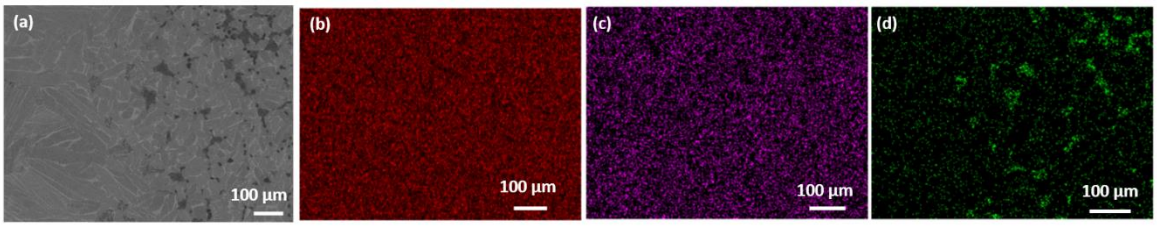

Figure 6.10: *EDX map of Ti64 through to Ti64+5vol.% SiC region; (a) SEM of FGM, (b) EDX map of Ti, (c) EDX map of V, (d) EDX map of Si*

Figure 6.11 shows micro-hardness maps for different regions of the FGM. A matrix of 7x9 using a load of 10g was used to obtain better readings of each phase's micro-hardness contribution. In figure 6.11a an SEM micrograph of the indentation matrix is shown for the Ti64+5vol.% SiC region with its corresponding micro-hardness map. It can be seen from the map that the strengthening phases are not homogenously spread out along the matrix, which has resulted in a variation of micro-hardness readings. Some regions have coalesced with neighbouring strengthening phases resulting in stress concentrations, while other regions are very lean showing limited strength contributions as indicated by the micro-hardness map, particularly in the top section of the microstructure. Figure 6.11b shows an SEM micrograph with an indentation matrix of the FGM area with Ti64+10 vol.% SiC. From observing the corresponding micro-hardness map, it can be seen that the micro-hardness evolution is more homogenous due to the neighbouring strengthening phase coalescing and bridging, creating a more uniform network of hard phases that could act as stress concentrators and areas of failure due to the brittle nature of the hard phases. It is important to note that the indents in the harder phase are represented by smaller indents than those in the Ti64 areas that are represented by bigger indents and a smaller micro-hardness value.

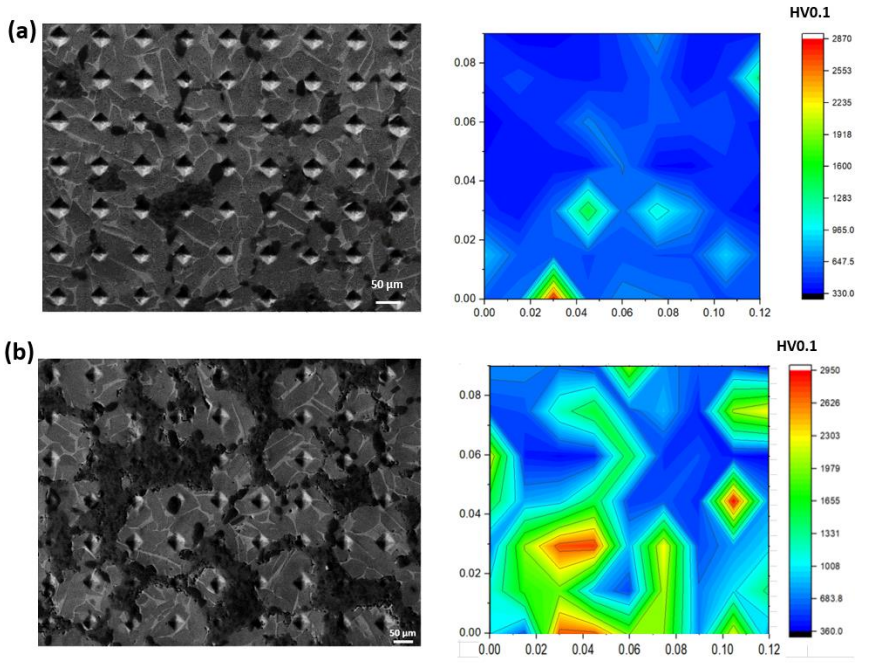

Figure 6.11: *SEM micrograph and corresponding contour maps for micro-hardness matrix using a load of 10g and spacing of 15µm: (a) Ti64+5vol.% SiC (b) Ti64+10vol.% SiC*

6.3.3.2 Compression testing of FGM

Compression testing was carried out due to the reason that in tribological applications, components experience compressive stresses over tensile stresses. Mechanical properties of the FGM were evaluated by conducting compression tests at five different regions of the FGM: unreinforced Ti64 (FGM 1), Ti64+5vol.% SiC to Ti64+10 vol.% SiC (FGM 2), Ti64+10vol.% SiC (FGM 3), Ti64+5vol.% SiC (FGM 4) and the interface between unreinforced Ti64 and Ti64+5 vol.% SiC is (FGM 5). The compressive yield strength, ultimate compressive strength (UCS) and ductility of the different layers of the FGM are listed in table 6.1.

Table 6.10: *Compressive properties at room temperature for Ti64-SiC FGM*

FGM	Yield strength (MPa)	UCS (MPa)	Ductility (%)
FGM 1 (0%)	1570	2201	17.2
FGM 2 (5-10%)	1985	2865	9
FGM 3 (10%)	2042	3263	7.8
FGM 4 (5%)	1780	2620	11.1
FGM 5 (0-5%)	1883	2486	12.3

As predicted, there is an increase in yield strength as the reinforcement volume fraction increases, while ductility decreases. It is evidently clear than introducing SiC particles improved the ultimate compressive strength (UCS) of reinforced FGM in comparison with unreinforced Ti64. For instance, Ti64 (FGM 1) has a UCS of 2201 MPa lower than that for Ti64 + 5 vol.% SiC (FGM 4), which has a UCS of 2620 MPa, an increase of 16% in UCS. Further reinforcing Ti64 with 10 vol.% SiC (FGM 3), results in a significant strength improvement of 3263 MPa, an increase of 33%. However, ductility suffered with increased yield strength with FGM 3 having a ductility reading of 7.8% compared to FGM 1 with 17.2%. For samples that are at the interface, in this study Ti64 to Ti64+5vol.% SiC (FGM 5), the UCS is 2486 MPa an 11.5% strength increase with a ductility that isn't significantly reduced. This can be rationalised in terms of the rule of mixture (ROM) as there is roughly an equal volume of both unreinforced Ti64 microstructure and reinforced Ti64 with SiC microstructure in FGM 5. Finally, the interface between Ti64+5vol.% SiC and Ti64+10vol.% SiC (FGM 2), displays a UCS of 2865 MPa with a ductility of only 9%, revealing a more brittle nature. Figure 6.12 shows a graphical representation of the compressive properties of the five FGM samples.

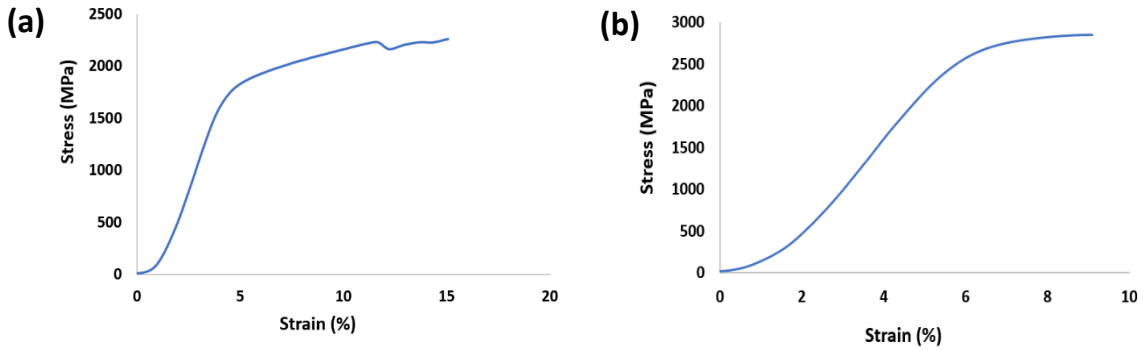

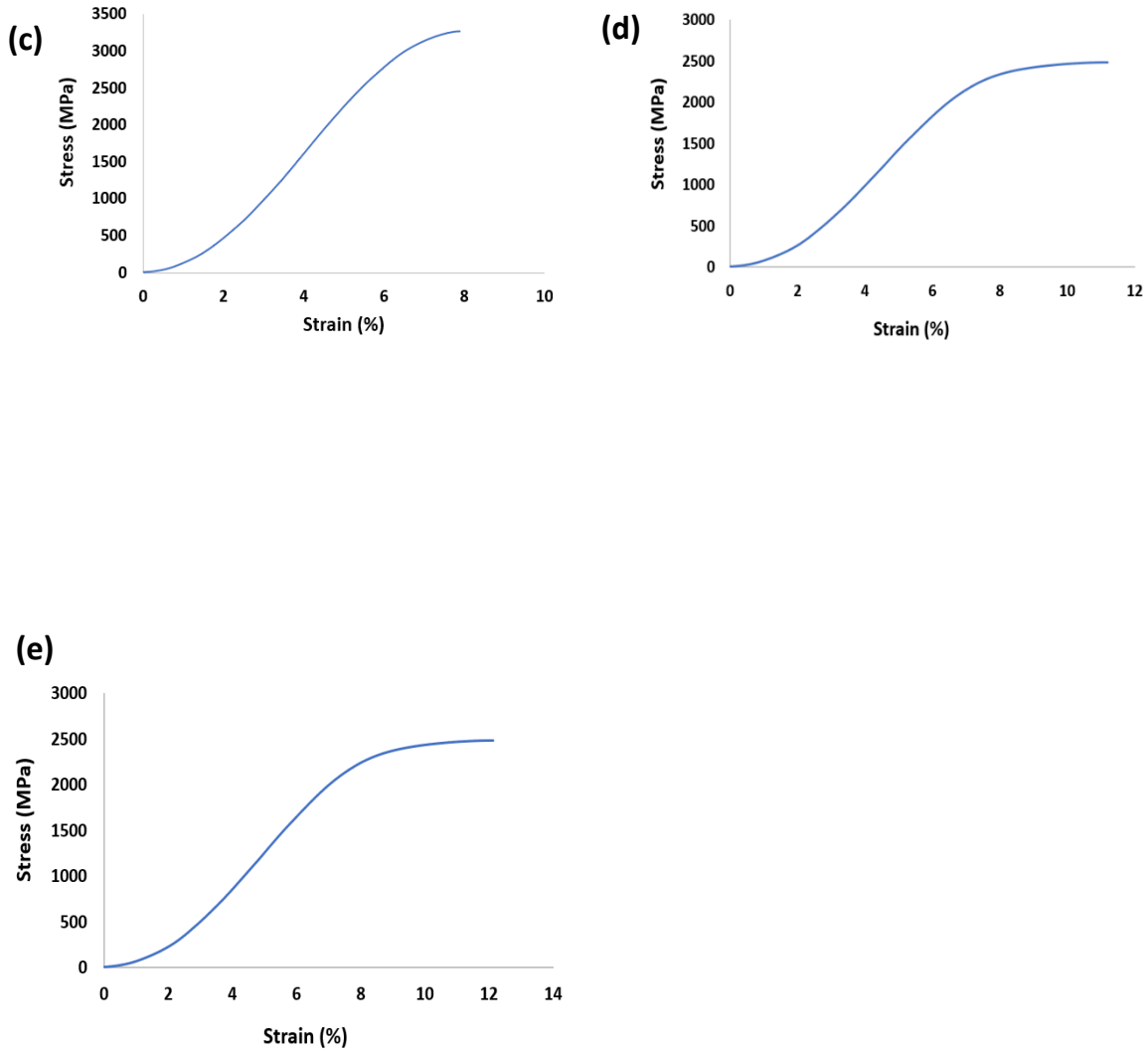

Figure 6.12: *Compressive stress strain diagrams of FGM: (a) FGM 1, (b) FGM 2, (c) FGM 3, (d) FGM 4, (e) FGM 5*

6.3.3.4 Fracture behaviour

Figure 6.13 shows the SEM micrographs of the fracture surfaces of the various regions of the five FGM samples that were compression tested. It can be seen from the fracture surfaces of FGM 1 presented in figures 6.13a-b that ductile fracture is the dominant mechanism of fracture due to the presence of dimples that represent a high amount of plastic deformation and is in agreement with the high ductility figure recorded in Table 6.1. The FGM 1 fracture surface also displays a crack initiation and propagation, confirming the brittle nature of the sample. In figure 6.13c the fracture surface of the interface between Ti64 and Ti64+5vol.% SiC is shown for FGM 5. The grading is quite clearly visible from the two different contrasts displayed in the micrograph due to the different densities of the

materials. In figures 6.13d-e it can be clearly seen that the cracks are initiating from the rich reinforcement regions that have the hard brittle phases and propagating along that region, showing a more brittle in nature, and the crack could have initiated from an agglomerated reinforcement region could be due to the high stress concentration levels. Furthermore, the hard *in situ* formed phases that are protruded in figure 6.13e could indicate and further confirm that the load is transferred from the softer Ti matrix to the stiffer silicide and carbide phases. Figure 6.13f shows the Ti64 region of FGM 5, whereby dimples and tearing features are visible, further evidence of the ductile nature of the FGM sample during compressive loading. FGM 3, compromising of Ti64 + 10 vol.% SiC is shown in figures 6.13g-h, revealing worse crack propagation along the brittle reinforcement zones and a higher fraction of loose debris of hard phases that is in agreement with it having lowest ductility recorded in table 6.1. Figure 6.13h, reveals that cleavage fracture took place, due to the high volume fraction of 10 vol.% SiC incorporated the brittleness of the *in situ* formed phases. FGM 4 displayed in figures 6.13i-j, is Ti64 + 5 vol.% SiC, and it can be clearly seen from the fractography that even though the dominant fracture mechanism is brittle, evident from the cleavage fracture and cracks present, it shows signs of plasticity and a ductile nature in terms of features, such as dimples and tearing ridges, and having ductility confirmed as being recorded as satisfactory at 11.1% in table 1. Finally, FGM 2,shown in figures 6.13k-L, it can be clearly seen that the left side is Ti64 + 5 vol.% SiC and the right side is Ti64 + 10 vol.% SiC. The change from a more ductile but brittle region on the left to a more brittle and less ductile region on the right can be clearly observed in the fractography in figure 6.13k.

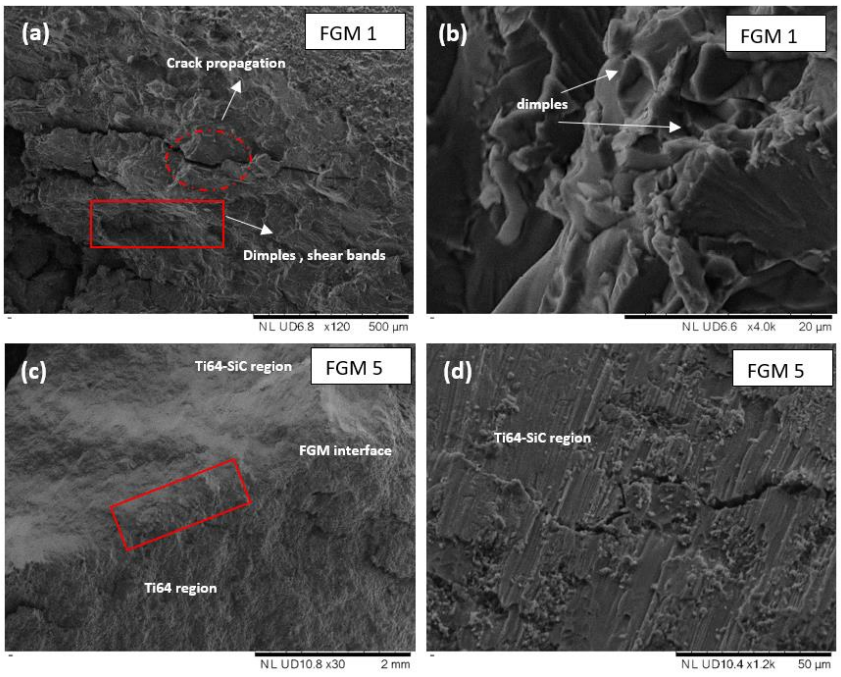

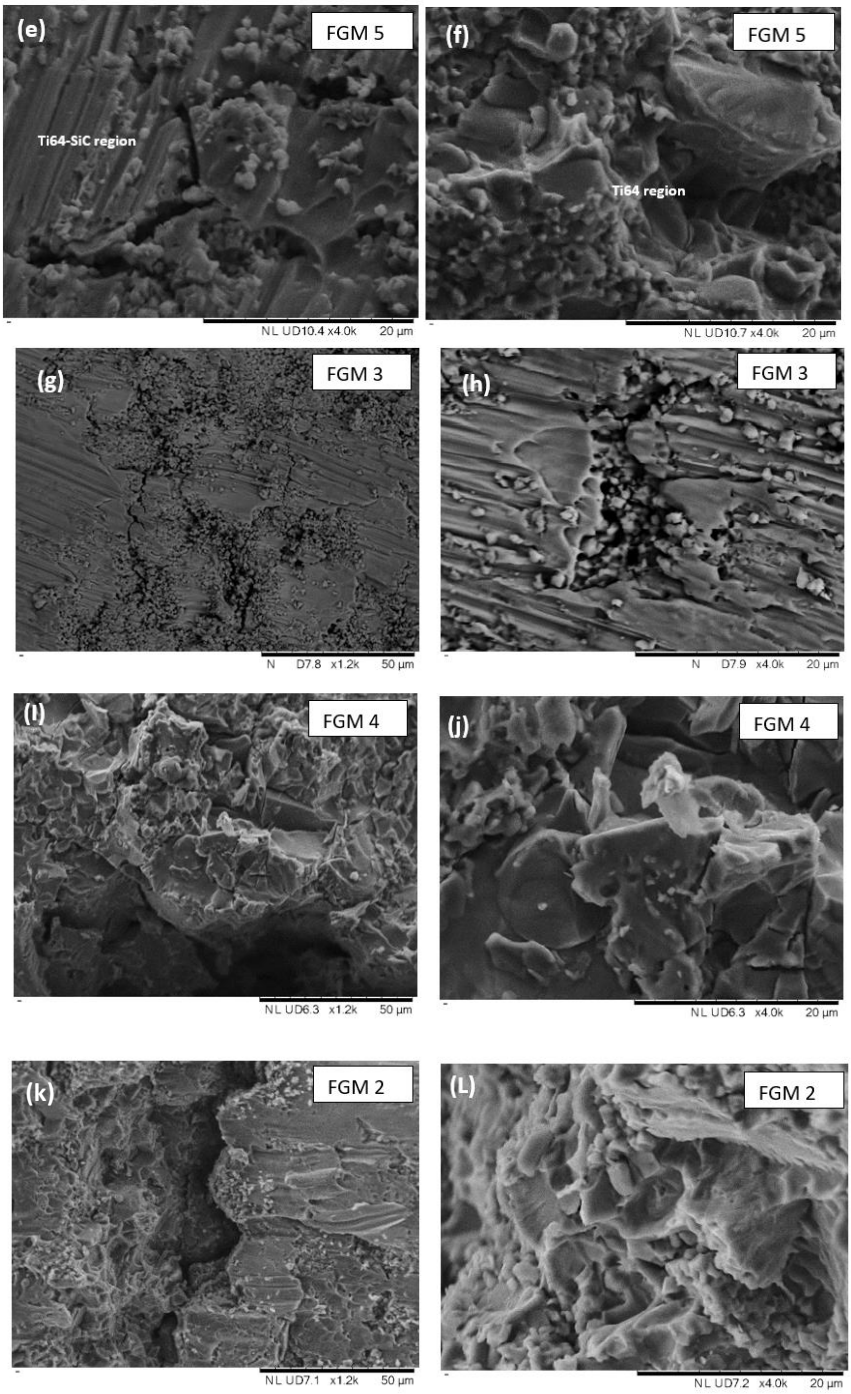

Figure 6.13*: Fracture surface of FGM, (a-b) FGM 1, (c-f) FGM 5 , (g-h) FGM 3, (i-j) FGM 4, (k-l) FGM 2*

6.3.3.5 Tribological properties

6.3.3.5.1 Worn surfaces

Figure 6.14 shows the SEM of the worn surfaces of the three distinctive layers of the FGM. In figure 6.14a the worn surface of monolithic Ti64 are visible with deep ploughed grooves suggesting

deformation of the plastic had occurred due to the abrasive wear mechanism taking place. As the volume fraction of the reinforcement is increased to 5 vol.%, presented in figure 6.14b, there are signs of abrasive wear with less deep ploughed grooves and micro-cutting due to the increased micro-hardness of the reinforced region compared to the unreinforced Ti64 region. This can be mainly attributed to the higher volume fraction of strengthening phases such as TiC and Ti_5Si_3, and the load transfer from the softer matrix to the stiffer reinforcing phases. However, signs of delamination can be seen, indicating that a weak interfacial bond existed between the reinforcing phases and the matrix, potentially due to the relatively large reinforcement starting powder size compared to the matrix. Increasing the volume fraction to 10 vol.% SiC, as seen in figure 6.14c, resulted in further debris forming. It had been expected that the wear would decrease as the reinforcement volume fraction was increased due to the higher recorded micro-hardness, but this was not the case due to the weak interfacial bonding between the matrix and reinforcement, resulting in three body abrasive wear occurring.

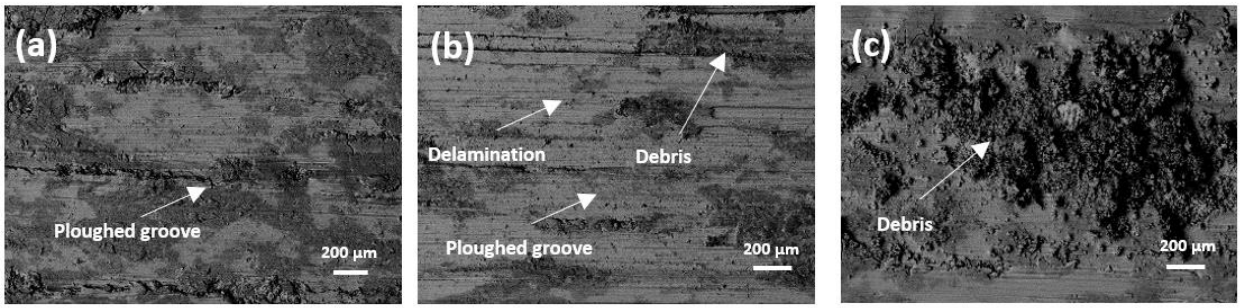

Figure 6.14*: SEM micrographs of worn surfaces: (a) Ti64 region, (b) Ti64 + 5 vol.% SiC region, (c) Ti64 + 10 vol.% SiC region*

6.3.3.5.2 COF

Figure 6.15 shows the recorded COF data of the different regions of the FGM during the wear test. The unreinforced region of Ti64, represented by the orange line, had an average COF of 0.44 over the duration of 750 cycles and was highly unstable. The region of the FGM reinforced with 5 vol.% SiC, shown by the blue plot, resulted in the COF value dropping considerably to approximately 0.34 . This could be attributed to the increase in micro-hardness of the reinforced region of the matrix in comparison to the unreinforced region of Ti64, as well as a strong interfacial bond between the matrix and reinforcement. Further increasing the reinforcement volume fraction to 10 vol.% SiC, results in a dramatic increase in the COF value making it even more unstable than the unreinforced FGM. This can

be explained since, even though the recorded micro-hardness of Ti64 + 10 vol.% SiC FGM region was the highest, the COF was high and unstable due to three body abrasive wear mechanism taking place attributed to the agglomeration of SiC reinforcement at certain regions and the weak interfacial bond due to the relative size of reinforcement and matrix, resulting in delamination of hard phases. Even though the average values were quite distinctive, the variation of the COF plot between different tested materials are large although the test was repeated three times per sample in order to ensure that the data collected were not anomalies and tested at three different locations at each sample which could suggest there was a microstructural inhomogeneity in the samples, hence resulting in a large deviation in the plot.

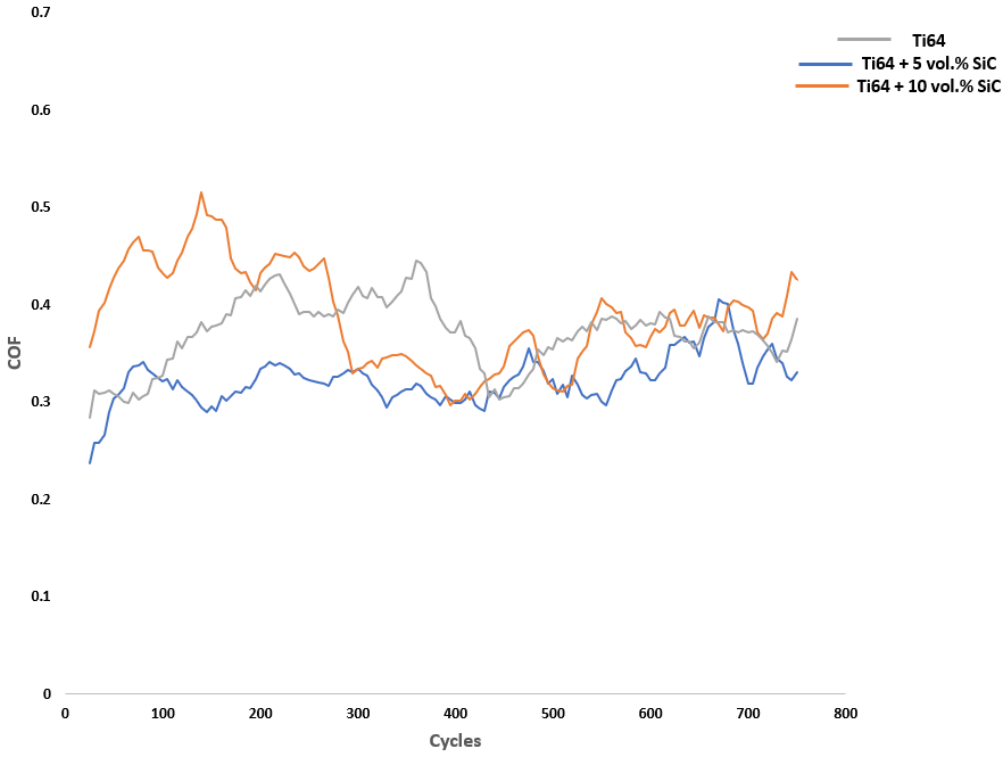

Figure 6.15: *COF data of different regions of Ti64/SiC FGM*

7 Conclusions

This study was conducted to analyse the synthesis of Ti64/SiC FGM with three layers of varying reinforcement volume fraction by use of the PM HIP technique and examined the mechanical and tribological behaviour of the resultant FGM at various regions. The microstructural evolution was thoroughly investigated in terms of phase evolution and how that impacted the micro-hardness along the gradient layers. Furthermore, compression properties at various regions of the FGM were tested and rationalised in terms of the microstructural evolution. The conclusions are as follows:

1) Ti64/SiC FGM was successfully prepared by the PM HIP technique at a temperature of 1160^{o}C,with no visible pores, full consolidation of the composite and synthesis of hard phases accomplished

2) Synthesis of an FGM composite with no visible cracks at the interfaces and a clear trend of increasing micro-hardness with the progression from the unreinforced FGM region to the reinforced FGM region, attributed to the harder phase and potential silicon diffusion into Ti matrix, resulting in an even greater micro-hardness for Ti64 close to interface area.

3) The FGM shows good compression properties even at the interface between the Ti64+ 5 vol.% SiC and Ti64+ 10vol.% SiC regions, with a satisfactory ductility of 9%.

Acknowledgements

The authors acknowledge the Centre of Doctoral Training in Innovative Metal Processing (IMPaCT), funded by the Engineering and Physical Sciences Research Council (EPSRC), and the National Structural Integrity Research Centre (NSIRC), for funding this PhD at the University of Birmingham.

References

[1] H. Attar, S. E. Haghighi, D. Kent, M. Dargusch,. *Recent developments and opportunities in additive manufacturing of titanium based matrix composites, A review, Int. J. Mach. Tools Manuf*, vol.133, 2018, pp. 418-419.

[2] J. Zhang, Y. Zhang, W. Lei, S. Karnati, F. Liou, J. Newkirk., *Microstructure and properties of functionally graded materials Ti6Al4V/TiC fabricated by direct laser deposition,* Rapid prototyping J., vol.24, 2018, pp.677-687

[3] M. Hayat, H. Singh, Z. He, P. Cao., *Titanium metal matrix composites* : An overview, Compos. Pt. A-Appl. Sci. Manuf., vol.121, 2019, pp.418-438

[4] X. Shen, C. Zhang, Y. Yang, L. Liu ., *On the microstructure, mechanical properties and wear resistance of an additively manufactured Ti64/metallic glass composite,* Addit. Manuf., vol.25, 2019, pp.499-510

[5] S. Udupa, R. Shrikantha, K.V. Gangadharan., *Functionally graded composite materials*: An overview, Procedia Materials Science, vol.5, 2014, pp.1291-1299

[6] L. Li, J. Wang, P. Lin, H. Liu., *Microstructure and mechanical properties of functionally graded TiC_p/Ti6Al4V composite fabricated by laser melting deposition,* Ceramics International, vol.43(18), 2017, pp.16638-16651

[7] S.N. Naveen Kumar, R.M. Devarajaiah, T. Ram Prabhu., *Review on aluminium based functionally graded composites,* Materials Today, vol.39, 2021, pp.1743-1749

[8] N. Sindhu, R. Goyal, T. Pullan, Unnikrishnan, T.P.D. Rajan, Sreemanu, S. Vadakke Madam., *Study on Al/TiB_2 functionally graded metal matrix composites,* Materials Today, vol.44, 2021, pp.2945-2951

[9] M. Naebe, K. Shirvanimoghaddam., *Functionally graded materials: a review of fabrication and properties,* Appl. Mater. Today, vol.5, 2016, pp.223-245

[10] R. Ekici, M. Kemal Apalak, M. Yildirim., *Indentation behaviour of functionally graded Al–SiC metal matrix composites with random particle dispersion*, Composites: Part B, vol.42, 2011, pp.1497-1507

[11] N. Radhika, J. Sasikumar, JL. Sylesh, R. Kishore ., *Dry reciprocating wear and frictional behaviour of B4C reinforced functionally graded and homogenous aluminium matrix composites,* J. Mater. Res. Technol., vol.2(9), 2020, pp.1578-1592

[12] K.M. Shorowordi, T. Laoui, A.S.M.A. Haseeb, J.P. Celis, L. Froyen., *Microstructure and interface characteristics of B4C, SiC and Al2O3 reinforced Al matrix composites: a comparative study,* J Mater Process Technol, vol.142, 2003, pp.738-743

[13] O. Carvalho, M. Buciumeanu, S. Madeira, D. Soares, F.S. Silva, G. Miranda., *Optimization of AlSi-CNTs functionally graded material composites for engine piston rings,* Materials and Design, vol.80, 2015, pp.163-173

[14] E. Salama, S. Morad, A. Esawi., *Fabrication and mechanical properties of aluminum-carbon nanotube functionally-graded cylinders,* Materialia, vol.7, 2019

[16] K. Panda, K. Chandran., *Titanium-Titanium Boride (Ti-TiB) Functionally Graded Materials through Reaction Sintering: Synthesis, Microstructure, and properties*. Metallurgical and Materials Transactions A, Vol.34, 2003.

Chapter 7: P/M Hot Isostatic Pressing of TMCs: Influence of Reinforcement Type, HIP Temperature and Reinforcement Volume Fraction on Microstructural Evolution, Mechanical and Tribological Properties

Abstract

Ti-6Al-4V (Ti64) titanium metal matrix composite (TMC) was reinforced with titanium diboride (TiB_2). Particles with varying volume fractions (5-10 vol.%) by use of powder metallurgy (PM) hot isostatic pressing (HIP) technique. In addition, the as-received mechanically alloyed (MA) titanium-silicon carbide (Ti-SiC) nanocomposite and titanium-titanium carbide (Ti-TiC) nanocomposite were successfully prepared by HIP. The following study investigated the influence of HIP temperature (950^{o}C and 1040^{o}C) on microstructural evolution and consolidation behaviour of the HIPped nanocomposites, and how that influenced the mechanical properties, such as micro-hardness and tribological behaviour, e.g. coefficient of friction (COF) and wear. Additionally, the influence of the reinforcement volume fraction (vol.%) on the mechanical and tribological behaviour of Ti64+TiB_2 TMCs were investigated thoroughly. The techniques used to characterise the TMCs were scanning electron microscopy (SEM) and x-ray diffraction (XRD), whilst the dry-sliding reciprocating test with the capability to record (COF data was conducted to assess the tribological properties. Furthermore, structure-property relations of the TMCs were analysed using the rule of mixture (ROM) in order to predict micro-hardness values, and strengthening mechanisms were also discussed. Some of the key findings of the study were that the COF of Ti64 + 10 vol.% TiB_2 was higher than that of Ti64 + 5 vol.% TiB_2, mainly due to three-body abrasive wear, which is attributed to the weak interfacial bonding between the reinforcement and matrix. Ti-TiC had the lowest COF value due to its high micro-hardness value and homogenous microstructure; this could be attributed to the MA route selected. Moreover, the micro-hardness increases and low COF value of Ti-TiC and Ti-SiC could be attributed to Orowan strengthening mechanism caused by the resistance of the nanoparticles used as reinforcement. The

experimental and theoretical values of micro-hardness were in agreement, which validate the modified ROM Reus model.

7.1 Introduction

Titanium (Ti) and its alloys are known to offer high specific strength, weight reductions and corrosion resistance in comparison with nickel and steel alloys [1], making them a good fit for petrochemical and structural applications. However, titanium and its alloys do suffer some shortcomings, such as low wear resistance, low Young's modulus and are not suitable for high temperature applications above 700℃ [2]. This is where titanium metal matrix composites (TMCs) come into play. By reinforcing the titanium matrix with hard ceramic particles, such as silicon carbide (SiC) [3], titanium diboride (TiB) [4], tungsten carbide (WC)[5], titanium nitride (TiN) [6], the wear and thermal resistance of the composite can be improved. PM is used as the standard for TMC fabrication in industry since ex-situ techniques such as ingot metallurgy are deemed not suitable for TMCs manufacturing due to the high reactivity of Ti with oxygen [7]. Some of the challenges of TMCs fabrication using PM technique are the powder homogeneity, dispersion of the reinforcement in the matrix and the formation of brittle intermetallic phases [8]. Variables that can maximise and enhance the properties of the TMCs are the reinforcement size, volume fraction, reinforcement and matrix morphology, dispersion method, and most importantly, the interfacial bonding between the matrix and the reinforcement [9]. It should also be noted that it is widely reported in the literature that TMCs fabricated by use of an *in situ* route display a higher Young's modulus and specific strength compared with ex-situ fabrication techniques [10]. Oyelola et al.,[5] successfully synthesised a functionally graded (FG) Ti-6Al-4V /WC produced by direct energy deposition. It was reported that TiC containing W (tungsten) rich precipitates in the matrix, resulted in an increased hardness, and ultimately better wear properties. Kgoete et al.,[6] studied the oxidation resistance of spark plasma sintered Ti-6Al-4V/TiN composites. They found that the composites thermally oxidised and Ti-6Al-4V consolidated with TiN particles, which resulted in improved micro-hardness and high temperature characteristics. It is well documented in the literature that the foremost blending method for TMCs is mechanical alloying (MA) using low-energy ball milling [11]. Reported applications of TMCs are for use in thrusters, spray nozzles and compressor fan blades, as they are light weight and provide high wear resistance, corrosion resistance, and enhanced strength and hardness [12]. Weng et al.,[13] successfully produced a Ti_5Si_3/TiC reinforced Co-based coating on the surface of a Ti-6Al-4V matrix, which resulted in an enhanced tribological performance as a result of the in-situ formed phases.[14]. To date there has been little work carried out on HIP of Ti-TiC, Ti-SiC and Ti-WC nanocomposites, therefore, this study was conducted to analyse the effect of HIP temperature on consolidation, microstructural evolution and tribological performance of the different as-received MA TMCs reinforced with nano-sized WC, SiC and TiC composites. Furthermore, the work will also investigate the influence of reinforcement volume fraction on Ti64-TiB_2 composites fabricated

by the PM HIP method. As to the authors knowledge, there is not much work done on HIPping of Ti-TiC, Ti-SiC and Ti-WC nanocomposites.

7.2 Experimental

7.2.1 Materials

Grade 2 titanium (Ti) powder with a particle size range of 45-150 µm was MA with different nano-reinforcements such as WC (22.5 wt.%), TiC (25 wt.%) and SiC (42 wt.%). The as-received powder was MA and supplied by MBN Nanomaterialia, Italy. Argon gas atomised (AGA) Ti-6Al-4V (Ti64) powder with a particle size range of 15-45 µm was purchased from LPW Technology, UK, while titanium diboride (TiB_2) powder with an average particle size of 5 µm was purchased from Reade Advanced Materials, USA, and used as the reinforcement for the Ti64 matrix.

7.2.2 Powder HIP

The as-received MA composites were consolidated using HIP. Mild steel canisters with an outer diameter of 30.5mm, length of 70 mm and wall thickness of 2.03 mm were welded using Tig welding at the University of Birmingham facility. The canisters were then leak tested using a helium leak detector system (PFEIFFER VACUUM) to ensure they were gas tight at 10^{-7} mbarl/s. The canisters were then filled with powders in a glovebox (Saffron glovebox), outgassed overnight until they reached a vacuum level of at least 10^{-5} bar then hot crimped. In addition, the first set of canisters underwent HIP using an (EPSI machine, HIP). At 1040^{o}C, a pressure of 140 MPa and a 3h dwell time was applied for the MA powders and another set prepare by HIP at a sub ß-transus temperature of 950^{o}C, dwell time of 3h and a pressure of 140 MPa for the MA powders. In terms of the blended powders consisting of Ti64 and TiB_2, the canisters used HIP at 1160^{o}C, 140 MPa and a dwell time of 3h. Ti64 was roll blended with TiB_2 with volume fractions of 5 vol.% and 10 vol.% for a time duration of 6h.

7.2.3 Microstructural characterisation

In terms of microstructural characterisation, the as-received powders were analysed using an SEM and energy dispersive x-ray spectroscopy (EDS) in order to view powder morphology and the phases

present. Cross-sections of the powders were analysed using SEM in order to determine whether any internal defects such as porosities were present, which could affect densification and consolidation behaviour. The as-HIP samples were electrical discharge machine (EDM) cut, ground, polished and etched using Kroll reagent (92% H_2O, 2% HF and 6% HNO_3) for about 10 seconds for SEM and XRD analysis. SEM was used to observe microstructural evolution, and XRD to identify the different phases present in the samples post HIP. The machine used for XRD was the AXRD, manufactured by Protofrom (AXRD, Proto) with a wavelength (λ) of 1.5406°A and Cu Kα radiation and measurements collected at 0.02º step size and 1s time/step.

7.2.4 Tribological and mechanical properties

Micro-hardness matrix indentations of nine by seven (9x7) were conducted on the TMCs 15µm apart in order to study and understand the contribution of the different phases in relation to the strengthening effect on the composite. The measurements were taken using the (Wilson VH1202 , Buehler), with the lowest load of 10g in order to specifically assess the different phases individually and understand their contribution to the overall strength. Furthermore, 10 indentations using the spacing recommendations of the ASTM E384-17 standard and a load of 1 kg were also measured in order to obtain an average micro-hardness for the TMCs. In terms of studying the wear properties, the wear performance was investigated at room temperature using an in-house sliding reciprocating machine at the University of Birmingham that can record COF data. The counter-body used were Al_2O_3 balls with a 10mm diameter and high micro-hardness of approximately 1600 HV and the tests were carried at room temperature. The load used for the reciprocating dry sliding wear test was 20 N, with a sliding distance of 5 mm and sliding speed of 10 mm/s for a total of 750 cycles. The worn surfaces were further analysed under SEM and EDX in order to comprehend the dominant wear features present. Finally, the wear depth was measured and characterised using a (Infinitefocus microscope, Alicona).

7.3 Results and discussion

7.3.1 Powder Characterisation

Figure 7.1 shows the SEM micrographs of the as-received MA powders. As seen from figure 7.1a that the Ti (45-150µm) powder morphology is not spherical, being irregular in shape and resembling platelets. However, the nano TiC reinforcement is seen at figure 7.1a to be homogenously distributed on the Ti matrix with very few loose particles, displaying a strong interfacial bonding, which enhances the mechanical and tribological properties. Furthermore, figure 7.1b shows the powder morphology of the MA Ti-SiC TMC that is irregular and rocky in shape and reinforced with finely distributed nano-SiC particles with very few loose particles. Finally, figure 7.1c shows the powder morphology of Ti-WC whereby the nano WC reinforcement is homogenously decorating the Ti matrix. It is important to note that the irregular, rocky platelet shaped Ti matrix could affect the densification behaviour in comparison with a spherical powder morphology. Figure 7.1d shows the powder morphology of Ti64+5 vol.% TiB_2 that was roll blended (RB). It can be seen from the micrograph that the majority of the reinforcement powder is stuck to the surface of the Ti64 matrix. However, increasing the volume fraction of TiB_2 in Ti64 matrix to 10 vol.% has resulted in reinforcement clustering and a higher fraction of the particles not adhering to the matrix, as observed in figure 7.1e, is due to the relatively large reinforcement size in relation to the matrix and the RB mixing technique used.

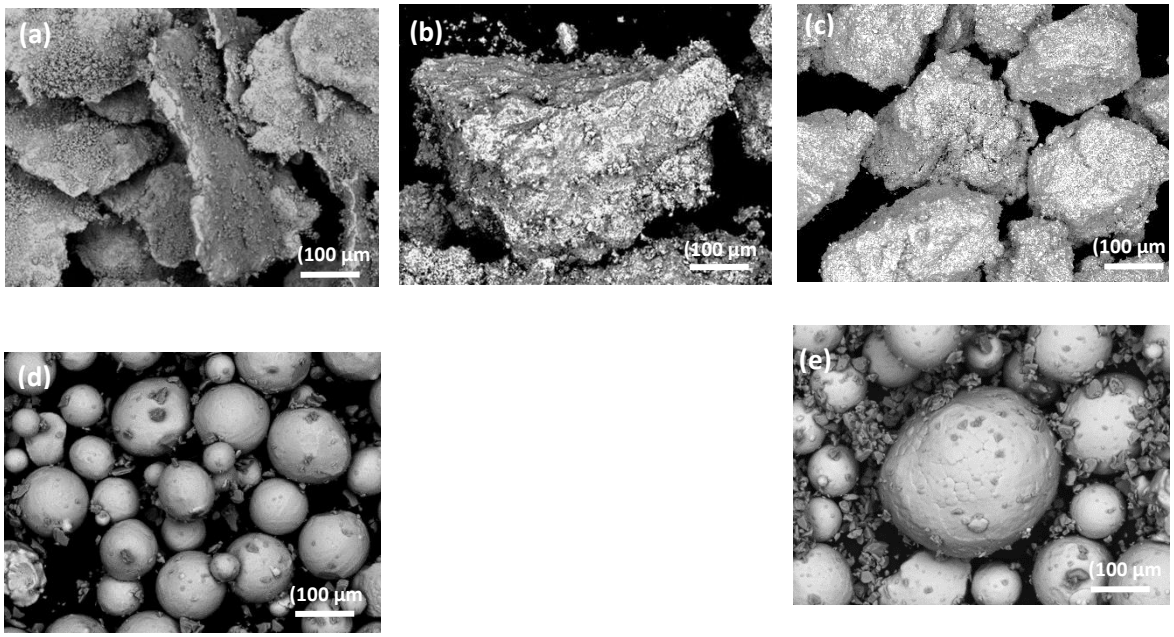

Figure 7.1: *SEM micrographs of as-received powders: (a) Ti-TiC (25 wt.%), (b) Ti-SiC (42 wt.%), (c) Ti-WC (22.5 wt.%), (d) Ti64 + 5 vol.% TiB_2, (e) Ti64 + 10 vol.% TiB_2*

Figure 7.2 shows an EDX mapping of the as-received powders in order to determine which powders were the reinforcements and whether they were homogenously distributed on the matrix powder. Figure 7.2a and 7.2b show large irregular Ti particles , with smaller TiC reinforcements stuck to the matrix , confirming that the MA powder was Ti-TiC. In figures 7.2c and 7.2d the EDX scan confirms that the large irregular powder morphology was Ti and that the small nanoparticles attached to the surface of the Ti matrix were silicon (Si) rich confirming that they were SiC nanoparticles. Finally, figures 7.2e and 7.2f confirmed that the large irregular flaky powder morphology observed in figure 7.1c was Ti, while the nanoparticles attached were WC dominant.

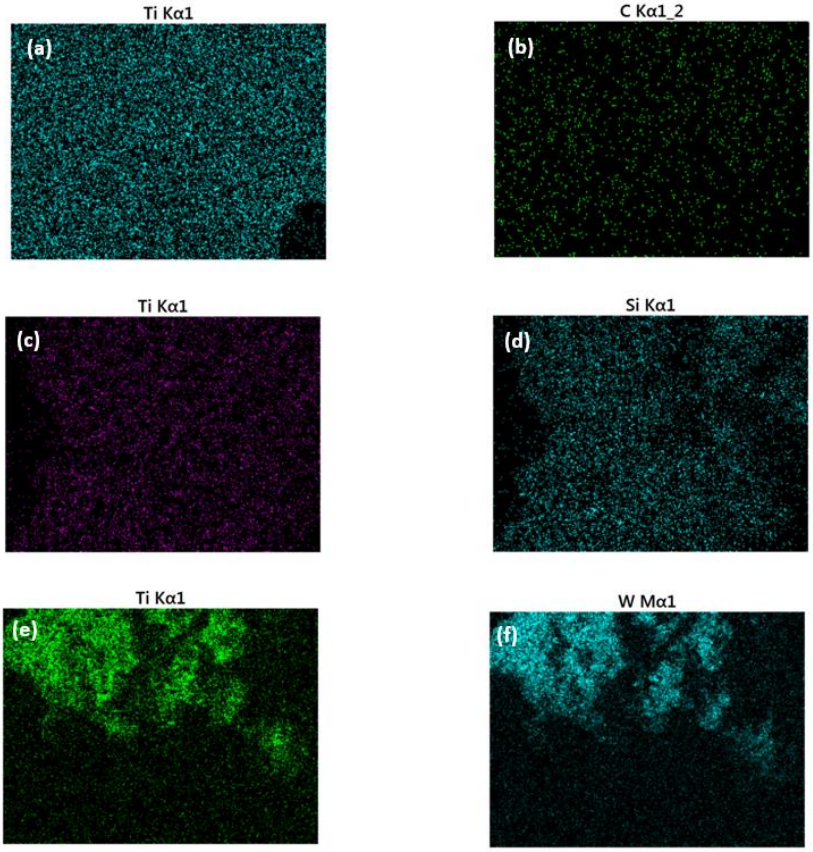

Figure 7.2: *EDX maps of as-received powders: (a-b) Ti-TiC (25 wt.%), (c-d) Ti-SiC (42 wt.%) , (e-f) Ti-WC (22.5 wt.%)*

Figure 7.3 shows the SEM cross-sections of the different as-received MA powders. The cross-sections were made by taking loose powders, grinding and polishing them for a few seconds at the lowest grinding and polishing settings and then taken into SEM for microscopy analysis. In figure 7.3a the cross-section of Ti-TiC revealed internal porosities and other defects due to micro-cracking originating from regions reinforced with the hard brittle TiC powder. Figure 7.3b shows the cross-section of Ti-SiC powders and clearly reveals more internal pores , cracking and defects, while the Ti-WC cross-section

presented in figure 7.3c displays no apparent porosities or cracking. The internal porosities and defects could explain the really low packing fraction and tap density.

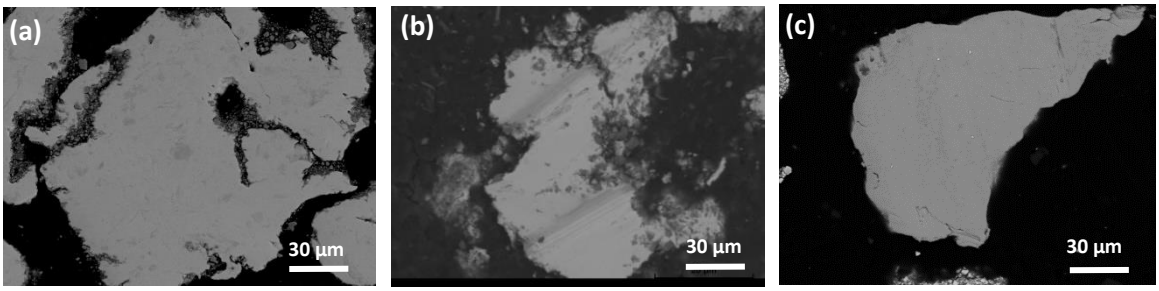

Figure 7.3: *SEM of as-received powder cross-sections: (a-b) Ti-TiC (25 wt.%), (c-d) Ti-SiC (42 wt.%), (e-f) Ti-WC (22.5 wt.%)*

7.3.2 Microstructural characterisation

Figure 7.4 shows SEM micrographs of HIPped and etched specimen microstructures. In figure 7.4a the microstructure of as-HIPped Ti-TiC presented was prepared at a HIP temperature of 950°C, while Figure 7.4b shows the microstructure of as-HIPped Ti-TiC at a HIP temperature of 1040°C. The transformation temperature for commercially pure (CP) Ti is approximately 882°C. HIPping at a higher temperature will stabilize the ß phase, since carbon (C) is an α stabilising element and an interstitial with a high solubility in Ti, as it diffuses into Ti, it will stabilise the α phase at a higher temperature. However, conducting HIP at elevated temperatures, such as 950°C and 1040°C, will stabilise the ß phase and would transform the Ti microstructure from the α phase to the β phase. It can be seen from the microstructure of Ti-TiC prepared at 950°C, in figure 7.4a, that the porosities are visible and that the temperature was not high enough to drive diffusion and ensure full consolidation. However, increasing the temperature to 1040°C, as seen in figure 7.4b, stimulated diffusion and the level of porosity was decreased. TiC is known to be a thermodynamically stable ceramic and is used in ex situ techniques, with no change in size or morphology, and no new chemical compounds are formed. However, it is widely reported that ex situ processing results in enhanced mechanical and tribological performance [10]. It is worth noting that the homogeneity of the TiC phase encasing the Ti matrix was excellent at both HIP temperatures of 950°C and 1040°C due to the MA route used, as seen in figure 7.4c and 7.4d, . In figures 4e-4h the influence of HIP temperature on the consolidation behaviour of Ti-SiC composite is presented. It can be clearly seen in figure 7.4e and figure 7.4g that HIPping at 950°C, did not ensure full consolidation with various porosity regions visible, and an incomplete *in situ*

reaction took place. On the other hand, raising the HIP temperature to 1040°C ensured full consolidation with no visible porosities and a complete *in situ* reaction, as seen in figure 7.4f and figure 7.4h. By observing the Ti-Si phase diagram at a temperature above 886°C and a Si weight percentage of in the region of 30-40 wt.% , it is expected that titanium silicide (Ti_5Si_3) would form [3]. Furthermore, by assessing the Ti-C phase diagram, it can be concluded that at a temperature range higher than 920°C, β-Ti and titanium carbide (TiC) would form. Ti-WC composites are shown in figures 7.4i and 7.4j, and it can be clearly seen that at 1040°C there was a lack of consolidation, large visible porosities and an incomplete *in situ* reaction . Figures 7.4k and 7.4l shows the microstructure of Ti64 + 5 vol.% TiB_2 composite HIPped at a temperature of 1160°C. In both microstructures that there are regions of TiB rich and TiB lean zones, due to the inhomogeneous distribution of TiB_2 during the mixing process and clustering that was visible in the powder morphology micrograph in figure 7.1d. It can also be seen that an *in situ* reaction took place between β-Ti and TiB_2 as explained by equation 7.1.

$$Ti + TiB_2 \longrightarrow 2TiB \qquad [7.1]$$

Increasing the volume fraction of TiB_2 to 10 vol.% , resulted in longer TiB whiskers at the β grain boundary, as displayed in figures 7.4m and 7.4n, which are denser, a coalescence between neighbouring TiB whiskers, which could result in strengthening of that region ,and the TiB whiskers were also seen to adhere to the prior particle boundaries (PPBs). The TiB phase has been confirmed by the XRD scan in figure 7.6a.

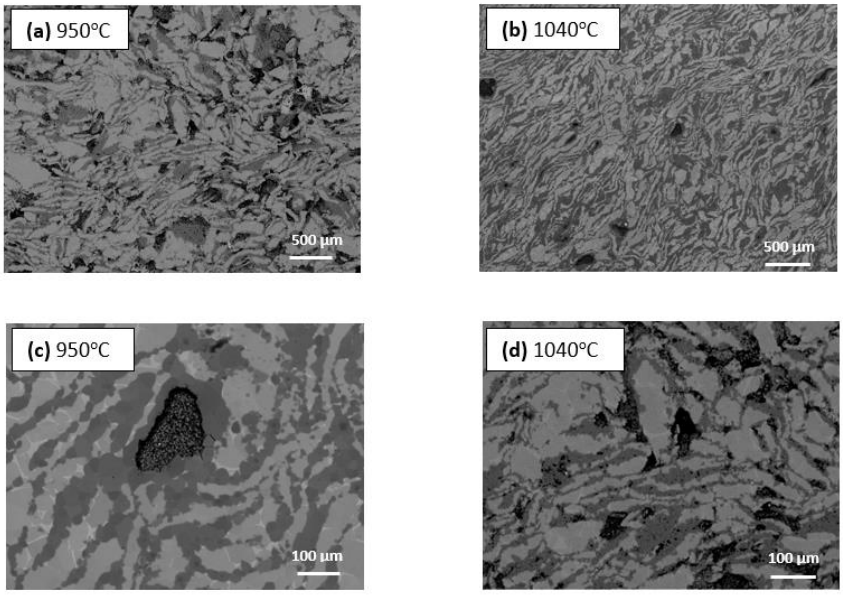

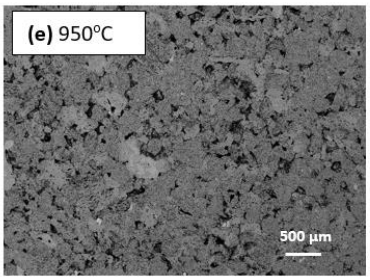
(e) 950°C
500 µm

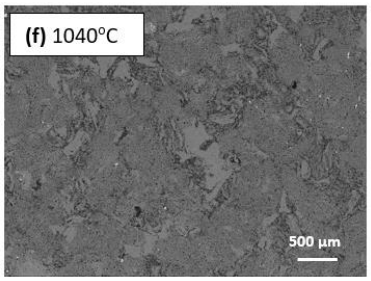
(f) 1040°C
500 µm

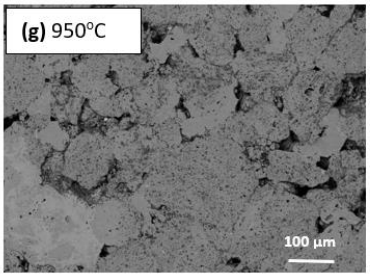
(g) 950°C
100 µm

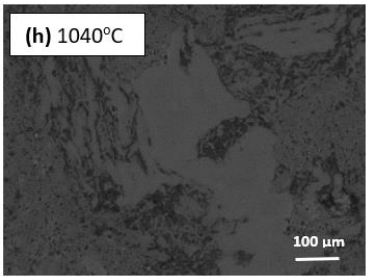
(h) 1040°C
100 µm

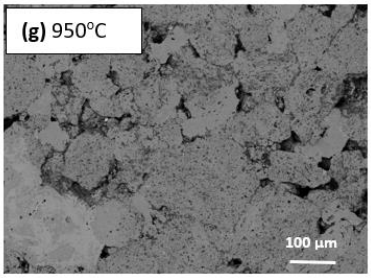
(g) 950°C
100 µm

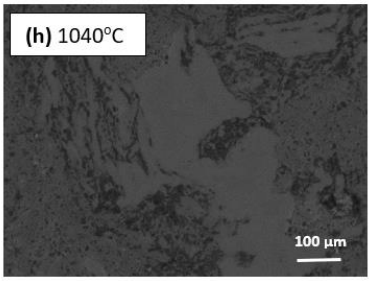
(h) 1040°C
100 µm

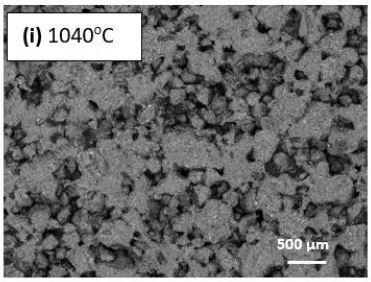
(i) 1040°C
500 µm

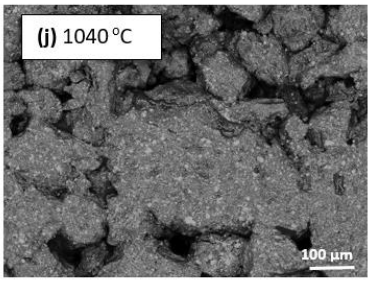
(j) 1040 °C
100 µm

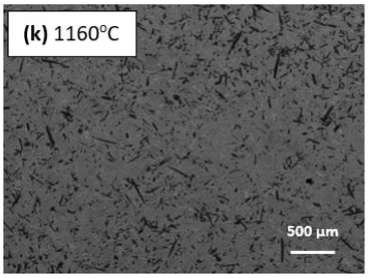
(k) 1160°C
500 µm

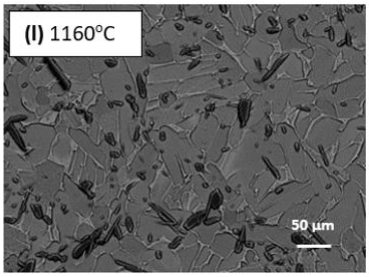
(l) 1160°C
50 µm

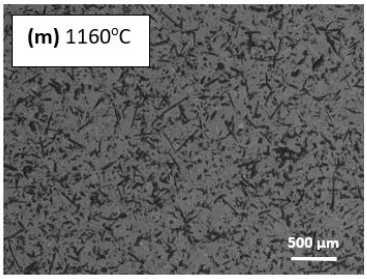
(m) 1160°C
500 µm

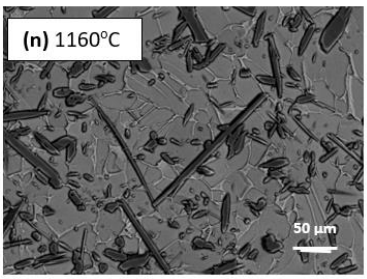
(n) 1160°C
50 µm

Figure 7.4: *SEM micrographs of as-HIPped microstructures: (a, c) Ti-TiC (950 °C), (b,d) Ti-TiC (1040 °C), (e,g) Ti-SiC (950 °C), (f,h) Ti-SiC (1040 °C), (i,j) Ti-WC (1040 °C), (k,l) Ti64 + 5 vol.% TiB_2 (1160 °C), (m, n) Ti64 + 10 vol.% TiB_2*

Figure 7.5 images shows the EDS of Ti-SiC composite prepared by HIP at a temperature of 1040°C. The layered EDS map presented in figure 7.5b confirms that the dark contrast precipitates are rich in Si, as indicated by the red areas. In figure 7.5e it can be seen that there is a small count of C present, which could have diffused into Ti matrix and strengthen the composite further. Finally, in figure 7.5f, a spectrum of the Ti-SiC composite shows a high peak of Ti, Si and a small peak of C, which could indicate the formation of the silicides and potentially carbide phases.

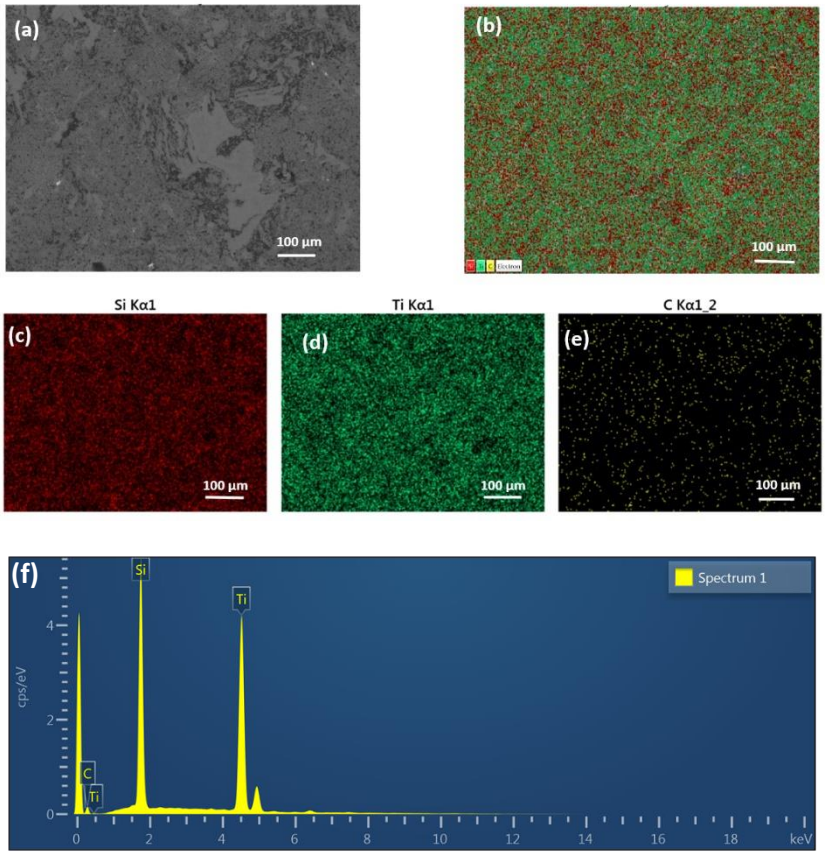

Figure 7.5: *EDX of Ti-SiC HIPped at 1040°C*

The XRD pattern displayed in figure 7.6a, shows the presence of TiB at approximately 41° and 42° but no sign of TiB_2 diffraction peaks, confirming that TiB_2 had fully reacted with Ti in-situ synthesising the TiB phase. The other peaks are α Ti with the exception of a small peak at approximately 38.5° that

corresponds to β Ti as the HIP temperature was 1160°C. The XRD pattern in figure 7.6b demonstrates that Ti and SiC successfully reacted to synthesise Ti_5Si_3 and TiC as highlighted by the cross and triangle in the figure respectively. The rest of the peaks represent the Ti matrix with the α/β phases shown. Figure 7.6c displays the XRD pattern of Ti-TiC, whereby the formation of the TiC phase peak can be detected. The Fe is detected as there was some canister diffusion zone material left on the sample.

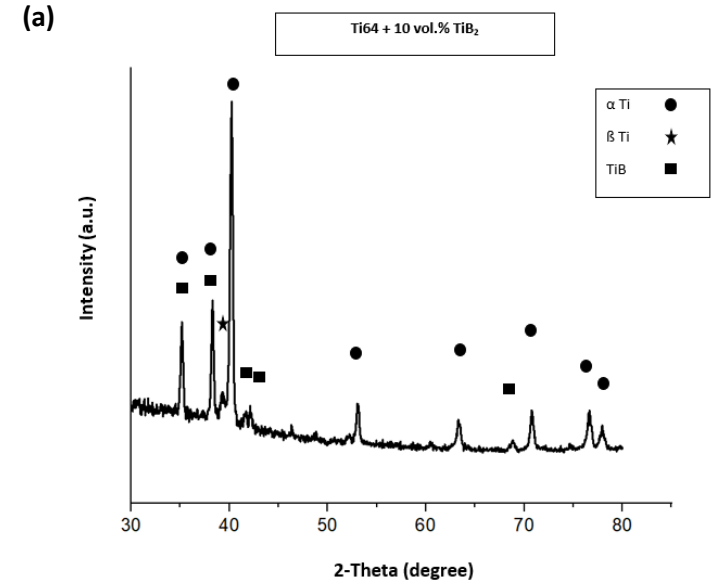

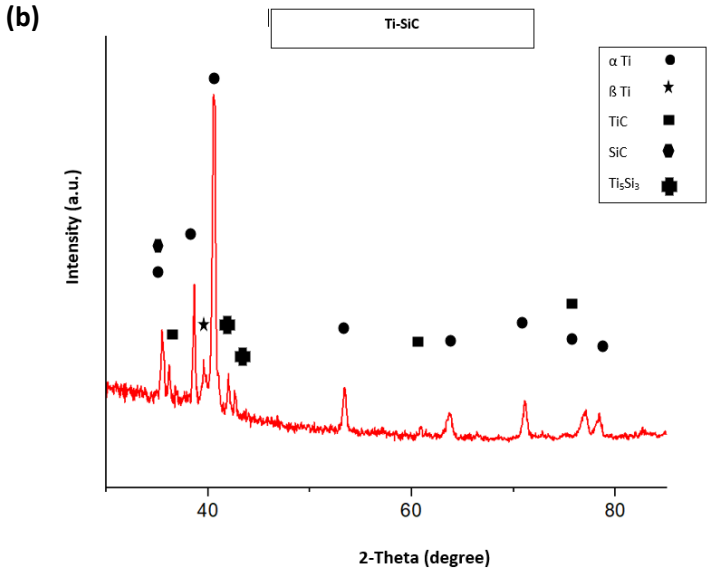

(c)

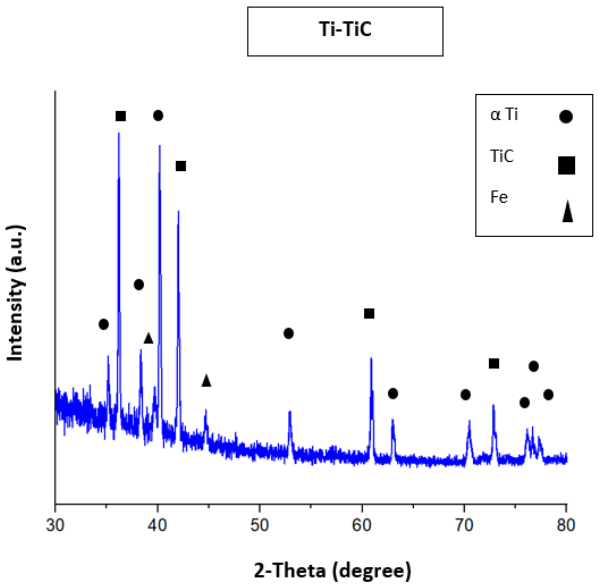

Figure 7.6: *XRD scans of as-HIPped samples (a) Ti64 + 10 vol.% TiB_2, (b) Ti-SiC, (c) Ti-TiC*

7.3.4 Mechanical properties

Figure 7.7a Shows the micro-hardness values for Ti64-TiB_2 composite measured using a 1kgf load. It can be clearly seen that increasing the reinforcement vol.%, attributes, in this instance from 5 vol.% to 10 vol.% improves the average micro-hardness of the material. This increase can be attributed to the hardening effect that was induced by the *in situ* formed TiB phase. The in-situ formation of TiB needles from the reaction:

$Ti+TiB_2 \rightarrow 2TiB$ (7.2) The resulting formed phases traits higher resistance to plastic deformation which results in the elevated hardness. Furthermore, increasing the vol.% of a hard reinforcement needle like TiB in a softer matrix such as Ti64, also increased hardness due to a reduction in the ductile material in the matrix., The TiB needles impede the Ti64 matrix and transfer the load from the softer matrix to the stiffer harder TiB phase due to the strengthening effect of the load transfer mechanism. It is important to note that the load transfer mechanism is extremely sensitive to the reinforcement volume fraction as seen by equation 7.3.

$$\Delta\sigma_{L.T} = 0.5 f_r \sigma_{ym} \qquad (7.3)$$

whereby f_r is the reinforcement volume fraction and σ_{ym} is the yield strength of the matrix.

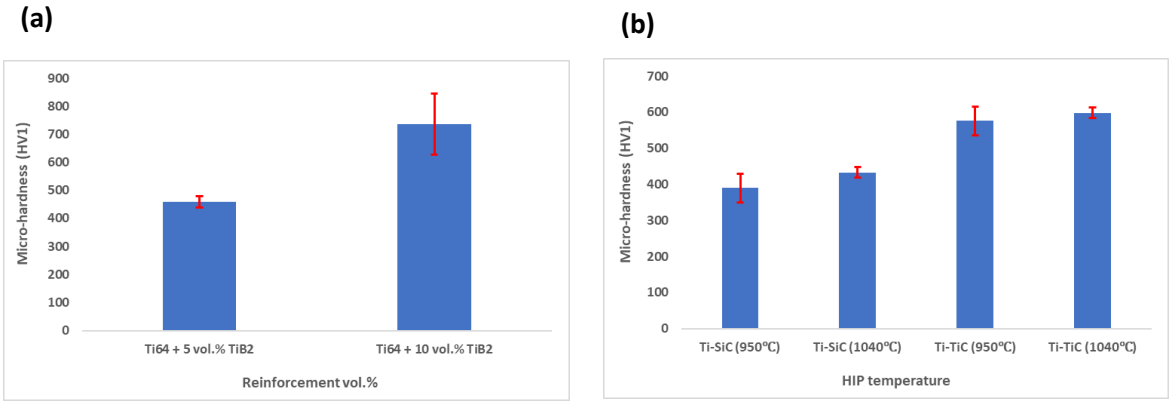

Figure 7.7: *(a) influence of reinforcement vol.% on micro-hardness of Ti64-TiB_2, (b) influence of HIP temperature on micro-hardness of Ti-SiC and Ti-TiC composites*

It is important to note that the standard deviation on the Ti64 + 10 vol.% TiB_2 was high at ±109HV suggesting an inhomogeneity in the composite microstructure, whereby some areas are rich in TiB needles and some areas are lean in TiB needles, which is ultimately due to the blending method used and the relatively large reinforcement volume fraction incorporated compared to the matrix and powder clustering. Figure 7.7b shows the micro-hardness of Ti-SiC and Ti-TiC as a function of HIP temperature. There is a clear trend of improved micro-hardness as the HIP temperature is increased from 950°C to 1040°C, and there are a number of explanations. In terms of Ti-SiC composite, it could be due to the retention of the hard phases of Ti_5Si_3, TiC and an increase in the retention of the harder β-Ti Phase, resulting in a higher load transfer effect. It could result in Si and C diffusion in the Ti matrix, which are both known to have a strengthening effect in Ti or it could be attributed to more consolidation and less porosities, and more regions of reinforcement overall.

7.3.5 Tribological properties

Figure 7.8 shows the worn surfaces of different as-HIPped composites, which commonly displayed as rough with ploughed grooves, delamination and wear debris, are typical features of abrasive wear mechanism due to the hard aluminium oxide (Al_2O_3) counter-body used resulting in severe plastic deformation. In figure 7.8a, the Ti64 + 5 vol.% TiB_2 worn surface is showed and it is clear that there

are signs of wear debris and delamination, which could be rationalised in terms of a weak interfacial bond between the reinforcement and matrix due to the large reinforcement size used relative to the matrix. As the reinforcement volume fraction is increased to 10 vol.% of TiB_2 as seen in figure 7.8b, the features of abrasive wear and wear debris are reduced due to the higher micro-hardness as shown in figure 7.7a. Figure 7.8c shows the worn surface of Ti-TiC composite that was prepared by HIP at 1040°C, and it can be clearly seen that there are signs of abrasive wear mechanism, such as delamination and wear debris. However, it should be noted that there is less delamination in comparison with Ti64 + 5 vol.% TiB_2 due to a higher micro-hardness of the composite and stronger interfacial bond between Ti reinforced with nano-sized TiC from a MA blending route.

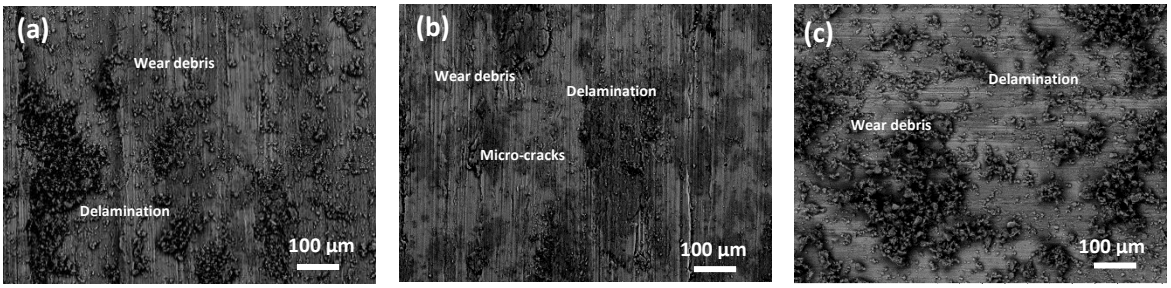

Figure 7.8: *SEM micrographs of worn surfaces (a) Ti64 + 5 vol.% TiB_2, (b) Ti64 + 10 vol.% TiB_2, (c) Ti-TiC HIPped at 1040°C*

Figure 7.9 shows the COF data of the composites, as a function of reinforcement vol.%, for Ti64 reinforced with TiB_2 and the Ti-TiC composites. The COF of Ti64 + 5 vol.% TiB_2 was recorded as 0.41 over the 800 cycles, while the COF of Ti64 + 10 vol.% TiB_2 was recorded as 0.43. The results achieved can be mainly attributed to three body abrasive wear mechanism, whereby the counter-body slide over the wear debris from the composite, . The main reason there is an increase in the wear debris and delamination of Ti64 + 10 vol.% TiB_2 can be mainly attributed to the weak interfacial bond between the reinforcement and the matrix due to the large size of the reinforcement particles (5 µm) relative to the matrix (15-45 µm) and the blending method used, which lead to an inhomogeneity in the blended powders and is clearly visible in the micrograph. The micro-hardness of the Ti64 + 10 vol.% TiB_2 composite had a standard deviation of 109 HV. Finally, the COF of Ti-TiC HIPped at 1040°C was recorded as 0.38 from the sliding reciprocating wear machine and averaged over three intervals and even though the microstructure was not fully consolidated as seen in figure 7.4c, it resulted in a better tribological performance in comparison with the fully consolidated Ti64+TiB_2. This, again, could be attributed to the improved homogeneity as a result of the MA technique used. The COF values of the TMCs are all within the range of variation and there was not a huge difference in COF values.

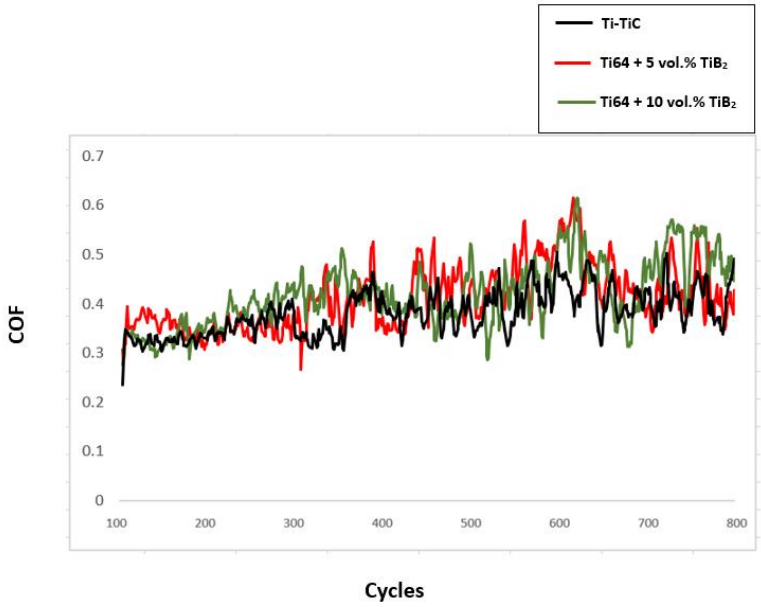

Figure 7.9: *COF data of the as-HIPped composites*

Figure 7.10 shows the wear rate of the as-HIPped composites. The volume loss of the samples were analysed using an Alicona optical profilometer. It can be clearly seen from the plotted wear rate in figure 7.10, that Ti64+10 vol.% TiB_2 exhibited the highest wear rate, followed by Ti64+5 vol.% TiB_2 and Ti-TiC. The results are in agreement with the COF data presented in figure 7.9 and the worn surface micrographs shown in figure 7.8. Even though the micro-hardness of Ti64+10 vol.% TiB_2 is higher than Ti64+ 5vol.% TiB_2, the wear rate is higher in Ti64+10 vol.% TiB_2, which could be attributed to the debonding of the reinforcement phase at higher volume fractions, resulting in three body abrasive wear and accelerating the wear rate.

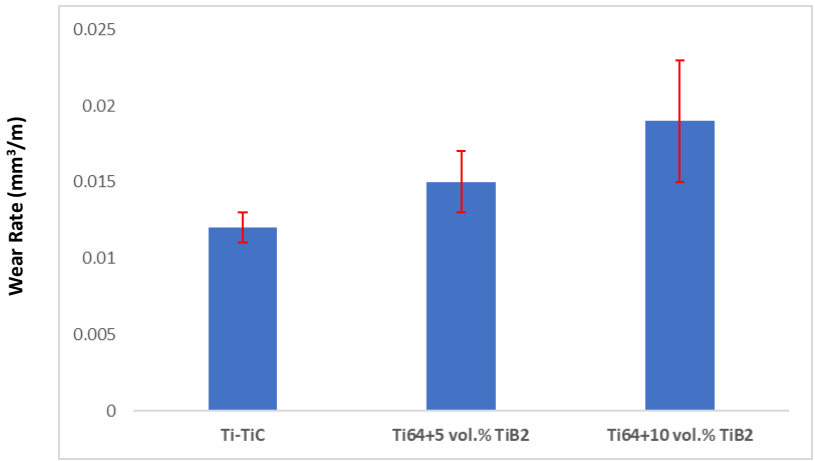

Figure 7.10: *Wear rate for Ti-TiC, Ti64 + 5 vol.% TiB_2 and Ti64 + 10 vol.% TiB_2*

7.3.6 Structure-property relations

In order to predict the structure-property relations, such as micro-hardness and compressive strength of the composites, the different contributing strengthening mechanisms will be explained and discussed in terms of how they influence the overall strength of the composite being analysed. Generally, the overall strength of a composite can be calculated in terms of the contributions of the load transfer mechanism, Hall-Petch grain refinement, dislocation strengthening and Orowan strengthening for nanocomposites. Moreover, in order to be able to predict the micro-hardness of composites based on the phase fractions of the formed phases, the ROM could be utilised in terms of the Hashin and Shtrikman upper bound (Voist) and lower bound (Reus) models [14]. The overall compressive strength of a composite can be calculated by using equation 7.4.

$$\sigma_{th} = \sigma_{ym} + \sigma_{H-P} + \sigma_{L.T} + \sigma_{CTE} + \sigma_{orowan} \qquad (7.4)$$

whereby σ_{ym} is the yield strength of the matrix, $\sigma_{H\text{-}P}$ is the Hall-Petch grain refinement, $\sigma_{H\text{-}P}$ is the load-transfer mechanism, σ_{CTE} is the dislocation strengthening mechanism due to the coefficient of thermal mismatch (CTE) between the matrix and reinforcement, and the σ_{orowan} is the strength induced from the Orowan strengthening mechanism due to the use of nano-reinforcements.

7.3.6.1 Hall-petch grain refinement

The Hall-Petch grain refinement equation depicts the influence of grain size on the strength of the composite and is expressed by equation 7.5.

$$\Delta\sigma_{H-P} = \sigma_o + kd^{-\frac{1}{2}} \qquad (7.5)$$

whereby σ_o is the starting stress for dislocation movement (845 MPa for Ti), k is s the Hall-Petch constant (for Ti = 0.3 MPa $m^{1/2}$ [15]) and d is the average grain size of the Ti matrix.

7.3.6.2 Load-transfer mechanism

The load-transfer mechanism is highly sensitive to the reinforcement volume fraction. The load is transferred from the softer matrix to the stiffer reinforcement, and the contribution to strength can be estimated using equation 7.6.

$$\Delta\sigma_{L.T} = 0.5 f_r \sigma_{ym} \qquad (7.6)$$

whereby σ_{ym} =845 MPa (yield strength of Ti matrix) was used and f_r is the volume fraction of reinforcement [16].

7.3.6.3 Dislocation strengthening via CTE mismatch

Dislocation strengthening using CTE mismatch is a prominent strengthening mechanism which arises from the CTE mismatch between the reinforcement and matrix. Dislocations are generated during the cooling process and the reinforcement particles at the grain boundaries will impede dislocation motion, hence strengthening the composite [17]. The expression used to calculate the strength contribution due to CTE mismatch is outlined in equation 7.7.

$$\Delta\sigma_{CTE} = \alpha G b \sqrt{\left(\frac{12\Delta T}{b(\frac{\Delta c.\, fr}{dr}}\right)} \qquad (7.7)$$

whereby G is shear modulus for (Ti = 44 GPa [18]), k is a constant for the material (for Ti= 1.25 [19]), b is Burger vector (for Ti= 0.29nm [15]), ΔT is the difference between the process temperature and room temperature, fr is the volume fraction of the reinforcement, dr is the reinforcement particle size, ΔC is s the thermal mismatch between matrix and reinforcement.

7.3.6.4 Orowan strengthening mechanism

The Orowan strengthening mechanism plays a dominant role by drastically increasing the strength of a composite through the incorporation of nanoparticles. This mechanism primarily works by

nanoparticles looping around the dislocations, inhibiting movement and strengthening the composite. The strength gain due to the Orowan strengthening mechanism can be calculated using equation 7.8.

$$\Delta\sigma_{orowan} = \frac{0.81\ MGb}{2\pi(1-\theta)^{\frac{1}{2}}} \frac{ln\frac{d_r}{b}}{\left(\frac{1}{2}d_r\sqrt{\frac{3\pi}{2f_r}-d_r}\right)} \qquad (7.8)$$

where G is shear modulus, b is burger vector, dr is particle size of reinforcement , fr is volume fraction of reinforcement (which are the same values as the those mentioned above in the dislocation strengthening mechanism), M is the Taylor factor (for Ti M=2.6 [20]) and Θ is the Poisson ratio (for Ti Θ=0.31 [21]).

7.3.6.5 ROM for micro-hardness

In terms of predicting the micro-hardness of composites, the ROM has been utilised in research, whereby Hashin and Shtrikman came up with upper bound (Voist) and lower bound (Reus) models to predict the micro-hardness depending on the microstructure [14]. In this study, since the matrix is soft and reinforced with stiffer phases, the Reus model is used as seen in equation 7.9.

$$H_{low} = (\frac{f_h}{H_h} + \frac{f_s}{H_s})^{-1} \qquad (7.9)$$

where f_h is the phase fraction of the harder phase, H_h is the micro-hardness of the harder phase, f_s is the phase fraction of the softer phase and H_s is the micro-hardness of the softer phase.

7.3.5.6 Deviation between experimental and theoretical data

Figure 7.11 shows a plot of the theoretical micro-hardness values for Ti64 reinforced with TiB_2 particles with varying vol.% (5-10 vol.%), and Ti-TiC composite HIPped at 1040°C. The theoretical values were calculated using the ROM, specifically the Reus model shown in equation 8. It can be observed that theoretical values are practically in agreement with the experimental micro-hardness values, with only a slight increase in the predicted values overall the experimental. The main reason for the deviation between theoretical and experimental values is that the equations do not consider the diffusion of C

and O into the Ti matrix, are well known to have a huge strengthening effect on Ti and the equations simply ignore those contributions into the yield strength values used for monolithic Ti in order to simplify the calculations. It is well known that the contribution of strength per each 0.01 wt.% of C in Ti matrix is roughly 7 MPa while a 0.01 wt.% of O has a strengthening effect of roughly 12 MPa in Ti matrix [22]. In addition, the deviation in values could also be attributed to the inhomogeneity of the blended powders of Ti64 reinforced with TiB_2 and an ineffective load transfer due to the microstructural inhomogeneity and weak interfacial bond between the matrix and relatively large sized reinforcement.

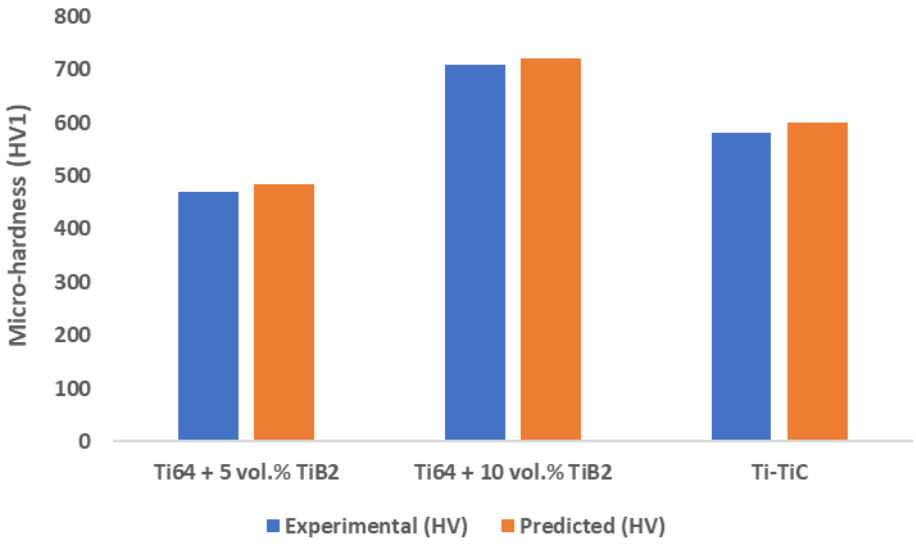

Figure 7.11: *Structure-property relations of micro-hardness using ROM Reus model*

7.4 Conclusions

The study looked into the influence of HIP temperature on the consolidation behaviour of as-received MA nanocomposite, such as Ti-SiC and Ti-TiC, and their respective mechanical and tribological behaviour. The influence of reinforcement vol.% on the mechanical and tribological behaviour of Ti64 reinforced with (5-10) vol.% TiB_2 particles mixed via roll blending were also investigated. Furthermore, the structural-property relations, namely the strengthening mechanisms, were extensively discussed in order to predict and rationalise the mechanical properties such as the micro-hardness. The conclusions are as follows:

(1) Ti-SiC composite prepared at a HIP temperature of 950^{o}C did not ensure full consolidation with large porosities visible, and an incomplete *in situ* reaction.

(2) The Ti-SiC composite at a HIP 1040^{o}C promoted more consolidation with less visible porosities and a better *in situ* reaction taking place, which resulted in the synthesis of the Ti_5Si_3 and TiC phases as confirmed by the XRD scan.

(3) Increasing the HIP temperature from 950^{o}C to 1040^{o}C resulted in increased retention of the TiC phase formation in Ti-TiC composite and a reduction in the porosity area and more *in situ* reaction taking place.

(4) TiB_2 reacted with Ti to form hard TiB needles as confirmed by the XRD scan. By increasing the vol.% of TiB_2 from 5 to 10 vol.% resulted in a higher retention of TiB needles that coalescence around neighbouring grain boundaries, further strengthening the agglomerated regions.

(5) The increase of micro-hardness observed with the with the 10 vol.% TiB_2 is mainly be attributed to the load transfer mechanism and grain refinement. The large standard deviation could be attributed to the inhomogeneity, which is inherent to the blending technique used and the relatively large reinforcement size of 5 μm.

(6) Increasing the HIP temperature from 950°C to 1040°C in Ti-TiC and Ti-SiC resulted in a higher micro-hardness, as a result of less porosity and improved retention of hard *in situ* formed phases.

(7) The experimental and theoretical values of micro-hardness are in agreement, validating the modified ROM Reus model. The small deviation in values could be attributed to O and C diffusion into Ti matrix, which are known to have significant strength contributions to the yield strength.

Acknowledgements

The authors acknowledge the Centre of Doctoral Training in Innovative Metal Processing (IMPaCT), funded by the Engineering and Physical Sciences Research Council (EPSRC), and the National Structural Integrity Research Centre (NSIRC), for funding this PhD project at the University of Birmingham.

References

[1] H. Attar, S. Haghighi, D. Kent, M. Dargusch., *Recent developments and opportunities in additive manufacturing of titanium based matrix composites: A review*, Int. J. Mach. Tools Manuf. Vol.133 ,2018, pp. 85–102

[2] T. Kuzumaki, O. Ujiiiye, H. Ichinose ., *Mechanical characteristics and preparation of carbon nanotube fiber-reinforced Ti composite,* Adv Eng Mater. Vol.2(7), 2000, pp.416-418

[3] C. Poletti, M. Balog, T. Schubert, V. Liedtke, C. Edtmaier., *Production of titanium matrix composites reinforced with SiC particles*, Compos Sci Technol. Vol.68(9), 2008, pp.2171-2177

[4] M. Selva Kumar, P. Chandrasekar, P. Chandramohan, M. Mohanraj., *Characterisation of titanium-titanium boride composites processed by powder metallurgy,* Mater Charact, Vol.73, 2012, pp.43-51

[5] O. Oyelola, P. Crawforth, R. M'Saoubi, A. Clare., *Machining of functionally graded Ti6Al4V/WC produced by directed energy deposition*, Addit.Manuf. Vol.24, 2018, pp.20-29

[6] F.M. Kgoete, A.P.I. Popoola, O.S.I. Fayomi., *Oxidation resistance of spark plasma sintered Ti6Al4V-TiN composites*, J. Alloys Compd., Vol.772, 2019, pp.943-948

[7] L. Huang, L. Geng., *Discontinuously Reinforced Titanium Matrix Composites: Microstructure Design and Property Optimization*. Singapore:Springer, 2017, pp.1-15

[8] S. Jeng, J. Yang, S. Aksoy., *Mechanical behaviour of SiC fibre-reinforced titanium/titanium aluminide hybrid composites*, J Mater Sci. Vol.27(19), 1992 , pp.5357-5364

[9] L. Geng, D.R. Ni, J. Zhang, Z. Zheng., *Hybrid effect of TiBw and TiCp on tensile properties of in situ titanium matrix composites*, J Alloy Compd., Vol.463(1), 2008, pp.488-492

[10] K. Kondoh, *Titanium metal matrix composites by powder metallurgy (PM) routes*. Titanium Powder Metallurgy. Boston:Butterworth-Heinemann; 2015. pp.277-297

[11] F. Kgoete, A. Popoola, O. Fayomi., *Oxidation resistance of spark plasma sintered Ti6Al4V-TiN composites*, J. Alloys Compd. Vol.772, 2019, pp.943-948

[12]] L. Wu, Z. Zhao, P. Bai, W. Zhao, Y. Li., *Wear resistance of graphene nano-platelets (GNPs) reinforced AlSi10Mg matrix composite prepared by SLM.* Applied Surface Science. Vol.503, 2020

[13] I. Shishkovsky, N. Kakovkina, V. Sherbakov., *Graded layered titanium composite structures with TiB2 inclusions fabricated by selective laser melting*. Compos. Struct. Vol.169, 2017, pp.90-96

[14] F. Weng, H. Yu, J. Liu, C. Chen, J. Dai, Z. Zhao., *Microstructure and wear property of the Ti5Si3/TiC reinforced Co-based coatings fabricated by laser cladding on Ti-6Al-4V*. Opt. Laser Technol. Vol.92, 2017, pp.156-162

[15] K. Kondoh., *Titanium metal matrix composites by powder metallurgy (PM) routes.* Titanium Powder Metallurgy. Boston:Butterworth-Heinemann; 2015. pp. 277–97

[16] K. Kim, *on the rule of mixtures for the hardness of particle reinforced composites*. Mater Sci Eng A. vol. 289, 2000, pp. 30-33

[17] H. Frost, M. Ashby ., *Deformation mechanism maps: the plasticity and creep of metals and ceramics.* Pergamon press; 1982.

[18] S. Li, K. Kondoh, H. Imai, B. Chen, L. Jia, J. Umeda, Y. Fu., *Strengthening behaviour of in situ-synthesized (TiC–TiB)/Ti composites by powder metallurgy and hot extrusion*. Mater Design. 2016; vol.95, pp.127–32.

[19] Y. Wu, W. Cassada, E. Lavernia., *Microstructure and mechanical properties of spray-deposited Al-17Si-4.5 Cu-0.6 Mg wrought alloy*. Metall Mater Trans. A1995;26(5), pp.1235–47.

[20] F.X. Li, P.D. Hao, J.H. Yi, Z. Chen, K.G. Prashanth, T. Maity, J. Eckert., *Microstructure and strength of nano-/ultrafine-grained carbon nanotube-reinforced titanium composites processed by high-pressure torsion*. Mater Sci Eng, A 2018, vol.722, pp.122–128

[21] W.J. Kim, Y.J. Yu., *The effect of the addition of multiwalled carbon nanotubes on the uniform distribution of TiC nanoparticles in aluminum nanocomposites*. Scripta Mater. 2014; vol.72, pp.25–28.

[22] H. Frost, M. Ashby., *Deformation mechanism maps: the plasticity and creep of metals and ceramics*. Pergamon press; 1982.

[23] M.J. Starink, S.C. Wang *., A model for the yield strength of overaged Al–Zn–Mg–Cu alloys*. Acta Mater.2003, vol.51, pp5131–5150.

[24] Sanaty-Zadeh*, Comparison between current models for the strength of particulate-reinforced metal matrix nanocomposites with emphasis on consideration of Hall–Petch effect*. Mater Sci Eng, A 2012, vol.531, pp.112–118.

[25] K. Kim, *on the rule of mixtures for the hardness of particle reinforced composites,* Materials Science and Engineering A289, 2000, pp.30 – 33

[26] H. Ogden, R. Jaffee ., *The effects of carbon, oxygen, and nitrogen on the mechanical properties of titanium and titanium alloys*: Battelle Memorial Inst. Columbus, Ohio: Titanium Metallurgical Lab; 1955

Chapter 8: Conclusions and Future Work

8.1 Introduction

The work in this thesis is aimed to study and investigate the influence of powder characteristics such as the reinforcement type, volume fraction and size on the mechanical and tribological performance of TMCs. Furthermore, the study looks into the influence of process parameters such as HIPping temperature on the consolidation behaviour, microstructural evolution and *in situ* phase formation of TMCs using elemental powders such as B and GNPs and different blending routes such as roll blending and mechanical alloying. Moreover, an FGM was produced via P/M HIP. It is well known that the reinforcement size and volume fraction can drastically affect the mechanical and tribological behaviour through variable strengthening mechanisms such as Orowan strengthening , grain refinement and load transfer mechanism. Additionally, it is well reported that the difference between the CTE values between the reinforcement and the matrix can result in strengthening the TMC via dislocation strengthening which is also investigated in this work. This chapter briefly summarises the conclusions in Chapters 4,5,6 and 7.

8.2 Influence of HIP temperature on phase formation

Process parameters such as the HIPping temperature directly influence the microstructure, hence the mechanical and tribological properties of TMCs. For instance, Ti64 is generally HIPped at 920℃ below the ß-transus temperature of 980℃, to limit grain growth, retention of ß-Ti phase and enhance the mechanical properties such as strength and ductility. One of the major challenges with HIPping Ti64 and its TMCs is the large brittle diffusion zone that forms during HIPping above the ß-transus temperature as a result of the increased solubility of Fe in Ti and the formation of brittle intermetallic phases. In order to thoroughly understand the influence of the HIPping temperature on the phase formation of the TMCs, the TMCs such as Ti64 reinforced with varying volume fractions of SiC, were HIPped at sub ß-transus temperature of 950℃ and a dwell time of 6h and above ß-transus temperature of 1160℃ for a constant dwell time of 3h and pressure of 140 MPa. The following conclusions were deduced below:

- It can be concluded from the Ti64-SiC TMC work that the samples HIPped at sub-transus temperature of 950℃, showed a lack of consolidation due to the temperature being too low to initiate and enhance the diffusivity of Si and reduce the yield strength of SiC in order to close the pores and have a full consolidation.

- It was also concluded that the temperature was enough to initiate an incomplete in-situ reaction between the reinforcement and the matrix.

- It was also concluded that HIPping at 950℃ for 6h did not enhance diffusivity, consolidation and *in situ* phase formation as the main driver is temperature. The main advantage of HIPping at 950℃ was the small diffusion zone in comparison with HIPping beyond the ß-transus temperature which resulted in a large brittle intermetallic phase zone due to the increased solubility of iron (Fe) in Ti.

- Another conclusion is, it is well known that carbon (C) diffusivity is ten times faster than the diffusivity of Si in the ß-Ti phase field, and that the maximum possible solubility of Si in ß-Ti is roughly about 3.7%. Therefore, the phase formation of strengthening phases such as titanium carbide (TiC) and titanium silicide (Ti_5Si_3) precipitates increases significantly as the HIP temperature is raised beyond the ß-transus temperature. Furthermore, Ti reacts with C to form TiC precipitates [1].

In summary, the work investigating the influence of HIP temperature on phase formation in the Ti64-SiC in Chapter 5, it was concluded that HIPping Ti-6Al-4V/SiC composite at 950℃ has many regions of unconsolidated SiC. Incomplete in-situ reactions occur. In contrast, HIPping at 1160℃ ensures full synthetization of in-situ Ti_5Si_3 and TiC phase formation.

In terms of further understanding the influence of HIPping temperature on the *in situ* formation of phases and the consolidation behaviour of TMCs, HIPping temperatures of sub β-transus (920℃), (1040℃) and super-transus (1160℃) were studied in Chapter 4, concerning the elemental phase formation of TMCs using starting additives such as graphene nanoplatelets (GNPs) and boron (B). 1040 ℃ was selected specifically as it is below the ß-transus temperature based on calculations that took

into account the diffusion of C and O into the Ti matrix, which are both well known in raising the ß-transus temperature beyond 980℃ for Ti64. The following conclusions were derived:

- Increasing the HIP temperature from 920℃ to 1040℃ ensures full consolidation and complete *in situ* reaction for Ti64 reinforced with 1 vol.% GNP. HIPping at 920℃ shows a lack in consolidation with large visible porosities and incomplete *in situ* reaction.

- HIPping Ti64 reinforced with 1 vol.% GNP could enhance the mechanical properties of the TMC due the presence of nano-sized graphene and the refined grain size of Ti64 in comparison with HIPping at higher temperatures which resulted in grain growth.

- HIPping temperature of 1040℃ was selected based on estimating the O and C content which estimate the ß-transus temperature to be 1070℃, hence why 1040℃ was selected and investigated.

- HIPping Ti64 reinforced with 1 vol.% GNP at 1160℃ results in the coarsening of the *in situ* formed TiC phase, an increase in ß-Ti phase and a lamellar microstructure for Ti.

Moreover, the influence of HIPping temperature on the phase formation and microstructural evolution of Ti-based as-received nanocomposites and Ti64 reinforced with TiB_2 particles was investigated thoroughly in Chapter 7. The conclusions derived from the study are as follows:

- HIPping the As-received Ti-SiC nanocomposite at 950℃ showed a lack of consolidation but an incomplete reaction did take place between the reinforcement and matrix.

- Increasing the HIP temperature to 1040℃ shows more *in situ* reaction taking place between the matrix and reinforcement resulting in the formation of strengthening phases such as TiC and Ti_5Si3 as confirmed by the XRD scan. Furthermore, the microstructure showed less porosity and more consolidation over 950℃ due to more diffusion taking place.

8.3 Influence of reinforcement volume fraction on mechanical and tribological properties

Increasing the reinforcement volume fraction can result in enhanced strength and tribological behaviour, however it can also be detrimental in the sense of making the material more brittle and decreasing the inherent material ductility. The major issue with using a high volume fraction is that it could lead to agglomeration during the blending process, hence resulting in heterogenous properties along the microstructure. It is well known that increasing the reinforcement volume fraction strengthens the TMC due to multiple strengthening mechanisms coming into play such as mainly the load transfer mechanism, which is highly sensitive to reinforcement volume fraction, grain refinement due to the *in situ* formed hard phases that decorate the PPBs and dislocation strengthening which is highly sensitive to both the reinforcement size and volume fraction. The influence of reinforcement volume fraction on the properties was investigated in Chapter 4, 5, 6 and 7.

In Chapter 4, the influence of reinforcement volume fraction of GNPs on the mechanical and tribological behaviour of the TMCs were investigated and the following conclusions were drawn:

- Increasing the reinforcement volume fraction of GNP from 1 vol.% to 2 vol.% resulted in a higher micro-hardness which can be mainly attributed to the strengthening effect of the load transfer mechanism.

- The increase in reinforcement volume fraction resulted in a lower COF value which can be attributed to both a higher micro-hardness and the unreacted GNP on the surface which helped lubricate the TMC during the wear test as confirmed by the Raman spectra.

- In terms of CTE measurements, Ti64 reinforced with 2 vol.% of GNP recorded the lowest value , even against Ti64 reinforced with 1 vol.% GNP and 1 vol.% B and that could mainly be attributed to a higher volume fraction of GNP and more retention of TiC which has the lowest CTE value and based on the ROM, the measurement can be rationalised.

In Chapter 5, the influence of SiC volume fraction the mechanical and tribological behaviour. The following conclusions can be drawn and are summarised below:

- Increasing the volume fraction of the SiC reinforcement, resulted in a higher recorded micro-hardness which could be mainly attributed to a higher retention of hard phases such as TiC

and Ti_5Si_3 and the strengthening effect of the load-transfer mechanism mainly. On the other hand, it had a negative impact on the wear and COF values due to 3-body abrasive wear. The 3-body abrasive wear is apparent due to the weak interfacial bond between the reinforcement and matrix.

In chapter 7 other reinforcements were investigated such as titanium diboride (TiB_2) and the following conclusions are drawn below:

- Increasing the reinforcement volume fraction of TiB_2 from 5 vol.% to 10 vol.% resulted in a higher micro-hardness value due to the strengthening effect of the higher retention of TiB needles that formed due to the *in situ* reaction between Ti matrix and TiB_2 as confirmed by the XRD scan. The higher retained TiB needles coalescence around surrounding grain boundaries and strengthen certain regions more.

- The large standard deviation in micro-hardness could be attributed mainly to the blending route used and the large size of the reinforcement powder used at 5µm relative to the matrix size.

8.4 Influence of reinforcement size on the mechanical and tribological properties

The reinforcement particle size has a significant influence over the mechanical behaviour and the tribological properties of TMCs. Reducing the reinforcement particle size from micron size to nano-size can influence the mechanical and tribological behaviour positively due to mainly the attribution of the Orowan strengthening mechanism which is a dominant strengthening mechanism in nanocomposites. The influence of reinforcement particle size on the mechanical and tribological properties was investigated mainly in Chapter 5 whereby two different sizes of 5 µm and 20 nm were selected for the SiC reinforcement at a constant reinforcement volume fraction. The following conclusions were derived from the research:

- Reducing the reinforcement particle size from 5 µm to 20 nm resulted in a micro-hardness increase at a constant reinforcement volume fraction of 5 vol.%. The increase in micro-hardness can be attributed to grain refinement, orowan strengthening and dislocation strengthening mechanisms.

- Reducing the reinforcement particle size from 5 µm to 20 nm reduces the COF even in comparison with Ti64 reinforced with 10 vol.% SiC. Even though the micro-hardness of Ti64 reinforced with 10 vol.% SiC is higher, the interfacial bonding between the reinforcement and the matrix is weaker, resulting in 3-body abrasive wear to take place, hence increasing the wear rate.

- From the structure-property modelling, the biggest strength contribution was due to the Orowan strengthening mechanism. Reducing the reinforcement particle size from 5 µm to 20 nm increased the orowan strength contribution from 2.8 MPa to 282.2 MPa at a constant volume fraction of 5 vol.% reinforcement. The strengthening mechanism works by inhibiting dislocation movement due to the nanoparticle's role as obstacles.

- Another big contribution to the strength is due to the CTE mismatch between the reinforcement and the metal matrix as predicted by the structure-property model. It is known that dislocations can be generated in the metal matrix upon the cooling process and geometrically necessary dislocations are produced. However, the CTE mismatch strength contribution in nano-composites are not consistent with experimental data in other works [3] which is attributed to internal stresses generated due to the CTE mismatch are reduced drastically as the reinforcement particle size is reduced from the micron to the nano-scale.

8.5 Influence of FGM layers on mechanical properties

It is a well-known fact that increasing the volume fraction along different layers of an FGM can drastically tailor the microstructure to certain needs, hence result in varying mechanical and tribological behaviour along the gradient. Chapter 6 looked into synthesizing a Ti64 reinforced with varying vol.% of SiC FGM (0,5,10) vol.% via P/M HIP and test the mechanical properties such as the compressive strength, fractography and tribological behaviour. The conclusions derived from the work are as follows:

- Successfully HIPped a three layer Ti64/SiC FGM with no visible cracks at the interface which shows a strong bond between different gradient layers as shown by the crack free indents from the micro-hardness testing.

- The micro-hardness showed an increasing trend at different layers as the volume fraction of SiC was increased. Furthermore, Ti64 showed a higher recorded micro-hardness that the typical value in the unreinforced region which could be potentially due to Si diffusion into the Ti matrix which is known to have a profound effect on strength.

- The compressive values of the unreinforced region of Ti64 had a ductility of 17.2% and a yield strength of 1570 MPa. The fractography showed mostly regions of ductile fracture which can be seen by features such as the dimples that were highly present in the sample.

- There is a clear trend of decreasing ductility values as the reinforcement volume fraction is increased while the compressive yield strength increases with an increase in reinforcement volume fraction.

- The interface regions between unreinforced Ti64 and Ti64 reinforced with 5 vol.% SiC shows a compressive yield strength and ductility values that are in between unreinforced Ti64 and Ti64 reinforced with 5 vol.% SiC.

- As the reinforcement volume fraction increases, the brittle nature seen from the fractography increases as indicated by the increase in the cracks and cleavage fracture features. The cracks are initiated from the regions that have an agglomeration of the hard phases, acting as stress concentration areas which is undoubtedly an inherent issue related to the powder blending route used and the relatively large reinforcement size in comparison to the matrix powder.

8.6 Influence of blending method on the microstructural homogeneity and properties

It is well known that the blending route to process TMCs can influence the microstructural homogeneity, hence the mechanical and tribological properties. Chapter 5 investigated the influence of blending method on the microstructural homogeneity and the properties. The conclusions derived from the study are as follows:

- MA using ball milling ensured the reinforcement particles to stick to the matrix, improving interfacial bonding and resulting in less delamination after wear testing

- De-agglomerating the nano-particles using wet ultrasonication in ethanol as a process control agent prior to ball milling ensured that the reinforcement was not agglomerated, hence

further improving the distribution on the matrix and resulting in more homogenous properties such as micro-hardness as reflected by the lower error bar in comparison with roll blending

8.7 Comparison between different reinforcements on the mechanical and tribological properties

Selecting a suitable reinforcement for a TMC depends on many factors which includes the CTE mismatch between the matrix and reinforcement that can influence the thermal residual stresses in brittle reaction zones, the *in situ* formed phase and the processing temperature required to synthesize the phase, cost, density of reinforcement in comparison to the metal matrix that could determine how much or little of a reinforcement volume fraction can achieve a certain increase in strength contribution and stiffness. Chapter 4 looked into reinforcements such as B and GNP while Chapter 7 investigated different as-received MA nanocomposites using reinforcements such as SiC, TiC and micron sized TiB_2. The conclusions presented below will compare the different reinforcements in terms of the strength contributions, micro-hardness contributions, wear resistance and whether B and GNP as starting elemental additives are better than using TiB_2 and TiC. The conclusions are as follows:

- HIPping Ti64 + 5 vol.% TiB_2 (5 µm) at super ß-transus temperature results in the formation of TiB needles at the prior particles boundaries coalescing and forming a network-like structure.

- HIPping Ti64 + 1 vol.% B (1 µm) below the ß-transus temperature at 1040℃ due the oxygen interstitials content raising the temperature resulted in the formation of finer TiB needles and a more refined microstructure in comparison to using TiB_2 as a starting reinforcement.

- 1 vol.% B (1 µm) increased the micro-hardness of Ti64 from 330 HV to 380 HV which is a strength increase of 15%, while 5 vol.% TiB_2 (5 µm) increased the micro-hardness from 330 HV to 450 HV 36% which makes it less effective in strengthening the composite as more TiB_2 is required to achieve the same strength contributions as B. It is well reported that adding 0.05 weight percent (wt.%) reduced the prior ß grain significantly which is due to the *in situ* formation of TiB at the GB that acts as nucleation sites for ß grains [1]. Other reports also described those small additions of B resulted in a grain refinement of 2-3x [2]. The strength contributions could be attributed mainly to grain refinement.

8.8 Future work

Based on the research conducted in this thesis, the main parameters that influence the homogeneity of the mechanical and tribological properties of the TMC goes back to selecting sub-micron or nano-sized reinforcements to enhance the interfacial bonding and improve the properties of the composite, which in turn would depend on the powder processing route using in terms of blending whether MA using a process control agent or dry roll blending is used. Other important factors that influence the mechanical and tribological behaviour is selecting a reinforcement that would be chemically compatible with Ti, low CTE mismatch with Ti and close densities while providing high strength contributions. Finally, selecting the optimal HIPping temperature to ensure full reaction and *in situ* phase formation is vital, while making sure that the brittle intermetallic diffusion zone is relatively small especially when near net shape (NNS) component structural integrity and tolerances are important in an application.

8.8.1 Canister material selection

Mild steel is commonly used as a canister for HIP due to the ease of deformation [3]. However, when processing TMCs at high temperatures, a large diffusion zone with brittle intermetallic phases forms which can be a region of crack initiation and would result in reducing the structural integrity of NNS components. Grade 2 Ti can be investigated as a potential canister material to HIP NNS TMC components and the influence of canister material can be studied in terms of the diffusion zone size and part tolerances.

8.8.2 Other processing parameters

The HIP process has many parameters that can influence the microstructure, mechanical and tribological properties directly such as the cooling rate, HIP temperature, dwell time and pressure. The cooling rate can influence the grain size significantly and the EPSI HIP at the University of Birmingham has a jet cooling system which can cool at a rate of 100℃/min.

8.8.3 Mechanical testing

Compression testing could be investigated for the other TMCs and compressive yield strength, elastic modulus and strain can be extrapolated from the data. Other mechanical tests that could be

conducted are fatigue testing and high temperature properties such as creep resistance at elevated temperatures. In terms of fatigue, it is known that the high stiffness of ceramic reinforcements could improve fatigue life under high stresses for rotating components in jet engines for example, however it the debonding between the matrix and reinforcement could be a potential area of problem that should be looked into [4]. As to using TMCs in high temperature applications, assessing the creep behaviour is vital. It is known that most MMCs have the three stages of creep from the primary, steady state and tertiary state. The metal matrix will creep more noticeably than the ceramic reinforcement [5]. For example, it is reported that using SiC as a reinforcement will reduce the creep rate substantially until deformation is reached [6]. Tensile tests could also be carried out in order to assess the materials response to tensile loading applications in the aerospace field for instance.

8.8.4 Erosion-corrosion behaviour

For applications that require corrosion-erosion resistance such as geothermal power plants and the oil and gas industry pipelines, Ti and its alloys provide high corrosion resistance in comparison with other materials such as stainless steel [7]. Studying the influence of different reinforcement types, volume fraction and size on the corrosion-erosion behaviour could be beneficial in enhancing the resistance of the composite in harsh operating conditions.

8.8.5 Modelling

Finite element modelling of the shape change that occurs during the HIP process and model the shrinkage for complex shaped NNS components. Abouaf et al. [8], came up with a model to predict the densification by accounting for the effect of viscoplasticity, thermal effects and the powder characteristics. In addition to that, work by Yuan et al. [9] came up with a finite element model that predicts the dimensions of HIPped Ti64 using the equations governing the plastic yield without taking into account other densification mechanisms. The reason to simplify the model was due to the fact that more than 90% of the powder densification takes place from the plastic yield mechanism and the model shows good agreement with the final geometries [10]. The model used by Abouaf and Yuan could be employed in future work when NNS components for TMCs are investigated.

8.8.6 Characterization

Characterization techniques such as electron back scattered diffraction (EBSD) can be utilized to further study the influence of different reinforcement types, volume fractions and sizes on the grain size of the TMCs. In addition, high resolution transmission electron microscopy (HRTEM) can be utilized to confirm the confirm the generation of geometrically necessary dislocations and whether Orowan looping due to the incorporation of nanoparticles acts as a strengthening mechanism.

References

[1] Yu, Yang & Hui, Songxiao & Mi, Xujun & Ye, Wenjun & Gao, Qi., *0.1wt% Boron addition Effect on dynamic compressive mechanical properties of Ti-6Al-4V alloy,* MATEC Web of Conferences, 05018, 2016, 705018

[2] Gaddam. *Effect of Boron and Hydrogen on Microstructure and Mechanical Properties of Cast Ti-6Al-4V*, Licentiate Thesis, Lulea University of Technology, 2011, SE-971 87 Lulea, ISSN: 1402-1757, ISBN: 978-91-7439-300-2.

[3] Mcnamara, Karrina & Butler, J. & Gandhi, A.A. & Tofail ., *3.2.1 Powder Metallurgical Processing of NiTi Using Spark Plasma Sintering,* Comprehensive Materials Finishing, 2017, Vol.3, pp.336-346

[4] N. Chawla, Y. Shen., *Mechanical behaviour of particle reinforced metal matrix composites,* Adv. Eng. Mater., 2001, Vol.3(6), pp.357-370

[5] S. Schwenker, D. Eylon., *Creep deformation and damage in a continuous fiber-reinforced Ti-6Al-4V composite,* Metallurgical. Mater. Trans. A, Vol.27(12), 1996, pp.4193-4204

[6] C. Leyens, J. Hausmann, J. Kumpfert., *Continuous fiber reinforced titanium matrix composites: fabrication, properties, and applications,* Adv. Eng. Mater., 2003, Vol.5(6), pp.399-410

[7] S. Irukuvarghula, R. Khan, N. Ludford, F. Brownlie, A. Pearson, T. Hodgkiess, A. Sergi, M. Al Lawati, M. Attallah., *Development of Powder Metallurgy Based Metal Matrix Composites for Geothermal Applications,* Conference: World Geothermal Congress, 2020

[8] M. Abouaf, J. Chenot, G. Raisson, P. Bauduin., *Finite element simulation of hot isostatic pressing of metal powders,* International Journal for Numerical Methods in Engineering, 1988, Vol.25(1), pp.191-212

[9] W.X. Yuan, J. Mei, V. Samarov, D. Seliverstov, X. Wu., *Computer modelling and tooling design for near net shaped components using hot isostatic pressing,* Journal of Materials Processing Tech, 2007, Vol.182(1-3), pp.39-49

[10] K. Essa, R. Khan, H. Hassanin, M. Attallah, R. Reed ., *An iterative approach of hot isostatic pressing tooling design for net-shape IN718 superalloy parts,* Int. J. Adv. Manuf. Technol., 2016, Vol.83, pp.1835-1845